Genetic Control of Hypothalamo-Pituitary Axis Development and Function in Mice

Eva Szarek, BSc (Hons)

A thesis submitted for the degree of

Doctor of Philosophy

March 2011

School of Molecular and Biomedical Science

Discipline of Biochemistry

The University of Adelaide

Advisors: *Associate Professor Paul Thomas*
Professor Jeffrey Schwartz

Discipline of Biochemistry
School of Molecular and Biomedical Science
The University of Adelaide
Adelaide Australia 5000

Printed on acid-free paper at Kwik Kopy, Adelaide, South Australia.

For my parents,

Jan and Dorota Szarek

"Glands rarely become ill, but when they do,
they give their disease to the rest of the body"

Hippocrates, *Glands*, circa 500 B.C.

CONTENTS

LIST OF FIGURES

Figures in Appendices

LIST OF TABLES

Tables in Appendices

A NOTE ON NOMENCLATURE

Relevant nomenclature guidelines were taken into account when referring to genes and gene products throughout this thesis. To unambiguously refer to mouse (*Mus musculus*) genes and gene products, and to distinguish these from mammalian nomenclature, the following conventions were adhered to. Mouse gene names are italicized and in lower case, whereas gene products are non-italicized and the first letter is capitalized. Human gene names are italicized and all capitalized, whereas proteins are non-italicized and all capitalized. In addition, reference may be given to *Drosophila* genes and gene products. To differentiate these from mouse and/or human genes and gene products *Drosophila* genes are italicized and the protein are non-italicized and in lower case. Additionally, when referring to both the gene and protein, the protein name is given.

Species	**Gene (abbreviation)**	**Protein (abbreviation)**
Mouse	*Sox3*	Sox3 or mSox3
Human	*SOX3*	SOX3 or hSOX3
Drosophila	*sox3*	sox3

With reference to the Sox3 knock-out, transgenic and reporter mice, these will be referred within this thesis as follows:

Mouse Line	**Nomenclature within thesis**
Sox3-null	*Sox3*-null
Sox3-transgenic ($Sox3^{iRES\text{-}eGFP}$)	Extra-Sox3
Sox3-GFP reporter	Green-Sox3

With reference to the novel dwarf mouse line described herein, we have given this mouse line the name Tukkuburko. The name is the Kaurna Aboriginal word referring to "small mouse". The Kaurna Indigenous people are the custodians of the greater Adelaide region and their cultural and heritage beliefs are still important to the living Kaurna people today.

ABSTRACT

Congenital dysfunction of the hypothalamic-pituitary (HP) axis occurs in approximately one birth per 2,200 and is associated with a broad range of common disease states including impaired growth (short stature), infertility, hypogonadism poor responses to stress and slow metabolism (Pescovitz and Eugster, 2004). Although, a number of genes have been linked to diseases of the HP axis, the genetic cause in many patients remains unknown.

This thesis examines two aspects of HP axis development and function. The first aim was to identify *Sox3* targets by examining gene expression differences between three mouse lines: *Sox3*-null (mice lacking *Sox3*; loss of function), Extra-Sox3 (mice over-expressing Sox3; gain of function) and wild-type, by genome wide profiling using the Illumina BeadChip microarray platform. The second aim was to characterize the downstream effects relative to HP development in a novel recessive dwarf mouse model with pituitary hypoplasia and growth hormone (GH) deficiency, generated by N-ethyl-N-nitrosourea (ENU) mutagenesis that produces a point mutation in the gene for the enzyme tryptophanyl-tRNA synthetase (WARS).

The first project (*project 1*) examined *Sox3,* the causative gene associated with X-linked hypopituitarism (XH), in wild-type and transgenic mice. SOX3 is a member of the SOX (SRY-related HMG box) gene family of transcription factors that is expressed in progenitor cells of the mouse embryonic central nervous system (CNS) including the developing and postnatal hypothalamus (Rizzoti et al., 2004). It is the only member of the SOXB1 subfamily positioned on the X chromosome (Collignon et al., 1996; Stevanovic, 2003). Appropriate dose- and time-dependent expression of Sox3 in the developing hypothalamus is required for normal neuroendocrine function, particularly related to growth and growth hormone (GH). Changes associated with a loss-of-function and/or gain-of-function of *Sox3* may contribute to a better understanding of other important genes, currently not known, involved in XH and/or X-linked mental retardation. At this point, however, the mechanisms linking SOX3 to its direct targets and their interplay within other downstream signaling cascades regulating HP axis development remain unknown. In order to identify *Sox3*-dependent genes, in mice, I performed microarray analysis of RNA extracted from embryonic mouse heads at 10.5 days post coitum (dpc) and compared RNA from wild-type, loss-of-function (*Sox3*-null) and gain-of-function (Extra-Sox3) mice. Several emergent candidate genes were further tested by quantitative mRNA expression analysis (qPCR). One of these was Neurogenin-3 (Ngn3), which showed a 2.5-

fold decrease (P<0.001) in expression by microarray in *Sox3*-null (n=6), compared with wild-type (WT; n=6) mice and 1.8-fold decrease (P<0.001) by qPCR between *Sox3*-null (n=6) and WT (n=6) mice. To evaluate the relationship between Ngn3 and Sox3 at a cellular level immunohistochemistry was performed on 10.5 dpc and 12.5 dpc brains. In WT mice at 10.5 dpc and 12.5 dpc Ngn3 and Sox3 expression overlapped in a subset of cells across the ventral-midline of the developing hypothalamus. In addition and in contrast to WT mice, in *Sox3*-null mice, there were few Ngn3 positive cells, localized to the arcuate hypothalamic nucleus. Neurogenin-3 (Ngn3) is a member of the Neurogenin gene family of proneural basic helix-loop-helix proteins. Although previous data show the importance of Ngn3 during pancreatic development, there is no information on the mechanisms and actions of Ngn3 or a relationship between NGN3 action and SOX3 during hypothalamic development. These results suggest Ngn3 is a downstream target of *Sox3* that is contributing to appropriate development of the hypothalamic-pituitary axis.

The second study (*project 2*) aimed to characterize and further examine a novel recessive ENU mouse mutant, called Tukku[1], exhibiting HP axis dysfunction resulting in dwarfism, pituitary hypoplasia and GH deficiency. Adult Tukku mice are 30-40% smaller than their WT littermates. The primary focus was to characterize the dwarfism phenotype in relation to the somatotropic axis and to identify the causative gene. The mutation was identified as a leucine to proline substitution in tryptophanyl-tRNA synthetase (WARS), a member of the aminoacyl-tRNA synthetase (AARS) enzyme family that link amino acids to their specific tRNAs. For proper function of this enzyme the specific recognition of substrates is critical for the fidelity of protein synthesis. The *Wars* mutation is contained within the N-terminal WHEP domain, from residue 16-69, and likely causes the disruption of the alpha helical structure. The N-terminal WHEP domain has only been found in eukaryote Wars enzyme. Importantly, AARS have been linked to regulating the noncanonical activity of angiogenesis (Otani et al., 2002; Wakasugi, 2010; Wakasugi and Schimmel, 1999; Wakasugi et al., 2002b). Along with pituitary hypoplasia, Tukku mice show a significant reduction in pituitary GH and serum levels of IGF-1, suggesting the defect leading to pituitary hypoplasia involves brain regions implicated in growth of the anterior pituitary. The reduction in pituitary GH levels may also involve delivery of GH-releasing hormone (GHRH) to GH-secreting cells since preliminary data also indicate that WARS is expressed within blood vessels of the pituitary and hypothalamus. To assess this, quantitative mRNA expression analysis (qPCR) of GHRH and somatostatin (Sst) was

[1] *Tukku,* meaning 'small' in Kaurna Aboriginal language.

performed. qPCR revealed a decrease in both GHRH and Sst (fold change >2) indicating that the defect is likely to be within the hypothalamic hypophysial vasculature that extends and makes a connection with the pituitary. To evaluate the relationship between Wars and pituitary vasculature, immunohistochemistry was performed on pituitaries at 8-weeks postnatal. Pituitary sections were co-stained with antibodies against platelet endothelial cell adhesion molecule (PECAM) + Wars or vascular-endothelial cadherin (VE-Cadherin; an endothelial specific, transmembrane protein, which clusters at adheren junctions where it promotes homotypic cell-cell adhesion) + Wars. Wars immunostaining was expressed within the endothelial cells of the pituitary vasculature, both in the anterior and posterior pituitary. Both PECAM and Wars appeared co-expressed within the vascular wall. VE-Cadherin was expressed in vessels together with Wars.

Overall, the data gathered from these projects highlight important insights into the identification of *Ngn3* as a likely *Sox3* target gene (*project 1*) and have identified a novel dwarf mouse model with a genetic determinant of HP axis function (*project 2*). These results have application to the study of HP axis development, to the study of vascular development during embryology and postnatally, and to possible avenues of genetic screen testing and development of new treatments related to GH deficiencies.

STATEMENT OF CONTRIBUTION BY OTHERS TO THIS WORK

Ms Sandra Piltz contributed to routine technical assistance in the maintenance of mouse colonies as well as purification of genomic DNA and genotyping by PCR.

Mr Dale McAninch contributed to the validation of genes identified by microarray (Chapter 3. Identification of *Sox3* Target Genes, p.105). This work formed part of his honors thesis in 2008.

Dr Stuart Reed, Dr Chris Goodnow and the team from The Australian Phenomics Centre (Canberra, ACT, Australia) the dwarf mouse line generated and identified the mutated gene by sequencing used in Project 2 (Chapter 4. Novel Dwarf Mouse Generated by ENU Mutagenesis, p.151).

Ms Carlie Delaine, Ms Siti Hadzir and Dr Briony Forbes contributed to the analysis of pituitary growth hormone and serum IGF-1 levels (Figure 4-5, p.162).

Ms Nadia Gagliardi performed paraffin embedding of tissues, sectioning and histological staining of mouse ovaries and testis (Figure 4-17, p.188) and brains (using Cresyl violet stain; Figure 4-3, p.158).

Ms Chin Ng contributed to the analysis of the dwarf mouse line by generating murine Wars constructs for analysis of angiostatic activity in cell culture (Figure 4-14, p.181). Ms Chin Ng also performed western blotting of mouse brain, pituitary and kidney samples (Figure 4-12, p.178). This work formed part of her honors thesis in 2010 (Ng, 2010).

A/Prof Paul Thomas and Prof Jeffrey Schwartz provided critical reading and proofing of the thesis manuscript.

Eva Szarek was responsible for the remainder of the work.

DECLARATION OF ORIGINALITY

This work contains no material which has been accepted for the award of any other degree or diploma in any university or other tertiary instituition to Eva Szarek and, to the best of my knowledge and belief, contains no material previously published or written by another person, except where due reference has been made in the text.

I give consent to this copy of my thesis when deposited in the University Library, being made available for loan and photocopying, subject to the provisions of the *Copyright Act 1968*.

The author acknowledges that copyright of published works contained within this thesis (as listed below*) resides with the copyright holder(s) of those works.

I also give permission for the digital version of my thesis to be made available on the web, via the University's digital research repository, the Library catalogue and also through web search engines, unless permission has been granted by the University to restrict access for a period of time.

* **Szarek, E.,** Cheah, P. S., Schwartz, J., Thomas, P., 2010. Molecular genetics of the developing neuroendocrine hypothalamus. *Mol Cell Endocrinol*. 323**,** 115-23

_____

Eva Szarek, *B.Sc (Hons)*

ACKNOWLEDGEMENTS

There are many people that I would like to thank for making my Ph.D possible and for offering support along the way.

My sincerest gratitude goes to my advsors A/Prof Paul Thomas and Prof Jeffrey Schwartz for their guidance, encouragement and support. It has been an honor to work under your guidance and supervision. I am grateful to A/Prof Paul Thomas for his patience, persistence and wealth of knowledge in molecular biology; I have learned an enormous amount. I am grateful to Prof Jeffrey Schwartz for introducing me to and sharing with me his wealth of knowledge in the wonderful world that is the pituitary. Working with both of you has been an amazing experience, at the bench and over a few drinks. I would like to thank you both for giving me an amazing opportunity to pursue my Ph.D in the fascinating field of brain development and neuroendocrinology. Thank you for the discussion of ideas, for giving me the freedom to follow my intuition, for offering invaluable advice.

I would also like to thank all the members of the Thomas lab (past and present), for discussions, useful tips at the lab bench, and for being a fun group to work with.

To all my friends outside the lab, thank you for being so supportive and getting my mind off the Ph.D every now and then. I really appreciated it!

A very special thank you to my loving parents and family for believing in me and taking an interest in my project. Thank you for your encouragement, and ongoing support. A special thank you to my wonderful husband for putting up with my late nights and weekends in front of the computer and my less than seldom grumpy mood. I love you and… I can finally say… "koniec!"

ACRONYMS AND ABBREVIATIONS

3'UTR 3' untranslated region

ACTH Adrenocorticotropic hormone

ADH antidiuretic hormone (same as AVP)

AGRF Australian Genome Research Facility

AH anterior hypothalamus

ARC arcuate nucleus

AVP arginine vasopressin (same as ADH)

BAC Bacterial Artificial Chromosome

BCIP 5-Bromo-4-Chloro-3-Indolyl phosphate

BM basement membrane

BMP bone morphogenic protein

bp base pair

BSA bovine serum albumin

C-terminal carboxyterminal

cAMP cyclic adenosine mono phosphate

cDNA complimentary deoxyribonucleic acid

CH congenital hypopituitarism

ChIP chromatin immunoprecipitation

CNS Central nervous system

CoIP co-immunoprecipitation

DEPC diethylpyrocarbonate

DIG digoxigenin

DMEM Dubelcco's Modified Eagle Medium

DMN dorsal-medial nucleus

DMSO dimethylsulfoxide

DNA Deoxyribonucleic acid

dpc days post coitum

E Embryonic day

E. coli Escherichia coli

ECM extracellular matrix

EDTA ethylene diaminetetra acetic acid

EGF epidermal growth factor

eGFP enhanced green fluorescent protein

EGTA ethylenglycolbis-(2-aminoethyl)-tetraacetic acid

ENU N-ethyl-N-nitrosurea

FACS fluorescence activated cell sorting

FCS fetal calf serum

FSC forward scatter

FSH Follicle Stimulating Hormone

G1 First Generation

gDNA genomic DNA

GFP green fluorescent protein

GFP^{+} GFP-positive

GH Growth hormone

GHRH Growth-hormone-releasing hormone

GHRHR growth hormone-releasing hormone receptor

h hour

H_2O water

HEPES N-[2-hydroxyethyl]-piperazin-N'-[2-ethansulfonic acid]

HISS heat-inactivated horse serum

HMG high mobility group

HP hypothalamo-pituitary

IGF insulin-like growth factor

IGHD isolated growth hormone deficiency

IP immunoprecipitation

IPTG isopropylthiogalactosid

IRES internal ribosome entry site

kb kilobase pair = 1000bp

kDa Kilo Dalton

KO Knockout

LH Luteinizing hormone

M Molar

m mouse

MAPK mitogen-activated protein kinase

ME median eminence

min minute

ml millilitre

mM millimolar

MQ-H_2O milliQ *H_2O*

mRNA messenger ribonucleic acid

mRNA messenger RNA

NBT *4-nitroblue tetrazolium chloride*

N-terminal *aminoterminal*

ng *nanograms*

NGN/Ngn *neurogenin*

NGN3/Ngn3 *neurogenin-3*

nM *nanomolar*

ORF *Open reading frame*

OT *oxytocin*

P *postnatal day*

PAGE *polyacrylamide-gel electrophoresis*

PBS *Phosphate buffered saline*

PCR *Polymerase Chain Reaction*

PDGF *platelet-derived growth factor*

PFA *paraformaldehyde*

PI *propidium Iodide*

PKA *protein kinase A*

PKC *protein kinase C*

POA *preoptic area;*

POMC *Pro-opiomelanocortin*

PVN *paraventricular nucleus;*

qPCR *quantitative real-time polymerase chain reaction*

qRT-PCR *quantitative real-time polymerase chain reaction*

r *rat*

RE *restriction emzyme*

RIN *RNA integrity number*

RNA *ribonucleic acid*

rpm *revolutions per minute*

rRNA *ribosomal RNA*

RT *reverse transcription*

rt *room temperature*

RT-PCR *reverse transcriptase-polymerase chain reaction*

SCN *supra-chiasmatic nucleus;*

SDS *sodium dodecyl sulfate*

SHH *sonic hedgehog*

SOCM *Sox consensus motif*

SON *supra-optic nucleus;*

SOX *Sry-related HMG box containing*

SSC *Salt Sodium Citrate*

Sst *somatostatin*

TE *Tris-EDTA*

tg *transgenic*

TGFβ *transforming growth factor-beta*

TRH *Thyrotropin-releasing hormone*

TRIS *Tris-(hydroxymethyl)-aminomethan*

TrpRS *tryptophan-tRNA synthetase (see also WARS)*

TSH *Thyroid-stimulating hormone*

U *units*

UTR *untranslated region*

VEGF *vascular endothelial growth factor*

VMN *Ventro-medial nucleus;*

WARS *see also TrpRS*

WT *wild-type*

XH *X-linked hypopituitarism*

zf *zebrafish*

µg *microgram*

µM *micromolar*

PUBLICATIONS

First author publications arising from the work presented within this thesis. A copy of this publication can be found in the Publications section of this thesis.

Szarek, E., Cheah, P. S., Schwartz, J., Thomas, P., 2010. Molecular genetics of the developing neuroendocrine hypothalamus. Mol Cell Endocrinol. 323**,** 115-23.

CONFERENCE PRECEEDINGS

The results described in this thesis have been presented as seminar communications at the following conferences:

Szarek, E., Read, S., Forbes, B., Delaine, C., Schwartz, J., Thomas, P. A novel ENU mutation, WARS, causes dwarfism in mice. *Gold Coast Health and Medical Research Conference,* Gold Coast, Queensland, Australia. December 2nd-3rd 2010

Szarek, E., Read, S., Forbes, B., Delaine, C., Schwartz, J., Thomas, P. A Novel ENU mutation, WARS, causes dwarfism in mice. *Program in Developmental Endocrinology and Genetics (PDEGEN) Research Conference*, National Institutes of Health, Bethesda, MD, USA. July 9th 2010.

Szarek, E., Read, S., Forbes, B., Schwartz, J., Thomas, P. Identification of the sequence responsible for and further phenotypic characterization of a novel dwarf mouse produced by ENU-induced mutagenesis. *Gold Coast Health and Medical Research Conference*, Gold Coast, Queensland, Australia. December 3rd – 4th 2009.

Szarek, E., Lovell-Badge, R., Schwartz, J., Thomas, P.Q. Expression of NGN3 in the developing hypothalamus: dependence on and co-localization with SOX3 in the mouse model of altered pituitary function. *ENDO2009*, Washington DC, USA. June 10th – 13th 2009.

1 Introduction

I. Molecular Genetics of the Hypothalamic-Pituitary Axis

The developmental programs that guide the formation of the mammalian endocrine and neuroendocrine organs involve complex regulatory networks, resulting in highly specialized cells capable of secreting a diverse set of peptide hormones. Cell-specific peptide hormone expression has proven to be an essential molecular tool in delineating temporal as well as spatial gene regulatory pathways that govern the development of the hypothalamic-pituitary (HP) axis.

This chapter focuses on providing an introduction to the molecular regulation of mammalian pituitary and hypothalamic development and function. Specifically, focusing on the importance of the transcription factors Sox3 during HP axis development, hypothalamic control of growth hormone secretion and angiogenesis. It is important to note that, although the development of the hypothalamus and pituitary is a highly interdependent process, the pituitary develops *in tandem* with the specific hypothalamic nuclei that ultimately regulate homeostatic responses in the mature organism.

A. Vertebrate Hypothalamic Development

The following sections provide a brief overview of the structure, function and the development of the hypothalamus and formed the introduction of a published review

article (Szarek et al., 2010); a copy of the review article may be found in the Publications section of this thesis.

1. Structure and function of the hypothalamus

The vertebrate hypothalamus is located ventral to the thalamus and dorsal to the pituitary gland at the mediobasal region of the central nervous system (CNS). It extends from the optic chiasm (located anteriorly) to the mammillary body (located posteriorly) and is organized into four distinct rostral-to-caudal regions: preoptic, anterior, tuberal, and mammillary. It is also divided into three medial-to-lateral areas: periventricular, medial and lateral. The periventricular hypothalamus contains four distinct cell clusters: the paraventricular nucleus (PVN), arcuate nucleus (ARC), suprachiasmatic nucleus (SCN), and the periventricular nucleus (PeVN; Figure 1-1, p.25). The medial hypothalamic zone is comprised of the medial preoptic nucleus, the anterior hypothalamus (AH), the dorsomedial nucleus, the ventromedial nucleus (VMN) and the mammillary nuclei. The lateral hypothalamus consists of the preoptic area (POA) and hypothalamic area. Throughout the hypothalamus are hypothalamic neurosecretory cells divided into two populations: the parvicellular and magnocellular neurosecretory systems. The former consists of neurons controlling the release of specific anterior pituitary neurohormones into the hypophysial system: thyrotropin-releasing hormone (TRH; located within the medial part of the medial parvicellular subdivision of the PVN), corticotropin-releasing hormone (CRH; located within the lateral part of the medial parvicellular subdivision of the PVN), growth hormone-releasing hormone (GHRH; located within the lateral part of the ARC), somatostatin (Sst; located within the PeVN), gonadotropin-releasing hormone (GnRH; located within the medial POA), dopamine (DA; located within the medial part of the ARC and detected by the enzymatic activity of tyrosine hydroxylase (TH)) and, the recently discovered gonadotropin-inhibiting hormone (GnIH; located within the dorsomedial nuclei in rodents; Figure 1-1, p.25). The magnocellular neurosecretory system consists of neuronal cells secreting the hormones, vasopressin (AVP) and oxytocin (OT) from axons that project directly into the posterior pituitary (neurohypophysis) and release the peptides systemically in response to various homeostatic cues (osmotic, cardiovascular and reproductive). For in-depth information and discussion on the magnocellular neurosecretory system please refer to (Caqueret et al., 2006).

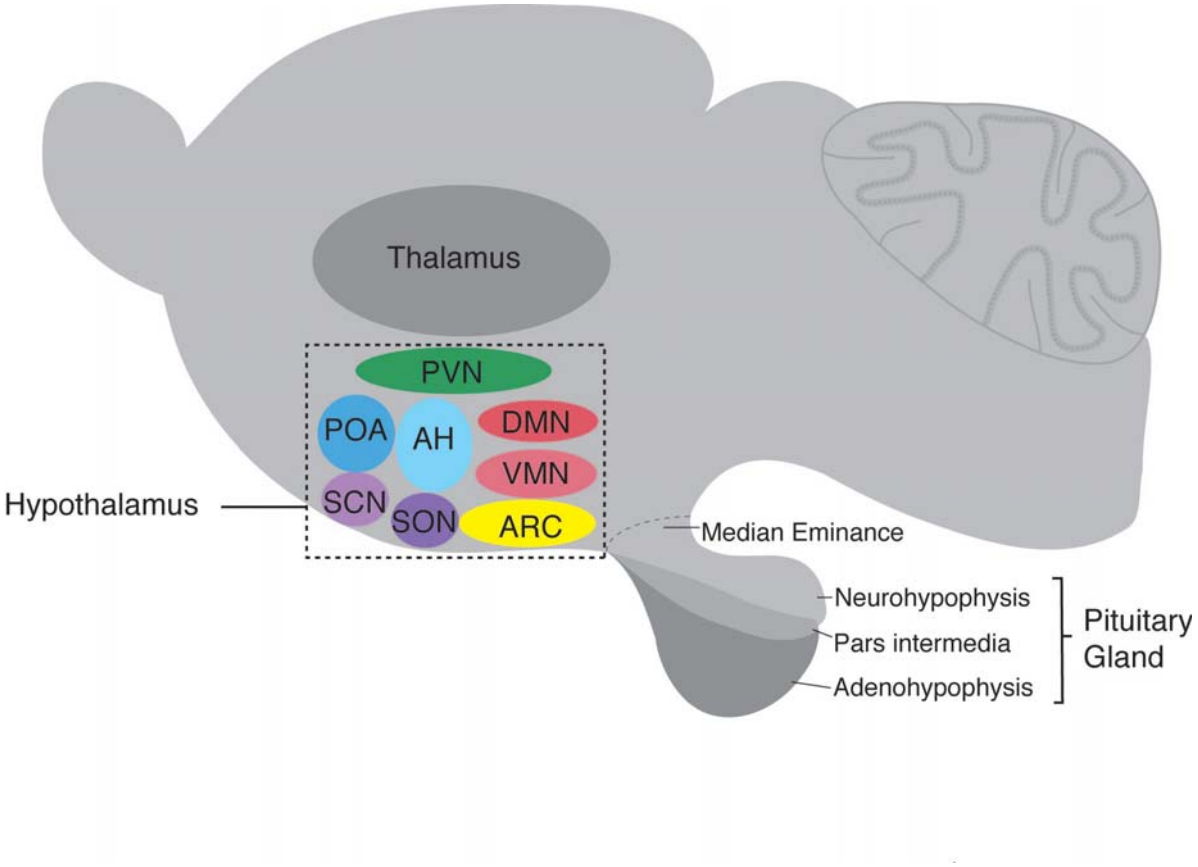

Figure 1-1 Illustration of the organization of the hypothalamic nuclei in the mouse brain
Lateral view of the organization of the hypothalamic nuclei. The hypothalamus is organized into distinct zones containing tight clusters of cell bodies. B. Representation of the neuroendocrine hypophysiotropic factors and their neuronal projections through the median eminence (ME) and into the adenohypophysis (anterior pituitary). PVN: paraventricular nucleus; POA: preoptic area; AH: anterior hypothalamus; SCN: supra-chiasmatic nucleus; SON: supra-optic nucleus; DMN: dorsal-medial nucleus; VMN: Ventro-medial nucleus; ARC: arcuate nucleus. Figure adapted from and appears in (Szarek et al., 2010).

2. *Development of the hypothalamus*

The hypothalamus develops from the ventral region of the diencephalon (Figdor and Stern, 1993) and, in the mouse, its primordium is morphologically evident from approximately 9.5 days post coitum (dpc; where 0.5 dpc is defined as noon of the day on which a copulation plug is present). Developmental studies performed in mice, chick and zebrafish indicate that sonic hedgehog (SHH) signaling plays an important role in the induction and early patterning of the hypothalamus (Manning et al., 2006; Mathieu et al., 2002; Szabo et al., 2009). Secretion of SHH from the murine axial mesendoderm, from 7.5 dpc, is essential for correct patterning of the anterior midline neuroaxis. In humans as well as in mice, mutations in the SHH/Shh gene (and several other components of this pathway) exhibit holoprosencephaly due to a failure of hypothalamic anlagen induction and optic field separation (Chiang et al., 1996; Schell-Apacik et al., 2003). Increased SHH activity leads to ectopic expression of hypothalamic markers in zebrafish, suggesting that SHH signaling has an instructive, rather than a permissive, role in shaping the

hypothalamus (Barth and Wilson, 1995; Hauptmann and Gerster, 1996; Rohr et al., 2001). Studies in chick embryos have shown that once the hypothalamic primordium is established, down-regulation of Shh is critical for the progression of ventral cells into proliferating hypothalamic progenitors, at least within the ventral tubero-mammillary (Manning et al., 2006). In addition, Shh down-regulation is mediated, to some extent, by local production of Bone Morphogenetic Proteins (BMPs), which belong to the transforming growth factor-beta (TGFβ) super-family of signaling proteins (Manning et al., 2006). This antagonism between SHH (ventral gradient morphogen) and BMP (dorsal gradient morphogen) in the hypothalamus is reminiscent of their opposing actions in dorsal-ventral patterning of the neural tube. However, this incorporates a temporal aspect (SHH early - BMP late) that appears necessary for establishing region-specific transcriptional profiles (Ohyama et al., 2008; Patten and Placzek, 2002). Although axial secretion of another member of the TGFβ super-family, NODAL, is also necessary for hypothalamic induction, the early lethality of Nodal mutants has precluded detailed assessment of its role in hypothalamic development in mice (Brennan et al., 2001; Conlon et al., 1994; Varlet et al., 1997). Genetic studies in zebrafish have shown that the Wnt signaling pathway is required for specification of the hypothalamic anlagen, its regionalization and neurogenesis (Kapsimali et al., 2004; Lee et al., 2006). Together, these studies have shown that hypothalamic induction and pattern formation depends on the activities of major protein signaling pathways involved in patterning, regional identity and cell fate determination.

For an in-depth and comprehensive review of the development of the hypothalamus and the important signaling and transcription factors please refer to the review located in the Publications section of this thesis (Szarek et al., 2010).

B. Vertebrate Pituitary Development

The pituitary gland (or hypophysis) is a central endocrine organ that regulates basic physiological functions, including growth, stress response, reproduction, metabolic homeostasis, and lactation. Distinct hormone-producing cells located within the anterior pituitary (or adenohypophysis) arise by extrinsic and intrinsic mechanisms from a common ectodermal primordium during development. Pituitary gland development has been studied extensively in the mouse. Although relatively little is known about human pituitary development, it seems that it mirrors that in rodents (Sheng et al., 1997). The purpose of this section is to provide an introduction to the integrated signaling and transcriptional events that affect precursor proliferation, cell lineage commitment, terminal differentiation and physiological regulation by hypothalamic tropic and pituitary factors.

1. Structure and function of the pituitary

The pituitary gland, located beneath the hypothalamus in the sella turcica, is composed of two anatomically and functionally distinct entities: (1) the adenohypophysis, derived from the oral ectoderm, and consists of the anterior lobe (or pars distalis), the intermediate lobe (or pars intermedia), and the pars tuberalis, a structure associated with the pituitary stalk; and (2) the neurohypophysis (or posterior lobe), of neural origin and is embryologically and anatomically continuous with the hypothalamus, consists of the posterior lobe (or pars nervosa) (Figure 1-2 A, p.28). As the primary site of endocrine action, the anterior pituitary contains at least five distinct cell types characterized by the six different hormones produced and secreted (Figure 1-2 B, p.28). Corticotropes, secrete adrenocorticotropic hormone (ACTH), a proteolytic product of pro-opiomelanocortin (POMC), which regulates metabolic function and the stress response through stimulation of glucocorticoid synthesis by inducing adrenal gland growth and activity. Thyrotropes, secrete thyroid-stimulating hormone (TSH) which regulate metabolism. Somatotropes, secrete growth hormone (GH) which regulate growth. Lactotropes, secrete prolactin (PRL) which regulate lactation. Gonadotropes secrete luteinizing hormone (LH) and follicle-stimulating hormone (FSH) which regulate sexual development and function. Intermediate lobe melanotropes, release α-melanocyte-stimulating hormone (αMSH), a product of the POMC gene. The adult human pituitary cell population, as determined by immunohistochemical techniques, consists of 50% of somatotropes, 10–25% lactotropes, 15–20% corticotropes, 10–15% gonadotropes, and 3–5% thyrotropes (Table 1-1, p.30) (Nussey and Whitehead, 2001). The anterior and intermediate lobes of the pituitary also contain non-hormone-secreting glial-like folliculostellate cells that act as functional units of a dynamically active cell network wiring the entire pituitary gland (Fauquier et al., 2002). In humans, the intermediate lobe is rudimentary and greatly reduced in structure and function. Both GH and PRL are composed of a single polypeptide, whereas TSH, LH and FSH are heterodimeric glycoprotein hormones, composed of a common α-subunit (αGSU) and distinct hormone-specific β-subunit (TSHβ, LHβ, FSHβ) that confers specificity and bioactivity. The production and secretion of these respective hormones is under the control of hypothalamic stimuli. A vascular link, consisting of long portal vessels, allows for efficient transport of hypothalamic neurosecretory hormones from the median eminence (located at the base of the hypothalamus) to the anterior/intermediate pituitary gland. In contrast, the posterior lobe *does not* contain endocrine cells, but axons of the magnocellular neurons, from the hypothalamus project directly here and approximately 100,000 axons form the hypophysial nerve tract (Nussey and Whitehead, 2001). These axons *release* (in response to electrical excitation) two major peptide hormones, AVP and OT. AVP and OT

regulate blood volume homeostasis and reproductive function, respectively. Surrounding the nerve terminals are modified astrocyte cells known as pituicytes, that appear to have an important role in the local control of hormone release (Nussey and Whitehead, 2001).

Figure 1-2 Schematic representation of the structure of the pituitary

(A) The normal pituitary is bean-shaped and has multiple components. (1) The neurohypophysis (posterior lobe) is an extension of the hypothalamus that descends into the sella turcica (saddle-shaped depression in the sphenoid bone at the base of the skull). Nerve terminals located here secrete hormones that are produced in the cell bodies of hypothalamic ganglion cells of the infundibulum and are supported by pituicytes (glial cells). (2) The adenohypophysis (anterior pituitary), derived from the oral ectoderm and ascends as Rathke's pouch during development, is composed of hormone-secreting epithelial cells, known as adenohypophysial cells. These cells lose contact with the oral ectoderm where the bone of the sella forms; this region is known as the anterior lobe (*pars distalis*). (3) The intermediate lobe (*pars intermedia*) is composed of epithelial cells from the posterior limb of Rathke's pouch and is well developed in most mammals, but only rudimentary in humans. The cell population here is melanotropes. (4) The *pars tuberalis*, a small rim of the adenohypophysis around the pituitary stalk, contains mostly gonadotropes. (B) The adenohypophysis is composed of six cell types each making hormones supported in acini by folliculostellate cells. Corticotropes (blue) make adrenocorticotropin (also known as adrenal corticotropic hormone (ACTH)), which stimulates the production of glucocorticoid by the adrenal cortex of the adrenal gland (located on top of the kidney). Somatotropes (orange) synthesize growth hormone (GH), which regulates bone and muscle growth and helps maintain lean body mass in adults. Lactotropes (red) produce prolactin (PRL), which acts to inhibit gonadal function and stimulates the production of breast milk during and after pregnancy. Mammosomatotrope (not shown), bihormonal cells that synthesize GH and PRL, represent a fluid cell population that differentiates into somatotropes and into lactotropes during growth phases and pregnancy, respectively. Thyrotropes (yellow) synthesize thyrotropin (or thyroid-stimulating hormone (TSH)), which stimulates production of thyroid hormone from the thyroid gland. Gonadotropes (light pink) produce follicle-stimulating hormone (FSH) and luteinizing hormone (LH), which regulate germ-cell development and sex steroid hormone production in the gonads (ovary in the female; testis in the male).

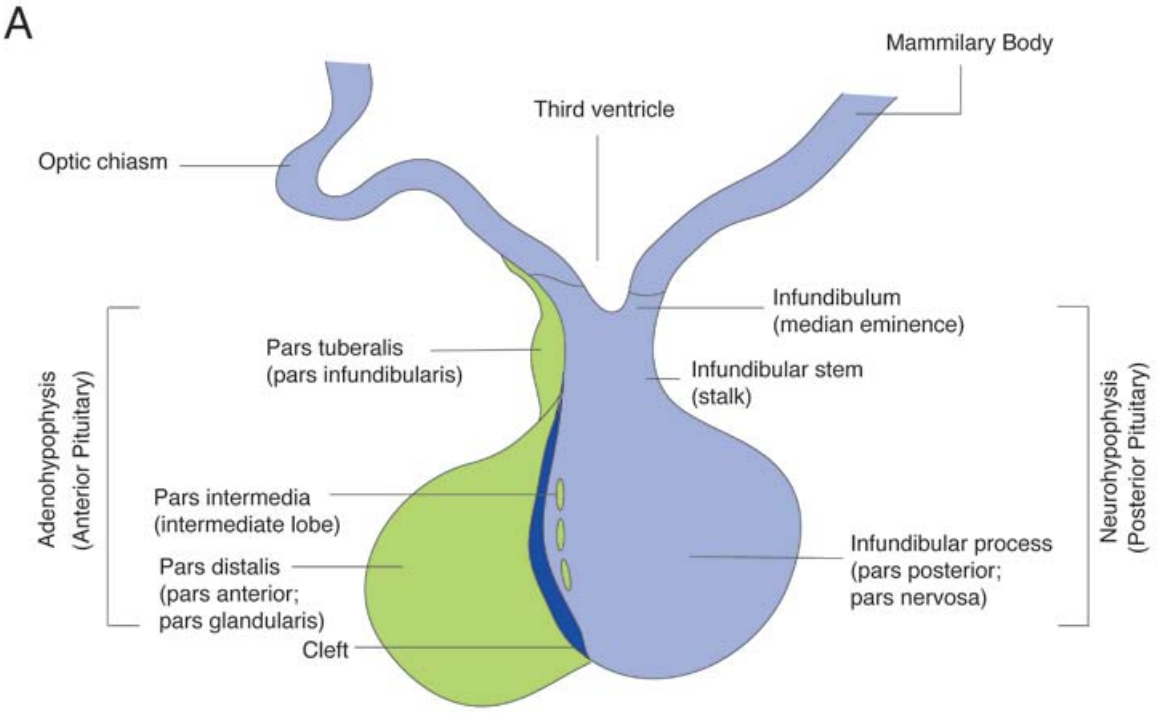
A
Mammilary Body
Third ventricle
Optic chiasm
Infundibulum
(median eminence)
Pars tuberalis
(pars infundibularis)
Infundibular stem
(stalk)
Adenohypophysis
(Anterior Pituitary)
Neurohypophysis
(Posterior Pituitary)
Pars intermedia
(intermediate lobe)
Infundibular process
(pars posterior;
pars nervosa)
Pars distalis
(pars anterior;
pars glandularis)
Cleft

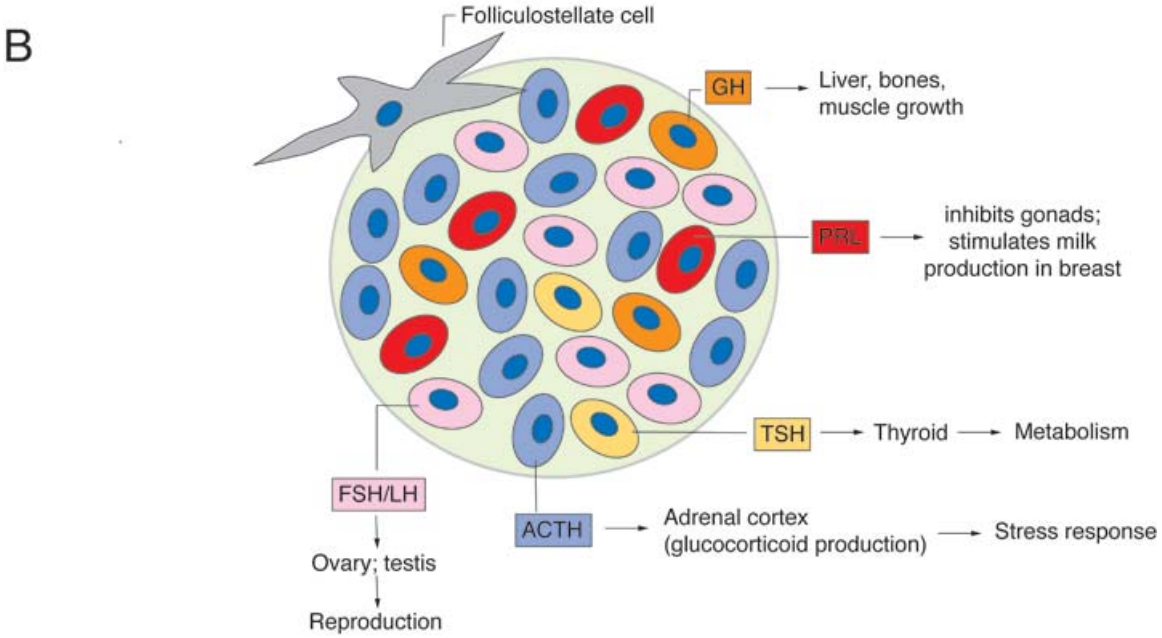
B
Folliculostellate cell
GH
Liver, bones,
muscle growth
PRL
inhibits gonads;
stimulates milk
production in breast
TSH
Thyroid
Metabolism
FSH/LH
ACTH
Adrenal cortex
(glucocorticoid production)
Stress response
Ovary; testis
Reproduction

Table 1-1 Hormone secretions of the anterior lobe of the pituitary gland and their control
TSH, thyroid stimulating hormone; ACTH, adrenocorticotropin hormone; LH, luteinizing hormone; FSH, follicle stimulating hormone; GH, growth hormone. [1]Basophils - stain with basic dyes; [2]Acidophils - stain with acidic dyes; (+), stimulatory; (-), inhibitory. Adapted from (Nussey and Whitehead, 2001)

Pituitary Cell type	Hormone	% Pituitary cell population	Hypothalamic hormone	Predominant hypothalamic nucleus of synthesis
Thyrotrope[1]	TSH	3–5%	TRH (+) Somatostatin (-)	Paraventricular, anterior periventricular
Corticotrope[1]	ACTH	15–20%	CRH (+)	Paraventricular, supraoptic
Gonadotrope[1]	LH FSH	10–15%	GnRH (+)	Arcuate
Somatotrope[2]	GH	40–50%	GHRH (+) Somatostatin (-)	Arcuate, anterior periventricular
Lactotrope[2]	Prolactin	10–25%	Dopamine (-) TRH (+)	Arcuate, paraventricular, unknown

2. *Development of the pituitary*

The development of the pituitary gland, a composite organ of dual origin in vertebrates, is a complex process involving the coordinated spatial and temporal expression of transcription factors and signaling molecules. Given the fact that all distinct hormone-producing pituitary cells arise from a common ectodermal primordium, the patterning, architecture and plasticity is remarkable. During organogenesis the anterior/intermediate and posterior lobes have distinct embryologic origins. However, in the mature organ these structures are fused together despite performing different functions independently of each other. The posterior lobe, of neuroectoderm origin, originates from the base of the diencephalon as an extension of the infundibulum (Figure 1-3, p.32) (Kaufman, 1992). The anterior and intermediate lobes arise from an invagination of the roof of the primitive oral cavity known as Rathke's pouch (Kaufman, 1992). In humans, Rathke's pouch is observed as a distinct structure by the fourth week of gestation (approximately embryonic day (E) 9 and E11 in mouse and rat development, respectively) (Dubois et al., 1997; Dubois and Elamraoui, 1995; Ikeda et al., 1988). Through intense differentiation and proliferation (refer to Section 1I.B.3 Early patterning of the pituitary, p.31), Rathke's pouch gives rise to the anterior pituitary and the five phenotypically distinct pituitary cells (Asa et al., 1988). Experiments examining the fate mapping of the origin of the anterior pituitary cells in mice have demonstrated that the hypophysial or pituitary placode, one of the six cranial placodes that develops transiently as localized ectodermal thickenings in the prospective head of the developing embryo, appears at 8.0 dpc. The pituitary placode is located ventrally in the midline of the anterior neural ridge

and is continuous with the future hypothalamo-infundibular region, located posteriorly in the rostral region of the neural plate. By 8.5 dpc the neural tube has curved at the cephalic end and the placode appears as a thickening of the roof of the primitive oral cavity. From 9.0 dpc the placode invaginates dorsally to form a rudimentary Rathke's pouch, from which the anterior and intermediate lobes of the pituitary are derived. Development of Rathke's pouch begins with the formation of the 'rudimentary' pouch (Figure 1-3 A and B, p.32). The rudimentary pouch moves in the caudal direction where it becomes encased by proliferating mesodermal tissue, thus providing a clear separation of the 'definitive' pouch from the oral membrane (Figure 1-3 C). The definitive pouch pinches off from the stomodeum at 10.5 dpc. In humans this occurs at seven weeks gestation whereby at 13 weeks gestation the pituitary is morphologically distinct (Ikeda et al., 1988). The evagination of the neural ectoderm at the base of the developing diencephalon will give rise to the posterior pituitary. The dorsal side of Rathke's pouch becomes the intermediate lobe, whereas the anterior lobe results from the proliferation and differentiation of cells located on the ventral side (Figure 1-3 D). Between 10.5-12.0 dpc the pouch epithelium continues to proliferate as it closes and separates from the underlying oral ectoderm at 12.5 dpc. Subsequently, the progenitors of the hormone-secreting cell types proliferate ventrally from the pouch between 12.5-15.5 dpc to populate what will form the anterior pituitary lobe. The remnants of the dorsal portion of the pouch will form the intermediate lobe, whilst the lumen of the pouch remains as the pituitary cleft, separating the intermediate from the anterior lobe (Rizzoti and Lovell-Badge, 2005; Scully and Rosenfeld, 2002). Within the developing anterior pituitary, gonadotropes form in the ventral region, thyrotropes within the central region, whereas somatotropes and lactotropes, both derived from a common precursor, are found populating the dorsal region (Dasen and Rosenfeld, 1999; Kioussi et al., 1999). Corticotropes, located on the dorsal anterior lobe side, are also found loosely scattered within the anterior lobe rostral tip (Dasen et al., 1999; Kioussi et al., 1999). In mice, an early and transient thyrotrope population is located in the rostral region of the developing anterior lobe (Lin et al., 1994). The order in which differentiating anterior pituitary cell types arise during pituitary organogenesis is similar in most mammals (Dasen and Rosenfeld, 2001; Lin et al., 1994; Rhodes et al., 1994).

3. *Early patterning of the pituitary*

A brief summary of the signaling molecules and transcription factors implicated in mammalian pituitary development and their interactions in orchestrating the differentiation of Rathke's pouch into various cell types of the anterior and intermediate pituitary lobes follows. The ontogeny of signaling molecules and selected transcriptional

factors during mouse pituitary organogenesis are shown in Figure 1-4 (p.35). The signaling pathways and transcription factors critical for pituitary and hypothalamic development and function are listed in Table 1-2 (p.36). For an extensive review on the early steps in pituitary development please refer to the excellent review by Sheng and Westphal (Sheng and Westphal, 1999) and Zhu et al (Zhu et al., 2007b).

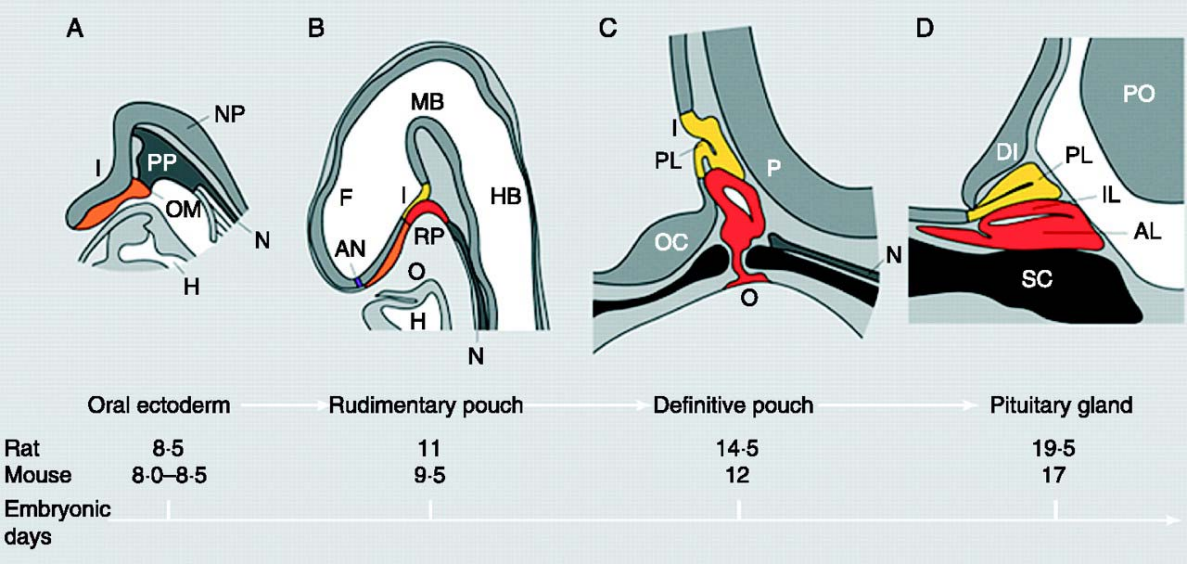

Figure 1-3 Schematic representation of the stages of pituitary development in rat and mice
Midsagittal or parasagittal section drawings of the rat embryos illustrating pituitary development. The corresponding stages in mouse and rat development are indicated. (A) The growth of the preinfundibular portion of the neural plate and the establishment of the presumptive Rathke's pouch area. (B) The formation of a rudimentary pouch. Note the absence of mesoderm between the pouch and the floor of the diencephalon. (C) The formation of a definitive pouch and the posterior lobe. Note the invasion of neural crest and mesenchymal tissue, and the separation of the brain and oral cavities. (D) A nascent pituitary gland. Abbreviations: I, infundibulum; NP, neural plate; N, notochord; PP, pituitary placode; OM, oral membrane; H, heart; F, forebrain; MB, midbrain; HB, hindbrain; RP, Rathke's pouch; AN, anterior neural pore; O, oral cavity; PL, posterior lobe; OC, optic chiasm; P, pontine flexure; PO, pons; IL, intermediate lobe; AL, anterior lobe; DI, diencephalon; SC, sphenoid cartilage. Adapted from (Schwind, 1928; Sheng and Westphal, 1999).

a. Signaling molecules

The patterning of the anterior pituitary primordium is directed by complex signals emanating both from the ventral diencephalon/infundibulum and from Rathke's pouch. The essential signals for Rathke's pouch development and for the timely and spatially organized process of pituitary cell type appearance are the same factors involved in patterning many other organs, namely, members of the growth factor/morphogens including Shh, FGF, BMP, Notch, and the Wnt families (Dasen and Rosenfeld, 1999). The role of epidermal growth factor (EGF) signaling in pituitary development, while important in somatotrope and lactotrope cell lineage development, is much less documented (Zhu et al., 2007b). Although the expression of the various signaling molecules varies, the essential

signaling molecules are expressed within the infundibulum, whereas others are located in the mesenchyme surrounding the pituitary, such as *Tgfbi* (or Transforming growth factor, beta-induced) which stimulates vascular endothelial growth factor (VEGF) production by folliculostellate pituitary cells (Renner et al., 2002) and some in the pouch itself (Brinkmeier et al., 2009). Thus, the regulation of pituitary development by signaling molecules is complex.

The maintenance of a balance of signaling pathways is necessary for normal pituitary growth and morphology. The most critical signaling molecules for pituitary development are NOGGIN (Davis and Camper, 2007), which is an antagonist of BMP signaling, transcription factor 7-like 2 (TCF7L2; T-cell specific, HMG-box) (Brinkmeier et al., 2003), a protein acting as a transcription factor that influences canonical[2] WNT signaling; and WNT5A, typically acting in the non-canonical pathway (Cha et al., 2004; Potok et al., 2008). Mutations in any of these signaling molecules can alter the development of Rathke's pouch and subsequently affect downstream signals involved in pituitary development. For example, an excess of BMP signaling in *noggin* mutant mice is associated with a reduction in the expression of fibroblast growth factor-10 (*Fgf10*), alteration in the SHH signaling domain, and results in Rathke's pouch containing multiple invaginations (Davis and Camper, 2007). Mice deficient in the *Tcf7l2* exhibit expansion of the *Fgf10* and *Bmp* signaling domains, and exhibit an abnormally large Rathke's pouch and oversized anterior lobe (Brinkmeier et al., 2007). Additionally, mice deficient in *Wnt5a* show expanded *Fgf* and *Bmp* signaling domains, with a dysmorphic Rathke's pouch but not markedly oversized (Potok et al., 2008). These examples highlight the disruption that can occur to one signaling pathway and signify the pleiotropic effects on other signaling pathways. This is a common theme of pituitary development.

Signaling molecules play an important role in the influence of spatial patterns of pituitary transcription factor expression, which subsequently leads to the emergence of the specialized hormone-producing pituitary cells. There is compelling evidence suggesting that alterations in signaling pathways affects the morphology and size of the organ more so than cell specification (Brinkmeier et al., 2007; Cha et al., 2004; Davis and Camper, 2007). For example, mouse mutants of *noggin, Wnt5a,* and *Tcf7l2* are each able to generate the 5 major hormone-producing cells of the anterior lobe despite variations in size and shape of the organ. The effects of various genetic lesions on pituitary growth and shape has been reviewed by (Rizzoti and Lovell-Badge, 2005).

2 In general the term canonical conform to orthodox or recognized rules whereas non-canonical does not behave according to the rules.

The development of the hypothalamus and pituitary is a highly independent process. However, signaling events between them generate transcriptional cascades that provide distinct hormone-secreting profiles of differentiated pituitary cell types.

b. Transcription factors

Numerous transcription factors play important roles during pituitary development and hormone production. Early-acting genes are not pituitary specific, and mutations in these genes cause defects in craniofacial development or other structures. For example, some of the homeobox genes have overlapping functions and multiple roles during ontogeny and include *Pitx1* and *Pitx2, Lhx3* and *Lhx4* (Charles et al., 2005; Ellsworth et al., 2008; Gage et al., 1999; Sheng et al., 1997). Mutations in some of these genes result in apoptosis and/or reduced cell proliferation, ultimately resulting in pituitary hypoplasia (Charles et al., 2008; Charles et al., 2005; Suh et al., 2002). Furthermore, genes downstream of some of the above-mentioned genes, such as *Nr5a1, Pitx2,* and *Gata2 (*all downstream of *Pitx2)* are able to result in tissue-specific disruption in mice (Zhao et al., 2001a, b). Specifically, GATA2, which is expressed in the pituitary during development and in adult gonadotropes and thyrotropes, plays an important role during gonadotrope and thyrotrope cell fate and TSH production (Charles et al., 2006). Mice with a pituitary-specific knockout of *Gata2* have reduced secretion of gonadotropins basally and compromised thyrotrope function (Charles et al., 2006).

Homeodomain transcription factors are another important class that play critical roles during pituitary development. Specifically, *Prophet of Pit1 (*or *Prop1)* and *Pou1f1* (also known as *Pit1*) are examples. *Prop1* is important for thyrotrope, somatotrope, lactotrope and gonadotrope development. Whereas, *Pou1f1* is required for thyrotrope, somatotrope, and lactotrope development. Mutations in the human ortholog of *Prop1* are the most common known causes of multiple pituitary hormone deficiency in humans (Cogan et al., 1998; Kelberman and Dattani, 2009; Mody et al., 2002; Wu et al., 1998). In mice, mutations of *Prop1* and *Pou1f1* show dramatic differences on fetal and neonatal pituitary development. *Prop1* mutants have poor pituitary vascularization and dysmorphology likely resulting, in part, from the failure of progenitors to migrate away from the proliferative zone and undergo differentiation (Ward et al., 2005). *Prop1* is required for normal N-Cadherin (*Cdh2*) expression, and changes in expression have been typically associated with epithelial to mesenchymal transition. Thus, the defect seen in *Prop1* mutants may result from failure to undergo epithelial to mesenchymal transition (Kikuchi et al., 2006; Kikuchi et al., 2007). On the contrary, mutations in mouse *Pou1f1* do not reveal

any obvious defects in pituitary vascularization or morphology, although the gland in hypoplastic.

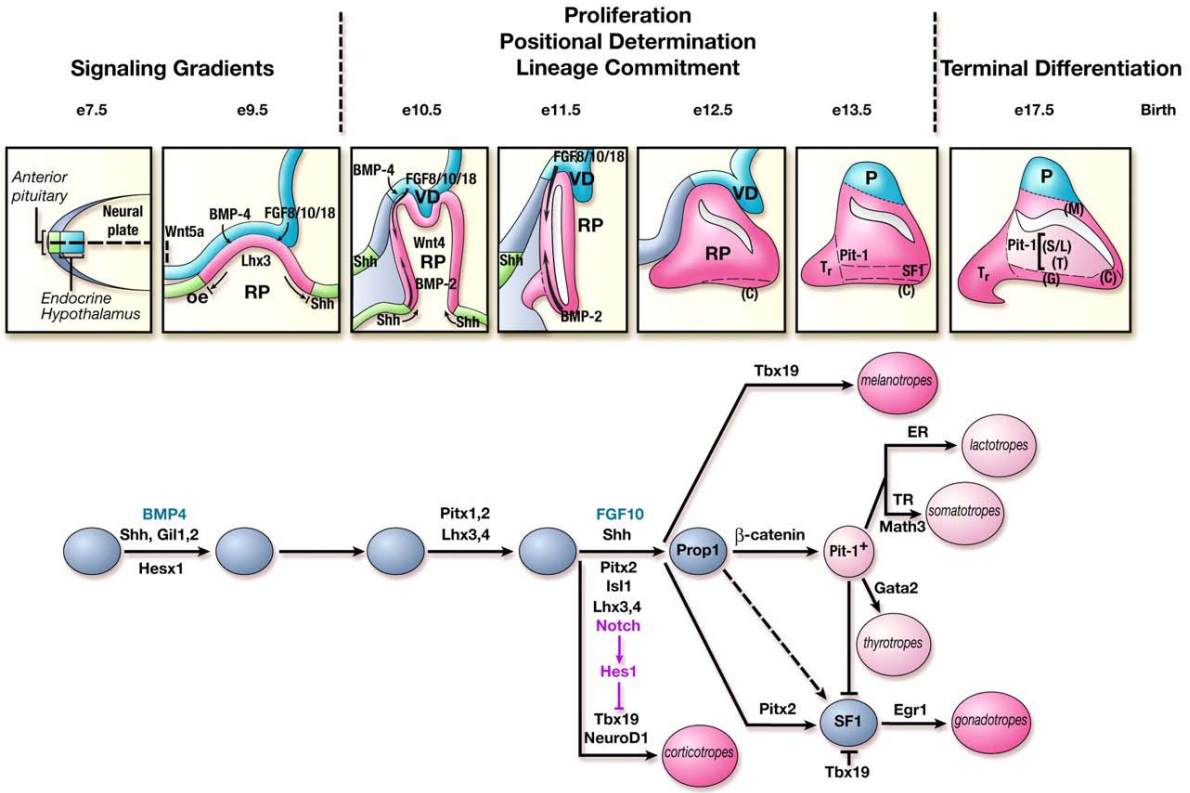

Figure 1-4 Ontogeny of signaling molecules and selected transcriptional factors during mouse pituitary organogenesis

The most anterior neural ridge gives rise to primordium of the anterior and intermediate lobes of the pituitary. The adjacent neural plate develops into endocrine hypothalamus and the posterior lobe of the pituitary gland. Ventral diencephalon, which expresses BMP4, FGF8/10/18, and Wnt5, makes direct contact with oral ectoderm and induces the formation of Rathke's pouch. Shh is expressed throughout the oral ectoderm except in the Rathke's pouch, creating a boundary between two ectodermal domains of Shh-expressing and -non-expressing cells. The opposing dorsal BMP4/FGF and ventral BMP2/Shh gradients convey proliferative and positional cues by regulating combinatorial patterns of transcription factor gene expression. *Pit1* is induced at e13.5 in the caudomedial region of the pituitary gland, which ultimately gives rise to somatotropes (S), lactotropes (L), and thyrotropes (T). Rostral tip thyrotropes (Tr) are Pit1 independent. Corticotropes (C) and gonadotropes (G) are differentiated in the most ventral part of the gland. The dorsal region of the Rathke's pouch becomes the intermediate lobe, containing melanotropes (M). The infundibulum grows downward and eventually becomes the posterior lobe (P). A number of transcription factors and cofactors regulating the lineage commitment and terminal differentiation of distinct cell types are illustrated in a genetic pathway. Adapted from (Scully and Rosenfeld, 2002; Zhu et al., 2007a).

Table 1-2 Signal pathways and transcription factors critical for pituitary and hypothalamic development and function

Hyp, hypothalamus; VD, ventral diencephalon; RP, Rathke's pouch; Tg, transgenic; KO, knockout; DKO, double knockout. Adapted from (Zhu et al., 2007a). For references to the individual genes please refer to (Zhu et al., 2007a).

C. The Hypothalamo-Pituitary Axis

1. *Anatomical and functional connections*

The pituitary gland (composed of the anterior and posterior lobes) is positioned below the brain in a midline pocket, or fossa, of the sphenoid bone, known as the sella turcica (Figure 1-5, p.39). The pituitary, whilst located outside the blood-brain barrier, maintains the anatomical and functional connections with the brain. The posterior lobe is embryologically and anatomically continuous with the hypothalamus, located in the basal part of the forebrain surrounding the third ventricle. Anatomically, the vertebrate hypothalamus is situated directly above the pituitary and consists of two distinct neuronal populations: the magnocellular and parvocellular neurons (Figure 1-6, p.40). The neuronal populations were described in Section 1I Molecular Genetics of the Hypothalamic-Pituitary Axis (p.23).

It is important to note that the HP axis consists of numerous vessels that help to define the relationship between these two structures. The blood supply of the hypothalamus and pituitary is discussed in the preceding section (refer to Section 1I.C.2 Blood supply of the hypothalamo-pituitary axis, p.38).

2. *Blood supply of the hypothalamo-pituitary axis*

The blood supply to the HP axis is complex but defines the functional relationship between the hypothalamus and anterior pituitary. Any interruption to the blood supply will impair hypothalamic control of anterior pituitary secretions. The hypothalamus receives its blood supply from the Circle of Willis (a circle of arteries supplying blood to the brain) whilst the anterior and posterior pituitary lobes receive arterial blood from the inferior and superior hypophysial arteries, respectively (Figure 1-7, p.41 and in Appendices Figure A 1, p.230). The capillary plexus of the inferior hypophysial artery drains into the dural sinus although some of these capillaries in the neural stalk form 'short' portal veins that drain into the anterior pituitary gland (Nussey and Whitehead, 2001). This constitutes only a small fraction of the circulation of the anterior lobe, which is one of the most extensively vascularized mammalian tissues. The major portion of the circulation arises from the 'long' portal veins that are formed from the capillary network of the superior hypophysial arteries; these provide blood to the nerve endings of the neurosecretory cells in the median eminence. Thus, hypothalamic releasing and inhibiting hormones are released into these hypophysial portal veins, through which they are transported to the endocrine cells of the anterior pituitary. It is here that these portal veins form a secondary capillary network into which anterior pituitary hormones are secreted. The capillaries in

the hypophysial portal system are fenestrated and thereby improve hormone delivery to the adenohypophysial cells. The venous channels from the anterior pituitary gland drain into the cavernous sinuses whereby they turn into the superior and inferior petrosal sinuses and into the jugular vein (Nussey and Whitehead, 2001).

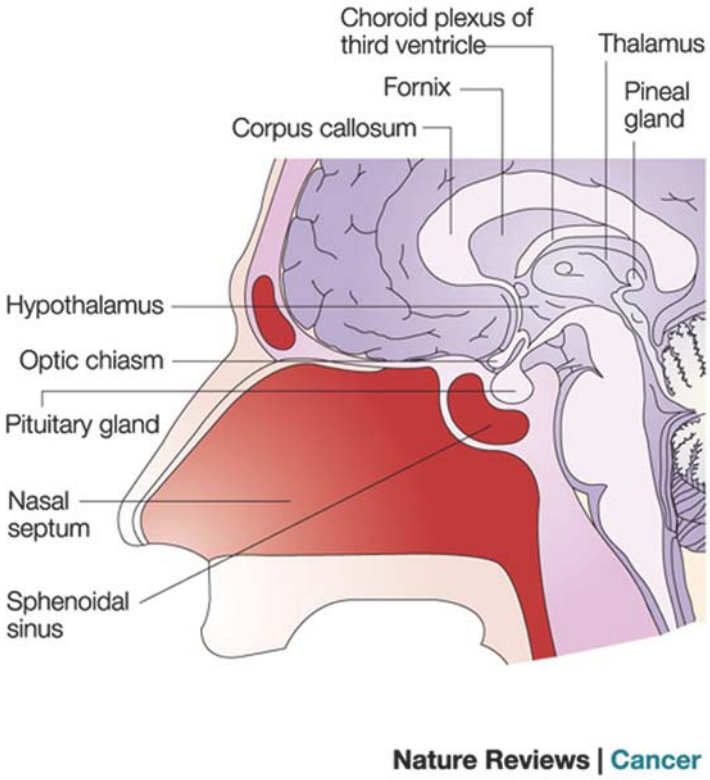

Figure 1-5 Anatomical location of the hypothalamus and pituitary in humans

Sagittal section through the midline showing the pituitary gland within the diaphragma sella (a fold that encases the pituitary), situated immediately posterior to the sphenoid sinus. The pituitary gland is the 'master' hormonal gland — comprising an anterior and posterior lobe1 — and is located at the base of the hypothalamus in the brain. A horizontal cross-section reveals three distinct anatomical areas — the central mucoid wedge and two lateral wings — within the anterior pituitary, and each hormone-secreting cell population is differentially distributed throughout the anterior pituitary. Adapted from (Heaney and Melmed, 2004).

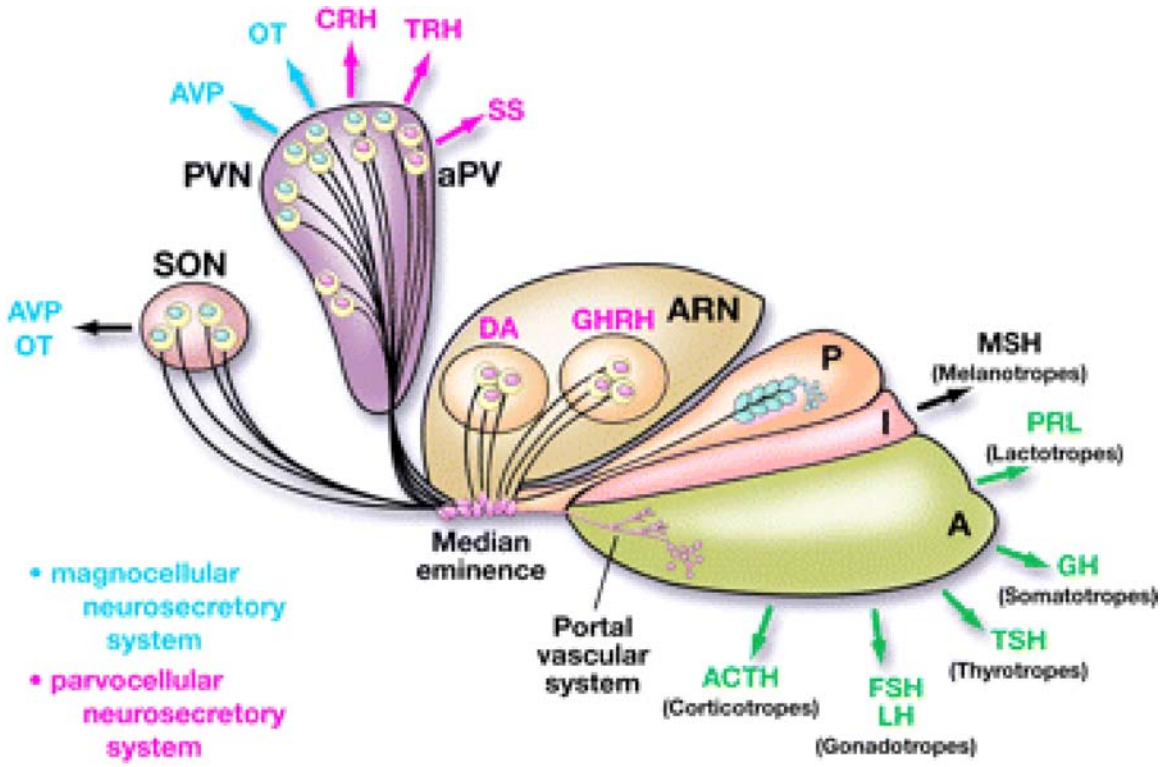

Figure 1-6 The hypothalamic-pituitary axis

Hormone synthesis and secretion from the pituitary gland are regulated by a series of peptide hormones released from hypothalamic neurons. The magnocellular neurosecretory system includes neurons in paraventricular hypothalamus (PVN) and supraoptic nucleus (SON) that synthesize oxytocin (OT) and arginine vasopressin (AVP) and release them from axonal terminals in the posterior lobe (P). Hormone synthesis and secretion in the anterior lobe of pituitary (A) are regulated by releasing factors produced by the parvocellular neurons and released into the portal vascular system. Corticotropin releasing hormone (CRH) and thyrotropin releasing hormone (TRH) are synthesized by neurons in the PVN. Growth hormone releasing hormone (GHRH) is synthesized by neurons of the arcuate nucleus (ARN) and the adjacent ventromedial nucleus. Somatostatin (SS) is mainly synthesized by neurons in anterior periventricular nucleus (aPV). The parvocellular neurons project to the medial eminence where they release hormones that are transported to the anterior pituitary by the portal vascular system. Adapted from (Zhu et al., 2007a).

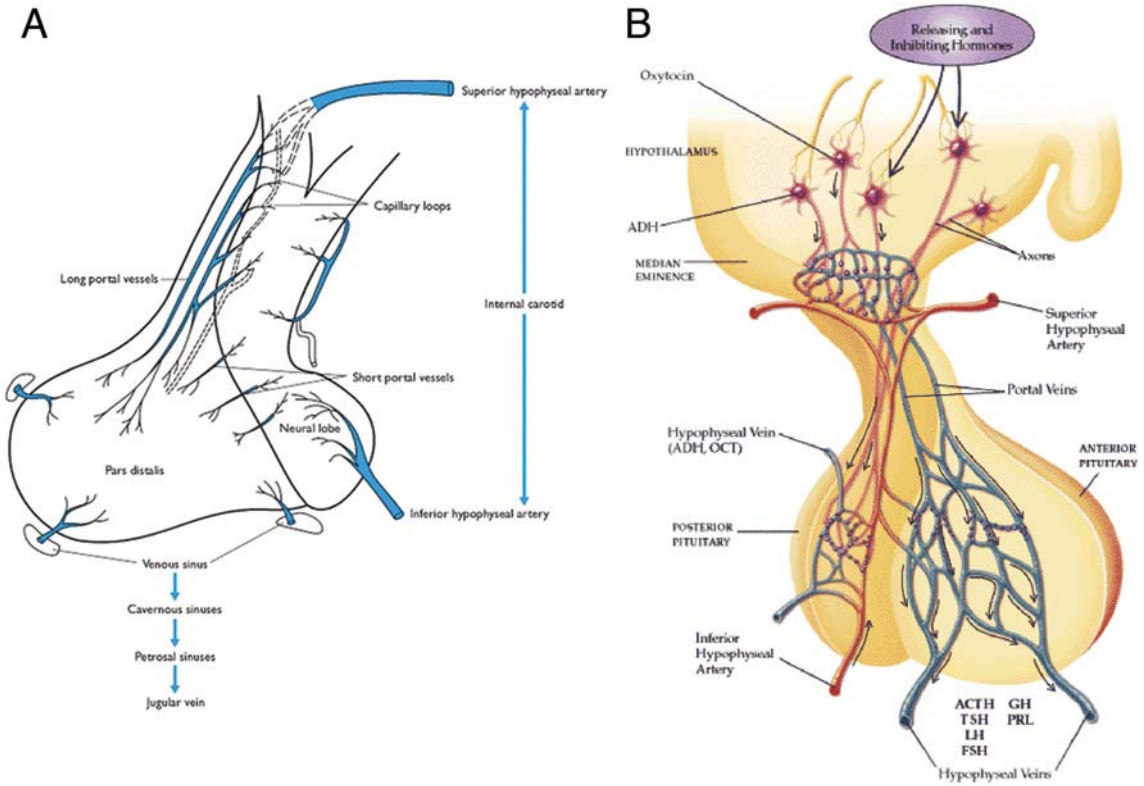

Figure 1-7 Diagrammatic representation of the blood supply and venous drainage of the hypothalamo-pituitary axis

(A) The anterior and posterior pituitary lobes receive blood from the inferior and superior hypophysial arteries. (B) Vasculature connection between the hypothalamus and pituitary. Abbreviations: ACTH, adrenocorticotropin; TSH, thyroid stimulating hormone; LH, luteinizing hormone, FSH, follicular stimulating hormone; GH, growth hormone; PRL, prolactin; ADH, antidiuretic hormone; OCT, oxytocin. Figure A adapted from (Nussey and Whitehead, 2001) and B from (Melmed, 2010).

3. *Angiogenesis*

The vascular system plays an important role ensuring that a sufficient supply of nutrients and oxygen is supplied from circulating blood to cells. There are two different mechanisms of vessel formation (Figure 1-8, p.42): vasculogenesis (or *de-novo* vessel formation), which involves differentiation of precursor stem cells to endothelial cells, and angiogenesis, the formation of new vessels that arise from preexisting capillaries (Risau, 1997). Vasculogenesis results in the formation of a primitive vascular network that undergoes expansion and remodeling via angiogenesis into a more mature vasculature. This vasculature comprises of large branching vessels and smaller capillaries. During embryonic development vessels initially form via vasculogenesis and later via angiogenesis, whereas new vessels in the adult predominantly arise via angiogenesis. The regulation of vasculogenesis and angiogenesis involves a delicate balance of pro- and anti-angiogenic factors (Hanahan and Folkman, 1996).

NOTE:
This figure is included on page 42 of the print copy of the thesis held in the University of Adelaide Library.

Figure 1-8 Vasculogenesis and angiogenesis
Vasculogenesis involves the formation of hemangioblastic blood islands and the construction of capillary networks from them. Angiogenesis involves the formation of new blood vessels by remodeling and building on older ones. Angiogenesis finishes the circulatory connections begun by vasculogenesis and builds arteries and veins from the capillaries. In this diagram, the major paracrine factors involved in each step are shown boxed, and their receptors (on the vessel-forming cells) are shown beneath them. Adapted from (Gilbert, 2000).

Firstly, vasculogenesis occurs with the involvement of three growth factors (as shown in Figure 1-8). The first important protein is the basic fibroblast growth factor (bFGF) FGF2. FGF2 is required for the generation of hemangioblasts (a multipotent cell, common precursor to hematopoietic and endothelial cells) from the splanchnic mesoderm (Gilbert, 2000). The second significant protein is vascular endothelial growth factor (VEGF). VEGF enables the differentiation of angioblasts, which are formed from hemangioblasts, and their multiplication to form endothelial tubes. The role of VEGF is discussed in greater detail below (see Section 4 Importance of VEGF and VE-Cadherin, p.43). The third protein is angiopoietin-1 (Ang1) which mediates the interaction between the endothelial cells and the pericytes—smooth muscle-like cells they recruit to cover them (Gilbert, 2000). Mutations of either Ang1 or its receptor, in mice, have resulted in the malformation of blood vessels and deficiency in the smooth muscles that usually surround them (Davis and Reed, 1996; Vikkula et al., 1996). Secondly, angiogenesis is also induced by the growth factors VEGF and bFGF, as well as platelet-derived growth factor (PDGF; which is necessary for the recruitment of pericyte cells that contribute to the flexibility of the capillary) (Lindahl et al., 1997), chemokines and others factors (as shown in Figure 1-8, p.42). VEGF acts on newly formed capillaries and causes loosening and degradation of the

extracellular matrix at certain points. This region contains exposed endothelial cells that are able to proliferate and sprout, ultimately forming a new vessel (Figure 1-9, p.44). FGF's play an important role whereby they alter the adhesiveness of the extracellular matrix (ECM) regulating endothelial-cell growth and differentiation during vessel formation. The loosening of the ECM may also allow capillary fusion that leads to formation of wider vessels, such as arteries and veins. Finally, the developed capillary network forms and is stabilized by TGF-β; which strengthens the ECM) and PDGF. The entire blood vessel formation process typically lasts several days or weeks and is tightly regulated by a variety of circulating and sequestered inhibitors that can suppress vascular endothelial proliferation (Adair et al., 1990) .

4. Importance of VEGF and VE-Cadherin in vascular development

VEGF is an angiogenic factor that plays an important role during blood vessel formation. A summary of the role and functions of VEGF are shown in Table 1-3 (p.46). Furthermore, the expression of VEGF and its receptors has been shown to be restricted to the vasculature during embryogenesis, indicating that these molecules play an important function during vascular development (Breier et al., 1995). In contrast, in adult tissue the gene expression of VEGF is quite minimal, except for in the adult kidney, where it is likely helping to maintain vasculature (Dvorak et al., 1995; Ferrara and Keyt, 1997). The expression of VEGF can be induced in various cell types such as during tumorigenesis (Baritaki et al., 2007; Oka et al., 2007; Plate and Risau, 1995; Soufla et al., 2006; Sun et al., 2005; Waldner et al., 2010) and wound healing (Ferraro et al., 2009; Ferte et al., 2009; Frank et al., 1995) implicating the VEGF-VEGF receptor gene family in pathological neovascularization (the formation of new blood vessels, i.e. capillary in-growth and endothelial proliferation in unusual sites, a finding typical of so-called 'angiogenic diseases', which include angiogenesis in tumor growth, diabetic retinopathy, hemangiomas, arthritis, psoriasis (Segen, 2006)).

Figure 1-9 Angiogenesis

(A) Schematic representation of the basement membrane (BM) in blood vessels. In the vasculature, the vascular BM interacts directly with the pericytes, which are on the outside, and the endothelial cells, which line the inside of the vessel. (B) Angiogenesis is associated with degradation and reformation of the vascular basement membrane (VBM). In response to growth factors and matrix metalloproteinases (MMPs), the VMB undergoes degradative and structural changes. This transition from mature VBM to provisional matrix promotes the proliferation and migration of vascular endothelial cells. Growth factors, such as vascular endothelial growth factor (VEGF), basic fibroblast growth factor (bFGF) and platelet-derived growth factor (PDGF), are released from the BM, and are also produced by fibroblasts and immune cells. This induces formation of an intermediate, and then a new (mature) VBM. Together with the vascular endothelial cells and pericytes, the VBM mediates formation of a new blood vessel. The degraded VBM during this process has a crucial role in regulating angiogenesis.

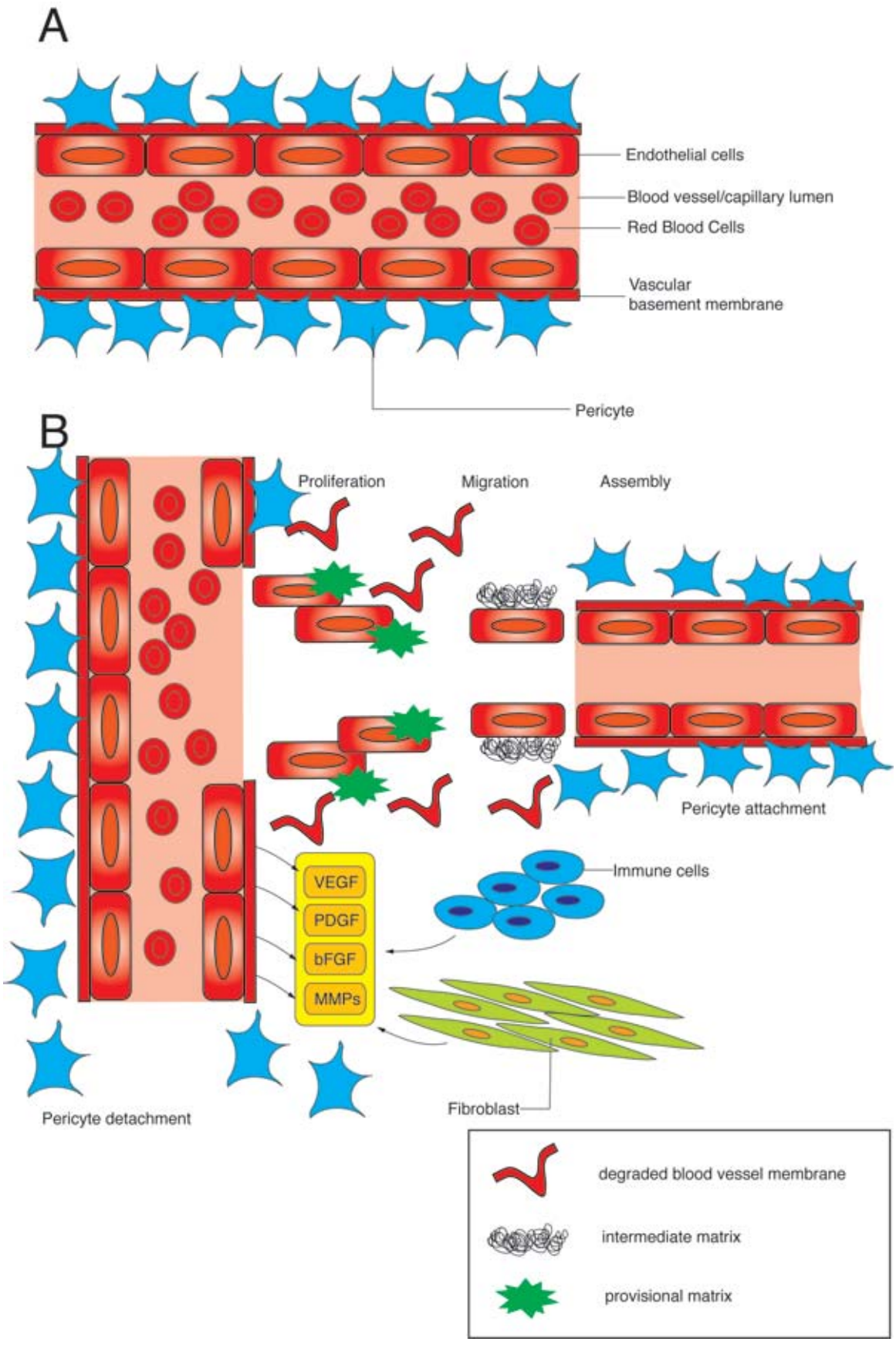
A
Endothelial cells
Blood vessel/capillary lumen
Red Blood Cells
Vascular
basement membrane
Pericyte
B
Proliferation
Migration
Assembly
Pericyte attachment
VEGF
PDGF
bFGF
MMPs
Immune cells
Fibroblast
Pericyte detachment
degraded blood vessel membrane
intermediate matrix
provisional matrix

Table 1-3 Important role and functions of VEGF during blood vessel formation
Information extracted and tabulated from (Carmeliet, 2000b).

Targeted inactivation of one VEGF allele results in haploinsufficiency and associated embryonic lethality, at around E9 in mice, due to abnormality in blood vessel development (Carmeliet et al., 1996). In contrast, conditional inactivation of the VEGF gene results in postnatal vascular impairment during development and endothelial survival that leads to an increase in death, stunted body growth, and impaired organ development (Gerber et al., 1999).

Vascular endothelial-cadherin (VE-Cadherin) belongs to the cadherin family of major cell adhesion molecules (CAMs) responsible for Ca2+-dependent cell-cell adhesion in vertebrate tissues (Alberts et al., 2002; Hynes, 1992). VE-Cadherin is the only member of the cadherin family to be found at endothelial junctions (Lampugnani et al., 1992) and its interactions are made via its cytoplasmic tail (containing three proteins of the armadillo family called β-catenin and plakoglobin, which both act to anchor cadherins to the cortical actin cytoskeleton (Gumbiner, 1996)). VE-Cadherin is activated when VEGF binds to its cognate receptor (Figure 1-10, p.49). Importantly, VE-Cadherin may play an essential role in implicating cell differentiation, growth, as well as migration (Dejana, 1996, 1997). In the mouse, the expression of VE-Cadherin has been localized to hemangioblasts from E7.5 onwards (Breier et al., 1996) and, thereafter, constitutively in all endothelial cells. Mice lacking a functional VE-Cadherin gene, or containing a mutant VE-Cadherin gene that lacks the β-catenin–binding cytoplasmic tail, or that does not express detectable VE-Cadherin levels, did not survive beyond E9.5 due to vascular insufficiency (Carmeliet et al.,

1999). A closer examination of wild-type and mutant mice has revealed that angioblasts were able to differentiate into endothelial cells and assemble into primitive vessels in the embryo and yolk sac, between E8.25–8.5. Accordingly, these results suggested that vasculogenesis was able to occur without VE-Cadherin. However, a closer look at E8.5 embryos revealed that certain vessels had few or even no lumen whilst others were dilated. Interestingly, in mutant embryo yolk sac endothelial cells, channels were seen disconnecting from their vascular branches. These vascular disconnection defects were more severe in mutant VE-Cadherin embryos between E8.75–E9.0 (a point when the wild-type primitive vascular is sprouting via angiogenesis and is remodeled into a vasculature network). Hence, normal functioning of VE-Cadherin essential for vasculogenesis, however it does play an important role in angiogenesis (i.e. the expansion, maturation, branching, and remodeling of vasculature).

NOTE:
This figure is included on page 48 of the print copy of the thesis held in the University of Adelaide Library.

Figure 1-10 The VEGF:VE-Cadherin Pathway

VEGFR-2 associates with VE-Cadherin, and when activated by VEGF, this receptor dimerizes causing the sequential activation of Vav2, Rac and PAK, through Src. This results in the serine phosphorylation of a conserved motif in the cytoplasmic tail of VE-Cadherin (SVR 665–667) by PAK, which is likely coordinated with the tyrosine phosphorylation of the VE-Cadherin–catenin complexes (dashed arrow) by Src. Serine-phosphorylated VE-Cadherin recruits β-arrestin, which promotes the consequent internalization of VE-Cadherin into clathrin-coated pits. Interestingly, the SVR motif is adjacent to the p120-binding region, which is conserved among all classical cadherins, thus raising the possibility that the association/dissociation of p120 with VE-Cadherin may regulate the status of phosphorylation of the SVR motif within the VE-Cadherin ICD and/or its interaction with β-arrestin. Tyrosine phosphorylation of VE-Cadherin and its associated molecules may be coordinated with the Src-dependent activation of Vav2 and Rac to regulate the dynamic disassembly and reassembly of adheren junctions. This process leads to the disassembly of endothelial-cell junctions, resulting in the enhanced permeability of the blood-vessel wall. Endosomal VE-Cadherin may be recycled to the cell surface, thus participating in the dynamic reorganization of adherens junctions during vessel remodeling. Furthermore, transactivation of VEGFR2 causes activation of two signaling cascades that are important for movement and vascular remodeling: first, activation of Src-family tyrosine kinases, the adaptor protein CrkII and CAS (Crk-associated substrate); and second, activation of PI3K-Alpha (Phosphatidylinositol 3-Kinase-Alpha), Akt Pathway and eNOS (endothelial Nitric Oxide Synthase), and the formation of NO (Nitric Oxide). In endothelial cells the predominant VEGFR2 that mediates eNOS phosphorylation is Flk1/KDR (Fetal Liver Kinase-1/Kinase-insert Domain-containing Receptor) leading to phosphorylation and stimulation of the PI3K-Akt1-eNOS pathway. VEGF receptor Flk1/KDR localizes to caveolae, while EDG1 receptor exists in both non-caveolae and caveolae membranes. After stimulation EDG1 translocates and concentrates in caveolae. Upon G-AlphaI protein-mediated activation of PLC (Phospholipase-C), intracellular Ca2+ levels increase and Ca2+ complexes with Calm (Calmodulin). The Ca2+/Calm complex then activates eNOS. Simultaneously, Ca2+ and Src family kinase-dependent transactivation of Flk1/KDR occurs, which stimulates Src family kinase and PI3K causing Akt1 and eNOS to be phosphorylated and activated. Schematic is a composite from two figures adapted from (Gavard and Gutkind, 2006) and Qiagen GeneGlobe Pathways (www.qiagen.com/geneglobe/pathwayview.aspx?pathwayID=199).

II. SOX FAMILY OF TRANSCRIPTION FACTORS

A. The SOX Family

The male sex determination gene Sry (sex-determining region of Y chromosome) was the first Sox (SRY-related HMG box) gene family member identified (Sinclair et al., 1990). Sox proteins contain a 79-amino acid HMG box domain that is responsible for sequence-specific DNA binding (Gubbay et al., 1990; Wright et al., 1993). Approximately 30 Sox genes have been identified, including 20 that are present in both the mouse and the human genome (Kiefer, 2007). Sox proteins have greater than 50% identity with the founding member Sry and are divided into eight subgroups (A-H) (Table 1-4, p.51 and Figure 1-12, p.52), based on phylogenetic analysis of HMG box regions. All Sox proteins are expressed during embryogenesis, and are involved in cellular differentiation, germ layer formation as well as organ development (Pevny and Lovell-Badge, 1997; Wegner, 1999). Members within each subgroup show highly restricted tissue specificity, with at least 12 members being expressed in the nervous system (Wegner, 1999). The B group is further divided into two subgroups: SoxB1 proteins (Sox1, 2, 3) containing transcriptional activation domains and SoxB2 proteins (Sox14, 21) containing repressor domains (Bowles et al., 2000). SoxB1 subfamily transcription factors are predominantly expressed within the early developing embryo, developing testis, and nervous system, and are vital for cell fate determination and cell differentiation during mouse development (Table 1-5, p.54), as shown by dominant negative and knockout mouse studies (Pevny and Lovell-Badge, 1997; Wegner, 1999).

B. The SOXB1 Subgroup

Sox1, Sox2 and Sox3 are assigned to the SoxB1 subgroup and share >95% HMG sequence homology (Figure 1-11, p.52). They are predominantly co-expressed in proliferating neural progenitors and stem cells of the embryonic CNS and function as transcriptional activators (Bylund et al., 2003). Members of the SoxB1 subgroup show considerable overlap in their expression patterns, and appear to be functionally redundant (Figure 1-12, p.55).

Table 1-4 SOX family of proteins

Abbreviations: CNS - central nervous system, ICM - Inner Cell Mass, PNS - Peripheral Nervous system. (Lefebvre et al., 2007; Pevny and Lovell-Badge, 1997)

Group	Gene	Chromosome	Expressed domain	Functions
A	*Sry*	Y	Genital ridge and testis	Male sex determination
B1	*Sox1*	8	Embryonic CNS, lens	Forebrain development, chromatin architecture, neuron migration
	Sox2	3	ICM, primitive ectoderm, CNS, PNS, embryonic gut, endoderm	CNS development, neuron fate commitment, embryonic organ development
	Sox3	X	Embryonic CNS, gonads	Specify stem cell identity, gonadogenesis, CNS development
B2	*Sox14*	9	Midbrain, Skeletal muscle	Neurogenesis - counteracts Sox1-3 activity to promote neuron differentiation
	Sox21	14	embryonic CNS	Neurogenesis - counteracts Sox1-3 activity to promote neuron differentiation
C	*Sox4*	13	Embryonic heart and spinal cord, adult pre-B and pre-T cells	-
	Sox11	12	Embryonic CNS, post-mitotic neurons	Organ development - lung, stomach, pancreas, spleen, eye and skeleton
	Sox12	2	Fetal Testis	-
D	*Sox5*	6	Adult testis	Skeletogenesis, neural crest development, gliogenesis
	Sox6	7	Embryonic CNS, adult testis	Cardiac conduction, skeletogenesis, gliogenesis, erythropoiesis
	Sox13	1	Kidney, Ovary, Pancreas	Lymphopoiesis
E	*Sox8*	17	Gliogenesis, Testis development, osteogenesis, neural crest	Cell fate commitment and maturation, CNS development, formation of neural crest and upkeep
	Sox9	11	Chondrocyte, genital ridge and adult testis, CNS, notochord	Male gonad development, cartilage condensation, apoptosis regulation
	Sox10	15	PNS, CNS	Neural crest, inner ear formation
F	*Sox7*	14	CNS, heart	Cardio genesis
	Sox17	1	Endoderm, testis	Endoderm formation, angiogenesis
	Sox18	2	Heart, lung, spleen, skeletal muscle, liver and brain of adult	Angiogenesis, vasculogenesis
G	*Sox15*	11	Pancreas	Skeletal Muscle regeneration
H	*Sox30*	11	Heart, brain, lung, testis, mesonephros	-

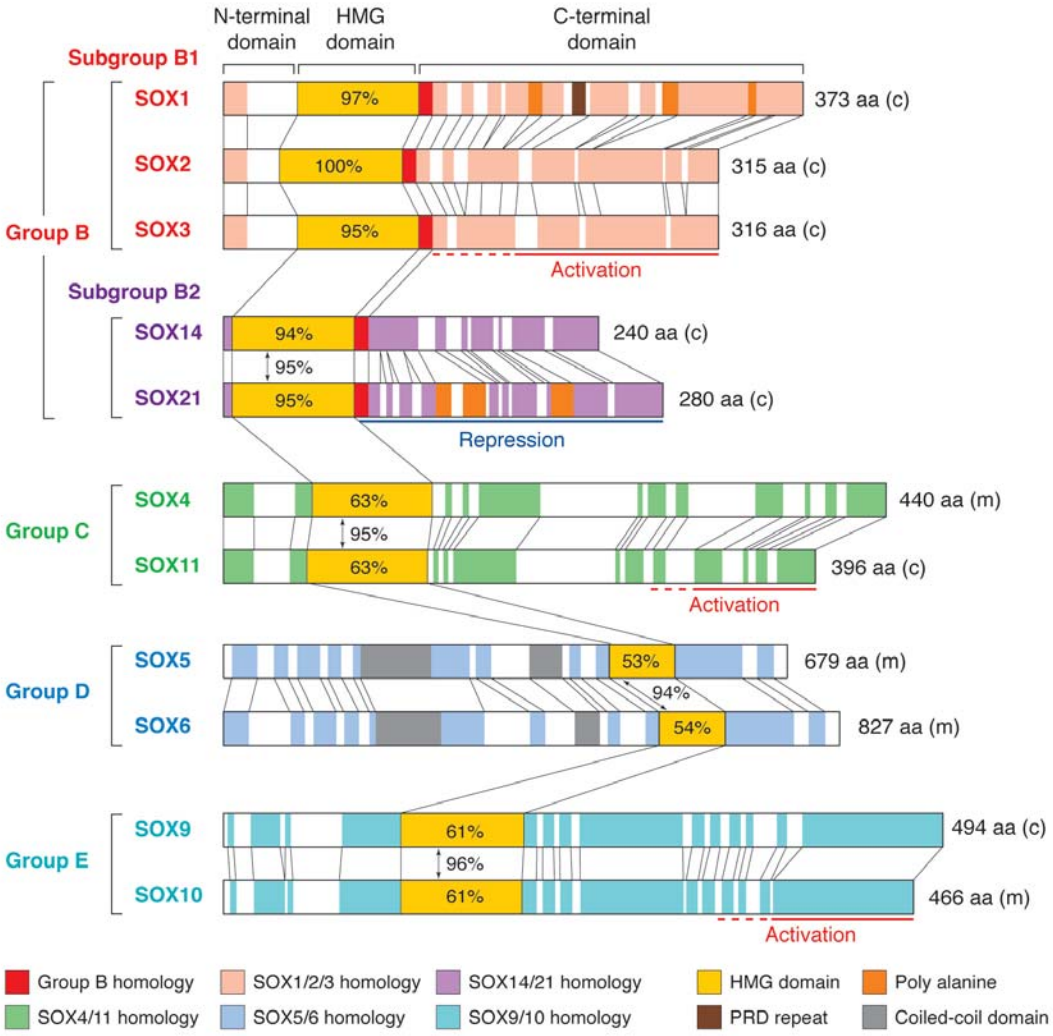

Figure 1-11 SOX family of proteins showing homology relationship

Representative SOX proteins of Groups B–E are shown schematically. Similarity scores of the high-mobility-group (HMG) domain amino acid sequences relative to that of SOX2, and between the group members, are indicated. Within each Group, amino acid sequences are highly conserved throughout the length, except Subgroups B1 and B2 of Group B. Group B is subdivided into Subgroups B1 (activators) and Subgroup B2 (repressors). Between Subgroups B1 and B2, the sequence similarity is found in 'Group B homology'5domain, in addition to the HMG domain. Between different Groups, similarity of the amino acid sequence is recognized only in the HMG domain. Protein sizes are shown in amino acid number, with species of protein origin (c, chicken; m, mouse). SOX5 and SOX6 are drawn in half scale. Activation and repression domains are shown by red and blue lines, respectively. PRD-repeat: His-Pro repeat originally found in Drosophila Paired protein; aa, amino acids. Figure and description obtained from (Kamachi et al., 2000).

Sox1, initially expressed at E8, is confined to neural precursors following neural induction (Pevny et al., 1998). By E9.5 Sox1 is detected throughout the entire length of neural tube and by E12.5 expression restricted to the ventricular and sub ventricular zones as well as the lens (Aubert et al., 2003). In mice, an absence of Sox1 results in a failure of differentiation in postmitotic neurons and is associated with seizures and lens defects (an area where Sox1 is uniquely expressed) (Ekonomou et al., 2005; Malas et al., 2003).

Sox2, the earliest transcription factor to be expressed in ectodermal cells, is largely restricted to the presumptive neuroectoderm following gastrulation. By E9.5 Sox2 is expressed throughout the brain, neural tube, sensory placodes, branchial arches and gut endoderm (Wood and Episkopou, 1999; Zappone et al., 2000). By E7.5 the expression of Sox2 is centered within the anterior neuroectoderm, but not within the posterior ectoderm (Zappone et al., 2000). By E9.5, Sox2 is expressed in neural stem cells of the developing neural tube throughout embryogenesis and well into adulthood (Avilion et al., 2003). Although, Sox2 cells within adulthood are restricted to the ventricular zone (Zappone et al., 2000). A recent study in mice (Kelberman et al., 2006) showed that heterozygous loss-of-function of *Sox2* results in abnormal anterior pituitary development, in particular a reduction in GH, LH and TSH (Kelberman et al., 2006). Homozygous deletion of Sox2 results in peri-implantation lethality preventing further studies because it is the only SoxB1 member expressed in the inner cell mass (Kelberman et al., 2006).

Sox3 is expressed in the developing CNS, including the developing and postnatal hypothalamus (Figure 1-12 B, p.55) (Rizzoti et al., 2004). It is the only member of the SoxB1 subfamily located on the X chromosome (Collignon et al., 1996; Stevanovic et al., 1993). Loss-of-function studies in mice have shown that *Sox3*, like Sox2, is required for the formation of the hypothalamo-pituitary axis (Rizzoti et al., 2004). However, as Sox3 is not expressed in Rathke's pouch, the defects in HP axis function in *Sox3*-null mice appear to have a hypothalamic origin (Rizzoti et al., 2004). SOX3 has been shown to bind the Sox Consensus Motif (SOCM) AACAAT, via its HMG box DNA binding domain (Bergstrom et al., 2000). Furthermore, SOX3 has been implicated as a transcriptional activator by means of reporter assays whereby increasing *Sox3* dosage leads to increased expression of a luciferase reporter construct containing either the SOCM or Hesx1 proximal promoter, identified as containing Sox binding regions (Wong et al., 2007; Woods et al., 2005).

Table 1-5 Expression and biological function of SoxB1 members

Modified and adapted from (Miyagi et al., 2009).

Gene	Chromosome	Expression domain	Functions
Sox1	8	Embryonic nerve system (CNS), lens, urogenital ridge	Lens development (induction and maintenance of gamma-crystallin gene expression) (Nishiguchi et al., 1998)
			Deletion in KO mice leads to microphthalmia, cataracts, and spontaneous seizures (Malas et al., 2003; Nishiguchi et al., 1998)
Sox2	3	Inner cell mass, primitive ectoderm, trophoblast stem cells, embryonic nerve system (CNS), lens, neurogenic regions in adult brain	Deletion in KO mice is embryonic lethal at implantation stage (involved in gene expression in FGF4 (Ambrosetti et al., 1997; Ambrosetti et al., 2000), Oct4 (Chew et al., 2005; Niwa et al., 2005), Nanog (Kuroda et al., 2005), UTF1 (Nishimoto et al., 1999), together with Oct-3/4)
			Induction of gamma- and delta-crystallin gene expression (Kamachi et al., 2001; Kondoh et al., 2004)
			Induction of Nestin gene expression in neural stem/progenitor cells (Josephson et al., 1998; Tanaka et al., 2004)
			Involved in its own expression in ES cells and neural stem cells (Miyagi et al., 2006; Miyagi et al., 2004; Tomioka et al., 2002; Uchikawa et al., 2003)
			Required for maintaining neural stem cell state and neurogenic potential (Bani-Yaghoub et al., 2006; Ferri et al., 2004; Miyagi et al., 2008; Overton et al., 2002; Taranova et al., 2006)
Sox3	X	Epiblast, embryonic CNS, lens, urogenital ridge	Required for early embryogenesis, gonadal function, and hypothalamo-pituitary axis formation (Rizzoti et al., 2004; Weiss et al., 2003)
			Ectopic expression leads to XX male sex reversal (Sutton et al., 2011)
			Candidate gene for human X-linked mental retardation syndromes (Laumonnier et al., 2002)

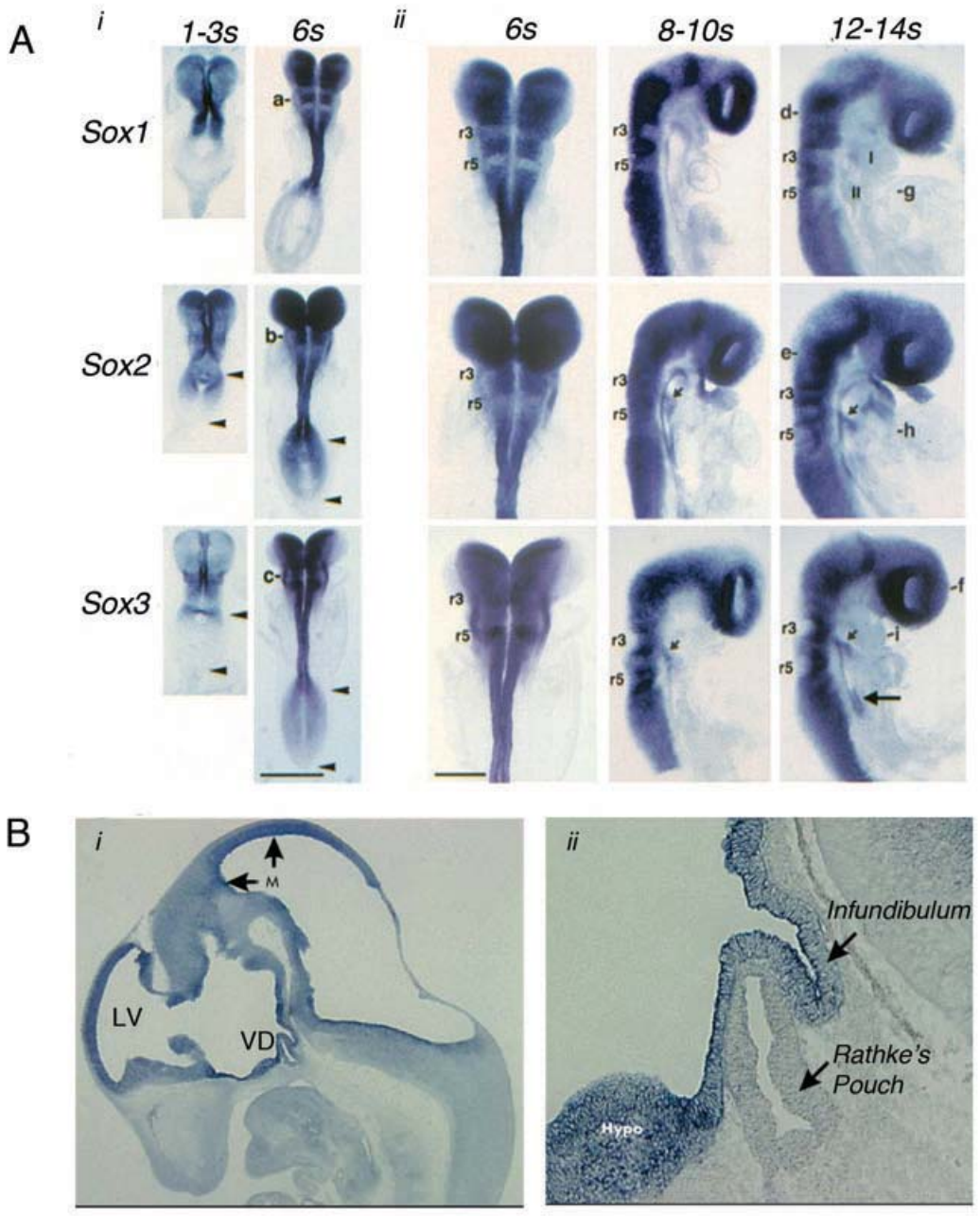

Figure 1-12 Expression of *Sox1*, *Sox2*, and *Sox3* in the developing mouse pituitary and central nervous system

(A) Whole mount *in situ* hybridization using *Sox1, Sox2* and *Sox3* antisense riboprobes on mouse embryos between 8.0 and 9.0 dpc (1-14 somites). Panel *i* shows 1-3 and 6-somite embryos flattened out and photographed from the dorsal aspect. Arrowheads demarcate the primitive streak. Panel *ii* shows detail of gene expression in the hindbrain. The 8-10 and 12-14 somite embryos were sagittally halved. Small arrows indicate expression of *Sox2* and *Sox3* in the ectoderm overlying the second branchial arch; large arrow indicates expression of Sox3 in the posterior region of the foregut. Key: s, somite; r, rhombomere; I, first branchial arch; II, second branchial arch. (B) Panel *i* represents a sagittal section from a mouse embryo 12.0 dpc showing strong *Sox3* expression in the infundibulum, the dorsal aspect of the lateral ventricle (LV), the ventral diencephalon (VD), and the roof and wall of the midbrain (M). Panel *ii* represents a sagittal section from a mouse embryo 11.5 days after conception, showing strong expression in the infundibulum and presumptive hypothalamus (Hypo). No signal was detected in the Rathke's pouch. Figure A adapted from (Wood and Episkopou, 1999) and B from (Solomon et al., 2004).

C. The Role of Sox3 in Hypothalamo-Pituitary Axis Development

1. *Sox3 is expressed throughout early embryonic development*

During commitment and specification of the forebrain primordium (E7.5-9.5 in the mouse), Sox3 is expressed throughout the neuroepithelium at high levels (Collignon et al., 1996; Wood and Episkopou, 1999). Patterning of the telencephalic vesicles by internal and external signaling centers establishes overlapping zones of transcription factor expression that ultimately control the emergence of the distinct forebrain derivatives. The progenitors of the hippocampus, the corpus callosum and the cortical projection neurons reside within the dorsal telencephalon and begin to differentiate at approximately E11.5. Sox3 expression in this region is maintained from E11.5 until at least postnatal day (P) 1 and is restricted to the self-renewing cell population in the ventricular zone. The ventral telencephalon, which gives rise to the cortical interneurons, also expresses Sox3 in the ventricular zone until at least E14.5. In the diencephalon, which gives rise to the hypothalamus, thalamus and optic nerves/retina, Sox3 is expressed at high levels in the infundibular recess, a midline evagination that is essential for posterior pituitary development as well as in the developing and postnatal hypothalamus (as shown in Figure 1-12 B, p.55). However, Sox3 is not expressed in Rathke's pouch (Collignon et al., 1996; Solomon et al., 2004).

2. *Sox3 plays an important role during brain development*

The role of Sox3 in the developing CNS has been examined in mice with *Sox3*-null mutations. *Sox3*-null mice have been generated using homologous recombination, whereby the *Sox3* open reading frame (ORF) is replaced with the enhanced green fluorescent protein (eGFP) ORF. Mice lacking functional *Sox3* exhibit variable phenotypes consistent with abnormalities in the HP axis including variable pituitary hormone deficiencies, dwarfism, and hypogonadism (Table 1-6, p.57) (Rizzoti et al., 2004; Rizzoti and Lovell-Badge, 2007; Weiss et al., 2003). Additionally, these mice exhibit CNS abnormalities including dysgenesis of the corpus callosum (Figure 1-13 A, p.58). Importantly, the ventral diencephalon appears expanded, relative to the normal V-shape seen in wild-type embryos and there is notable bifurcation and expansion of the dorsal side of Rathke's pouch (Figure 1-13 B, p.58). The later changes are most obvious from E11.5 through E14.5 (Rizzoti et al., 2004). Furthermore, the neuroepithelium precursor cells in this presumptive hypothalamic region have significant reduction in cellular proliferation (Rizzoti et al., 2004). Thus, *Sox3* undoubtedly contributes to correct morphogenesis of the hypothalamic primordium and for HP axis formation and research to date indicates the importance of Sox3 expression

during the early stages of development. Additionally, mice lacking *Sox3* have altered BMP/FGF8 expression in the ventral diencephalon that plays important roles in controlling differentiating cell types (Rizzoti et al., 2004).

Table 1-6 Phenotypes of *Sox3* transgenic mouse models
Adapted from (Alatzoglou et al., 2008)

3. *Importance of genetic background*

The laboratory mouse is one of the primary animal models for understanding the genetic and molecular basis of human biology and disease (Rosenthal and Brown, 2007). In the study out-lined in Chapter 3 (Identification of *Sox3* Target Genes, p.105 – *project 1*) *Sox3*-null mice were used. The importance of genetic background of *Sox3*-null mice is well established (Rizzoti et al., 2004; Rizzoti and Lovell-Badge, 2005, 2007). The *Sox3*-null mice in other studies were maintained on the C57/BL6 background, which suppressed the brain defect and enhanced the spermatogeneis defect. Whereas, the *Sox3*-null mice in *project 1* were maintained on a mixed background, and, although they had lost the dwarfism phenotype, they presented with abnormal morphogenesis of the hypothalamus, pituitary and midline CNS structures.

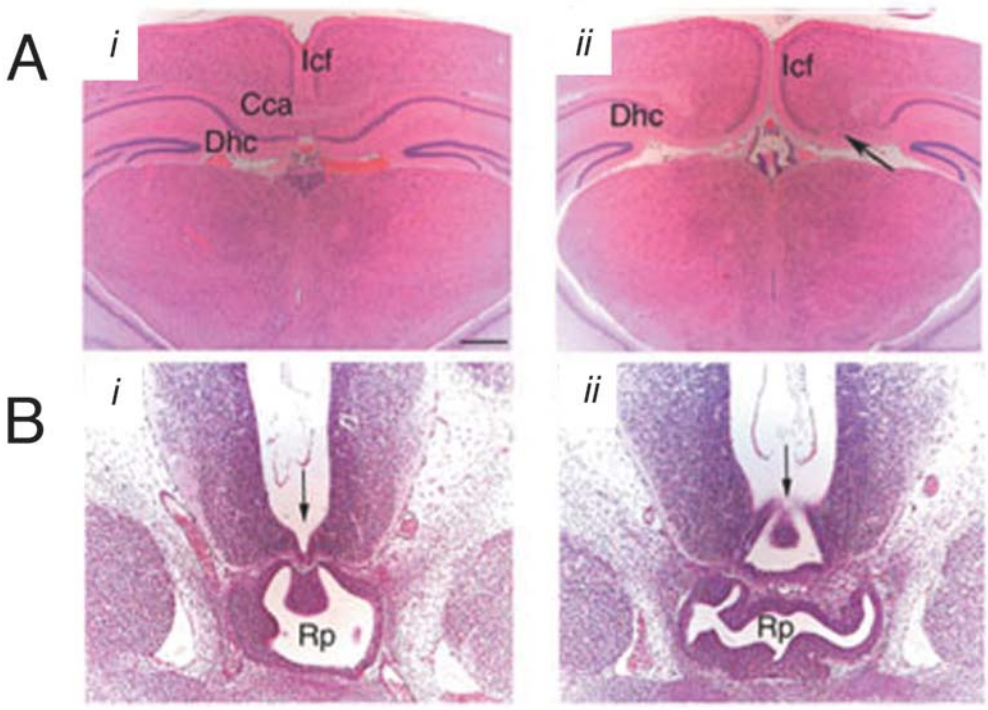

Figure 1-13 Abnormal morphogenesis of the hypothalamus, pituitary and midline CNS in *Sox3*-null mice

Transverse sections of 3-week-old (A) WT (i) and *Sox3*-null (ii) littermates, showing dysgenesis of the corpus callosum, and failure of the dorsal hippocampal commissure to cross the midline (arrow). (B) Coronal sections of E12.5 mouse embryos wild-type (i) and *Sox3*-null (ii) showing abnormal ventral hypothalamus and infundibulum (arrow), as well as a bifurcated Rathke's pouch. Abbreviations: Icf, intercerebral fissure; Cca, corpus callosum; Dhc, dorsal hippocampal commissure; Rp, Rathke's pouch. Adapted from (Rizzoti et al., 2004).

III. CONSEQUENCES OF MUTATIONS IN TRANSCRIPTION FACTORS: CONGENITAL HYPOPITUITARISM

Congenital Hypopituitarism (CH) is a clinical syndrome of deficiency in pituitary hormone production. Congenital defects may result from disorders involving the pituitary gland or hypothalamus and can result in morbidity, particularly when diagnosis is delayed (Mehta and Dattani, 2008).

A deficiency in GH is closely associated with CH (Lindsay et al., 1994; Mehta and Dattani, 2008; Mehta et al., 2009). GH deficiency is often accompanied by deficiencies in other anterior pituitary hormones or, in severe cases, deficiencies in all anterior pituitary hormones or panhypopituitarism, often arising during early childhood development (Alatzoglou and Dattani, 2009). Panhypopituitarism refers to involvement of all pituitary hormones; however, only one or more pituitary hormones are often involved, resulting in partial hypopituitarism. Untreated panhypopituitarism can be lethal.

CH has a significant genetic component that has been described in familial forms of the disorder. These familial forms often display autosomal recessive, autosomal dominant as well as X-linked recessive inheritance patterns (Procter et al., 1998; Thomas et al., 2001). Several genes have been identified involved in autosomal forms of CH, these include SOX3, SOX2, POU1F1, PROP1, HESX1, T-PIT and LHX3/4 (Table 1-7) (Agarwal et al., 2000; Kelberman and Dattani, 2006; Kelberman et al., 2006; Metherell et al., 2004; Rizzoti et al., 2004; Thomas et al., 2001; Thomas et al., 1995). A great majority of these genes were originally identified in mice as major players in pituitary development and were consequently associated with CH in humans. Comparatively, examination of the phenotypes observed in mouse mutants and patients with mutations in orthologous genes emphasize the conservation in the genetic program controlling mammalian HP development. This has undoubtedly emphasized the importance of mouse mutagenesis studies to further enhancing our understanding of CH in humans.

IV. THE GROWTH HORMONE AXIS

A. Growth-Hormone and Growth Hormone-Releasing Factor

GH plays an integral part in post-natal growth, development and contributes to important metabolic functions. As an anabolic hormone, GH provides widespread actions, many of which are mediated by insulin-like growth factors (IGFs), insulin growth factor-1 (IGF-1) and -2 (IGF-2), which are synthesized by the liver and in target tissues (Liu et al., 1993; Zhou et al., 1997). GH exerts its most profound effect on linear growth by stimulating proliferation of cartilage in the epiphyseal plates of long bones before they fuse. Furthermore, GH also increases total bone mass and mineral content by increasing the activity and the number of bone modeling units (Nussey and Whitehead, 2001). GH increases lean body mass, reduces adiposity by its lipolytic effects, and increases organ size and function, the latter effect being mediated by IGFs (Figure 1-14, p.61). Normal concentrations of GH are necessary to maintain normal pancreatic islet function. Thus, in GH deficiency, insulin secretion declines whilst an excess of GH reduces insulin-dependent glucose uptake causing a rise in insulin secretion to compensate for the GH-induced resistance.

Table 1-7 Transcription factors that affect pituitary function and are associated with autosomal forms of congenital hypopituitarism
Adapted from (Davis et al., 2010).

Gene	DNA binding Motif	Clinical features, Mouse phenotypes
Syndromic: affecting pituitary development and other head structure		
PITX	Paired/bicoid homeo	Rieger syndrome: eyes, teeth, umbilical defects Rarely, isolated GH deficiency, haploinsufficient in humans but not obvious in mice
OTX2	POU homeo	Anophthalmia, microphthalmia, hypopituitarism
LHX3	LIM homeo	GH, TSH, PRL, LH, FSH, ACTH, variable including rigid cervical spine, sensorineural deafness
LHX4	LIM homeo	GH, TSH, PRL, LH, FSH, ACTH, cerebellar and skull defects
SOX2	HMG box	Hypogonadotropic hypogonadism, rare isolated GH deficiency
SOX3	HMG box	Multiple Pituitary Hormone Deficiency, metal retardation
HESX1	Paired homeo	Variable induced septo-optic dysplasia and severe or mild pituitary hypoplasia or aplasia; GH, TSH, PRL, LH, FSH, ACTH, or Isolated Growth Hormone Deficiency
GLI2	Kruppel family	Holoprosencephaly, cleft lip, central incisor, hypopituitarism
Non-syndromic: affecting pituitary development and other peripheral organs		
PROP1	Paired homeo	Progressive Hypopituitarism, GH, TSH, PRL, LH, FSH, ACTH
POU1F1	POU homeo	GH, TSH, PRL
TPIT	T box	No human mutations described, mice have delayed growth, puberty
OTX1	POU homeo	No human mutations described, mice have delayed growth, puberty
Syndromic: affecting pituitary development and other peripheral organs		
NR5A1	Nuclear receptor	LH, FSH, 46,XY disorder of sexual development, hypogonadism, premature ovarian failure, adrenal failure

GHRH, a hypothalamic-releasing factor synthesized by neurons in the hypothalamic arcuate nucleus, stimulates somatotrope proliferation. Axons of GHRH neurons project to the median eminence and terminate on the capillaries of the pituitary portal system to stimulate GH release (Lin-Su and Wajnrajch, 2002). Somatotrope proliferation, and secretion of GH, is initiated by binding GHRH to the GHRH receptor (GHRHR), triggering a signaling cascade involving cAMP (Figure 1-15, p.62). Interestingly, during GHRH signaling cAMP does not exert its usual anti-proliferative effects, rather, in the somatotrope it mediates the *proliferative* actions of GHRH (Figure 1-16, p.63). Furthermore, GHRH is also involved in stimulating, although to a lesser extent, protein kinase C (PKC) (French et al., 1991) and mitogen-activated protein kinase signaling., which

is at least partially independent of both Protein Kinase A and Protein Kinase C signaling (Pombo et al., 2000). As a consequence, GHRH is able to activate multiple signaling mechanisms that are likely to be used to mediate the proliferative effects of GH.

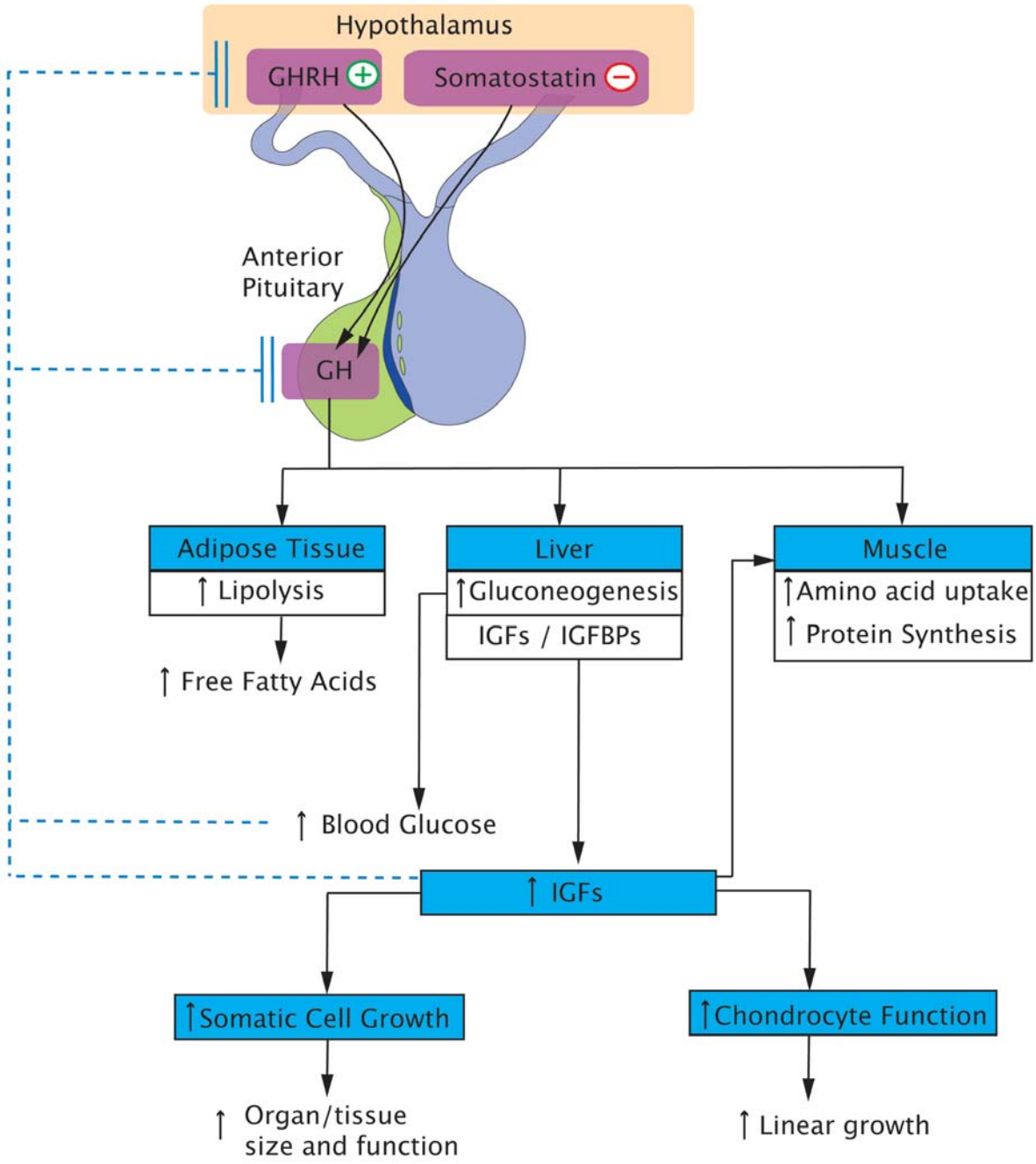

Figure 1-14 Major actions of growth hormone

GH has direct actions on adipose tissue, liver as well as muscle. However, many of the actions of GH are mediated by increasing the synthesis and release of insulin-like growth factors (IGFs), which stimulate DNA, RNA and protein synthesis in various organs and tissues thereby increasing both their size and function. GH also stimulates the synthesis and release of IGF binding proteins (IGFBPs), and these bind circulating IGFs. Their binding provides a reservoir of circulating IGFs. Dashed lines indicate the negative feedback resulting from the action of GH on peripheral tissues.

Figure 1-15 GHRH signaling pathway

Binding of GHRH to its receptor activates the α-subunit of the receptor-associated G-protein complex the (Gsα) of the closely associated G-Protein complex, thus stimulating membrane-bound AC (Adenylyl Cyclase) and increasing intracellular cAMP (cyclic Adenosine Monophosphate) concentrations. cAMP binds to and activates the regulatory subunits of PKA (Protein Kinase-A), which in turn release catalytic subunits that translocate to the nucleus and phosphorylate the transcription factor CREB (cAMP Response Element Binding protein). Phosphorylated CREB, together with its coactivators, p300 and CBP (CREB Binding Protein) enhances the transcription of various genes by binding to specific DNA elements within gene promoter regions, referred to as CREs (cAMP-Response Elements). The genes activated by GHRH and cAMP contain CREs in their promoter regions. CREB, via direct and indirect mechanisms, stimulates GH production via transcription of the GH gene as well as increasing transcription of the GHRHR gene as part of a short positive feedback loop. Adapted from Qiagen GeneGlobe Pathways (www.qiagen.com/geneglobe/pathwayview.aspx?pathwayID=199).

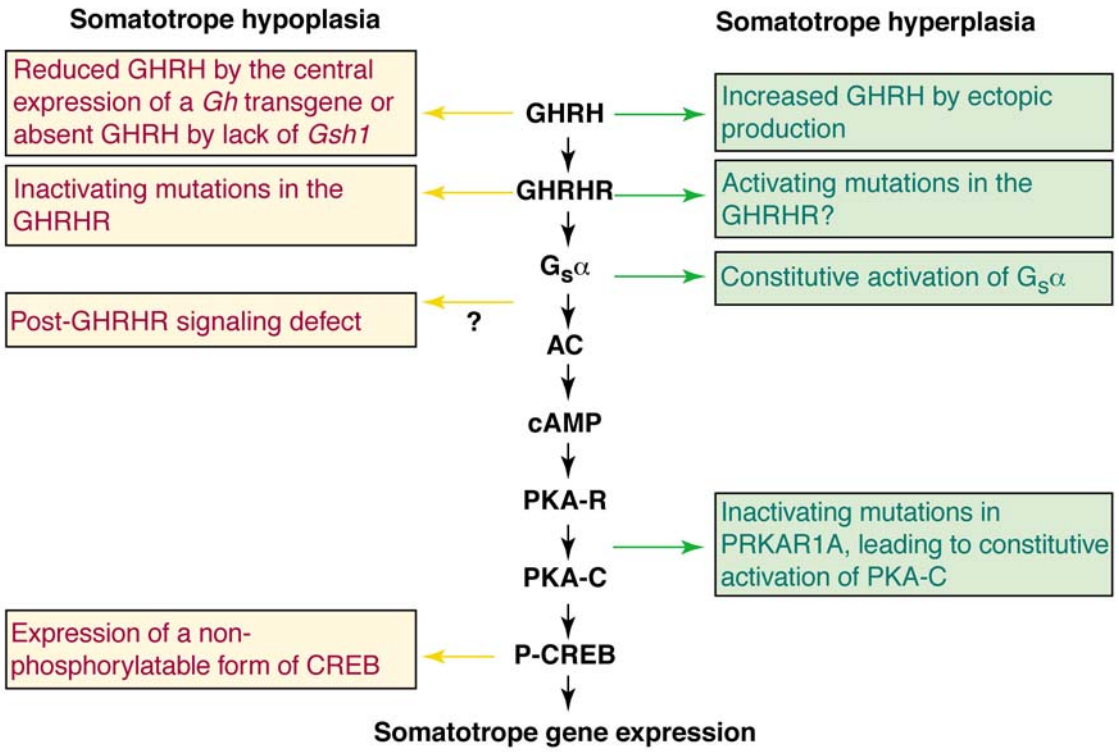

Figure 1-16 Spontaneous and experimental alterations in the GHRH signaling pathway that result in either somatotrope hypoplasia or hyperplasia

Abbreviations: AC, adenylyl cyclase; cAMP, cyclic adenosine monophosphate; GHRH, growth hormone-releasing hormone; GHRHR, GHRH receptor; Gsα, α-subunit of the receptor-associated G-protein complex; gsh1, genetic-screen-homeobox protein 1; P-CREB, phosphorylated cAMP-response element-binding protein; PKA-C, catalytic subunits of protein kinaseA; PKA-R, regulatory subunits of protein kinase A; PRKAR1A, protein kinase cAMP-dependent regulatory type 1α(a specific PKA-R). Adapted from (Frohman and Kineman, 2002a).

B. Growth Hormone Deficiency

Abnormal structure of the GH molecule or gene deletion as well as mutations in GHRH or GHRHR can lead to conditions such as isolated growth hormone deficiency (IGHD)(Alatzoglou and Dattani, 2010; Illig et al., 1971; Molina et al., 2003; Phillips et al., 1981) or GHR mutations lead to primary GH insensitivity (such as Laron Syndrome, a severe growth hormone-resistant short stature condition transmitted as an autosomal recessive trait) (Laron et al., 1966).

IGHD is the most common pituitary hormone deficiency resulting from congenital or acquired causes. The reported incidence of congenital IGHD is approximately 1 in 4,000–10,000 live births (Mullis, 2005). The known genes that are involved in the genetic etiology of IGHD include those encoding for GH (specifically *GH1*, the gene encoding GH), GHRHR, and transcription factor SOX3 (Laumonnier et al., 2002) and HESX1 (Thomas et al., 2001). There are four types of familial IGHD (Table 1-8, p.65): autosomal recessive (type

IA and IB), autosomal dominant (type II) and X-linked recessive (type III) (Procter et al., 1998). Mutations in *GH1* result from autosomal recessive (type 1A or type 1B) or dominant inheritance (type II). Mutations in GHRHR, resulting from autosomal recessive inheritance (type II), were first implicated in the etiology of IGHD in the spontaneous dwarf mouse model, known as the '*little mouse*'. The phenotype stems from a homozygous missense mutation (Asp60Gly) in the extracellular domain of the receptor gene (Gaylinn et al., 1999). Anterior pituitary development is not affected in the '*little mouse*', however the pituitary is hypoplastic and contains fewer than 10% of the expected number of somatotropes as well as other pituitary cells. The examination of this mouse model led to the finding that signaling via GHRHR is essential for the proliferation of the somatotrope lineage. Approximately 10% of patients with familial IGHD have mutations within the *GHRHR* (Salvatori et al., 2001). Children with *GHRHR* mutations often present with severe GH deficiency and short stature. However, they rarely present with neonatal hypoglycemia and microphallus, as seen in patients with *GH1* mutations. The reasons for this discrepancy remain undetermined, although it may likely reflect the degree of GH deficiency seen in these patients.

V. GENERATION OF NOVEL MICE BY ENU MUTAGENESIS

Traditional methods of generating animal mutants have involved the use of controlled exposure to mutagenic chemicals, notably ethyl nitrosurea (ENU), ethyl methylsulfonate or high doses of X-rays as well as more specific gene targeting (Strachan and Read, 1999) . Recently, there have been numerous large-scale mutagenesis screens on mice (Aigner et al., 2008; Bokryeon et al., 2009; Boles et al., 2009; Bradeen et al., 2006; Hagge-Greenberg et al., 2001; Kermany et al., 2006; Pawlak et al., 2008; Rathkolb et al., 2000; Reijmers et al., 2006; Rolinski et al., 2000; Soewarto et al., 2000). It is no surprise that mice have been the most widely used animal models of human disease. Mice can be maintained in breeding colonies at reasonable costs. They have a relatively short lifespan (~2-3 years) and generation time (~3 months; the average female mouse can produce four to eight litters of six to eight pups). Due to their ease of breeding, complex-breeding programs, such as those involving large-scale mutagenesis screens, can be organized for the production of recombinant inbred strains and congenic strains. Thus, the genetics of the laboratory mouse has been extensively studied for decades, and, not surprisingly, the phenotype of many mutants has been documented. The identification of these phenotypes has been made possible with the use of backcross methods and the availability of numerous polymorphic markers. Importantly, many of the mutations in mice show conservation with humans and have been well documented. This information has proven

to be extremely useful in identifying genuinely homologous single gene disorders in mouse and human.

Chapter 4 of this work examines a novel recessive dwarf mouse generated by ENU mutagenesis. The generation of these mice is detailed in Materials and Methods Chapter 2II.B.2 Dwarf Mouse Line Generated by ENU Mutagenesis, p.74.

Table 1-8 Isolated growth hormone deficiencies associated with severe short stature
hGH, human growth hormone; IGHD, isolated growth hormone deficiency; MRI, magnetic resonance imaging. Modified and adapted from (Pescovitz and Eugster, 2004)

NOTE:
This table is included on page 65 of the print copy of the thesis held in the University of Adelaide Library.

VI. HYPOTHESIS, AIMS AND SIGNIFICANCE

A. *Project 1*: Identification of *Sox3* Target Genes

While the role of Sox3 during brain development has been extensively studied, the target genes of *Sox3* remain unidentified. Hence, the first goal of this project was to identify potential direct/indirect target genes, and to focus in on the HP axis. It was hypothesized that comparisons between the three mouse lines would provide one, if not many, potential direct/indirect target genes identified by whether their expression was up- or down-regulated in the initial microarray investigation and subsequent validation experiments. Thus, the aim of the study was to examine the gene expression profiles associated with *Sox3*-deletion and Sox3-overexpression using cDNA microarray. Genes differentially expressed were predicted to have biological activity influencing differentiation, survival and proliferation. Furthermore, changes associated with a loss-of-function and gain-of-function of Sox3 may contribute to a better understanding of other important genes, currently not known, involved in X-linked hypopituitarism and/or X-linked mental retardation.

B. *Project 2*: Novel Dwarf Mouse Generated by ENU Mutagenesis

Growth-retarded mice present an invaluable model to elucidate the molecular mechanisms involved in regulating growth, body size, and the genetic influences thereon. There have been many growth-retarded mouse models generated from spontaneous genetic dwarfism mutations. These mutant models have provided a useful system with which to elucidate the mechanisms of GH regulation and transcription factor interplay. However, dwarfism is not limited to disorders affecting genes of the pituitary gland (e.g. *GH1*) and hypothalamus (*GHRHR*). This study identified and further examined a novel recessive ENU mouse mutant, called *Tukku*, exhibiting HP axis dysfunction resulting in dwarfism, pituitary hypoplasia and GH as well as GHRH deficiency. The mutation was identified as a leucine to proline substitution (L30P) in tryptophanyl-tRNA synthetase (*Wars*), a member of the aminoacyl-tRNA synthetase enzyme family that link amino acids to their specific tRNAs. The overall aim of this study was to characterize the primary pathology of the dwarfism phenotype, focusing specifically on the somatic-growth axis, to understand the function of the mutation in regulating the HP axis (*Aim 1*); confirm the mutation by sequencing (*Aim 2*); and examine the expression of the mutant protein, specifically focusing on the HP axis (*Aim 3)*

2 Materials and Methods

I. BUFFERS AND SOLUTIONS

A. Commercially Obtained

1. Compounds, buffers and solutions

Table 2-1 Compounds, buffers and solutions

Name	Supplier
Bovine Serum Albumin (BSA)	Sigma Aldrich
DEPC H_2O	Invitrogen
Agarose (DNA Grade)	Progen Biosciences
Chloroform	Sigma Aldrich
Phenol:Chlorofom:Isoamyl alcohol	Sigma Aldrich
Trizol	Invitrogen
Formaldehyde Solution (40%)	AnalaR (MERCK Pty Ltd)
Tween 20 Solution (10%)	Bio-Rad Laboratories (Hercules, CA)

2. Histology

The following solutions were prepared by Nadia Gagliardi, Anatomical Sciences, University of Adelaide, Adelaide, Australia: Haematoxylin, Eosin, Cresyl, and Masson Trichome.

3. Indicators, antibodies and enzymes

Table 2-2 Indicators and antibodies

Name	Supplier
5-bromo-4-chloro-3-indolyl phosphate, BCIP	Roche
Digoxenin-11-UTP	Roche
4-nitroblue tetrazolium chloride, NBT	Roche
Anti-digoxigenin-AP, Fab fragments	Roche

Table 2-3 Antibodies used in the detection of proteins by immunofluorescence analysis

Name	Type	Source	Dilution	Reference
GFP	Goat polyclonal	Rockland	1:400	(Sutton et al., 2011)
Ngn3	Mouse monoclonal	Dr. Michael German, Diabetes Center, University of California, San Francisco, USA.	1:1000	(Lee et al., 2001)
PECAM (CD-31)	Rat polyclonal	Santa Cruz	1:100	(Sutton et al., 2011)
Sox3	Goat polyclonal	R&D	1:100	(Rizzoti and Lovell-Badge, 2007; Sutton et al., 2011)
Wars	Mouse monoclonal; raised against the human N-terminus of residues 50-150	Abcam	1:1000	-
VE-Cadherin (CD-144)	Goat polyclonal	R&D	1:500	(Huber et al., 2002)

Table 2-4 Secondary fluorescence antibodies used in the detection of proteins by immunofluorescence.

When more than one type is listed, this indicates that, depending on the combinations of primary antibodies used, species-appropriate combinations of secondary sera were used.

Name	Type	Source	Dilution
Alexa-488	Donkey anti-Goat	Invitrogen	1:400
Cyanine-3	Donkey anti-Rabbit, -Mouse and -Goat	JacksonImmunoResearch	1:400
Cyanine-5	Donkey anti-Rabbit, -Mouse and -Goat	JacksonImmunoResearch	1:400
Prolong Gold Antifade Mounting Medium with DAPI	-	Invitrogen	-

Table 2-5 Enzymes

Name	Supplier
Proteinase K	Sigma Aldrich
Restriction endonucleases	New England Biolabs
SP6 RNA Polymerase	Roche
T4 Polynucleotide Kinase, 3' phosphatase free	Roche
T4 DNA Ligase	Roche
T4 DNA Polymerase	New England Biolabs
T7 RNA Polymerase	Roche
Taq DNA Polymerase, Recombinant	Invitrogen
ABI Prism™ Dye Terminator Cycle Sequencing Ready Reaction Mix	Perkin-Elmer

4. *Specialty kits*

Table 2-6 Specialty kits

Name	Supplier
Applied Biosystems RNA to cDNA	Applied Biosystems
BCA Protein Assay	Pierce
FAST SYBR	Applied Biosystems
High Pure PCR Preparation Kit	Roche
MasterAmp™ PCR Optimization Kit (without ammonium sulfate)	Epicentre Biotechnologies
pGem®-T Vector System I	Promega
QIAquick PCR Purification Kit	QIAGEN
QIAGEN® Plasmid Midi Kit	QIAGEN
QIAshredder™	QIAGEN
Rat/Mouse Growth Hormone ELISA Kit (Cat. EZRMGH-45K)	Millipore
RNeasy® Mini Kit	QIAGEN
RNeasy® Plus Mini Kit	QIAGEN
Zymoclean™ Gel DNA Extraction Kit	Zymo Research

5. *Preparation of DNA oligonucleotides*

DNA oligonucleotides were synthesized and purified by Geneworks Pty Ltd (Thebarton, South Australia, Australia). Oligonucleotides were designed using Primer3 (http://frodo.wi.mite.edu/primer3/) (Rozen and Skaletsky, 2000) and were analyzed using NetPrimer (http://www.premiersoft.com/netprimer/). NetPrimer, a free web tool, allows for the analysis of oligonucleotide secondary structures including hairpins, self-dimers, and cross-dimers, ensuring the availability of the oligonucleotide for the reaction as well as minimizing primer-dimer formation. Gene-specific primer pairs used in qPCR experiments were designed to cross intron-exon boundaries.

Table 2-7 PCR primers for genotyping *Sox3*-null mice

Sequence is in the 5′ → 3′ direction. Abbreviations: m, mouse; F, forward primer; R, reverse primer. In parenthesis is the primer reference number for the lab.

Primer Name	Sequence
m*Sry*F1 F (288)	CAC TGG CCT TTT CTC CTA CC
m*Sry*R1 R (289)	CAT GGC ATG CTG TAT TGA CC
EGFP F (238)	ATG GTG AGC AAG GGC GAG GAG CTG TT
EGFP R (239)	CTG GGT GCT CAG GTA GTG GTT GTC
Gapdh F (234)	CTT GCT CAG TGT CCT TGC TG
Gapdh R (235)	ACC CAG AAG ACT GTG GAT GG

Table 2-8 PCR primers for genotyping *Sox3* transgenic and GFP reporter mice

Sequence is in the 5′ → 3′ direction. Abbreviations: m, mouse; F, forward primer; R, reverse primer. In parenthesis is the primer reference number for the lab.

Primer Name	Sequence
mTg*Sox3* F Primer (342)	CTG GGT TAG AGA GCA GCA TCC
mTg*Sox3* R Primer (343)	GAG TGT TGG AGG GGG TTG AG
NSXRch10WT R Primer (347)	GTC CTA CTC CCT CAA CAC CTG TC
m*Sry*F1 F (288)	CAC TGG CCT TTT CTC CTA CC
m*Sry*R1 R (289)	CAT GGC ATG CTG TAT TGA CC

Table 2-9 PCR primers for genotyping the dwarf mouse line

Sequence is in the 5′ → 3′ direction. F, forward primer; R, reverse primer. In parenthesis is the primer reference number.

Primer Name	Sequence 5′ → 3′
D12Mit7_F (632)	CCG GGG ATC TAA AAC TAC AT
D12Mit7_R (633)	TCT AAT CTC AGC CCA ATG GT
D12Mit79_F (634)	GAG GGA TGG ATG CAA TAG TCA
D12Mit79_R (635)	AAT CCA GCA TCT GAT TAA ACT CC

Table 2-10 qPCR primers used for the validation of microarray results (*Project 1*)

Sequence is in the 5′ → 3′ direction. F, forward primer; R, reverse primer.

Gene	Forward Primer (F) and Reverse Primer (R) in the 5′ → 3′ direction
Nenf	F: GGA TCC AGC AGA CCT CAC TC R: TGG CTT TGT ACA CCT TGC TG
GAPDH	F: ATG CCA GTG AGC TTC CCG TTC AGC R: ACC CAG AAG ACT GTG GAT GG
Ngn3	F: CCC CAG AGA CAC AAC AAC CT R: AGT CAC CCA CTT CTG CTT CG
Sox3	F: GAA CGC ATC AGG TGA GAG AAG R: GTC GGA GTG GTG CTC AGG
Sfrp1	F: AGT TGA AGT CAG AGG CCA TCA R: CCA GCT TCA AGG GTT TCT TCT
Nfya	F: ACA CAA CCA GCA GTG GAC AA R: CCA TCA TGA CCA TTC CTC CT

Table 2-11 qPCR primers used for analyzing *Ghrh* and *Sst* in dwarf mouse hypothalamic extracts (*Project 2*)

Sequence is in the 5′ → 3′ direction. F, forward primer; R, reverse primer.

Gene	Forward Primer (F) and Reverse Primer (R) in the 5′ → 3′ direction
Ghrh	F: CTGTATGCCCGGAAAGTGAT R: AAGGCTTCATCCTTGGGAAT
Sst	F:CCCCAGACTCCGTCAGTTT R: CCTCATCTCGTCCTGCTCA

B. Laboratory Prepared Buffers and Solutions

Table 2-12 Laboratory prepared general buffers and solutions

Name	Ingredients	Use
1xGlycine-Tris-HCl-SDS	192mM Glycine, 25mM Tris-HCl, 0.1% SDS	western blots
Agarose gel loading dye (6X)	30% glycerol, 0.2% (w/v) bromophenol blue, 0.2%(w/v) xylene cyanol	PCR
Coomassie Blue	8% ammonium sulphate, 1.6% phosphoric acid, 0.08% CBB G-250 and 20% methanol	SDS-PAGE
Embryo Lysis Buffer	50mM KCl, 10mM Tris-HCl (pH 8.3), 2mM MgCl2, 0.1mg/mL Gelatin, 0.45% Nonident P40, 0.045% Tween 20	protein extraction
Formaldehyde (4%)	4% formaldehyde (diluted from 40%) in 1× PBS	Tissue fixative
Gel drying solution	35% ethanol, 5% glycerol	SDS-PAGE
Gel fixative solution	40% ethanol, 10% acetic acid	SDS-PAGE
Hybridization buffer	50% formamide (deionised), 5× SSC, 2% Blocking Reagent (Boehringer Mannheim), 0.1% Tween-20, 0.5%	*in situ* hybridization
lysis buffer (embryonic yolk-sac/tail)	1M Tris; 0.5M EDTA; 5M Extra-Sox3; 10% SDS	Phenol:Chloroform extraction
No-EDTA whole-extract cell lysis buffer	420mM NaCl, 25% glycerol, 0.5% NP-40, 1.5mM MgCl, 20mM Hepes (pH7.5)	protein expression
PBST	1× PBS, 0.1% Tween 20	various
Phosphate Buffered Saline (PBS)	30mM NaCl, 2.5mM KCl, 10mM Na2HPO4, 30mM NaH2PO4, HCl to pH 7.4	various
SDS loading buffer (2x)	62.5mM Tris-HCl pH 7.0, 4% SDS, 15% Glycerol, 0.02% Bromophenol Blue	SDS-PAGE
Sodium Citrate Buffer	0.1% (w/v) sodium citrate, 0.1% Triton X-100, 1× PBS	various
TBE (20X)	1.8 M Tris, 1.8 M boric acid, 0.05 M EDTA, pH 8.3	various
Western blot transfer buffer	192mM Glycine, 25mM Tris-HCl, 15% Methanol	western blots

II. MOUSE BREEDING AND LINES

A. Maintenance and Breeding

1. *General maintenance*

All mice used in this study were bred at the University of Adelaide Laboratory Animal Services. All procedures were approved by the University of Adelaide Animal Ethics Committee and conformed to *Australian Code of Practice for the Care and Use of Animals for Scientific Purposes* guidelines (National Health and Medical Research Council, 2004). Mice were housed in groups of two to six, with autoclaved, white pine shavings as bedding, under 12-hour light/12-hour dark photoperiods (lights on at 0600 h), with *ad libitum* access to water and food. The University of Adelaide Laboratory Animal Services performed general maintenance of the colonies in addition to obtaining tail snip samples for genotyping.

2. *Timed matings*

Females (one and/or two; no more than two) were housed with the designated male in one cage overnight for approximately 16-h. The presence of a vaginal copulation plug was taken as evidence of mating, and noon of the day of discovery was defined as 0.5 days post coitum (dpc) was defined as noon of the day of discovery. The University of Adelaide Laboratory Animal Services performed checking of copulation plugs.

B. Mouse Lines

1. *Sox3 transgenic lines*

To gain insight into the development of the HP axis in XH, three mouse models, previously generated, were used: (1) lacking *Sox3* (*Sox3*-null) (Rizzoti et al., 2004), (2) over expressing Sox3 (Extra-Sox3) (Sutton et al., 2011) and (3) normal levels of Sox3 (Green-Sox3) (unpublished mouse line, P. Thomas). Each line was generated using enhanced-green fluorescent (eGFP) protein or an internal ribosome entry site-enhanced-GFP (IRES-eGFP) reporter cassette (described below). The use of GFP in mouse molecular genetics and generation of transgenic mouse models has become an extremely versatile tool for tracking and quantifying biological entities as well as in high-throughput screening and gene discovery. GFPs have been identified in a wide range of coelenterates, and, while recently the number of cloned GFPs has expanded, to date the best-characterized proteins are those from the jellyfish *Aequorea victoria* and the anthazoan *Renilla reniformis*.

a. *Sox3-null*

The *Sox3*-null mouse line was generated using homologous recombination in embryonic stem cells (Rizzoti et al., 2004). Briefly, the *Sox3* ORF was replaced with a marker gene encoding enhanced eGFP protein downstream. This allowed the expression of eGFP to be driven by *Sox3* regulatory sequences. *Sox3*-null mice exhibit a range of phenotypes, as described in Chapter 1II.C The Role of Sox3 in Hypothalamo-Pituitary Axis Development (p.56).

b. *Extra-Sox3*

The Extra-Sox3 mouse line was generated using BAC-recombineering. Briefly, these mice were generated by pronuclear injection, using a modified 36kb *Sox3* genomic fragment containing all of the known regulatory elements required for Sox3 expression (Brunelli et al., 2003). To enable detection of the transgene, an IRES-eGFP reporter cassette was inserted into the 3′ untranslated region (3′UTR) of *Sox3* using homologous recombination. The transgene construct was derived from a modified BAC clone (RP23-174O19) containing IRES-eGFP reporter cassette. Interestingly, one mouse phenotype, with XX male sex-reversal was identified (Sutton et al., 2011). Only mice that *did not* show XX male sex-reversal were used in this body of work. Extra-Sox3 mice exhibit specific developmental defects in forebrain structures that resemble XH patients. Extra-Sox3 embryos exhibit live-GFP signal in the CNS in a Sox3 pattern. However, it is not yet clear how much Sox3 is generated in these embryos.

c. *Sox3-GFP reporter (Green-Sox3)*

A Sox3-eGFP reporter transgenic mouse line expressing normal levels of Sox3 (Green-Sox3) were generated (by A/Prof Paul Thomas) from a modified BAC in which the *Sox3* ORF was replaced with the eGFP coding sequence. A 36kb fragment, which contains identical regulatory sequences that were used to generate the Extra-Sox3 mice, was microinjected to generate transgenic founders. These mice express normal levels of Sox3 in eGFP cells and were generated to serve as a wild-type controls for gene profiling (by microarray) and related experiments.

In all mice the insertion of the eGFP reporter enables detection of transgene expression by epifluorescence microscopy and in a pattern consistent with that of Sox3. Schematic representation of the *Sox3*-null, Extra-Sox3 and Sox3-GFP (Green-Sox3 reporter) constructs is shown in Figure 3-1 (p.106) of Chapter 3 Identification of *Sox3* Target Genes.

2. *Dwarf Mouse Line Generated by ENU Mutagenesis*

Dwarf mice were generated at The Australian Phenomics Centre (APC, Australian National University, Canberra, Australia) using N-ethyl-N-nitrosurea (ENU) mutagenesis. It is worth noting that the breeding schemes used in generating ENU mutations vary according to the allelic characteristics required (that is, whether screening for dominant or recessive mutations) and the strains required for subsequent gene mapping (Acevedo-Arozena et al., 2008). For dominant mutations, ENU-treated males (G0) are crossed with wild-type females to produce G1 individuals that are then assayed for the dominant mutation (Acevedo-Arozena et al., 2008). For recessive mutations, pedigrees are bred by intercrossing the offspring of a G1 individual (G2) or crossing them back to the original G1, thus making homozygous mutations in a proportion of G3 offspring (Figure 2-1, p.75).

Briefly, the generation of dwarf mice involved, a single 250-mg/kg dose of ENU (Sigma Aldrich, St. Louis, MO, USA) that was injected intravenously into 8-week-old male C57BL/6 mice. Mice were returned to their cages, for approximately 4 weeks to recover and then crossed to untreated C57BL/6 females. G1 mice were screened for obvious external abnormalities. Animals with a phenotype of interest, in this case, animals that were dwarf, were mated to wild-type C57BL/6 mice.

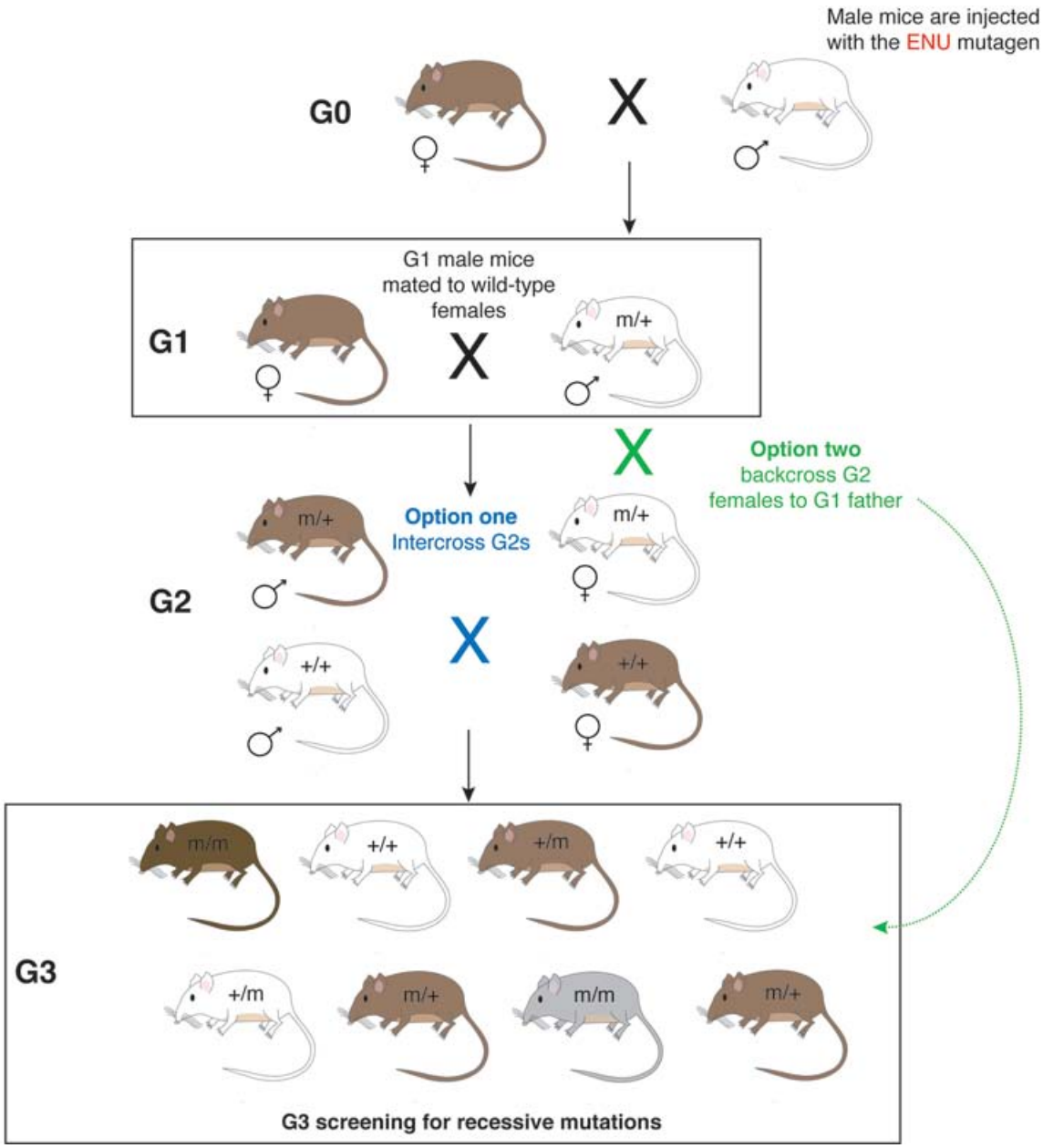

Figure 2-1 Strategy of ENU breeding for screening recessive pedigrees

Male mice are treated with N-ethyl-N-nitrosourea (ENU) and after a period of sterility are mated to wild-type (+/+) females. G1 male mice, heterozygous for N-ethyl-N-nitrosourea (ENU)-induced mutations (m/+), are mated to wild-type females. Their offspring (G2) are then either intercrossed or mated back to the original G1. Recessive (+/m) and dominant (m/+) mutations can then be detected in the resultant G3 progeny. Coat colors are shown as different to emphasize what the mutagenized strain and the wild-type females should be from different inbred strains so that G3 mice can be used for mapping purposes.

III. EMBRYO AND TISSUE COLLECTION

A. Embryo Collection

Pregnant females were dissected at various developmental time points (as discussed in results of each chapter). Embryos were dissected free of maternal decidual tissue and studied under a dissection microscope (Nikon SMZ1000 GFP Dissection Microscope, Nikon, Japan) attached to an Olympus DP70 Camera (Olympus, Japan) with a short-wave U, which excites eGFP at 485/20 nm. For embryos collected from the Sox3 mouse lines, one application of eGFP fluorescence was to determine the extent of expression; this was in addition to confirmation of genotype by PCR. Embryos were photographed for documentation under both the bright light exposure and eGFP fluorescence (Figure 2-2, below). Mouse embryos were staged according to somite numbers (Figure 2-3, p. 77), although some variation was observed in developmental stage both between and within litters at the given embryonic ages.

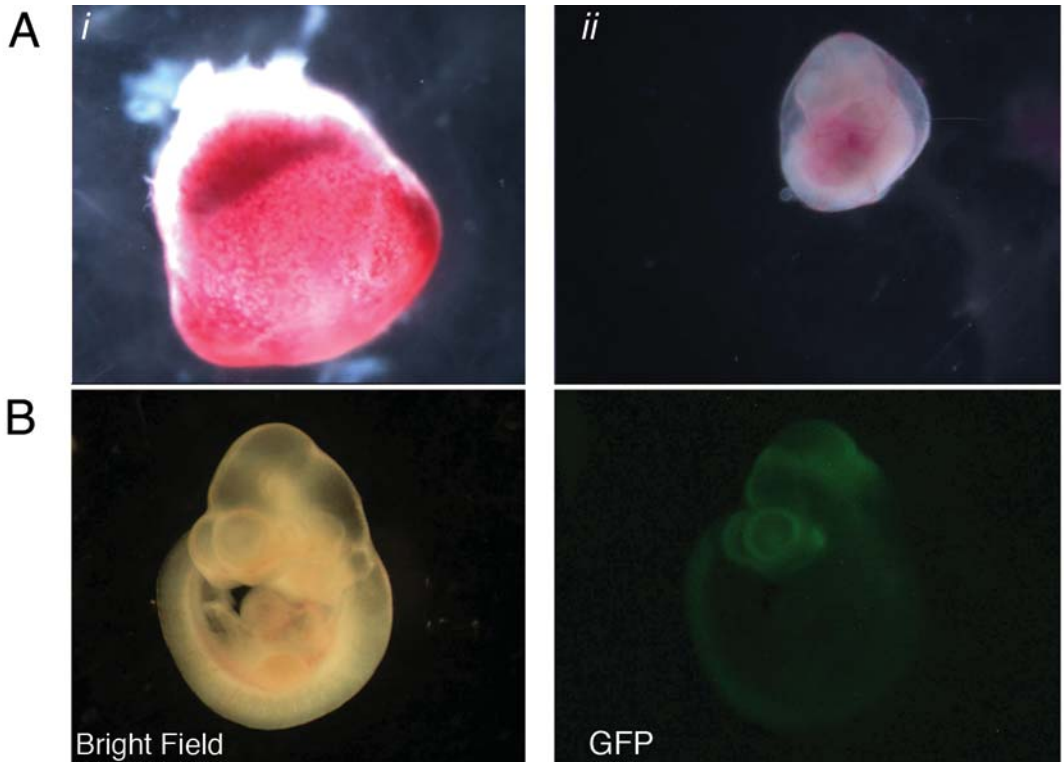

Figure 2-2 Embryo dissection at 10.5 dpc showing live GFP in *Sox3*-null embryos
(A) Representative image of a dissected embryonic pod (*i*) at 10.5 dpc and the yolk sac, containing a mouse embryo (*ii*), dissected from the pod shown in (*i*). (B) Bright field and live-GFP images of the *Sox3*-null embryo dissected and shown in A.

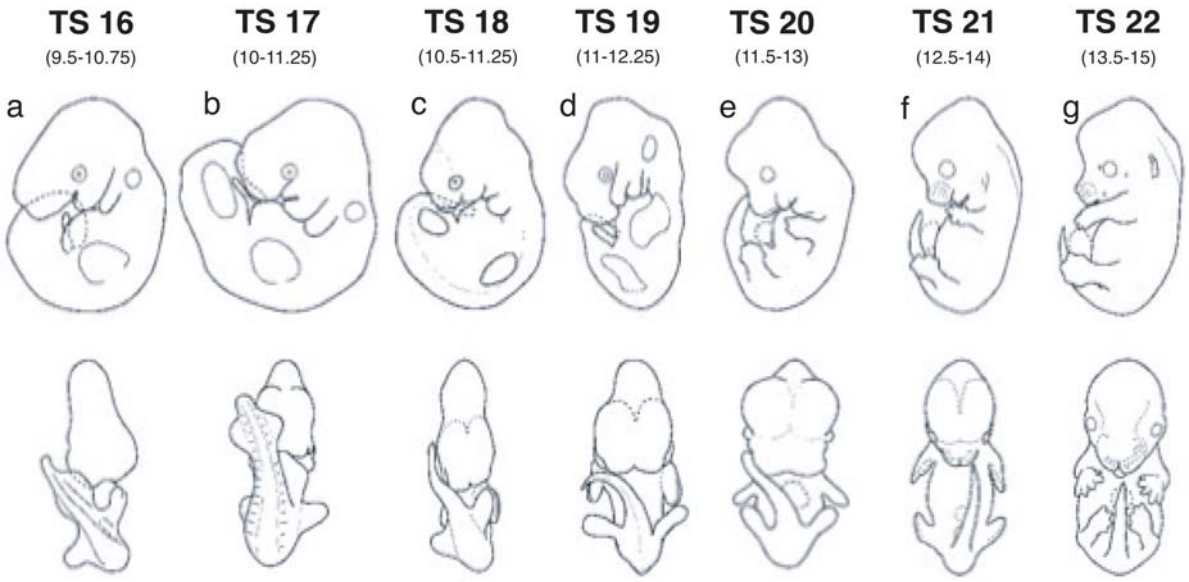

Figure 2-3 Theiler staging of mouse embryos between 9 – 15 dpc
(a) Posterior neuropore closes, Formation of hind limb & tail buds, lens plate, Rathke's pouch; the indented nasal processes start to form30-34 somites. Absent thin & long tail. (b) Deep lens indentation, advanced development of brain tube, tail elongates and thins, umbilical hernia starts to form 35-39 somites. Absent nasal pits. (c) Closure of lens vesicle, nasal pits, cervical somites no longer visible 40-44 somites. Absent auditory hillocks, anterior footplate. (d) Lens vesicle completely separated from the surface epithelium. Anterior, but no posterior, footplate. Auditory hillocks first visible 45-47 somites. Absent retinal pigmentation and sign of fingers (e) Earliest sign of fingers (splayed-out), posterior footplate apparent, retina pigmentation apparent, tongue well-defined, brain vesicles clear 48-51 somites. Absent 5 rows of whiskers, indented anterior footplate. (f) Anterior footplate indented, elbow and wrist identifiable, 5 rows of whiskers, umbilical hernia now clearly apparent 52-55 somites. Absent hair follicles, fingers separate distally. (g) Fingers separate distally, only indentations between digits of the posterior footplate, long bones of limbs present, hair follicles in pectoral, pelvic and trunk region 56-~60 somites. Absent open eyelids, hair follicles in cephalic region. For full descriptions of Theiler staging and mouse anatomy visit http://genex.hgu.mrc.ac.uk/Atlas/intro.html

B. Tissue Collection and Processing

1. RNA processing of mouse embryonic 10.5 dpc mouse heads used in microarray analysis

Pregnant female mice were culled by cervical dislocation at 10.5 dpc. Embryos were dissected free from decidual tissue in cold RNAase-free PBS. Heads dissected at the 2nd branchial arch and immediately placed into RNeasy Solution (Qiagen, CA, USA) and stored at -80C until ready to extract RNA. A small section of the embryonic tail tip was removed from each embryo for genotyping.

Total RNA was isolated using the RNeasy Protect Cell Mini Kit (Qiagen, CA, USA) following manufacturer instructions. Whole heads were briefly disrupted using sonication (5 seconds, 50kHz) in order to produce suspensions without aggregates, and then homogenized using QIAshredder columns (Qiagen, CA, USA) to reduce viscosity

caused by high-molecular-weight cellular components and cell debris. Purified total RNA was resuspended in 50µL of RNAase-free water. A maximum of 12 extractions were done at any one time to minimize loss of RNA quality. Determination of RNA integrity and concentration are described in Section XIV.B Analysis of RNA Quality, p.93.

2. *RNA processing of hypothalamic sections used in mRNA expression analysis by qPCR*

Hypothalamic regions were dissected (as shown in Figure 2-4) and explants were processed using Trizol™ (Invitrogen, CA, USA) as per manufacturer's instructions. The Trizol™ method of RNA extraction is better suited for extracting RNA from large tissue samples, such as brain.

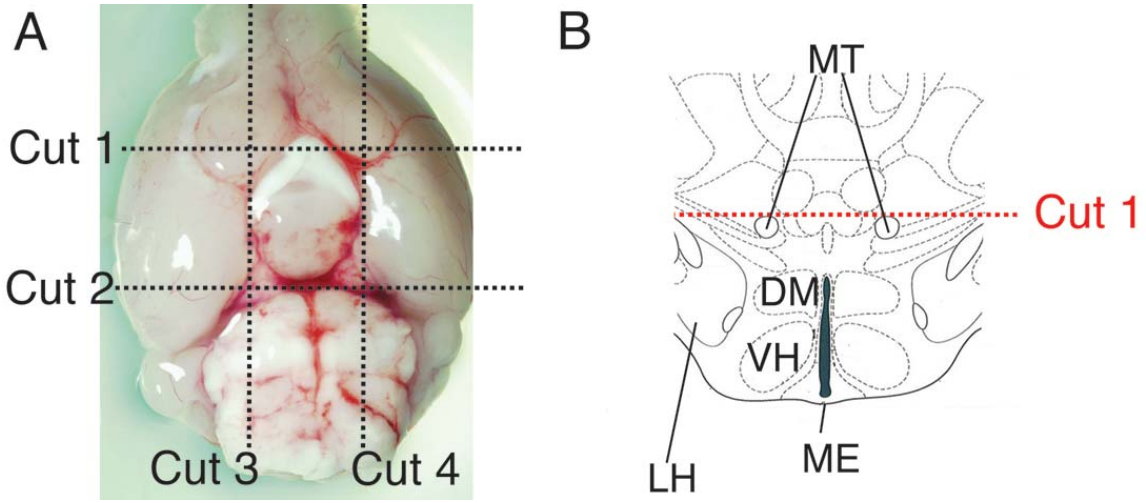

Figure 2-4 Schematic representation of hypothalamic dissection in 8-week old mice
(A) Ventral view of a wild-type mouse brain, showing the hypothalamic (Hyp) region and the optic chiasm (OCh). Dotted lines indicate the dissection path. (B) Coronal view through the region cut in A by Cut 1. To completely isolate the hypothalamic region a further three cuts were made (indicated by red dotted lines). Abbreviations: MT, mammillothalamic tract; DM, dorsomedial hypothalamic nuclei; VH, ventromedial hypothalamic nuclei; LH, lateral hypothalamic nuclei.

Briefly, once RNA was extracted, 50ng of each sample was reverse transcribed using the High Capacity RNA-to-cDNA kit (Applied BioSystems, CA, USA). qPCR was performed using Fast SYBR Green Master Mix (Applied BioSystems, CA, USA) and run on an ABI 7500 StepOnePlus System (Applied BioSystems, CA, USA).

3. *Isolation of protein from whole pituitaries for GH analysis*

Whole pituitaries were dissected from dwarf and wild-type animals, placed in microfuge tubes and snap frozen in dry ice (dry ice slurry made with isopentane and dry ice in a metal container). Samples were stored at -80C until ready for processing.

Protein extraction commenced with the addition of 100µl lysis buffer (No-EDTA whole-extract cell lysis buffer: 420mM NaCl; 25% Glycerol; 0.5% NP-40; 1.5mM MgCl; 20mM Hepes pH 7.5; H_2O) containing 15µl protease inhibitor cocktail (Protease Cocktail Inhibitors, Mini Protease Inhibitor Cocktail, Roche, CA, USA; Roche Cat No. 11 836 153 001). Pituitaries were sonicated in lysis buffer for 30 seconds then incubate on ice for 30 minutes. Pituitaries were then incubated at 4C on a nutator mixer[3] for 2 hours and then centrifuged (4C max speed) for 15 minutes. The supernatant was collected and protein concentration was determined using BCA™ Protein Assay (Pierce, Rockford, IL, USA) according to manufacturer's protocol and using bovine serum albumin as the standard.

4. *Fixation and Tissue Preparation*

a. *Frozen Sections*

Embryonic tissues (embryos from the *Sox3* transgenic and null mouse lines as well as pituitaries from dwarf and wild-type animals) were collected at the indicated stages and fixed in 4% paraformaldehyde (PFA) in phosphate-buffered saline (PBS, 0.1M) at 4C overnight (for sectioning). Following overnight incubation tissue samples were washed 3 times for 10 minutes each in PBS (0.1M) to remove residual 4% PFA and then cryoprotected in 30% sucrose (made in 0.1M PBS) at 4C. Tissue samples were embedded in OCT (Tissue-Tek, Sakura Finetek, The Netherlands) and snap frozen in isopentane (Prolabo, Barcelona, Spain) cooled by dry ice. Embedded embryos were cut in serial sections (10-12µm; sagittal and/or coronal) using a Leica CM1900 Cryostat (Leica, Germany). Sections were mounted onto Superfrost Plus Slides (Menzel-Glaser, Braunschweig, Germany).

b. *Paraffin Sections*

Brain, ovary and testis tissue from dwarf and wild-type mice were processed into paraffin according to standard processing procedures (Bancroft and Gamble, 2007) by Nadia Gagliardi, Histology Services, School of Medical Science, University of Adelaide. Sections were mounted onto Superfrost Plus Slides (Menzel-Glaser, Braunschweig, Germany).

C. Preparation of Tail Tip Genomic DNA for PCR Genotyping

Genomic DNA (gDNA) from embryonic and adult mouse was isolated from tail tips (approximately 2mm; obtained at time of weaning or at embryo dissection) using the traditional phenol/chloroform method (Sambrook and Russell, 2001) or using the High

[3] a gentle three dimensional rotating, rocking mixer which is at a constant 20° angle @ 24rpms.

Pure PCR Template Preparation Kit (Roche Applied Science, Mannheim, Germany). The High Pure PCR Template Preparation Kit provided a less toxic and laborious method for the extraction of gDNA from adult mouse and embryonic tail tip. The protocol followed manufacturer specifications.

The traditional phenol/chloroform method used digested mouse-tail samples overnight (approximately 16-h at 55C) in lysis buffer (1M Tris; 0.5M EDTA; 5M Extra-Sox3; 10% SDS) and Proteinase K (5mg/ml). The following day the digest mix was centrifuged (14,000rpm; 5 minutes) to spin down undigested mouse tail-hair and other debris. The supernatant was transferred into a new microfuge tube to which Phenol:Chloroform:Isoamyl alcohol (1:1:1 ratio; Sigma Aldrich, St. Louis, MO, USA) was added. The digest mix was vortexed and spun (14,000rpm; 2 minutes). The top layer was transferred to a new tube and an equal volume of chloroform (approximately 180µl) was added. Again, the mix was vortexed and centrifuged (14,000rpm; 2 minutes). The top layer was transferred to a new tube and an equal volume of 100% isopropanol was added. Entire mix was vortexed and centrifuged (4C; 14,000rpm; 20 minutes). The supernatant was removed and 150µL 70% ethanol was added, followed by another vortexing and centrifugation at 4C 14,000rpm for 10 minutes). The final step involved removing the supernatant and air-drying the DNA pellet for 5-10 minutes. DNA was resuspended in 200µL of deionised H_2O.

IV. PCR GENOTYPING

PCR genotyping was carried out using the s1000 Thermal Cycler (Bio-Rad, Hercules, CA, USA).

A. *Sox3* Transgenic Lines

The genotyping of *Sox3* transgenic mouse lines involved a multiplex PCR assay using 2 X MasterAmp Premix buffer (Epicentre® Biotechnologies, Madison, Wisconsin, USA) and Taq DNA Polymerase, Recombinant (Invitrogen, CA, USA). Standard reaction conditions were 50ng each primer, 2U Taq DNA Polymerase (Invitrogen, CA, USA) and up to 10ng template DNA in a 20µl reaction. The 2 X MasterAmp Premix buffers (Epicentre® Biotechnologies, Madison, Wisconsin, USA) were Buffer J (Epicentre® Biotechnologies, Madison, Wisconsin, USA) for use in PCR assays for *Sox3*-null, and D, Extra-Sox3 and Green-Sox3 reporter mice lines. DNA fragments were analyzed by electrophoresis on an ethidium bromide stained agarose gel (1-1.5%). Primer sets used for genotyping are shown

in Table 2-7 (p.70) and Table 2-8 (p.70). Cycling conditions are shown on the next page in Table 2-13.

Table 2-13 PCR analysis cycling conditions for *Sox3* transgenic and null mouse lines

Mouse Line	Cycle	Time
Sox3-null		
	Denaturation	30 seconds at 95°C
	Elongation/35 cycles	30 seconds at 95°C
		1 minute at 60 °C
		2 min at 72 °C
	Extension period	5 min at 72°C
	Hold	22°C
Sox3-transgenic		
	Denaturation	30 seconds at 95°C,
	Elongation/35 cycles	30 seconds at 95°C
		1 minute at 60 °C
		40 seconds at 72 °C
	Extension period	5 min at 72°C
	Hold	22°C
Sox3-GFP Reporter		
	Denaturation	30 seconds at 95°C,
	Elongation/35 cycles	30 seconds at 95°C
		1 minute at 60 °C
		40 seconds at 72 °C
	Extension period	5 min at 72°C
	Hold	22°C

B. ENU Generated Dwarf Mice

The genotyping of the dwarf mouse line involved a multiplex PCR assay using 2 X MasterAmp Premix buffer (Epicentre® Biotechnologies, Madison, Wisconsin, USA) and Taq DNA Polymerase, Recombinant (Invitrogen, CA, USA). Standard reaction conditions were 50ng each primer, 2U Taq DNA Polymerase (Invitrogen, CA, USA) and up to 10ng template DNA in a 20µl reaction. The 2 X MasterAmp Premix Buffer K (Epicentre® Biotechnologies, Madison, Wisconsin, USA) was used. Genotyping of the dwarf mice was done using microsatellite markers. Microsatellite marker primer pairs for the genome scan were designed by the Australian Phenomics Facility (APF; Canberra, ACT, Australia) and were purchased from GeneWorks Pty Ltd (Thebarton, South Australia, Australia).

Primer sets used for genotyping dwarf mice are shown in Table 2-9 (p.70). Cycling conditions are shown in the table below (Table 2-14).

Table 2-14 PCR analysis cycling conditions for dwarf mouse lines.

Step/Cycle Number	Time/Temperature
Denaturation	20 seconds at 94°C,
Elongation/35 cycles	20 seconds at 55°C
	20 seconds at 72 °C
Extension period	3 min at 72°C
Hold	10°C

V. MOUSE PHYSIOLOGICAL STUDIES

A. Growth Analysis of Dwarf Mice

1. *Weight over time*

a. *Post-weaning*

Mice from the dwarf colony (wild-type, homozygous and heterozygous) were weighed at weaning, between 21-29 days, by Laboratory Animal Services (The University of Adelaide, South Australia, Australia). Each mouse was then weighed again at postnatal day (P) 30 and every 10 days thereafter, until mice reached P130. A total of 5 mating pairs were set-up. These produced a sufficient number of mice per sex and genotype (Table 2-15).

Table 2-15 Mouse numbers used in growth analysis over time
Abbreviations: P, postnatal day; +/dw, heterozygous dwarf; dw/dw, homozygous dwarf.

Sex	Genotype	Total Numbers Started	Numbers of Mice (per date and used in statistical analysis)	Comments
Female	wild-type	4	4 mice per date	No deaths recorded
	+/dw	8	P30-P40, n=8 P50, n=7 P60 > n=6	1 death recorded after P50 and 1 death recorded after P40. This reduced the number for all proceeding dates.
	dw/dw	5	P30-P50, n=5 P60 > n=4	1 death recorded after P50 This reduced the number for all proceeding dates.
Male	wild-type	6	P30-120, n=6 P130, n=4	2 deaths recorded after P130 This reduced the number for all proceeding dates.
	+/dw	7	P30-P50, n=7 P60>, n=6	1 death recorded after P60 This reduced the number for all proceeding dates.
	dw/dw	7	P30-120, n=7 P130, n=6	1 death recorded after P130 This reduced the number for only this time point.

b. *Pre-Weaning*

To further examine the extent of dwarfism, mice were examined at P1, P7 and P14. For each time point 3 breeding pairs were set up and pups were collected on the specified days (Table 2-16, p.69). Pups were sacrificed by CO_2 inhalation and then photo-documented against a ruler (showing cm; to show relative growth). Tail tips were taken for genotyping.

Table 2-16 Mouse numbers used in growth analysis at P1, P7 and P14
Abbreviations: P, postnatal day; F, female; M, male; +/dw, heterozygous dwarf; dw/dw, homozygous dwarf.

	Total Numbers		
Genotype	**P1**	**P7**	**P14**
wild-type	F: n=4 M: n=4	F: n=4 M: n=4	F: n=3 M: n=1
+/dw	F: n=3 M: n=1	F: n=5 M: n=4	F: n=2 M: n=4
dw/dw	F: n=4 M: n=3	F: n=2 M: n=2	F: n=3 M: n=1

2. *Body Length*

Body length, the distance between the tip of the nose and the base of the tail, was measured (centimeters) in 8-week old wild-type (n=6) and homozygous dwarf (n=6) mice.

B. Pituitary Growth Hormone Levels

To determine pituitary hormone level of GH, whole pituitaries were dissected, and processed for protein as described in Section III.B.3 Isolation of protein from whole pituitaries for GH analysis (p. 78). Pituitary GH levels were measured by the Rat/Mouse Growth Hormone ELISA Kit (Cat. EZRMGH-45K; Millipore, St. Charles, MO, USA) according to manufacturer protocol. This Rat/Mouse Growth Hormone ELISA kit is used for the non-radioactive quantification of GH in rat or mouse serum, plasma, tissue extracts or cell culture media samples. One kit is sufficient to measure 39 unknown samples in duplicate. Whole extract pituitary protein was measured for wild-type (male and female, n=4/sex), heterozygous (male and female, n=4/sex), and homozygous (male and female, n=4/sex) 8-week old mice. The ELISA assay was performed by Carlie DeLaine and Siti Hadzir (The University of Adelaide, Australia). Results were analyzed and graphed by Eva Szarek.

C. Blood Biochemistry: Examining IGF-1 levels

Blood was collected from 8-week old wild-type, heterozygous and homozygous dwarf mice by cardiac puncture following cervical dislocation. These samples were from mice whose whole pituitaries were processed for protein used in the GH ELISA (described above). Due to IGF-1 kit limitation, samples from wild-type and homozygous dwarf males and females (n=3 per group) were analyzed.

Blood (approximately 100-300µl/cardiac puncture per mouse) was collected into microfuge tubes and stored on ice. Blood samples were centrifuged and the serum was

collected into new microfuge tubes and stored at -80C until processing. IGF-1 assay (performed by Siti Hadzir and Carlie Delaine (The University of Adelaide, Australia)) was performed using the mouse IGF-1 kit (Catalogue Number DY791; R&D Systems, Minneapolis, MN, USA) as per manufacturer's instructions.

D. Expression of Hypothalamic GHRH and Sst by qPCR

To quantitate hypothalamic levels of *Ghrh* and *Sst*, hypothalami were surgically removed (as shown in Figure 2-4, p.78). *Ghrh* and *Sst* levels were measured in hypothalamic extracts by qPCR. The qPCR method is described in Section XVI (p.102).

E. Statistical Analysis

Data were expressed as mean±SEM, unless otherwise stated, for the indicated number of observations. Statistical significance of difference between groups was determined by using 2-tailed Student's t test or one-way ANOVA followed by appropriate post hoc tests.

VI. PURIFICATION OF DNA FOR SEQUENCING

A. Purification of DNA from Agarose Gels

DNA bands excised from agarose gels were purified using the Zymoclean™ Gel DNA Recovery Kit (Zymo Research, Irvine, CA, USA), according to the manufacturer's protocol.

B. Sequencing

DNA was sequenced using the ABI PRISM® BigDye™ v3.1 Terminator Ready Reaction Cycle Sequencing Kit with AmpliTaq™ DNA polymerase, FS (Applied BioSystems). Typically a sequencing reaction contained 1µL of purified double-stranded template DNA, 50 ng/µl of primer, 1.5µL of BigDye v3.1 Terminator mix, 5µL Better Buffer and Milli-Q water up to a 20 µL volume. Reactions were performed using the s1000 Thermal Cycler (Bio-Rad, Hercules, CA, USA), with the following conditions: 35 cycles of 96C for 3 minutes, 96C for 10 seconds, 50C for 10 seconds, and 60C for 4 minutes. Afterwards, the samples were purified as follows. Products were precipitated for 15 minutes at room temperature (~22C), following the addition of 60µL of 100% isopropanol and 20µL MQ-H_2O to each 20µL sequencing reaction. Precipitated DNA was pelleted by centrifugation for 5 minutes at 14,000 rpm and the supernatant was carefully removed by

pipetting. The pellet was washed by briefly vortexing in 200µL of 75% isopropanol. After 5 minutes of centrifugation at 14,000 rpm the supernatant was carefully removed, and the pellet was air-dried. Running of Dye Terminator gels was conducted by the Sequencing Centre at the Institute of Medical and Veterinary Science (Adelaide, Australia), and the output was returned as a Macintosh®-compatible chromatogram file that was then analyzed using freely available 4Peaks Software (Mek&Tosj, Amsterdam, The Netherlands) on the Mac OSX platform (http://mekentosj.com/science/4peaks/).

VII. BACTERIAL TECHNIQUES

A. Media and Solutions

All bacterial cell culture media (Table 2-17) as well as glassware was autoclaved (121C) prior to use and aseptic techniques were implemented to prevent contamination. Bacterial culture medium was prepared with distilled and deionised water. Where indicated, ampicillin was added from a sterile stock solution to the media after autoclaving. Bacteria were cultured in Luria Broth (LB) medium, supplemented with ampicillin (50µg/ml; D-(−)-α-Aminobenzylpenicillin sodium salt; Sigma Aldrich, St. Louis, MO, USA) to select for transformed populations. Bacterial cultivation was carried out at 37C overnight with constant agitation (225 rpm). Bacterial colonies were grown on Luria agar (L-agar) plates supplemented with ampicillin (50µg/ml).

Table 2-17 Bacterial growth media composition

Name	Composition
Luria broth (LB)	1% (w/v) bactotryptone; 0.5% yeast extract: 1% Extra-Sox3; pH 7.0; supplemented with ampicillin (100µg/mL)
Luria agar (L-agar) plates	LB; 1.5% (w/v) bactoagar supplemented with ampicillin (100µg/mL)
Super Optimal broth with Catabolite repression (SOC)	2% bactotryptone; 0.5% yeast extract; 10 mM Extra-Sox3; 2.5 mM KCl; 10 mM MgCl2; 10 mM MgSO4; 20 mM glucose.

B. Preparation of Chemically Competent *E.coli*

Escherichia coli (*E. coli*) strain DH5α® (Invitrogen Corp., CA, USA) cells were made chemically competent by the calcium chloride protocol, originally described by Cohen and colleagues (Cohen et al., 1972), and later modified by Sambrook and colleagues (Sambrook and Russell, 2001).

C. Bacterial Transformation by Heat Shock

In general, transformation of *E. coli* with plasmid DNA was performed by heat shock, using chemically competent DH5α® cells. DH5α® chemically competent cells were

prepared as follows. All cells were stored in 50 µl aliquots at –80C. Transformation was carried out using chemically competent E. coli DH5α® cells (Invitrogen, CA, USA) by performing heat shock. Briefly, chemically competent E. coli DH5α® cells (Invitrogen, CA, USA) were thawed on ice (from -80C). Plasmid DNA (~50ng) was directly added to 100µl of competent *E. coli* DH5α®(Invitrogen, CA, USA) cells and incubated on ice for 30 minutes. Bacteria were subsequently 'heat shocked' in a water bath at 42C for 30 seconds, and then returned to ice for 2 minutes. Pre-warmed SOC medium (250µl) was added to the bacteria, which were incubated at 37C for 1 hour with constant agitation (225 rpm). Aliquots of the transformed bacteria were plated (20-200µl) onto L-agar plates supplemented with ampicillin (50µg/ml) (Boehringer Mannheim, Australia), to select for bacteria expressing the appropriate antibiotic marker. L-agar plates were incubated at 37C overnight.

A single colony was selected from the L-agar plate and inoculated into 25ml of LB medium supplemented with ampicillin (50µg/ml) (Boehringer Mannheim, Australia) and incubated at 37C overnight with vigorous shaking (300 rpm). Bacterial cell cultures were grown to a cell density of approximately 3–4 x 10^9 cells per ml. The bacteria cultured overnight were pelleted and used for purification of plasmid DNA, as outlined below.

D. Purification of Plasmid DNA

The purification of plasmid DNA was carried out using the QIAfilter Plasmid Midi Kit (Qiagen, CA, USA). This method was used for the purification of DNA used for generating in situ hybridization probes. The procedure followed manufacturer's protocol. Briefly, overnight bacterial cultures were pelleted by centrifugation at 6000x g for 15 min at 4C and re-suspended in 4ml of Buffer P1 (Qiagen, CA, USA). 4 ml of Buffer P2 (Qiagen, CA, USA) was added and mixed thoroughly by vigorously inverting the sealed tube 4–6 times. The reaction was incubated at room temperature (15–25C) for 5 minute. Following the 5-minute incubation 4 ml of chilled (4C) Buffer P3 (Qiagen, CA, USA) was added and the solution was mixed immediately and thoroughly by vigorously inverting the tube 4–6 times. The lysate was transferred immediately into the barrel of the QIAfilter Cartridge and incubated at room temperature (15–25C) for 10 minutes. The lysate was filtered into a QIAGEN-tip 100 (Qiagen, CA, USA), previously equilibrated with 4ml of QBT Buffer (Qiagen, CA, USA), and allowed to enter the resin by gravity flow. The QIAGEN-tip 100 was washed in 2 x 10ml Buffer QC (Qiagen, CA, USA). DNA was eluted in 5ml Buffer QF (Qiagen, CA, USA). DNA was precipitated in 3.5ml room-temperature isopropanol and centrifuged at 15,000x g for 30 minutes at 4C. The DNA pellet was washed in 2ml of 70% ethanol at room temperature and centrifuged at 15,000x g for 10 minutes at 4C. The pellet

was air-dried for 10 minutes and re-suspended in 10mM tris-EDTA (TE) Buffer (pH 8.0) [10 mM Tris-HCl, pH 8.0; 1 mM EDTA]. To quantify nucleic acid purity, concentration and yield of DNA obtained from this plasmid purification process, spectrophotometric analysis on individual samples was conducted using a spectrophotometer. In addition, the success of the plasmid purification procedure was confirmed on an analytical gel. Small aliquots were removed during the purification procedure from the following four steps: 1. The cleared lysate; 2. flow-through; 3. combined Buffer QC (Qiagen, CA, USA) wash fractions, and 4. Buffer QF (Qiagen, CA, USA) eluate. 2µl of each sample was run on a 2% agarose gel for analysis of fractions at each stage.

VIII. FLUORESCENCE IMMUNOHISTOCHEMISTRY

The preparation of sections for immunohistochemistry is outline in Section 4 Fixation and Tissue Preparation (p.79).

Cryosections were washed in PBS + 0.1% Tween-20 (PBS-T), pre-blocked in 10% heat-inactivated sheep serum (HISS) in PBS-T and incubated overnight at 4C with primary antibody solutions made in 10% HISS in PBST in a humidified chamber. Following incubation, sections were washed in PBS, followed by incubation in a humidified chamber (air tight container containing wet paper towel) with secondary antibodies for 5-8 h at room temperature. Sections were mounted and examined using microscope. Refer to Table 2-3 (p.68) for a list of primary antibodies and Table 2-4 (p.68) for a list of secondary fluorescence antibodies used in the detections of proteins by immunofluorescence (immunostaining).

IX. *IN SITU* HYBRIDIZATION

A. Purification of Plasmid DNA by Restriction Enzymes

cDNA inserts were isolated from plasmid DNA by restriction enzymes (RE; New England Biolabs) in the appropriate buffers (New England Biolabs), as specified by the manufacturer. Plasmid DNA (4µg) was digested for 1 hour at 37C using the appropriate RE in a final solution of a 1x reaction buffer in 50µl. 100-200 ng of uncut and cut digest was separated by elecrophoresis on a 1% agarose gel using a 1x Tris Borate Electrophoresis buffer (TBE; pH 8.0). To the remaining ligation 50µl Milli-Q H_2O was added followed by addition of 100µl Phenol:Chloroform:Isoamyl alcohol (Sigma Aldrich, St. Louis, MO, USA) vortexing and centrifugation at 14,000 rpm for 2 min. The aqueous layer (top layer) was removed into a new microfuge tube and ethanol precipitated using 1/10 sodium acetate

(1/10 of the volume obtained from aqueous layer) plus 2 volumes ethanol (100%) (2 x volume of aqueous layer). The precipitate was frozen at -20C for 30 mins followed by centrifugation at 14,000 rpm for 15 min. The supernatant was removed and discarded. The remaining pellet was washed in 500µl 70% ethanol by centrifugation at 14,000 for 10 mins and resuspended in 10µl of MQ-H_2O. The digest was run on a 1% agarose gel to visually confirm the digest had been successful.

B. Transcription Reaction and Generation of In Situ Hybridization Probes

Digoxigenin (DIG)-labeled RNA probes were generated using T3, T7, or SP6 RNA polymerases and a DIG-RNA labeling mix (Roche Applied Science, Mannheim, Germany).

C. *In Situ* Hybridization

Embryos were harvested (as described in which Section III.A Embryo Collection, p.76). Embryonic tissue sections were processed, sectioned and hybridized using DIG-labeled antisense RNA probes and detected with anti-DIG antibodies coupled to alkaline-phosphatase-conjugated antibody against DIG according to published protocols. For color development, 4-nitroblue tetrazolium chloride (NBT) and 5-bromo-4-chloro-3-indolyl phosphate (BCIP) were used as substrates. Labeled preparations were imaged using a Zeiss AxioPlan2 (Carl Zeiss, Germany) with an attached Fujix DS-515 color camera (FujiFilm, Australia) and attached monitor.

X. MORPHOLOGY STAIN

A. Hematoxylin and Eosin

Frozen sections were air dried for several minutes, to remove moisture, then stained with 0.1% Mayer's Hematoxylin (Anatomical Sciences, University of Adelaide, Adelaide, Australia) for 20 seconds followed by a 5 min rinse, in cool running water, and removed once water was clear. Sections were then immersed in 0.5% Eosin (1.5g dissolved in 300ml of 95% ethanol), dipped approximately 12 times, followed by quick dip in water, until the eosin stoped streaking (about 4-6 dips). Dehydrated in 50% ethanol (10 seconds), 70% ethanol (10 seconds), 95% ethanol for (30 seconds) and 100% ethanol (1 minute). The final step was to immerse sections into Histolene (2 times for 2 minutes each; Fronine, New South Wales. Australia). Sections were mounted and a coverslip affixed with DEPEX mounting medium (Anatomical Sciences, University of Adelaide, Adelaide, Australia).

Paraffin sections were run through a series of deparaffinizing solutions prior to following the procedure.

B. Cresyl Staining

The Cresyl staining method is used for the detection of Nissl bodies in the cytoplasm of neurons on formalin-fixed, paraffin embedded tissue sections. The Nissl body will stain a purple-blue color. This stain is commonly used for identifying the basic neuronal structure in brain and spinal cord tissue.

Paraffin brain sections were processed for Cresyl Staining by Nadia Gagliardi (Anatomical Sciences, University of Adelaide, Adelaide, Australia). Brain sections were cut at 10μm onto Superfrost Plus Slides (Menzel-Glaser, Braunschweig, Germany). The Cresyl staining procedure is as follows: sections are deparaffinized in 95% (15 minutes), 75% (1 minute), and 50% (1 minute) ethanol, rinse sections in distilled H_2O 2 minutes and then into fresh distilled H_2O for 1 minute. They are stained with 0.1% cresyl violet for 5 minutes and rinsed the section in distilled water for 3 minutes. The sections are then dehydrated in 95% alcohol for 10 dips followed by 100% alcohol for 10 dips. Sections are cleared in Histolene (Fronine, New South Wales. Australia) and cover slips are mounted with DEPEX mounting medium (Anatomical Sciences, University of Adelaide, Adelaide, Australia).

C. Masson Trichome

The Masson Trichome stain is used for the detection of collagen fibers in tissues that have been formalin-fixed or paraffin-embedded sections, and may be used on frozen sections. Collagen fibers will stain blue and the nuclei will stain black. Background will stain red.

Paraffin testis sections were processed for Masson Trichome staining by Nadia Gagliardi (Anatomical Sciences, University of Adelaide, Adelaide, Australia). Sections underwent the following procedure: Deparaffinize and rehydrate through 100% alcohol, 95% alcohol 70% alcohol. Wash in distilled water. Followed by staining in Weigert's iron hematoxylin working solution for 10 minutes. Sections were rinsed in running tap water for 10 minutes. Then counterstained in Biebrich scarlet-acid fuchsin solution (Biebrich scarlet, 1% aqueous, Acid fuchsin, 1% aqueous, Acetic acid, glacial 1%) for 10-15 minutes. This was followed by washing in distilled water and differentiated in phosphomolybdic-phosphotungstic acid solution (5% Phosphomolybdic acid, 5% Phosphotungstic acid) for 10-15 minutes or until collagen was not red. The sections were transferred directly (without rinse) to aniline blue solution and stained for 5-10 minutes. Rinse briefly in distilled water

and differentiate in 1% acetic acid solution (Aniline blue 2.5 g, Acetic acid, glacial 2 ml, Distilled water 100 ml) for 2-5 minutes. Wash in distilled water. Dehydrate very quickly through 95% ethyl alcohol, absolute ethyl alcohol (these step will wipe off Biebrich scarlet-acid fuchsin staining) and clear in xylene. Cover slips were mounted with DEPEX mounting medium (Anatomical Sciences, University of Adelaide, Adelaide, Australia).

XI. PROTEIN IMMUNBLOT

The western blotting protocol was used by Chin Ng (2010) during her Honors work and contributed to Figure 4-12 (p.178). The following method is adapted from her work (Chin Ng, 2010).

A. Tissue Collection

Tissue for western blotting was obtained from wild-type and homozygous dwarf adult 5-month old mouse brain, pituitary and kidney.

B. Whole Cell Extract

Whole cell extraction was performed on ice to prevent protein denaturation. A minimal amount of Whole Cell Extract Lysis Buffer (420mM NaCl, 25% glycerol, 0.5% NP-40, 1.5mM MgCl, 20mM Hepes (pH7.5)) and fresh Protease Cocktail Inhibitors (Sigma Aldrich, St. Louis, MO, USA) were added to each tissue sample (7 ml for brain sample, 5 ml for kidney and 50 µl for pituitary). Tissue homogenization was performed in lysis buffer using a blade and grinder followed by incubation at 4C on a nutator for 30 minutes. Samples were centrifuged at 13,000 rpm for 15 minutes at 4C. The supernatant was collected and stored at -80C until ready for processing. The supernatant was collected and protein concentration was determined using Bradford Protein Assay (described below) using bovine serum albumin as the standard.

C. Determining Protein Concentration Using Bradford Protein Assay

Protein concentrations were determined using Bradford Protein Assay. A bovine serum albumin (BSA) standard curve was generated by using serial dilution of bovine serum albumin with MQ-H_2O (0µg/ml to 2,000µg/ml). Protein samples from brain, kidney and pituitary were diluted 1:10 and 1:100 in MQ-H_2O. Both bovine serum albumin standards and protein samples were repeated in duplicate. Bio-Rad Protein Assay Dye Reagent Concentrate (Bio-Rad, Hercules, CA, USA) was diluted 1:4 and 200µl of the diluted Bio-Rad Protein Assay Dye Reagent (Bio-Rad, Hercules, CA, USA) was combined

into each well containing 10µl of the protein. Absorbance was measured at 600nm and concentration determined from the standard curve generated from the bovine serum albumin standards.

D. Sodium Dodecyl Sulfate Polyacrylamide Gel Electrophoresis

20ng of protein was loaded into each well in a 1:1 ratio of protein samples to 2x sodium dodecyl sulfate polyacrylamide gel electrophoresis (SDS-PAGE) loading buffer and were denatured by heating at 95C for 5 minutes. Samples were centrifuged at 13,000 rpm for 1 minute before loading into well of SDS-PAGE gels. All samples were loaded on discontinuous SDS-PAGE gels comprising of 4% stacking gel and 10% resolving gel. Gels were run at 100V in 1xGlycine-Tris-HCl-SDS buffer (192mM Glycine, 25mM Tris-HCl, 0.1% SDS) until the dye front had run off the bottom of the gel. Proteins were visualized with Coomassie Blue gel staining (procedure is not outline as data is not shown within this body of work; please refer to the work by Chin Ng (Ng, 2010)).

E. Protein Immunblot (Western Blot Preparation)

Following SDS-PAGE gels were transferred to nitrocellulose membranes using wet transfer. Gels were sandwiched into a cassette with nitrocellulose membrane and transferred in Western Blot Transfer Buffer at 250mA for 1.5 hour at room temperature. Post-transfer, nitrocellulose membrane was blocked in 5% skim milk/PBST at room temperature for 1-2 hours. Nitrocellulose membranes were washed in PBST (x3 10 minutes) then incubated overnight at 4C with primary antibody: anti-WARS (ab58054, mouse monoclonal; Abcam, Cambridge, MA, USA; 1:1,000 in PBST) and anti-GAPDH (mouse monoclonal, clone GAPDH-71.1; Sigma Aldrich, St. Louis, MO, USA; 1:5,000 in PBST). The following day, the nitrocellulose membrane was washed 3 x 10 minutes with PBST and incubated with HRP-conjugated donkey-anti-mouse secondary antibody (Rockland, Gilbertsville, PA, USA) diluted into 1:5,000 in 1% skim milk/PBST for 1 hour at room temperature with gentle agitation. Nitrocellulose membranes were washed a final time (3 x 10 minutes) and developed in Western Lightening Plus ECL luminol reagents (PerkinElmer, Waltham, MA, USA) for 5 minutes and exposed to X-ray film.

XII. CELL DISSOCIATION

Two methods of cell dissociation were preformed to determine optimal collection and sorting of GFP-positive (GFP^+) cells, with the aim of using these in microarray analysis. These are described below.

A. *Method 1*: Cell Dissociation using Trypsin

Embryonic heads, at 10.5 dpc, were dissociated using trypsin, as described in (Bouchard et al., 2005). Briefly, embryonic heads were dissociated into a single cell suspension using a 24-gauge needle followed by incubation at 37C for 45 minutes in 6 well plates containing 500µl of 1% trypsin (Invitrogen, CA, USA) in PBS. The reaction was stopped by transferring the single-cell suspension into 4ml of cold Gibco® Dubelcco's Modified Eagle Medium (DMEM; Invitrogen, CA, USA) containing 10% FCS. Cells were centrifuged for 2 min at 4C at 1,000rpm. The cell pellet was resuspended in phenol-red free DMEM (Invitrogen, CA, USA) containing 1% Fetal Calf Serum (FCS; Invitrogen, CA, USA) and 1µg/ml propidium iodide (PI; Sigma Aldrich, St. Louis, MO, USA). Cells were sorted according to fluorescence levels of GFP^+ and PI^- using the BD FACS Vantage SE with FACSDiVa Option (BD Bioscience, MD, USA), detailed in Section XIII Fluorescence Activated Cell Sorting (p. 92).

B. *Method 2*: Cell Dissociation using Dispase II and Collagenase B

The cell dissociation method using dispase II and collagenase B is described in (Beverdam and Koopman, 2006). Briefly, 10.5 dpc whole embryo heads were dissected in ice-cold 1xPBS and then enzymatically dissociated in dissociation medium composed of Hank's Balanced Salt Solution (Sigma Aldrich, St. Louis, MO, USA) containing 1 mg/ml collagenase B (Roche Applied Science, Mannheim, Germany), 1.2 U/ml Dispase II (Roche Applied Science, Mannheim, Germany) and 5 U/ml DNase1 (Sigma Aldrich, St. Louis, MO, USA) for 50-60 minutes at 37C while shaking. Cells were further dissociated mechanically using a P1000 Gilson pipette and a 23-gauge syringe. Finally, cells were passed through 40µm cell strainers (Falcon BD Biosciences), rinsed with ice-cold 1xPBS, spun down and resuspended in 1ml of phenol-red free DMEM supplemented with 1% FCS containing 1µg/ml PI. Cells were sorted according to GFP^+ and PI^- fluorescence as detailed below (see Section XIII Fluorescence Activated Cell Sorting).

XIII. FLUORESCENCE ACTIVATED CELL SORTING

GFP^+ cells were sorted on the BD FACS Vantage SE with FACSDiVa Option (BD Bioscience, MD, USA), with technical assistance provided by Sandy McIntyre, The Institute of Medical and Veterinary Science, Adelaide, South Australia. The apparatus was run at 28psi using a 90µm nozzle. GFP fluorochromes were excited with a 488 nm argon laser and 530 nm collection filters were used to detect GFP and regulate deflection. GFP^+ cells were

collected into RNAprotect Reagent (Qiagen, CA, USA) or phenol-red free DMEM containing 1% Fetal Calf Serum (FCS) for further analysis.

Cells were first gated on a histogram; GFP^+ expressing cells were visualized on a forward/side scatter plot. Cells were 'back-gated' on the forward/side scatter plot to eliminate debris prior to analysis; this also eliminated auto-fluorescence of the sample. An analysis plot was generated with FITC fluorescence on the X-axis and PI on the Y-axis. Ten thousand GFP-expressing cells were gated, and the number of these cells expressing GFP analyzed. Data were expressed as GFP^+ cells per 10,000 total events.

XIV. MICROARRAY USING THE ILLUMINA BEADCHIP

A. RNA Preparation

The preparation of RNA for use in microarray is outlined in Section III.B.1 RNA processing of mouse embryonic 10.5 dpc mouse heads used in microarray analysis (p.77).

B. Analysis of RNA Quality

A variety of procedures are in common use for analysis and quantification of RNA (Fleige and Pfaffl, 2006). Recent analysis comparing the various methods (Ribogreen, Agilent Bioanalyzer, spectrophotometer, Nanodrop and more recently the Bio-Rad Experion) for quantification of the same RNA samples clearly demonstrate that no two methods produce the same data and that it is inadvisable to compare quantification data obtained using the different methods (Bustin, 2005). Therefore, throughout this work RNA analysis and quantification was consistently determined using the Agilent 2100 Bioanalyzer (Agilent Technologies, Palo Alto, CA, USA) together with the RNA 6000 Nano LabChip (Agilent Technologies, Palo Alto, CA, USA).

RNA samples were stored at -80C until ready to be sent off for microarray analysis. The Agilent 2100 Bioanalyzer, which uses microfluidics to size-separate and quantitate RNA, measures the amount of 28S and 18S ribosomal RNA; high-integrity RNA has a 28S:18S ratio of ~2.0. Additionally, it also calculates an RNA Integrity Number (RIN), which considers the full size distribution of RNA, not just the 28S and 18S rRNA, and is considered a more accurate assessment of overall integrity (Schroeder et al., 2006). Figure 2-5 shows representative electropherograms used to train the RIN software and shows the varying levels of RNA intactness (Mueller et al., 2004).

All samples used for microarray analysis demonstrated ratios >1.6 and <1.9. High-integrity RNA with a RIN value greater than 7.5 were selected for further analysis. RNA

extracted from embryo heads with the highest possible RIN were used as individual samples for microarray hybridization. All purified products were stored at −80C.

Figure 2-5 Electropherograms used in the analysis of RNA quality using the Agilent 2100 Bioanalyzer
(A) Sample electropherograms used to train the RNA Integrity Number (RIN) software. Samples range from intact (RIN 10), to degraded (RIN 2). (B) Electropherogram detailing the regions that are indicative of RNA quality. (C) Electropherogram showing the varying levels of intactness. Adapted from (Mueller et al., 2004).

C. The Illumina® BeadChip Technology

Microarray analysis was performed using the llumina® Whole-Genome Expression BeadChip MouseWG6v1.1 Sentrix-6, containing approximately 47,000 probes that cover more than 19,000 genes from the mouse genome assembled from the NCBI database (Illumina Inc, 2010). Each Illumina® BeadChip Sentrix-6 BeadChip allows the interrogation of six RNA samples in parallel and produces data that can be treated as coming from six independent microarrays. Physically, each Illumina® BeadChip Sentrix-6 BeadChip consists of twelve equally spaced strips of beads (Figure 2-6, below). Each pair of adjacent strips comprises a single microarray and is hybridized with a single RNA sample. The BeadChip contains 3µm beads that have been tagged with hundreds of thousands of copies of a unique 25-mer address oligonucleotide followed by a gene-specific 50-mer oligonucleotide, that are randomly assembled onto each array. Each array is made up of approximately 1.6 million beads and provides an approximate 30-fold redundancy per oligonucleotide (Illumina Inc, 2010). The unique address oligonucleotide enables the location of each bead to be identified (Figure 2-7, p.97).

NOTE:
This figure is included on page 96 of the print copy of the thesis held in the University of Adelaide Library.

Figure 2-6 Physical layout of twelve equally spaced strips in a Illumina® Sentrix-6 BeadChip
Each array is made up of a pair of strips, one-below the other (Illumina Inc, 2010).

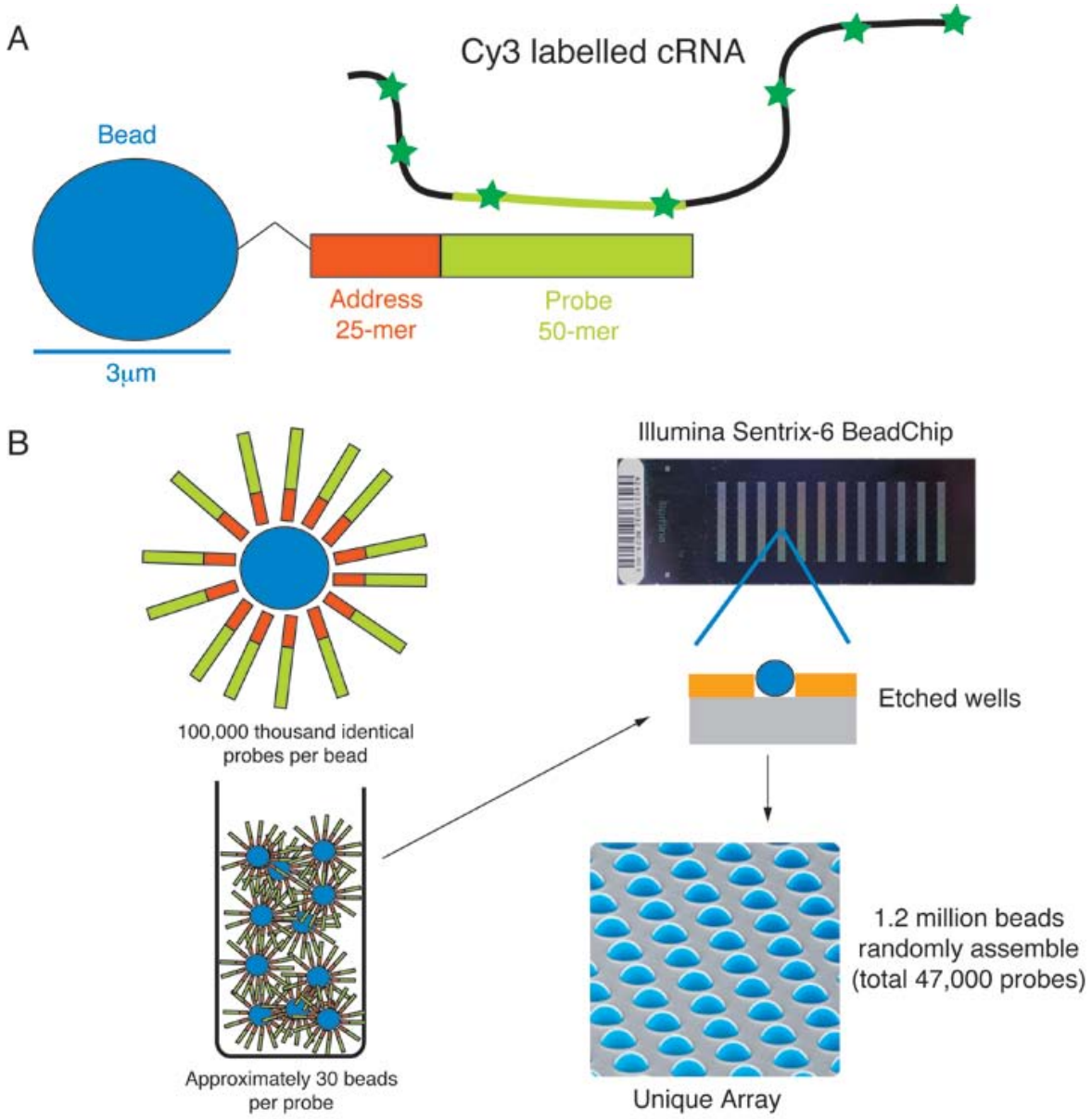

Figure 2-7 Schematic view of an Illumina® bead coupled with an oligonucleotide, consisting of the address code and a 50 base gene-specific sequence

(A) Schematic representation of a single 3µm bead with a single oligonucleotide attached. Each oligonucleotide features a unique 25-mer address sequence to help locate the beads' position on the assembled array and a 50-mer probe sequence which is specific to the gene of interest. (B) Each 3µm bead has hundreds of thousands of copies of a single oligonucleotide attached. Approximately 30 beads of the 47,000 different probes are assembled randomly into etched wells on a chip producing a unique array.

D. Microarray Processing

All microarray processing (from RNA amplification to hybridization) was carried out at the Australian Genome Research Facility (AGRF; Melbourne, Australia) using the Illumina® Sentrix Mouse-6 v1.1 Expression BeadChip (Illumina Inc, San Diego, CA). These high-density oligonucleotide arrays comprise over 47,000 probes to query expression profiles of the mouse genome. Content is based on the RefSeq, RIKEN FANTOM2 databases and other data sources.

1. RNA amplification

Fragmented aRNA (2µg) was hybridized to the Illumina® BeadChip in duplicate and hybridized for 16-h at 45C.

RNA was linearly amplified in two consecutive rounds using the Illumina® RNA Amplification Kit (Illumina Inc, San Diego, CA) following the manufacturer's instructions. The procedure was conducted at AGRF. For information purposes the amplification procedure consists of reverse transcription with an oligo-(dT) primer bearing a T7 promoter using ArrayScript™, a reverse transcriptase (RT) engineered to produce higher yields of first strand cDNA than wild-type enzymes. ArrayScript™ catalyzes the synthesis of virtually full-length cDNA, which is the best way to ensure production of reproducible microarray samples. The cDNA then undergoes second strand synthesis and clean-up to become a template for in vitro transcription with T7 RNA Polymerase. To maximize cRNA yield, Ambion's proprietary MEGAscript® in vitro transcription (IVT) technology is used in the kit to generate hundreds to thousands of anti-sense RNA copies of each mRNA in a sample. The labeled aRNA produced with the kit was then used for hybridization with the Illumina Sentrix Mouse-6 v1.1 array (Illumina Inc, San Diego, CA).

2. Hybridization to the Illumina® BeadChip

Hybridization to Illumina® Mouse-6 Version 1.1 BeadChips was conducted at the AGRF (Melbourne, Australia) using standard Illumina® protocols (as per manufacturer instructions). There were two biological replicates of the entire experiment, making a total of eighteen arrays on three BeadChips.

The Illumina® BeadChip analyzes whole-genome gene expression using a direct hybridization approach. Each sample is biotin-labeled, then amplified RNA (aRNA) is generated, via a cDNA intermediate, and this produces thousands of antisense copies of each original mRNA molecule (refer to Figure 2-7, p.97). The labeled aRNA from one sample is hybridized in duplicate onto two individual arrays (to provide technical

replicates). Illumina® BeadChip uses single fluorescence, Cy3 conjugated streptavidin, for the detection of gene expression, allowing the quantitative detection of RNA at each bead location via fluorescence excitation and detection. The average fluorescent intensity is then determined by averaging the fluorescent intensity for each bead and for each probe (this is repeated for each array). The generation of aRNA, aRNA labeling, array hybridization, fluoresce detection, and data retrieval were performed by the Australian Genome Research Facility (AGRF; Melbourne, Victoria, Australia).

3. *Array design*

Please refer to Chapter 3III.C Microarray Analysis for a description of the microarray experimental design. This is represented in Figure 3-4 (p.115) and outlines the array design of the three chips used.

E. Data Collection and Analysis

Microarray data was sent to me on DVD and contained three folders. One folder contained the Illumina® BeadChip images of each slide. Images were included so as to be visually assessed for quality (uniform hybridization and the absence of large artifacts). The two remaining folders contained normalized (or background-subtracted) data, and non-normalized (or non-background subtracted) data. The normalized data was used in downstream statistical analysis.

1. *Statistical programming environment for analyzing microarray data*

Data was analyzed using the R statistical environment (http://www.r-project.org/) (Ihaka and Gentleman, 1996) and IlluminaGUI packages (http://illuminagui.dnsalias.org/) (Schultze and Eggle, 2007) on the MacOSX.

2. *Normalizing data*

The purpose of normalization is to remove non-biological sources of variation. In a microarray experiment, there are many sources of variation. These include dye biases from the efficiency of dye incorporation, experimental variability in the hybridization and processing steps and differences between experimental conditions for replicate slides.

IlluminaGUI provides the option to choose from three different normalization techniques that are based on different assumptions concerning the nature of the raw data (Schultze and Eggle, 2007): quantiles-method (Bolstad et al., 2003), the variance stabilization and normalization (vsn)-method (Huber et al., 2002) and the QSpline-method (Workman et al., 2002). Quantile normalization is based on transforming each of the array

specific distributions of intensities so that they have the same values of quantiles (Deshmukh and Purohit, 2007). The vsn-method builds upon the fact that the variance of microarray data depends on the signal intensity and that a transformation can be found after which the variance is approximately constant (Huber et al., 2002). It is like the logarithm at the upper end of the intensity scale, approximately linear at the lower end, and smoothly interpolates in between. The vsn-method assumes that less than half of the genes on the arrays are differentially transcribed across the experiment. An advantage of vsn-transformation over log-transformation is that vsn works also on values that are negative after background subtraction. The QSpline normalization method uses quantiles from array signals and target signals to fit smoothing B-splines. The splines are then used as signal-dependent normalization functions on the signals of x. The target signals can be from another array or could be means calculated from multiple arrays (Workman et al., 2002).

For the experiment outlined herein quantile normalization was employed. Quantile normalization is useful for normalizing across a series of conditions where it is believed that a small but intermediate number of genes may be differentially expressed – as is hypothesized (refer to Chapter 3II Aims , p.107).

3. Statistical analysis to determine differentially expressed genes

Three statistical approaches were used to identify differentially expressed genes:

- Linear model of microarray data analysis (LIMMA)

  fits linear models to each gene in order to identify differentially expressed genes. LIMMA identifies candidates based on the p-value, the probability that the values obtained can be achieved randomly, and a B value, the log of the odds that the gene is differentially expressed. Genes with low p-values and high B values are the most likely candidates for differential expression.

- Significance Analysis of Microarrays (SAM)

  identifies genes with significantly differing expression levels between sets of samples, as long as an a-priori hypothesis is present that some genes will have significantly different mean expression levels between different sets of samples (Ideker et al., 2000);

- t-test

  helps to determine the data's signal to noise ratio for each gene and identifies the statistical chance that the gene is differentially expressed.

4. *Data collation*

To collate the data a PERL script was written to easily manage and combine the data. The PERL script is provided in the Appendices - PERL script used in the collation of microarray statistical data (p.203).

The complete comparison of all the data obtained from the microarray experiment is located in the Appendices - Microarray DATA showing differentially expressed genes (p.210).

F. Criteria for the Identification of Differentially Expressed Genes

Microarray data, having been analyzed using three independent statistical methods (LIMMA, SAM, and t-test), identified 226 differentially expressed genes that were detected by all three tests (Appendices - Microarray DATA showing differentially expressed genes, p.210). I focused my initial efforts on examining genes involved in hypothalamic/pituitary development, therefore I selected genes based on the following criteria:

- Low p-value

  A low p-value (p) indicates statistical significance to the degree of differential expression. A P<0.05 is accepted as statistically significant.

- High fold change

  A high fold change increases the likelihood of reproducibility by qPCR.

- Expression within the developing brain, in particular within the HP axis.

  Determining whether the gene is expressed in the developing brain involved searching GeneBank and literature search (PubMed search).

XV. cDNA Generation

RNA obtained from embryonic tissue (refer to Section III.B.1 RNA processing of mouse embryonic 10.5 dpc mouse heads used in microarray analysis, p.77) and from adult brains (refer to Section III.B.2 RNA processing of hypothalamic sections used in mRNA expression analysis by qPCR, p.78) was reverse transcribed using the Applied BioSystems High Capacity RNA-to-cDNA kit (Applied BioSystems, CA, USA) as per manufacturer's instructions. 500ng of each sample of starting RNA was reverse transcribed used and concentration determined by spectrophotometer reading. A final volume of 20µL of cDNA was generated. cDNA was diluted 1:10 with Milli-Q water and stored at -20C in 10µL aliquots.

XVI. qPCR

Real time PCR, also called quantitative real time PCR (qPCR/qrt-PCR/qRT-PCR) is the technique of choice to amplify and simultaneously quantify a targeted DNA molecule. qPCR is highly sensitive and allows quantification of rare transcripts and small changes in gene expression. The simplest detection technique for newly synthesized PCR products in qPCR uses the SYBR Green I fluorescence dye that binds specifically to the minor groove double-stranded DNA (Morrison et al., 1998).

qPCR was performed using Fast SYBR Green Master Mix (Applied BioSystems, CA, USA) according to manufacturer's protocol and run on an ABI 7500 StepOnePlus thermo-cycler (Applied BioSystems, CA, USA) with the following parameters: 95C for 20secs, 39 cycles of 95C for 3secs, 60C for 30secs. Followed by generating a dissociation curve, done by increasing the sample temperature in 0.5C increments and measuring fluorescence levels after each increment. Each reaction was performed in triplicate, unless otherwise noted.

XVII. SOFTWARE PROGRAMS

The following software packages were used in the generation/analysis and/or presentation of data and/or results throughout this work. All packages were run on the Mac Operating System (Mac OSX Leopard), unless otherwise noted.

- Word and Excel 2008 (Microsoft, California, USA)
  Word-processing package in which this work was written in.
- Endnote X2 (Thomson Reuters, USA)
  Bibliographical database program.
- 4Peaks v1.7 (Mek&Tosj, Amsterdam, The Netherlands)
  Visualize and edit DNA sequences.
- R Project (University of Auckland, New Zealand)[4]
  Software environment for statistical computing and graphics.
- Adobe Photoshop CS4 (Adobe System Incorporated, USA)
  Photo editing and construction of compiled figures/graphs.
- Adobe Illustrator (Adobe System Incorporated, USA)
  Diagram and figure line-vector drawing package.
- ConceptDraw Pro (Odessa Corporation, USA)
  Diagramming platform for generation of flow charts.
- SPSS 19 (IBM Corporation, NY, USA) used on Windows XP (Microsoft, USA)
  Statistical package.
- SigmaPlot (Systat Software Inc, USA) used on Windows XP (Microsoft, USA)
  Graph drawing package.
- Chimera[5]
  Visualization and analysis of molecular structures and related data.

[4] Initially written by Robert Gentleman and Ross Ihaka, University of Auckland, New Zealand. http://www.r-project.org/

[5] The package is freely available for Windows and Mac computers from the following link http://www.cgl.ucsf.edu/chimera/

This page has been left blank intentionally.

3 Identification of *Sox3* Target Genes

I. INTRODUCTION

Sox3, a member of the high mobility group (HMG) family of transcription factors, is expressed in neural progenitor cells (Brunelli et al., 2003; Stevanovic, 2003) and in the gonads (Raverot et al., 2005; Sutton et al., 2011). The correct dosage of SOX3/*Sox3*, a transcription factor member of the SOXB1 family, is essential for brain, specifically hypothalamic and pituitary development (Rizzoti et al., 2004). Critically, the target genes regulated by *Sox3* have not been identified. The identification of *Sox3* target genes is crucial for better understanding *Sox3* function. In the mouse embryo, Sox3 is highly expressed within the developing brain at 10.5 dpc (Chapter 1II.C The Role of Sox3 in Hypothalamo-Pituitary Axis Development, p.56). Given its robust expression at 10.5 dpc it is speculated that *Sox3* target genes are activated at this stage. This includes both direct targets, whereby SOX3 binds to the promoter/regulatory region of these target genes thereby activating gene expression, as well as indirect target genes. Indirect target genes are not directly bound by Sox3 but are regulated via transcription regulators, which are targets of *Sox3*, and are likely to be affected by *Sox3* loss. The SOXB1 family members (*Sox1-3*) are

transcriptional activators (Bylund et al., 2003). Using transgenic mice that lack *Sox3,* direct targets are likely to be identified (by being down-regulated), although indirect targets may also be identified (by either being up- or down-regulated).

The aim of the work described in this chapter was to identify potential *Sox3* target genes using three mouse lines, *Sox3*-null, Extra-Sox3 and Green-Sox3 (Figure 3-1, below), by large-scale gene profiling using microarray technology (also see Chapter 2II.B.1 Sox3 transgenic lines, p.72). The three mouse lines chosen for this study have a Sox3-GFP reporter cassette inserted, thereby enabling GFP-positive (GFP^+) cells to be sorted and used in downstream microarray applications. This chapter describes the use of the Illumina BeadChip, a novel microarray, for the identification of *Sox3* target genes. Moreover, I describe here the identification of a potential *Sox3* target gene, *Neurogenin-3* (*Ngn3*). Ngn3 is a member of the basic helix-loop-helix transcriptional factor family that play important roles in vertebrate neurogenesis and are expressed in neural and endocrine precursor cells, in particular the endocrine cell types in the pancreas (Gradwohl et al., 2000; Sommer et al., 1996). Notably, Ngn3 has been shown to co-localize with Sox3 in proliferating germ cells during spermatogonial differentiation, and is decreased in the absence of *Sox3* (Raverot et al., 2005). Thus, suggesting a potential functional link between Sox3 and Ngn3.

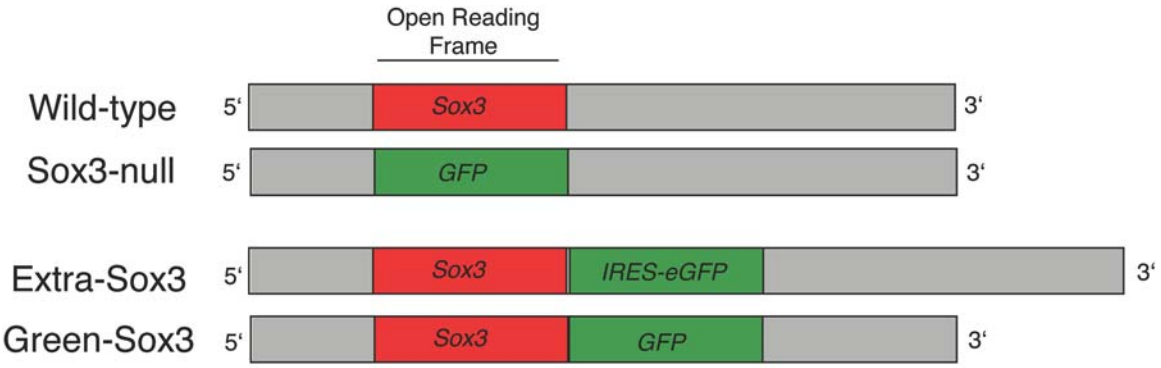

Figure 3-1 Schematic representation of the wild-type, *Sox3*-null, Extra-Sox3 and Green-Sox3 (GFP-reporter) mice.

Sox3-null mice was generated using homologous recombination whereby the SOX3 open-reading frame (ORF) was replaced with the marker gene encoding GFP protein downstream. This permitted the expression of GFP driven by the Sox3 regulatory sequences. Extra-Sox3 mice were generated using BAC-recombineering using an IRES-eGFP reporter cassette that was inserted into the 3'UTR of *Sox3* using homologous recombination. Green-Sox3 (GFP-reporter) mice, containing identical regulatory sequences that were used to generate the Extra-Sox3 mice, were generated from a modified BAC in which the *Sox3* ORF was replaced with the eGFP coding sequence. These mice express normal levels of Sox3 in eGFP-expressing cells.

II. AIMS

The overall aim of this project was to identify *Sox3* target genes, using microarray analysis to compare gene expression in wild-type, *Sox3*-null and Extra-Sox3 mice embryonic heads at 10.5 dpc.

My specific aims were to:

- Identify potential *Sox3* target genes by microarray analysis (*Aim 1*);
- Verify microarray results using qPCR (*Aim 2*);
- Examine the expression of Sox3 and the potential *Sox3* target gene(s) that are up- and/or down-regulated as a consequence of a loss of *Sox3* (*Aim 3*).

III. RESULTS

AIM 1: IDENTIFY POTENTIAL *SOX3* TARGET GENES BY MICROARRAY ANALYSIS

As *Sox3* is an essential regulator of HP axis development, to further investigate the function of *Sox3* in HP axis formation I set out to identify novel target genes by microarray analysis. This approach was based on the premise that gene expression differences in the brain region of wild-type, Sox3-null and Extra-Sox3 embryos would be detected by gene expression profiling. This approach required several technical difficulties to be addressed. Initially, the aim was to collect GFP-positive (GFP^+)[6] cells by FACS and extract RNA from these cells in preparation for microarray processing.

A. Cell Dissociation and FACS sorting of GFP-positive cells for use in Microarray Analysis

The overall aim was to identify target genes of *Sox3*. The first step was to isolate and collect GFP^+ cells from the three transgenic mouse lines: Green-Sox3, Extra-Sox3 and *Sox3*-null. Once isolated, the GFP^+ cells would be used for microarray analysis using the Illumina MouseRef-6 BeadChip. 50ng total RNA would be required from each transgenic mouse line.

Using FACS, I attempted to isolate 5,000-10,000 live GFP^+ cells from the CNS of individual *Sox3*-null, Extra-Sox3 and wild-type embryos. These numbers are based on a similar study (Bouchard et al., 2005) whereby 5,000 GFP^+ cells yielded 5-10ng RNA (or 30-80µg after two rounds of amplification). Two methods of cell dissociation, using trypsin (*method 1*) and using a combination of dispase II and collagenase B (*method 2*), were trialed to determine which method generated the most viable GFP^+ cells per embryo. All samples were collected at 10.5 dpc following the protocols described in Materials and Methods (Chapter 2XII Cell Dissociation, p.91).

Sorting profiles of cells obtained using trypsin as the dissociation medium (*method 1*) are shown in Figure 3-2 A (p.112), and profiles of cells obtained using a combination of dispase II and collagenase B in the dissociation medium (*method 2*) are shown in Figure 3-2 B (p.112). In each experiment three controls were used based on the presence or absence of

[6] a '+' indicates positive for GFP and '-' indicates negative for GFP. These superscripts are used to indicate presence of GFP as well as propidium iodide (PI) in FACS.

GFP and propidium iodide (PI; membrane impermeant nucleic acid stain that is generally excluded from viable cells. Thus, it is commonly used for identifying dead cells).

The controls, used to set the 'gate' during FACS, were as follows:

- GFP$^-$PI$^-$

  Cells identified as GFP-negative (GFP$^-$) and PI-negative (PI$^-$) collected from wild-type embryos that did not express GFP and were not selectively stained for dead cells. PI$^-$ cells are viable. This is the negative control and we would not expect to see sorting of either GFP$^+$ and/or PI$^+$ cells.

- GFP$^-$PI$^+$

  Cells identified as GFP-negative and PI-positive collected from wild-type embryos that did not express GFP but were selectively stained for dead cells. This control helps to set the PI sorting gate. We would expect to see FACS of PI$^+$ cells only.

- GFP$^+$PI$^-$

  Cells identified as GFP-positive and PI-negative collected from embryos expressing GFP and were not selectively stained for dead cells. This control helps to set the GFP sorting gate. We would expect to see FACS of GFP$^+$ cells only.

Samples, used in the sorting of GFP$^+$PI$^-$ cells, were obtained from individual GFP$^+$ embryos from litters from the three mouse lines. Each GFP$^+$ sample was stained with PI to eliminate, by sorting, any cell debris and dead cells (as I was only interested in collecting viable GFP$^+$ cells).

The results from one cell sorting experiment comparing cell dissociation methods (*method 1* and *method 2*) are shown in Figure 3-2 A and B. Results are from two independent *Sox3*-null 10.5 dpc litters. The controls GFP$^-$PI$^-$ (*i*), GFP$^-$PI$^+$ (*ii*), GFP$^+$PI$^-$ (*iii*) and one cell sorting result (*iv*) are shown. The scatter plot (showing side scatter (SSC) and forward scatter (FSC)) used in gating the cells is shown (inset). Using trypsin-containing medium (*method 1*) yielded very few GFP$^+$ cells per embryo (572 GFP$^+$PI$^-$ cells; Figure 3-2 A *iv*). In contrast, using a combination of dispase II and collagenase B (*method 2*), yielded 1,017 GFP$^+$PI$^-$ cells (Figure 3-2 B *iv*). Similar results were shown in repeat experiments (data not shown).

The use of trypsin-containing medium did not provide reliable yields of positive cells (GFP$^+$PI$^-$) per embryo. This method resulted in a high yield of cell debris (as shown by the scatter plots in Figure 3-2 A *i – iv*). The distribution of the dots in the scatter plot can distinguish one type of cell from another. This enables the creation of a gate around one particular cell population for further analysis. The larger cells (or cell debris) are represented as higher values along the y-axis (SSC), while the more granular cells (those

containing more objects inside the cell enabling laser refraction) are represented as higher values along the x-axis (FSC). In Figure 3-2 A and B the cells of interest are gated (measured along FSC x-axis; blue selection) and form a tight population. Whereas, cell debris (measured along SSC y-axis; black dots) does not form a tight population, rather they are more dispersed.

The use of the more gentle cell dissociation method, using a combination of collagenase B and dispase, as previously described elsewhere (Beverdam and Koopman, 2006) provided a higher yield of GFP^+PI^- cells per embryo, than seen with trypsin-containing medium. This method utilized collagenase B, from *C. histolyticum*, which is a protease with specificity for the **X**-Gly bond in the sequence Pro-**X**-Gly-Pro, where **X** is most frequently a neutral amino acid. Such sequences are found in high frequency in collagen, but only rarely in other proteins. Dispase II, a metalloenzyme produced by *Bacillus polymyxa*, has been classified as an amino-endo peptidase suitable for tissue disaggregation and subcultivation procedures since it does not damage cell membranes (Stenn et al., 1989). Thus, unlike trypsin, which has the ability to damage the cell membrane under prolonged or excessive trypsin concentrations, the combination of collagenase and dispase provide a more gentler dissociation medium. The use of this method proves to be more effective in collecting a higher yield of GFP^+PI^- cells.

Although the use of a combination of dispase II and collagenase B provided a higher yield this would not provide the required number of GFP^+PI^- cells to generate 50ng RNA. In a similar study (mentioned above), 5,000-10,000 GFP^+PI^- cells were collected by FACS per embryo (Bouchard et al., 2005). For each embryo, the total RNA from a minimum of 5,000 cells was reverse-transcribed followed by two rounds of amplification (as total RNA isolated per embryo was low; 5-10 ng), and yielded 30-80 µg of aRNA (Bouchard et al., 2005). My data showed, using the combination of collagenase and dispase cell dissociation method, an average yield of 1,000 GFP^+PI^- cells per embryo. Based on Bouchard *et al* data as an estimate of required yield, 5,000 GFP^+ cells per embryo would generate 5 ng. Obtaining the minimum of 50ng total RNA per embryo would not be achievable. Approximately 50,000 GFP^+ cells would need to be collected from 10 embryos that would need to be pooled into one sample, and in triplicate for per mouse line (Green-Sox3, Extra-Sox3 and *Sox3*-null). Thereby requiring at least 30 GFP^+ embryos per mouse line. Given that, on average, 25% of each litter (or 2 pups from an average litter size of 8) would produce homozygous pups carrying GFP, 10 GFP^+ embryos would be pooled from, at least five matings. This method would prove extremely time consuming, and would require the use of sizeable numbers of embryos. Therefore, an alternative approach was

derived that involved isolating the entire embryonic head at 10.5 dpc from which total RNA was extracted and analyzed by microarray.

B. Extraction of RNA from Whole Mouse Embryonic Heads for use in Microarray Analysis - RNA Quality Analysis

Total cellular RNA was isolated from the 10.5 dpc embryonic heads from *Sox3*-null, Extra-Sox3 and wild-type mouse lines (see Materials and Methods Chapter 2III.B.1 RNA processing of mouse embryonic 10.5 dpc mouse heads used in microarray analysis, p.77). RNA size and quality was assessed via the Agilent 2100 Bioanalyzer.

Figure 3-3 (p.114) shows the RNA quality analysis of the samples used in microarray analysis. All RNA samples were of the highest quality based on their RNA integrity number (RIN) (refer to Materials and Methods Chapter 2XIV.B Analysis of RNA Quality, p.93). RNA used as individual samples for each mouse line sample and pooled RNA samples from wild-type and *Sox3*-null mouse lines had a RIN of 8-10. Only in the Extra-Sox3 pooled samples were there two samples with RIN of 7.9 and 7.8. The other two samples had RIN in the range of 8-10.

C. Microarray Analysis

Microarray analysis was performed, as outlined in Material and Methods (see Chapter 2XIV.D.2 Hybridization to the Illumina® BeadChip, p.98 and Chapter 2XIV.D.3 Array design, p.99).

Figure 3-4 (p.115) shows the microarray outline and experimental design. For each experimental group: *Sox3*-null, Extra-Sox3 and wild-type RNA samples were collected. From each experimental group two RNA samples were collected from individual embryonic heads. The third group contained a pooling of RNA obtained from 4 embryonic heads. Each sample was hybridized in duplicate across three Illumina BeadChip slides. Hybridizing in duplicate was a strategy employed to eliminate/reduce errors between/within slides.

Figure 3-2 Fluorescence activated cell sorting of GFP$^+$ mouse 10.5 dpc embryonic heads comparing two cell dissociation methods: trypsin (*method 1*) and a combination of dispase II and collagenase B (*method 2*)

(A) Trypsin method used for cell dissociation and FACS. (B) Dispase II and Collagenase B method used for cell dissociation and FACS. In each experiment, performed on independent days, *Sox3*-null litters were used. Three controls were used: GFP$^-$PI$^-$ (collected from wild-type embryos; shown in *i*), GFP$^-$PI$^+$(collected from wild-type embryos shown in *ii*), and GFP+PI- (collected from GFP$^+$ embryos, shown in iii). The remaining GFP$^+$ embryos in the litter were sorted for GFP$^+$ cells and stained with PI, to identify any cell debris and dead cells (*iv*). The genotype (wild-type or *Sox3*-null) of each embryo is shown. The corresponding scatter plot used in gating the cells is also shown. FACS graphs were generated using FCSExpress V3.0 (DeNovo Software, Los Angeles, California, USA)

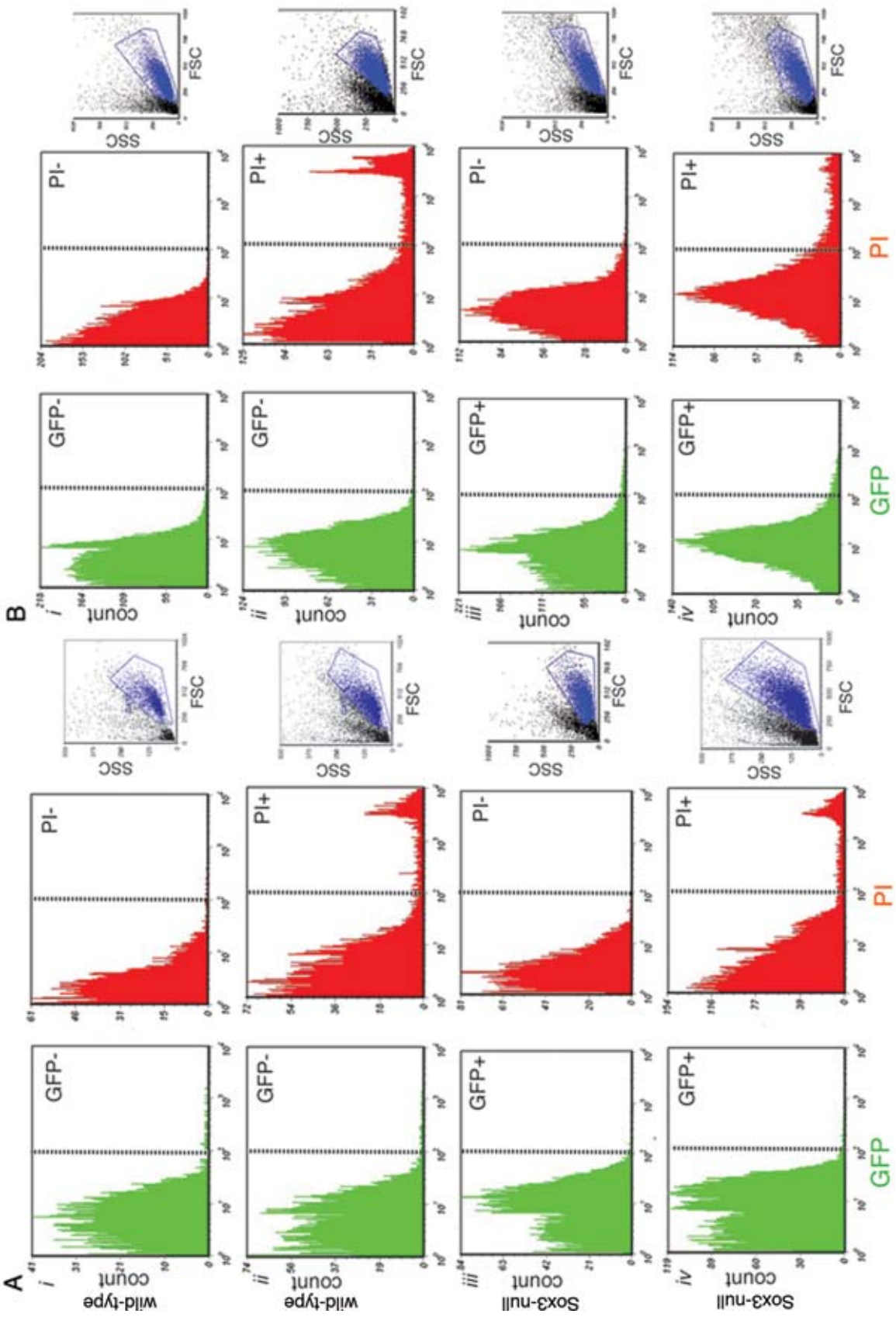
A
B
wild-type
Sox3-null
GFP-
GFP+
PI-
PI+
GFP
PI
SSC
FSC
count

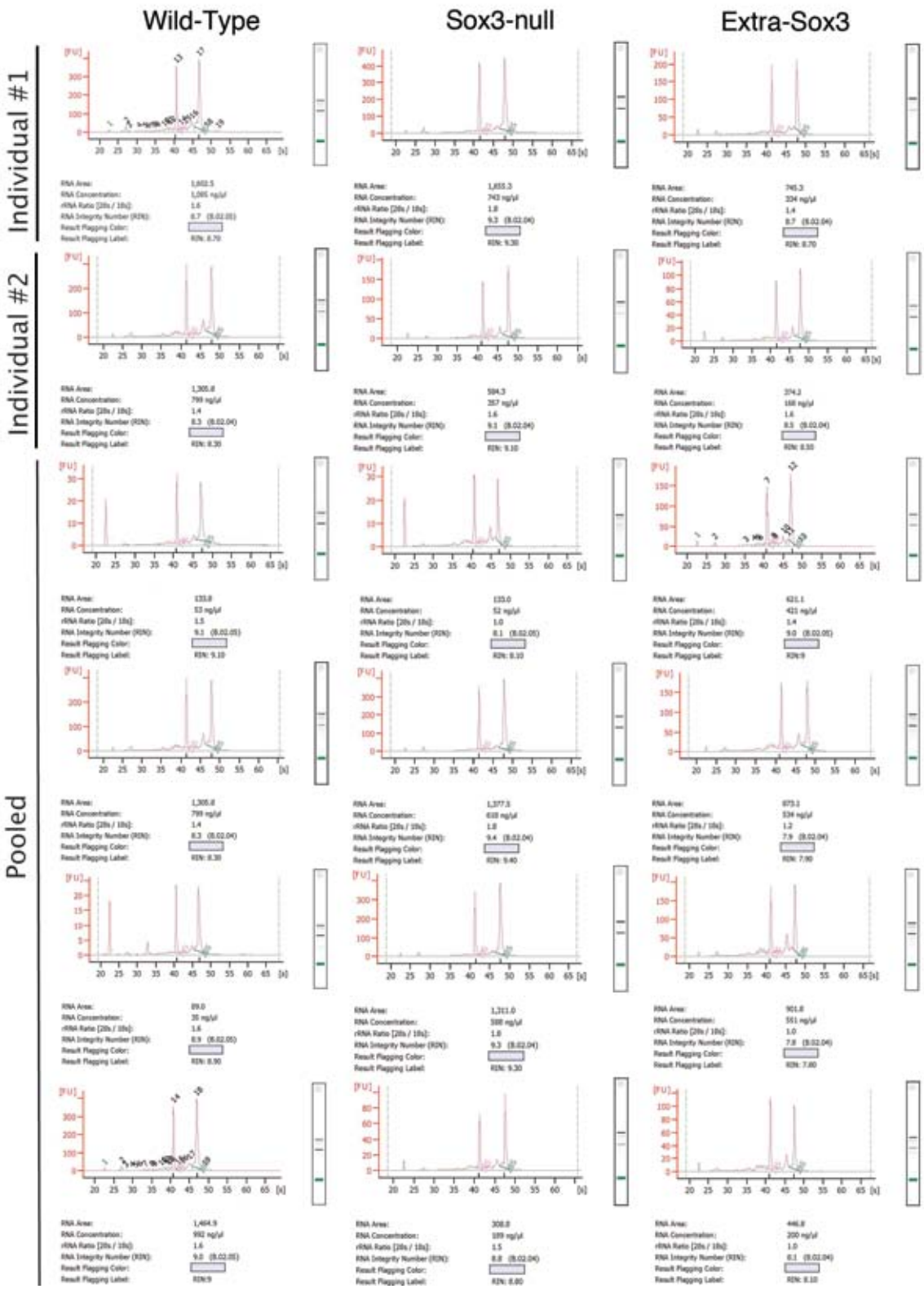

Figure 3-3 RNA quality from whole mouse embryo heads used in microarray analysis
RNA quality analysis, as determined by Agilent Bioanalyzer, of all samples used in microarray analysis.

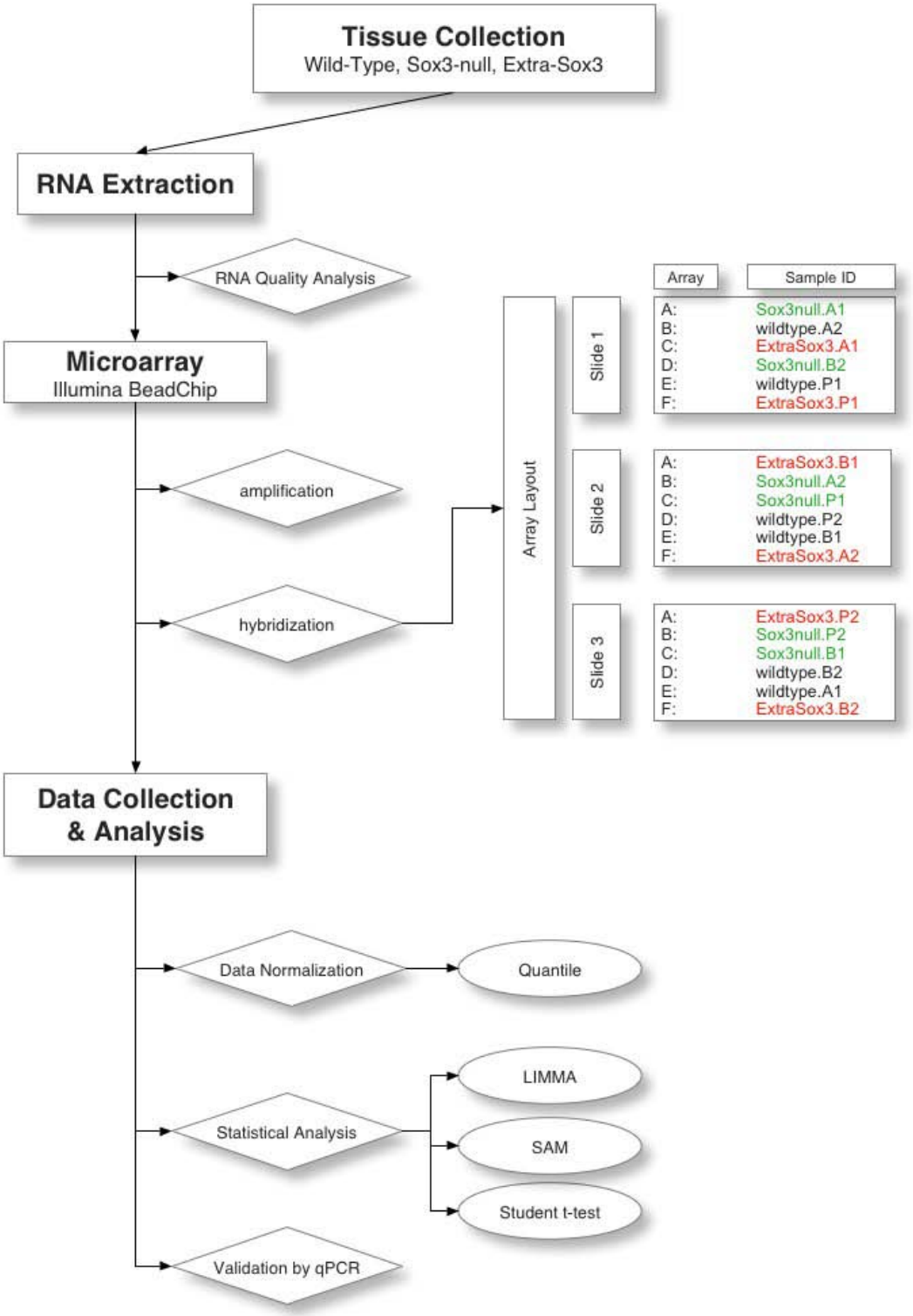

Figure 3-4 Microarray experimental outline and design

Schematic overview of the microarray process, from tissue collection to data analysis and the final step of validation by qPCR, showing the Illumina BeadChip array organization. For each experimental group: *Sox3*-null (green text), Extra-Sox3 (red text) and wild-type (black text) three samples of RNA were collected. From each experimental group two RNA samples (A and B) were collected from individual embryonic heads and hybridized in duplicate (A1, A2 and B1, B2). The third group contained a pooling of RNA obtained from 4 embryonic heads, and was also hybridized in duplicate (P1 and P2).

D. Normalizing Microarray Data

Data was first normalized by two methods: quantiles-method (Bolstad et al., 2003) and the vsn-method (Huber et al., 2002). Data is represented by box-plots and is shown normalized using the quantile-method (Figure 3-5, p.117):

- Non-background subtracted microarray data sets that have
  not been normalized (Figure 3-5 a)

  been quantile normalized (Figure 3-5 b)
- Background subtracted microarray data set that
  not been normalized (Figure 3-5 c)

  been quantile normalized (Figure 3-5 d)

Background subtraction removes the non-specific background intensities of the scanner images and then undergoes quantile-normalization. These box plots reveal that the non-background subtracted data has a greater degree of variation between and within arrays prior to normalization and is likely to contain more variation when determining which genes are differentially expressed. Hence, non-background subtracted data is not suitable for downstream analysis. Thus, for the analysis of differentially expressed genes the background-subtracted data normalized using the quantile-normalization method was employed in downstream data analysis.

To further analyze the differences between arrays the data was plotted using M versus A plots to show the log-intensity ratio ($M=\log_2(G1/G2)$) versus the mean log intensity ($A=\log_2\sqrt{(G1 \times G2)}$) for all the genes present on the array (Figure 3-6, p.119). MA-plots for single channel microarray platforms are computed from the means and differences of log-expression values from two microarrays. Such plots were introduced and used by Bolstad et al (Bolstad et al., 2003). Determining the MA plot gives a quick overview of data distribution. In many microarray experiments the general assumption is that the expression levels of most of the genes would not be changed and so the majority of the points on the M plot (y axis) would be located at 0 (since Log(1) is 0). If the majority of points are not located at 0, then a normalization method such as LOESS regression should be applied to the data before statistical analysis (Causton et al., 2003). The MA plots shown in Figure 3-6 (p.119) compare the MA plots for non-normalized (background subtracted) data versus quantile-normalized (using background subtracted) data. Both the non-normalized and quantile-normalized MA plots indicate that all points on the M plot are located at 0. Therefore, the data did not need to undergo further normalization methods before statistical analysis.

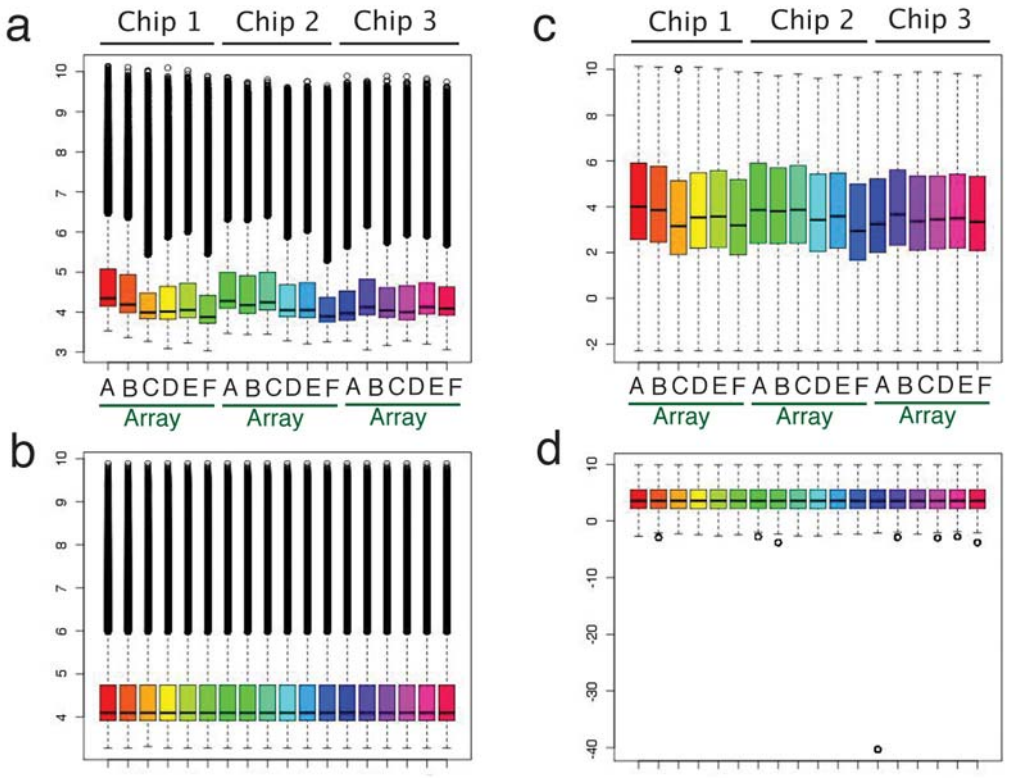

Figure 3-5 Box-plots showing intensity distributions before and after normalization of non-background subtracted and background subtracted data sets

Box plots are used to determine the distribution of intensity signals across an array, thereby verifying the comparability of all arrays within an experiment. Non-background subtracted data shown prior to normalization (a) and then after quantile-normalization (b). Background subtracted data shown prior to normalization (c) and then after quantile-normalization (d). Box plots were generated using IlluminaGUI in the R programming environment. (a) and (c) show reference to the chips (chip 1-3) and the arrays within each chip (A-F).

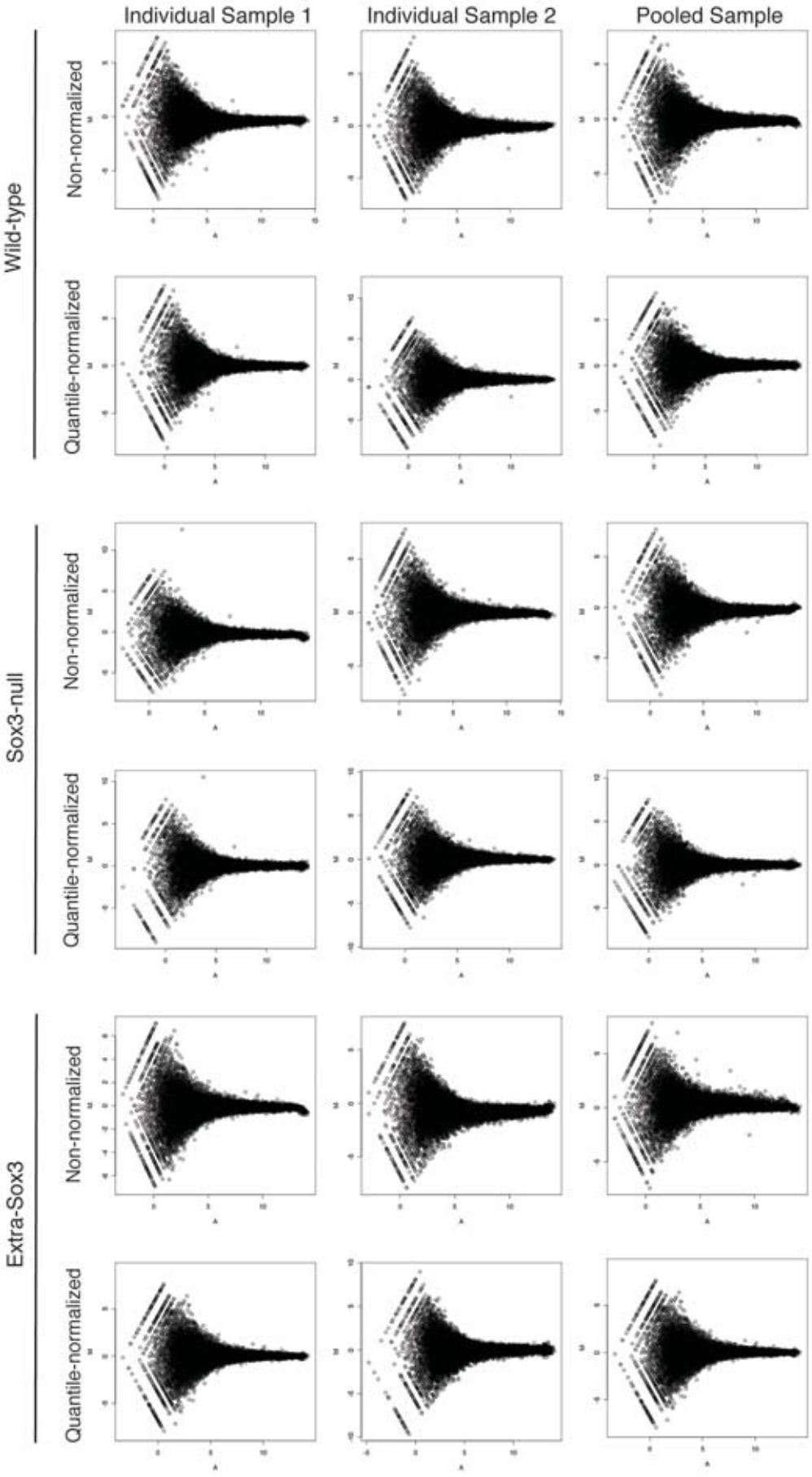
Individual Sample 1
Individual Sample 2
Pooled Sample
Wild-type
Sox3-null
Extra-Sox3
Non-normalized
Quantile-normalized

Figure 3-6 M versus A plots prior and after quantile normalization of background subtracted arrays
Plots show between-array symmetry around a horizontal line through zero. Each duplicate array for the groups was located on a different slide, providing more control over possible variations. Plotting this data on MA plots shows that there is little variation between arrays of the sample, both before normalization (non-normalized data) and after (quantil-normalized data). No non-linearity was seen in either non-normalized or quantile normalized data therefore further normalization, such as using LOESS regression was not required to have been applied to the data before statistical analysis.

E. Identification of Differentially Expressed Genes

Differentially expressed genes were identified by statistical methods as described in Materials and Methods Chapter 2XIV.E Data Collection and Analysis (p.99) and Chapter 2XIV.F Criteria for the Identification of Differentially Expressed Genes (p.101).

The initial focus for identifying differentially expressed genes was on *Sox3*-null versus wild-type because this enables the identification of down-regulated genes (as determined by having a negative fold change) in the *Sox3*-null mice relative to wild-type.

To identify genes that were differentially expressed, three statistical methods were employed: LIMMA, SAM, and t-test. These methods are described in detail in Materials and Methods Chapter 2XIV.E.3 Statistical analysis to determine differentially expressed genes (p.100). By using three methods I was able to deduce which genes were down-regulated in each test. I focused my initial efforts on examining genes involved in hypothalamic/pituitary development, and therefore I selected genes based on the following criteria:

- Low p-value

  A low p-value (P) indicates statistical significance to the degree of differential expression. A $p<0.05$ is generally accepted as statistically significant.

- High fold change (as indicated by a negative value)

  A high fold change increases the likelihood of reproducibility by qPCR.

- Expression within the developing brain, in particular within the HP axis.

  Determining whether the gene is expressed in the developing brain involved searching GeneBank and literature search (PubMed search).

During the statistical analysis process an Honors student in the lab, Dale McAninch, as part of his honors work, contributed in the validation of differentially expressed genes. Dale selected genes based on their connections to brain development or expression within progenitor cells. These genes were selected from the microarray list generated from t-test statistical data; 122 genes were identified as being differentially expressed with a fold change greater than 2 in *Sox3*-null relative to wild-type (Table 3-1, p.123). I examined genes that were detected by all three statistical methods, detailed below. Initially choosing six genes best fitting the selection criteria: genes that were down-regulated - *Clcn7, Enpp5, Gpr125,* and genes that were up-regulated - *Pdrg1, Rpo1-4* and *Tomm22* (data not shown). These genes were chosen based on their large differences in gene expression which could be reproduced and seen by qPCR, and potentially indicate

accuracy of microarray statistical data analysis. When these genes were analyzed by qPCR there was no correlation when compared to the microarray statistical analysis (data not shown). These results indicate that either the samples tested by qPCR analysis were not similar in their expression profiles (the microarray samples and qPCR samples came from different litters and were collected at individual times) to those used in the microarray or that these genes have been detected as false-positive by microarray and subsequently there is no change seen by qPCR validation (McAninch, 2008). To further analyze the microarray data, Dale selected 50 differentially expressed genes identified by microarray, and validated these by qPCR. The results are tabulated and located in the Appendices - Microarray Validation by qPCR (p.232) (McAninch, 2008). In summary, none of the genes tested by qPCR agreed with the microarray data.

To further examine the reason for such a large false-positive discovery rate, Dale examined the gene expressions of positive control genes (known to be expressed): *Sox3*, *GFP* and Xist (X-inactivated specific transcript; an RNA gene located on the X chromosome of placental mammal acting as a major effector of the X inactivation process whereby its RNA is responsible for the random silencing of one of the X chromosomes in somatic cells of XX individuals), and is not expressed within XY somatic cells. As described previously, the *Sox3* ORF has been replaced with the GFP ORF in *Sox3*-null mice, thus GFP, the second positive control, is expressed in cells that would normally express Sox3. Therefore, Sox3 should only be detectable in wild-type samples and GFP only in *Sox3*-null samples. Microarray data found *Sox3* expressed in wild-type samples but not in *Sox3*-null samples, however GFP was not detected in either the wild-type or the *Sox3*-null samples. The probe on the microarray detects enhanced GFP (eGFP) that has approximately 30% silent base substitutions compared with GFP. This is the likely reason why the microarray did not detect the GFP in the *Sox3*-null samples. Nevertheless, using qPCR primers for GFP Dale was able to detect both eGFP and GFP indicating expression in *Sox3*-null but not wild-type samples. Furthermore, *Xist* was only expressed in female, but not male, samples. These results are shown in Appendices - Table A 2 Average intensity values for *Xist, Sox3, β-Actin* and *GFP* (p.233). Additionally, microarray data revealed that *Sox3* was down-regulated in *Sox3*-null mice and up-regulated in Extra-Sox3 mice, as expected. Further supporting that, although there is a high false-positive discovery rate, the microarray was able to identify positive control genes.

My analysis of differentially expressed genes was based on statistical detection by all three tests (LIMMA, SAM and t-test) comparing *Sox3*-null samples relative to wild-type. A total of 45 genes were identified as down-regulated (negative fold change) by all three

statistical tests (Table 3-2, p.126). All of these genes had a fold change greater than 2 using t-test and SAM statistical methods. Only 18 genes were identified as down-regulated in *Sox3*-null mice using the LIMMA statistical method, again each gene had a fold change greater than 2 relative to wild-type.

F. Genes Chosen for qPCR Validation

Four differentially expressed genes were selected that were expressed in the developing hypothalamus at 10.5 dpc and that also showed a low p value and a high fold change (as per selection criteria detailed above). A literature search was also conducted and the most biologically relevant gene from this list was *Ngn3* (Raverot et al., 2005). As shown in the Table 3-4 (p.127), *Nfya, Ngn3, Sfrp1*, and *Nenf* were down-regulated, as indicated by the fold change, in *Sox3*-null mice. In Extra-Sox3 mice, only *Sfrp1* was also down-regulated and *Nenf* was up-regulated. *Sfrp1* and *Nenf* were the only genes from this list that were detected by the three statistical methods. Due to the initial focus for identifying differentially expressed genes on *Sox3*-null relative to wild-type and the high false-positive discovery rate, specific genes detected by the Extra-Sox3 microarray data are referred to as needed. As shown by Dale, *Pdrg1, Rpo1-4* and *Tomm22,* which were all highly up-regulated in Extra-Sox3 samples, relative to wild-type, did not show this same trend by qPCR. Therefore, I focused on the results obtained from *Sox3*-null relative to wild-type in addition to literature searches to focus in on genes likely to be targets of *Sox3* and are expressed in the developing hypothalamus, at 10.5 dpc.

Table 3-1 Down-regulated genes identified by microarray analysis and t-test statistical analysis in *Sox3*-null 10.5 dpc embryonic heads

Data is sorted by fold change (FC). For comparison the FC and p-value for results obtained by LIMMA and SAM statistical methods are shown.

Gene/Symbol	LIMMA		SAM		t-test	
	FC	P-value	FC	P-value	FC	P-value
Fcer1g					-92.12	0.00E+00
5730538E15Rik	-5.13	2.13E-09	-10.63	1.00E-04	-53.27	0.00E+00
Ndufb10	-3.27	6.82E-05			-51.77	0.00E+00
Sox3	-5.94	1.86E-09	-44.09	0.00E+00	-44.09	0.00E+00
Xist	-4.57	1.45E-04	-30.09	0.00E+00	-30.09	1.00E-04
5430404G13Rik	-4.32	2.72E-07	-19.40	0.00E+00	-19.40	0.00E+00
1110060M21Rik	-4.00	2.94E-11	-16.55	0.00E+00	-16.55	0.00E+00
Mll5					-12.10	8.10E-03
Gpr125	-3.51	6.19E-10	-10.77	0.00E+00	-10.77	0.00E+00
AB041568			-10.17	0.00E+00	-10.17	0.00E+00
9430077D24Rik	-3.22	2.30E-06	-8.75	0.00E+00	-8.75	0.00E+00
2610511O17Rik					-7.90	0.00E+00
Olig1					-7.82	0.00E+00
matrix-remodelling associated 7			-7.21	0.00E+00	-7.21	0.00E+00
A630076G18Rik					-7.06	1.00E-04
Clcn7	-2.72	5.01E-09	-6.49	0.00E+00	-6.49	0.00E+00
Drctnnb1a			-5.96	3.50E-03	-5.96	2.90E-03
Uap1	-2.63	2.20E-08	-5.70	0.00E+00	-5.70	0.00E+00
2410146L05Rik	-2.49	9.98E-10	-5.65	0.00E+00	-5.65	0.00E+00
Elovl4	-2.45	9.18E-11	-5.44	0.00E+00	-5.44	0.00E+00
Ddr1	-2.43	6.71E-10	-5.34	0.00E+00	-5.34	0.00E+00
A430106J12Rik	-1.17	2.23E-04			-5.30	0.00E+00
Ppan	-2.47	4.90E-09	-5.25	0.00E+00	-5.25	0.00E+00
2310038D14Rik	-2.74	3.29E-05	-4.61	1.00E-03	-4.61	0.00E+00
Nrxn3					-4.53	1.00E-04
Mrps10	-2.90	1.16E-04	-4.33	2.90E-03	-4.33	0.00E+00
Plod2	-2.17	9.28E-06	-4.28	0.00E+00	-4.28	0.00E+00
Atf7ip	-2.06	1.30E-09	-4.15	0.00E+00	-4.15	0.00E+00
9630038C08Rik					-4.05	1.50E-03
Kif3a	-2.38	2.52E-05	-3.95	1.00E-03	-3.95	0.00E+00
2410112O06Rik	-2.42	4.62E-05	-3.90	1.60E-03	-3.90	0.00E+00
F830002E14Rik			-3.82	4.10E-03	-3.82	1.00E-04
B3galt6					-3.74	0.00E+00
A930009K04Rik	-1.89	4.52E-05	-3.66	0.00E+00	-3.66	0.00E+00
Sfrp1			-3.58	3.00E-04	-3.58	0.00E+00
Rps13	-2.28	1.03E-04	-3.58	2.00E-03	-3.58	0.00E+00
Bbs4	-2.03	3.55E-04	-3.53	6.00E-04	-3.53	0.00E+00
Robo3			-3.52	2.40E-03	-3.52	0.00E+00
Srd5a2l	-1.77	2.00E-06	-3.50	0.00E+00	-3.50	0.00E+00

3100003M19Rik	-1.80	7.46E-08	-3.50	0.00E+00	-3.50	0.00E+00
Slit2			-3.46	2.90E-03	-3.46	1.50E-03
Trim11					-3.44	5.00E-04
6330527O06Rik	-1.92	5.97E-05	-3.44	3.00E-04	-3.44	0.00E+00
Hmgn3	-1.79	7.92E-09	-3.41	0.00E+00	-3.41	0.00E+00
Lhx1			-3.34	2.50E-03	-3.34	0.00E+00
E230012J19Rik			-3.31	1.00E-04	-3.31	0.00E+00
Cox7a2l					-3.27	2.78E-02
Mpg	-2.32	2.76E-04			-3.26	0.00E+00
6330414G21Rik			-3.22	2.70E-03	-3.22	0.00E+00
Cops5	-1.66	3.54E-04	-3.21	1.30E-03	-3.21	1.10E-03
A730085F06Rik					-3.01	3.10E-03
LOC235497	-1.58	2.88E-08	-2.98	0.00E+00	-2.98	0.00E+00
Srp9					-2.94	5.40E-03
1200013A08Rik	-1.76	2.52E-05	-2.94	1.00E-03	-2.94	0.00E+00
Fbxo44	-1.57	8.66E-05	-2.94	0.00E+00	-2.94	0.00E+00
8430408J09Rik	-1.60	6.40E-05	-2.90	4.00E-04	-2.90	0.00E+00
LOC381820	-1.52	3.80E-06	-2.88	0.00E+00	-2.88	0.00E+00
2610109H07Rik			-2.85	0.00E+00	-2.85	0.00E+00
Cobl	-1.61	1.20E-05	-2.84	4.00E-04	-2.84	0.00E+00
G630034H08Rik	-1.64	1.30E-04	-2.83	1.80E-03	-2.83	0.00E+00
2810406K13Rik	-1.82	3.16E-04	-2.82	3.50E-03	-2.82	0.00E+00
Lhx1			-2.77	4.20E-03	-2.77	0.00E+00
9430091F09Rik	-1.63	1.73E-04	-2.75	2.10E-03	-2.75	0.00E+00
2900009C24Rik	-1.49	1.49E-04	-2.71	3.00E-04	-2.71	0.00E+00
Asrij	-1.40	3.62E-06	-2.67	1.00E-04	-2.67	0.00E+00
0610034P02Rik			-2.66	0.00E+00	-2.66	0.00E+00
MGC67181			-2.66	4.00E-04	-2.66	0.00E+00
C030034J23Rik					-2.65	1.82E-02
Nfya	-1.52	3.63E-05	-2.63	7.00E-04	-2.63	0.00E+00
Ephb2	-1.32	2.18E-04	-2.62	3.00E-04	-2.62	0.00E+00
A330055K22Rik			-2.57	7.00E-04	-2.57	0.00E+00
Dner	-1.65	2.12E-04	-2.56	4.10E-03	-2.56	0.00E+00
Grb10			-2.54	1.10E-03	-2.54	3.00E-04
Kcnq2					-2.53	2.00E-04
6330415B21Rik	-1.27	2.37E-04	-2.53	2.00E-04	-2.53	0.00E+00
E130216C05Rik			-2.52	3.00E-04	-2.52	0.00E+00
9330161A03Rik					-2.48	1.00E-04
1810006K23Rik	-1.33	2.01E-06	-2.44	1.00E-04	-2.44	0.00E+00
Sncg					-2.43	1.00E-04
Viaat					-2.41	7.70E-03
LOC380983			-2.40	4.30E-03	-2.40	1.00E-04
C430002D13Rik	-1.27	1.69E-05	-2.39	0.00E+00	-2.39	0.00E+00
Neurog2					-2.37	4.00E-04
1200003M09Rik	-1.22	2.38E-05	-2.34	0.00E+00	-2.34	0.00E+00
Cspg3	-1.44	1.68E-04	-2.34	4.10E-03	-2.34	0.00E+00
Zfp330	-1.29	2.18E-04	-2.33	8.00E-04	-2.33	0.00E+00
AW121567					-2.33	8.00E-04
Hspcb					-2.33	7.00E-04

Gria2					-2.33	1.90E-03
Kptn	-1.22	3.38E-07	-2.31	1.00E-04	-2.31	0.00E+00
Dpysl2					-2.31	0.00E+00
Tce1	-1.20	1.43E-06	-2.26	1.00E-04	-2.26	0.00E+00
Fgfr1op2			-2.26	6.00E-04	-2.26	0.00E+00
Phip	-1.17	3.84E-08	-2.25	0.00E+00	-2.25	0.00E+00
LOC381795	-1.15	5.27E-06	-2.25	0.00E+00	-2.25	0.00E+00
Rab6	-1.23	3.81E-05	-2.24	1.20E-03	-2.24	0.00E+00
9630023C09Rik					-2.24	7.60E-03
Anapc13	-1.23	5.77E-06	-2.23	6.00E-04	-2.23	0.00E+00
LOC277193			-2.22	4.00E-04	-2.22	0.00E+00
Slc15a2					-2.22	1.11E-02
4930441L02Rik	-1.14	3.38E-06	-2.21	1.00E-04	-2.21	0.00E+00
9030607L20Rik	-1.16	1.98E-04	-2.20	1.00E-04	-2.20	0.00E+00
1700008D07Rik	-1.13	1.44E-04	-2.19	0.00E+00	-2.19	0.00E+00
Zfp288					-2.14	2.50E-03
Myt1	-1.18	6.90E-05	-2.14	1.20E-03	-2.14	0.00E+00
LOC434147	-1.15	5.99E-05	-2.13	5.00E-04	-2.13	0.00E+00
9130023D20Rik	-1.10	5.27E-05	-2.10	4.00E-04	-2.10	0.00E+00
Dcx	-1.24	2.71E-04			-2.10	0.00E+00
Twsg1	-1.06	1.46E-05	-2.08	1.00E-04	-2.08	0.00E+00
3110035E14Rik					-2.08	9.00E-04
Rab3d	-1.05	4.36E-07	-2.08	0.00E+00	-2.08	0.00E+00
2310004H21Rik	-1.07	1.63E-05	-2.08	1.00E-04	-2.08	0.00E+00
5830420C15Rik	-1.02	1.13E-04	-2.06	5.00E-04	-2.06	0.00E+00
4930427A07Rik					-2.05	1.79E-02
2900063K03Rik			-2.05	3.20E-03	-2.05	1.00E-04
5730406F04Rik			-2.05	1.70E-03	-2.05	2.00E-04
Caskin1			-2.05	0.00E+00	-2.05	0.00E+00
1110029I05Rik	-1.03	1.35E-07	-2.03	1.00E-04	-2.03	0.00E+00
4930524J08Rik					-2.03	7.00E-03
A230057G18Rik					-2.02	3.00E-04
Dncl2b			-2.02	3.30E-03	-2.02	0.00E+00
Snap25					-2.01	7.00E-04

Table 3-2 Down-regulated genes identified by microarray analysis using three statistical analyses (LIMMA, SAM, and t-test) in *Sox3*-null 10.5 dpc embryonic heads

Data is sorted by fold change (FC).; from highest to lowest in t-test.

	LIMMA		SAM		t-test	
Gene/Symbol	**FC**	**p value**	**FC**	**p value**	**FC**	**p value**
5730538E15Rik	-5.1277	2.13E-09	-10.6268	1.00E-04	-53.2700	0.00E+00
Sox3	-5.9436	1.86E-09	-44.0923	0.00E+00	-44.0900	0.00E+00
Xist	-4.5653	1.45E-04	-30.0888	0.00E+00	-30.0900	1.00E-04
1110060M21Rik	-4.0015	2.94E-11	-16.5538	0.00E+00	-16.5500	0.00E+00
Gpr125	-3.5126	6.19E-10	-10.7668	0.00E+00	-10.7700	0.00E+00
9430077D24Rik	-3.2237	2.30E-06	-8.7502	0.00E+00	-8.7500	0.00E+00
Clcn7	-2.7239	5.01E-09	-6.4869	0.00E+00	-6.4900	0.00E+00
Uap1	-2.6270	2.20E-08	-5.6980	0.00E+00	-5.7000	0.00E+00
2410146L05Rik	-2.4916	9.98E-10	-5.6477	0.00E+00	-5.6500	0.00E+00
Elovl4	-2.4503	9.18E-11	-5.4367	0.00E+00	-5.4400	0.00E+00
Ddr1	-2.4344	6.71E-10	-5.3356	0.00E+00	-5.3400	0.00E+00
Ppan	-2.4674	4.90E-09	-5.2533	0.00E+00	-5.2500	0.00E+00
Mrps10	-2.9045	1.16E-04	-4.3344	2.90E-03	-4.3300	0.00E+00
Plod2	-2.1671	9.28E-06	-4.2751	0.00E+00	-4.2800	0.00E+00
Atf7ip	-2.0578	1.30E-09	-4.1455	0.00E+00	-4.1500	0.00E+00
Kif3a	-2.3807	2.52E-05	-3.9492	1.00E-03	-3.9500	0.00E+00
2410112O06Rik	-2.4229	4.62E-05	-3.9019	1.60E-03	-3.9000	0.00E+00
Rps13	-2.2836	1.03E-04	-3.5838	2.00E-03	-3.5800	0.00E+00
Bbs4	-2.0322	3.55E-04	-3.5259	6.00E-04	-3.5300	0.00E+00
Srd5a2l	-1.7693	2.00E-06	-3.5049	0.00E+00	-3.5000	0.00E+00
Hmgn3	-1.7852	7.92E-09	-3.4079	0.00E+00	-3.4100	0.00E+00
Cops5	-1.6609	3.54E-04	-3.2102	1.30E-03	-3.2100	1.10E-03
1200013A08Rik	-1.7594	2.52E-05	-2.9408	1.00E-03	-2.9400	0.00E+00
Fbxo44	-1.5650	8.66E-05	-2.9410	0.00E+00	-2.9400	0.00E+00
Cobl	-1.6142	1.20E-05	-2.8374	4.00E-04	-2.8400	0.00E+00
G630034H08Rik	-1.6440	1.30E-04	-2.8348	1.80E-03	-2.8300	0.00E+00
9430091F09Rik	-1.6267	1.73E-04	-2.7513	2.10E-03	-2.7500	0.00E+00
Asrij	-1.3992	3.62E-06	-2.6724	1.00E-04	-2.6700	0.00E+00
Nfya	-1.5250	3.63E-05	-2.6300	7.00E-04	-2.6300	0.00E+00
Ephb2	-1.3213	2.18E-04	-2.6180	3.00E-04	-2.6200	0.00E+00
Dner	-1.6453	2.12E-04	-2.5586	4.10E-03	-2.5600	0.00E+00
C430002D13Rik	-1.2678	1.69E-05	-2.3871	0.00E+00	-2.3900	0.00E+00
1200003M09Rik	-1.2216	2.38E-05	-2.3381	0.00E+00	-2.3400	0.00E+00
Cspg3	-1.4418	1.68E-04	-2.3408	4.10E-03	-2.3400	0.00E+00
Zfp330	-1.2933	2.18E-04	-2.3318	8.00E-04	-2.3300	0.00E+00
Kptn	-1.2239	3.38E-07	-2.3100	1.00E-04	-2.3100	0.00E+00
Tce1	-1.1950	1.43E-06	-2.2587	1.00E-04	-2.2600	0.00E+00
Phip	-1.1685	3.84E-08	-2.2526	0.00E+00	-2.2500	0.00E+00
Rab6	-1.2319	3.81E-05	-2.2424	1.20E-03	-2.2400	0.00E+00
Anapc13	-1.2317	5.77E-06	-2.2333	6.00E-04	-2.2300	0.00E+00

Myt1	-1.1812	6.90E-05	-2.1431	1.20E-03	-2.1400	0.00E+00
2310004H21Rik	-1.0735	1.63E-05	-2.0798	1.00E-04	-2.0800	0.00E+00
Rab3d	-1.0548	4.36E-07	-2.0800	0.00E+00	-2.0800	0.00E+00
Twsg1	-1.0638	1.46E-05	-2.0762	1.00E-04	-2.0800	0.00E+00
5830420C15Rik	-1.0229	1.13E-04	-2.0556	5.00E-04	-2.0600	0.00E+00

Table 3-3 List of four differentially expressed genes chosen for validation by qPCR showing the fold change as determined by the three statistical tests. Expression location of these genes is also shown
Sox3 is also shown for comparison. Abbreviations: PPHyp, Prependuncular hypothalamus; H, hindbrain; PedHyp, peduncular (caudal) hypothalamus; RSP, rostral secondary prosencephalon; M, midbrain; T, telencephalic vesicle; NA, no data available, FC, fold change; nd, not determined. P<0.05 unless otherwise indicated. [1] Expression location was found using Allen Brain Atlas (http://developingmouse.brain-map.org/). [2] (Wang et al., 2006a).

		ExtraSox3 vs Wild-Type			***Sox3*-null vs Wild-Type**			
Gene	**Gene Name**	**LIMMA FC**	**SAM FC**	**t-test FC**	**LIMMA FC**	**SAM FC**	**t-test FC**	**Expression Location at 11.5 dpc[1]**
Nfya	nuclear transcription factor-Y alpha	nd	nd	nd	-1.52	-2.63	-2.63	PedHyp, RSP
Ngn3	neurogenin 3	nd	nd	nd	nd	-2.53	nd	PedHyp, RSP
Sfrp1	secreted frizzled-related protein 1	nd	nd	-2.45	nd	-3.58	-3.58	PPHyp, H
Nenf	neuron derived neurotrophic factor	nd	20.88	nd	-4.00	-16.55	-16.55	NA, neurons[2]
Sox3	SRY-related HMG box-3	nd	36.00	nd	-5.94	-44.09	-44.09	RSP, PedHyp, M, T

AIM 2: CONFIRM MICROARRAY IDENTIFIED POTENTIAL *SOX3* TARGET GENES BY QPCR

G. Validation of Microarray Data by qPCR

qPCR was performed to validate the expression levels of four identified differentially expressed gene (refer to Table 3-3, p.127).

The genes chosen for validation by qPCR were selected based on exhibiting large degrees of change, which were of biological interest due to their response to a change in condition (in this case deletion of *Sox3*). Given that it was not practical to confirm by qPCR the many thousands of microarray-identified genes, the initial focus was to examine genes of interest that were based on their biological significance (refer to Materials and Methods Chapter 2XIV.F Criteria for the Identification of Differentially Expressed Genes, p.101).

In tandem, Dale's honors work (McAninch, 2008) focused on performing an extensive validation of differentially expressed genes that were identified by microarray (as outlined above). Briefly, all of genes examined demonstrated no change in expression between wild-type and *Sox3*-null 10.5 dpc embryos. Dale examined the two genes that had the highest predicted fold changes from the microarray (*Gpr125* at -9.36 and *Tomm22* at +18.68) by Northern blot analysis (data not shown; refer to McAninch, 2008). There was no change in gene expression for either gene between wild-type and *Sox3*-null samples by Northern blot. This data supported the lack of correlation observed between microarray and qPCR data (McAninch, 2008).

I performed validation by qPCR of the four genes: *Nfya, Ngn3, Sfrp1*, and *Nenf* in addition *Sox3*, which was used as a control. These genes were chosen as they were expressed in the developing hypothalamus at 10.5 dpc. All genes were normalized to *Gapdh* because it showed consistent readings for all samples. The relative expression levels were compared between the *Sox3*-null and wild-type mice (Figure 3-7, p.130). Only two cDNA series were analyzed twice each. Analysis was conducted on *Sox3*-null versus wild-type animals because it is easier to determine the accuracy of the microarray with qPCR data if in fact the gene identified is a target of *Sox3*; loss of *Sox3* would result in a loss of *Sox3* target gene. Relative expression of *Nfya, Ngn3, Sfrp1*, and *Nenf* was analyzed using RNA collected from embryos that were not used in the initially microarray analysis, as these RNA samples were precious with limited quantity and were stored for use to confirm expression of the identified gene. *Nenf,* and *Sfrp1* showed no significant change in gene expression by qPCR when comparing wild-type (n=3) and *Sox3*-null (n=3). However, *Nfya* had a modest decrease in expression and *Ngn3* expression was markedly decreased. Data was normalized to *Gapdh* and expression relative to wild-type. NFYA is a subunit of NFY which is a ubiquitous transcription factor (composed of NFYA, NFYB and NFYC) necessary for DNA binding (Krstic et al., 2007). Generally, NF-Y promotes and/or stabilizes the binding of transcription factors to nearby DNA-binding elements, attracts co-activators and, consequently, enhances transcription (Bellorini et al., 1997; Frontini et al., 2002; Ronchi et al., 1995). Furthermore, it NFY has been shown to be involved in the regulation of the *SOX3* promoter (Krstic et al., 2007). Thus, was not chosen for further analysis.

To confirm the decrease in *Ngn3*, I repeated the experiment in Extra-Sox3 as well as wild-type samples to determine whether there would be any change in *Sox3* and *Ngn3* expression in Extra-Sox3 samples (Figure 3-8, p.130). Both *Ngn3* and *Sox3* genes were normalized to *Gapdh*. *Sox3* expression was significantly decreased in *Sox3*-null samples, and was increased in Extra-Sox3 samples, but this result was not significant. *Ngn3*

expression was significantly decreased in *Sox3*-null samples, and was increased in Extra-Sox3 samples. The large error bars in this sample may be attributed to the different embryos that were collected from different litters. The transgene itself does not contain all the regulatory elements necessary and as such the integration of the Sox3$^{IRES\text{-}GFP}$ transgene is random whereby some Sox3-positive cells will express this (unpublished data, personal communication A/Prof Paul Thomas); some cells will express endogenous and exogenous levels. It must be noted that microarray analysis did not detect up-regulation of *Ngn3* (refer to Table 3-4, p.127).

To further verify that the decreased expression of *Ngn3* seen in independently collected embryonic heads from *Sox3*-null mice was an accurate representation, I proceeded to repeat the qPCR experiment using RNA samples that were obtained from wild-type and *Sox3*-null (n=6 per group) samples used in microarray analysis (Figure 3-9, p.131). *Sox3* and *Ngn3* expression was significantly decreased in *Sox3*-null samples. Due to the very limited amount of RNA used in microarray analysis there was only enough to perform this experiment once (in addition to my colleague's experiments (as outlined in McAninch, 2008).

All the genes listed (as shown in Table 3-4, p.127), except *Ngn3*, did not show differential expression by qPCR. Expression levels of *Sox3* and *Ngn3* were consistent with the microarray data; *Sox3* and *Ngn3* were down-regulated. These data suggest that microarray data accurately established differences in gene expression between the wild-type and *Sox3*-null whole embryonic head, at least for this particular gene and the positive controls (detailed above). Given the promising result of *Ngn3*, and the previous published result indicating that Sox3 is co-expressed with Ngn3 in spermatogonial cells (Raverot et al., 2005), I decided to focus on this gene and compare it's expression with Sox3 in the developing hypothalamus.

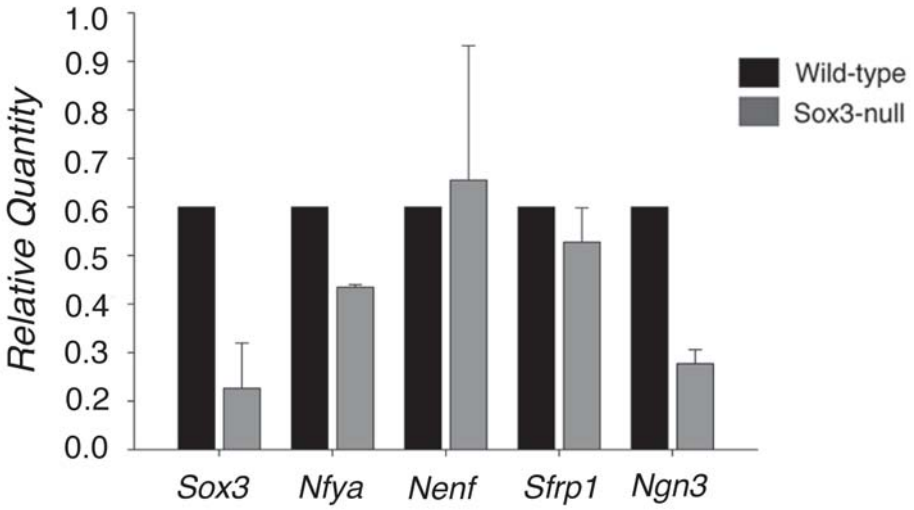

Figure 3-7 qPCR analysis showing relative quantitation of 10.5 dpc embryonic heads showing the expression profile of four microarray identified genes *Sox3*, *Nfya, Nenf, Sfrp1* and *Ngn3* in wild-type and *Sox3*-null mice

Normalized expression levels of each gene are shown relative to *Gapdh*. Two cDNA series were analyzed twice each. Error bars represent Standard Deviation of the two series.

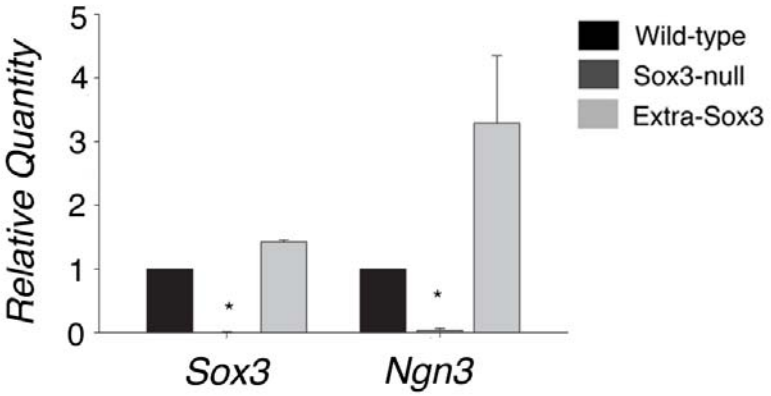

Figure 3-8 qPCR analysis showing relative quantitation of 10.5 dpc embryonic heads showing the expression profile of *Ngn3* and *Sox3* in wild-type, *Sox3*-null and Extra-Sox3 mice

Normalized expression levels of each gene are shown relative to GAPDH. Three cDNA series were analyzed thrice each. Error bars represent SEM of the three series. * $p<0.05$.

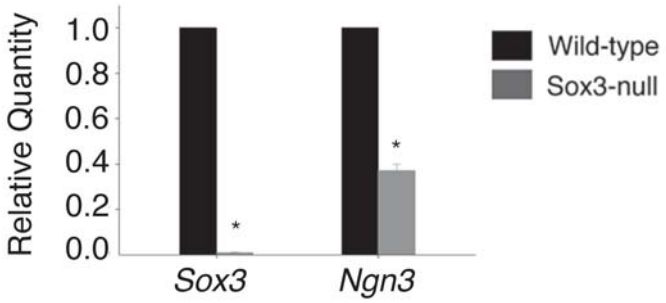

Figure 3-9 qPCR analysis showing relative quantitation of 10.5 dpc embryonic heads used in microarray analysis showing the expression profile of *Ngn3* and *Sox3* in wild-type and *Sox3*-null mice
Normalized expression levels of each gene are shown relative to GAPDH. Three cDNA series were analyzed thrice each. Error bars represent SEM of the three series. * $p<0.05$.

AIM3: EXPRESSION OF *SOX3* AND *SOX3* TARGET GENE(S)

H. *Ngn3* is Expressed in the Developing Hypothalamus

The expression of Ngn3 in the hypothalamus has not been previously characterized in mice, but has been studied in the developing zebrafish hypothalamus (Wang et al., 2001). Indeed, little is known about its role during HP axis development. Briefly, Ngn3, a bHLH transcription factor and member of the neurogenin family, plays a critical role in the specification of endocrine cells in pancreatic Islets of Langerhans cells (Gradwohl et al., 2000). In the pancreas, *Ngn3*-expressing cells have been identified to be progenitor cells fated to become islet endocrine cells (Gradwohl et al., 2000).

Given that *Ngn3* was decreased in *Sox3*-null, relative to wild-type, by both microarray and qPCR, together with the previous published result indicating that *Sox3* is co-expressed with *Ngn3* in spermatogonial cells (Raverot et al., 2005), I focused my efforts on examining the expression of *Ngn3* together with *Sox3* in the developing hypothalamus, between 10.5 dpc and 14.5 dpc.

Firstly, I examined mRNA expression of Ngn3 by *in situ* hybridization. The Ngn3 probe was kindly donated from DJ Anderson, Howard Hughes Medical Institute, California Institute of Technology (Pasadena, CA, USA). The generation of the plasmid used is described by (Sommer et al., 1996). *Ngn3* was expressed within the developing hypothalamus (Figure 3-10, p.135). *Ngn3* expressing cells appeared located more dorsal in *Sox3*-null sections. Although there was a slight difference in the section-plane between wild-type and *Sox3*-null, the region of *Ngn3* expression was decreased in the *Sox3*-null hypothalamus. Within the median eminence of the *Sox3*-null sections Ngn3 expressing cells were absent. Ngn3 was not detected in progenitor cells, as it is not on in the ventricular layer and does not appear to be expressed there. However, this may be attributed to the slight variation in location of the regions and the slight angle-variation when sections were cut.

I. Ngn3 is Co-expressed with Sox3 in the Developing Hypothalamus

To further examine the expression of Ngn3 and Sox3 during hypothalamic development I asked two questions. Firstly, does the expression of Ngn3 overlap with Sox3. Secondly, is the expression of Ngn3 decreased in *Sox3*-null mice, compared to age matched wild-type littermates. To answer these questions I used immunostaining as this technique enables one to examine overlapping expression. Furthermore, I examined

several developmental time-points (10.5-15.5 dpc) to gain a better understanding of expression during hypothalamic development.

The initial time point I examined was 10.5 dpc; the same time point used in microarray analysis. Coronal sections through the embryonic brain were obtained. As shown in Figure 3-11 A (p.136) Ngn3 is expressed in ventral hypothalamic cells and within the median eminence in wild-type sections. In *Sox3*-null mice there is an absence of Ngn3-positive ($Ngn3^+$) cells within the ventral hypothalamic region. A closer examination, by higher power magnification, revealed that not all Sox3-positive ($Sox3^+$) cells co-express Ngn3 (Figure 3-11 B, p.136). There is overlapping expression; we see $Ngn3^+Sox3^-$ cells, $Ngn3^-Sox3^+$ and $Ngn3^+Sox3^+$. This overlapping expression is restricted to the lateral (ventral hypothalamic) cells. Expression is consistent with the data presented by *in situ* (providing confidence that the Ngb3 antibody is specific).

The next time point I examined was 12.5 dpc to determine whether there was a loss of Ngn3 in any region of the hypothalamus and examine whether there was overlapping expression with Sox3. Embryos from wild-type and *Sox3*-null mice were collected at 12.5 dpc and sectioned in the coronal (Figure 3-12, p.137) and sagittal plane (Figure 3-13, p.138). Immunostaining of 12.5 dpc in coronal sections did not reveal any gross loss of $Ngn3^+$ cells in the hypothalamic region or within the median eminence of *Sox3*-null mice compared to wild-type. $Ngn3^+Sox3^+$ cells were not identified nor were there GFP^+Ngn3^+ cells in *Sox3*-null sections; GFP cells represent cells that would normally be expressing Sox3. Therefore, to examine further the possibility of a loss of $Ngn3^+$ expressing cells, sagittal sections were obtained, as these are able to show a greater region through the developing hypothalamus and Rathke's pouch. In sections from wild-type embryos $Sox3^+$ cells were expressed throughout the developing neuroepithelium (infundibulum and presumptive hypothalamus), whereas $Ngn3^+$ cells were localized to cells within the posterior infundibulum and presumptive hypothalamus. In sections from *Sox3*-null embryos there was an absence of $Ngn3^+$ cells within the posterior infundibulum (Figure 3-13 B *vi*), median eminence, dorsal to the Rathke's pouch, and the presumptive hypothalamus.

The next time point I examined was 14.5 dpc to further examine the expression of Ngn3 and Sox3 and determine whether Ngn3 'switches-off' during later development. Embryos from wild-type and *Sox3*-null mice were collected at 14.5 dpc and sectioned in the coronal plane (Figure 3-14, p.139). Immunostaining of 14.5 dpc in coronal sections did not reveal any gross loss of $Ngn3^+$ cells in the hypothalamic region or within the median eminence of *Sox3*-null mice compared to wild-type. However, $Ngn3^+$ cells were very scarce

in both wild-type and *Sox3*-null in the hypothalamic region. In wild-type Ngn3$^+$ cells were located within the ventral hypothalamic region, whereas in *Sox3*-null Ngn3$^+$ cells were located within the arcuate nucleus (on left region only in Figure 3-14). This variation in location of Ngn3$^+$ cells may be attributed to the slight difference in section processing between wild-type and *Sox3*-null embryos.

15.5 dpc embryos were also collected and immunostained for Ngn3 and Sox3, however no Ngn3$^+$ cells were observed (data not shown). This suggests that there is a small developmental window (at least between 10.5-14.5 dpc) during which Ngn3 cells are expressed within the developing hypothalamus and co-express with some Sox3-expressing cells.

In summary, at 10.5 dpc in the wild-type Ngn3 expression overlapped with Sox3 in cells located in the ventral hypothalamus and median eminence. In *Sox3*-null, Ngn3 was absent in the ventral hypothalamus. At 12.5 dpc, in coronal sections, there no gross loss of Ngn3+ cells in the hypothalamic region or within the median eminence of *Sox3*-null mice compared to wild-type. Examination of sagittal sections from wild-type and *Sox3*-null embryos revealed that there was an absence of Ngn3+ cells within the posterior infundibulum, median eminence (dorsal to the Rathke's pouch) and the presumptive hypothalamus of *Sox3*-null embryos. At 14.5 dpc, in coronal sections, there was no gross loss of Ngn3+ cells in the hypothalamic region or within the median eminence of *Sox3*-null mice compared to wild-type. At 15.5 dpc no Ngn3+ cells were detected. These data suggest that Ngn3 may be indirectly regulated by Sox3 (Figure 3-15, p.140).

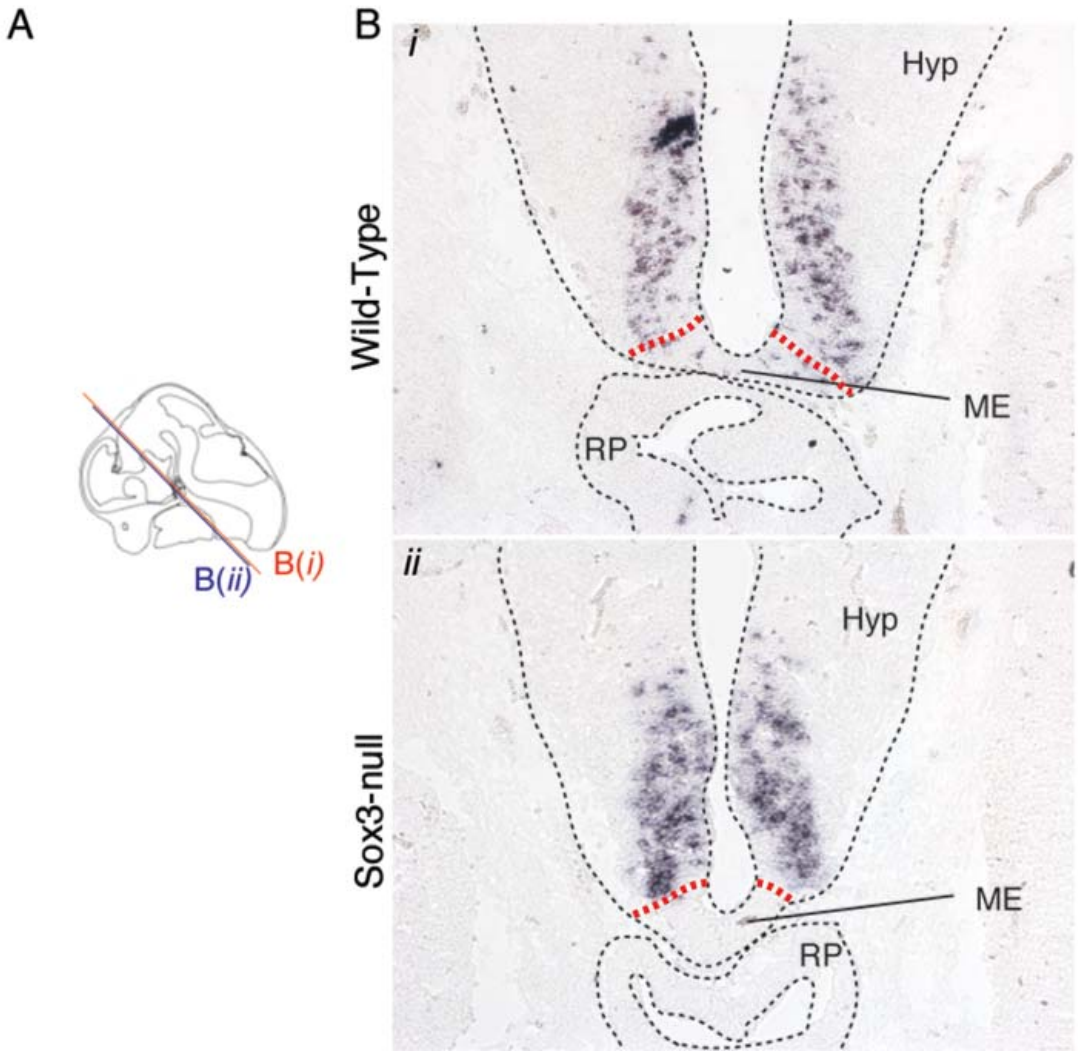

Figure 3-10 Expression of *ngn3* in the developing hypothalamus of wild-type and *Sox3*-null 12.5 dpc coronal sections by in situ hybridization.

(A) Schematic representation of a sagittally sectioned 12.5 dpc mouse embryo. Lines indicate the corresponding sections shown in B. Red dashed lines indicated the region of the median eminence. Black dashed lines represent the outline of the hypothalamus and Rathke's pouch (RP). (B) Expression of *ngn3* in the 12.5 dpc developing hypothalamus. Shown are adjacent coronal sections from wild-type (i) and *Sox3*-null (ii). *ngn3* transcript is detectable in the hypothalamic region. Abbreviations: Hyp, hypothalamus; ME, median eminence; RP, Rathke's Pouch.

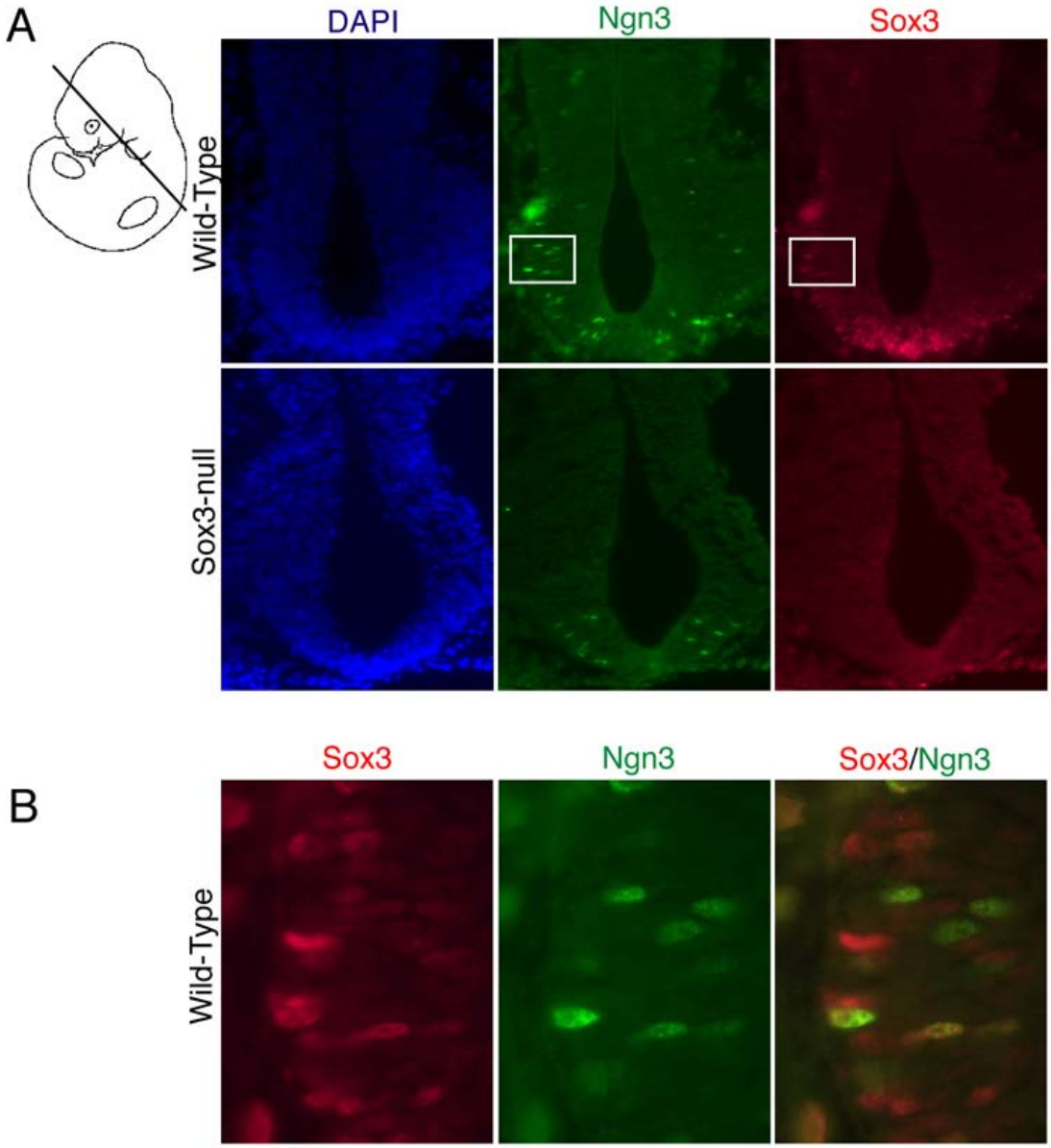

Figure 3-11 Ngn3 is co-expressed with Sox3 in the developing hypothalamus at 10.5 dpc wild-type and *Sox3*-null mice – coronal orientation.

(A) Coronal sections through the embryonic brain (region shown in mouse embryo schematic). Sections are slightly more posterior to the median eminence. *Sox3*-null mice show an absence in the ventral hypothalamic region. (B) High magnification images of wild-type region (as shown by box in A). Not all $Sox3^+$ cells co-express Ngn3. Co-expression (as shown in the merged image by yellow immunostaining) of $Ngn3^+Sox3^+$ is seen in few cells. Images were captured using a Zeiss Axioplan 2 microscope and AxioCam MRm with Axiovision software. Magnification 10x in (A) and 100x (oil) in (B).

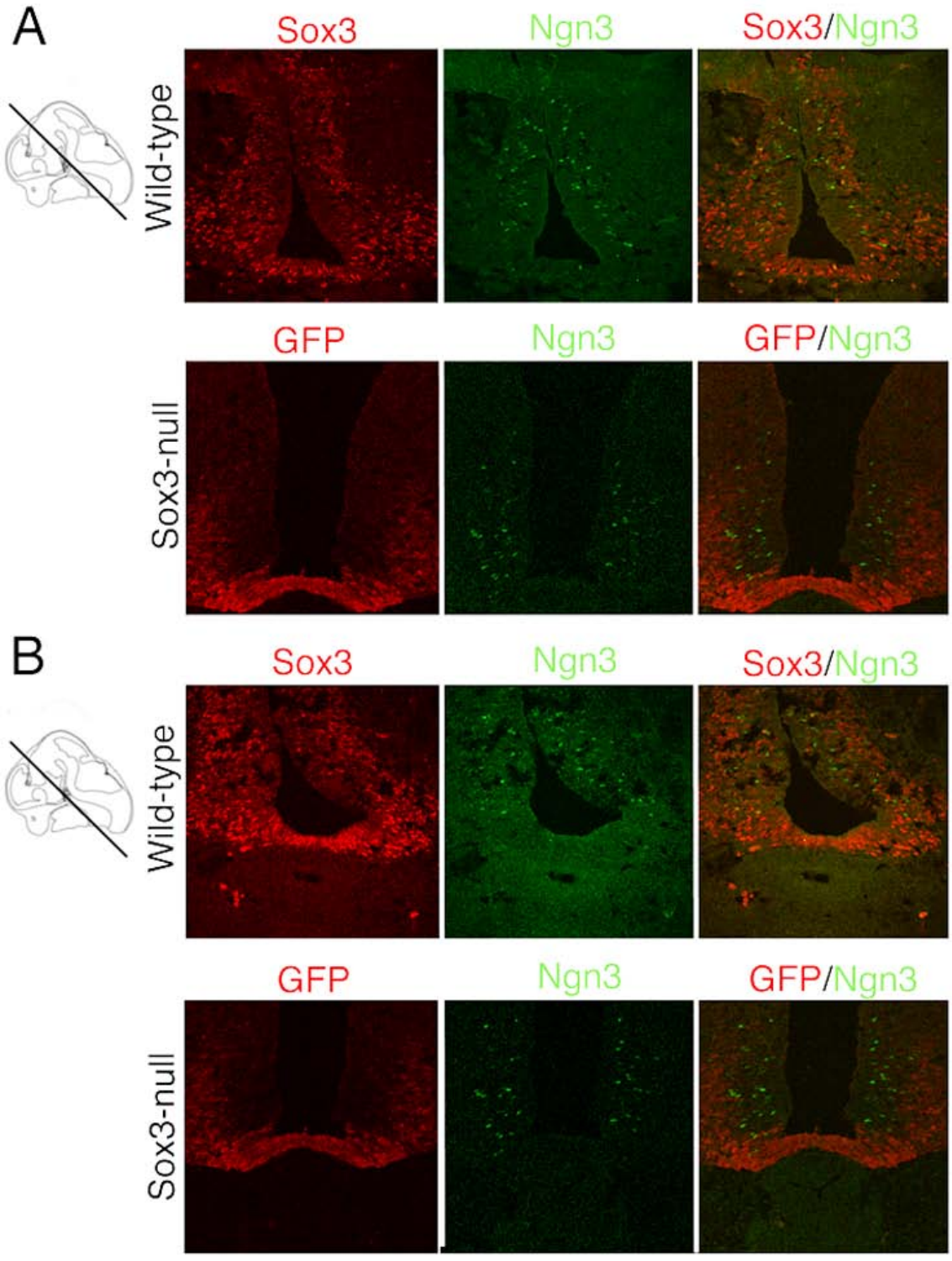

Figure 3-12 Expression of Ngn3 and Sox3 in the developing hypothalamus at 12.5 dpc wild-type and *Sox3*-null mice – coronal orientation

Coronal sections through the embryonic brain (region shown in mouse embryo schematic). (A) Sections are slightly posterior to the median eminence. There were no $Sox3^{+}Ngn3^{+}$ cells in either wild-type or *Sox3*-null sections. (B) Sections are slightly more anterior (to those in A). There was no distinct difference in expression of $Ngn3^{+}$ cells. Images were captured using a Zeiss Axioplan 2 microscope and AxioCam MRm with Axiovision software. Magnification 20x.

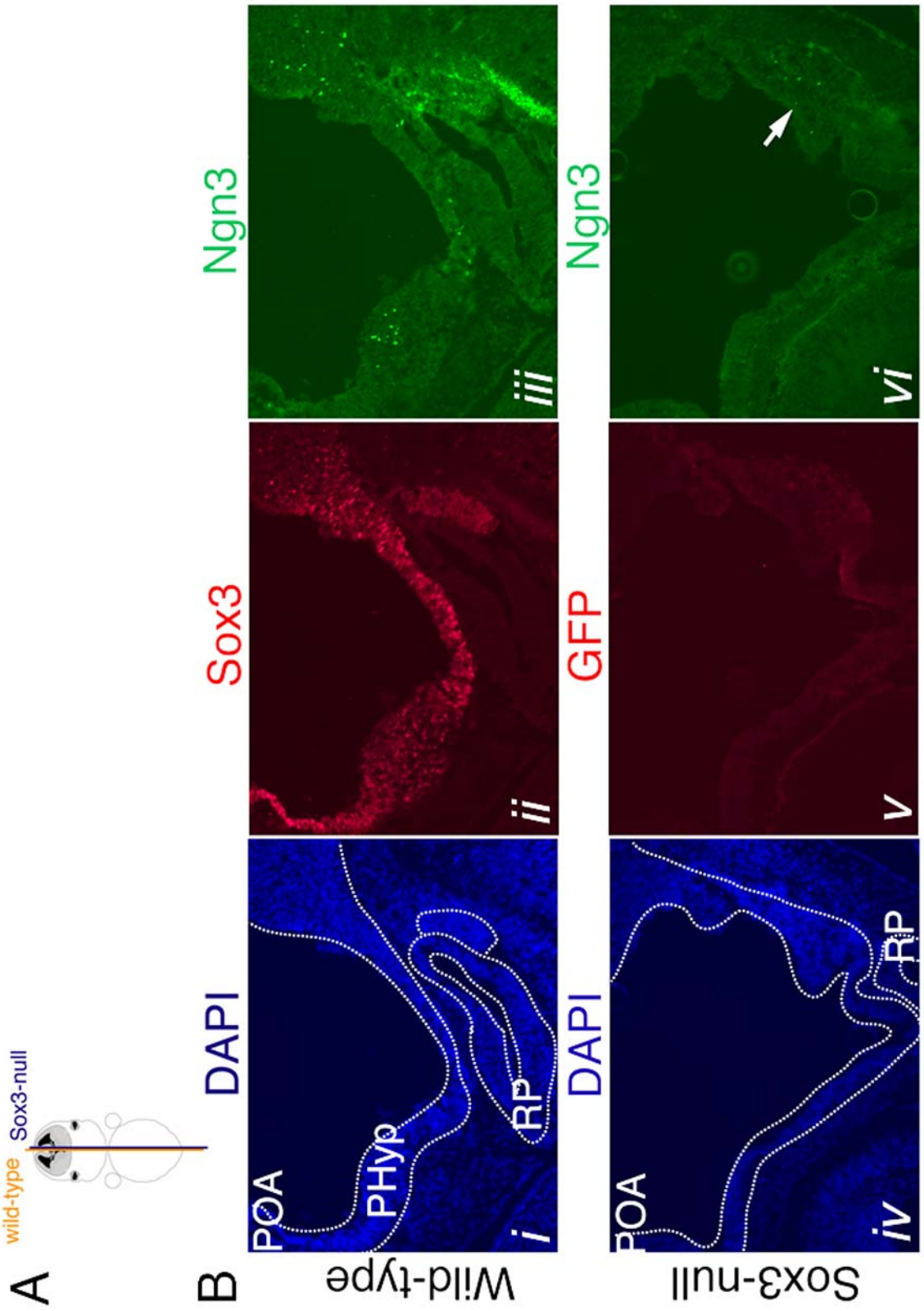

Figure 3-13 Expression of Ngn3 and Sox3 in the developing hypothalamus at 12.5 dpc in wild-type and *Sox3*-null mice – sagittal orientation

(A) Schematic representation of the embryonic brain. Lines indicate corresponding sections in B. (B) Ngn3^{+} cells are absent in the median eminence (arrow in panel *vi*), dorsal to the Rathke's pouch (RP). Images were captured using a Zeiss Axioplan 2 microscope and AxioCam MRm with Axiovision software. Magnification 20x. Abbreviations: POA, pre-optic area; PHyp, presumptive hypothalamus.

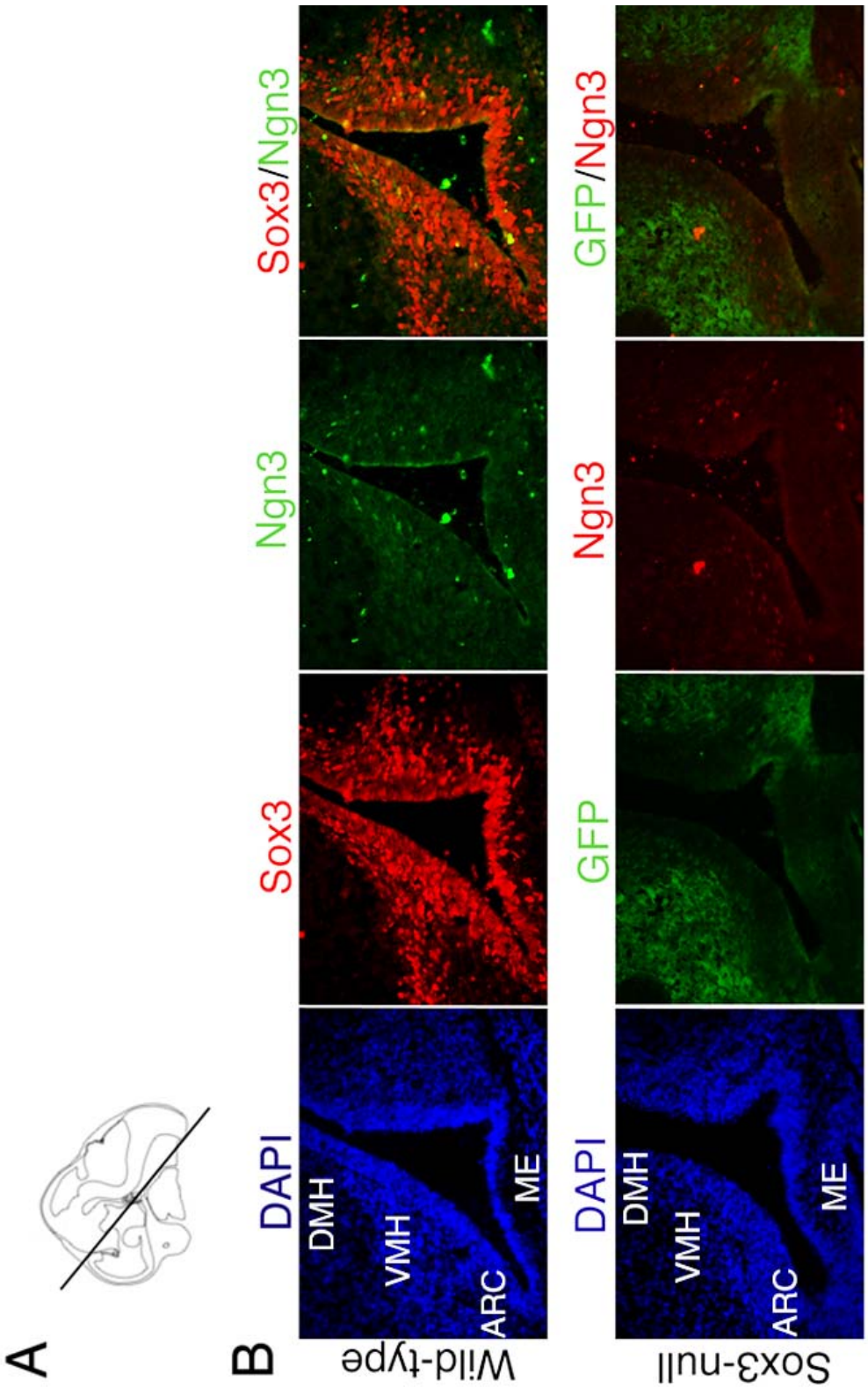

Figure 3-14 Expression of Ngn3 and Sox3 in the developing mouse hypothalamus at 14.5 dpc – coronal orientation.

(A) Schematic representation of coronal section through the embryonic brain. (B) *Sox3*-null mice show Ngn3^{+} (red) cells in the ventral hypothalamic area. In wild-type mice, Ngn3^{+} cells (green) are located ventral. Images were captured using a Zeiss Axioplan 2 microscope and AxioCam MRm with Axiovision software. Magnification 20x. Abbreviations: DMH, dorsal medial hypothalamus; VMH, ventromedial hypothalamus; ARC, arcuate nucleus; ME, median eminence.

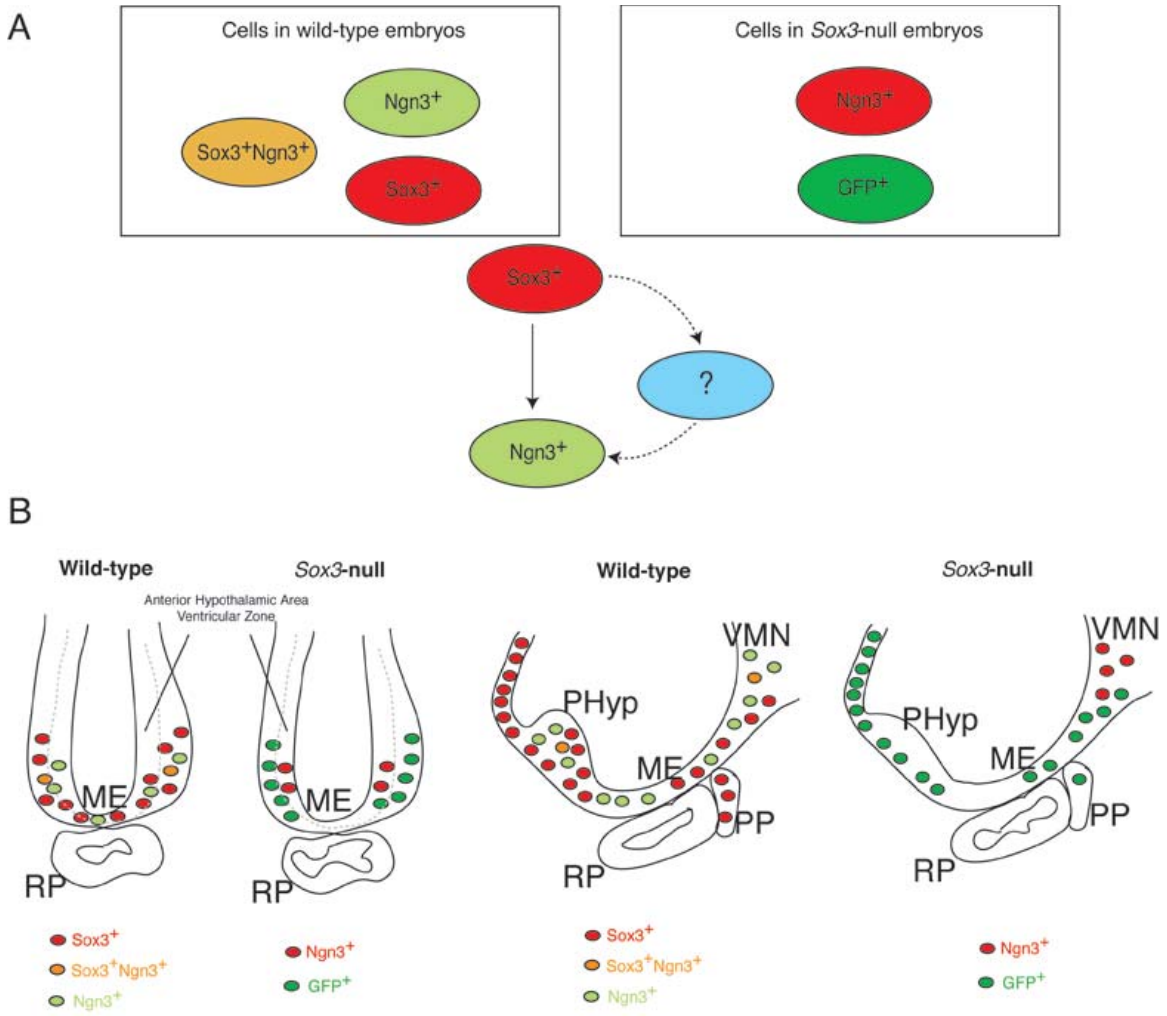

Figure 3-15 Model of Ngn3 and Sox3 cells during mouse HP axis development between 10.5 – 12.5 dpc.

(A) Schematic representation of the Ngn3+, Sox3+, GFP+, and Sox3+Ngn3+ cells detected in the developing hypothalamus at 10.5 dpc. (B) Schematic representation of the regions expressing Ngn3+, Sox3+, GFP+, and Sox3+Ngn3+ cells in wild-type and *Sox3*-null embryos at 10.5 dpc in the coronal plane and 12.5 dpc in the sagittal plane. Abbreviations: RP, Rathke's pouch; ME, median eminence PHyp, presumptive hypothalamus; VMN, ventromedial nucleus, PP, posterior hypothalamus.

IV. DISCUSSION

The function and expression of *Sox3* in brain development has been well studied in mice and humans and it's disruption/deletion has been linked to XH (Alatzoglou et al., 2008; Bergstrom et al., 2000; Brunelli et al., 2003; Bylund et al., 2003; Laumonnier et al., 2002; Neves et al., 2007; Nikcevic et al., 2008; Rizzoti et al., 2004; Rizzoti and Lovell-Badge, 2007; Stevanovic et al., 1993; Wang et al., 2006b; Woods et al., 2005). However, we do not know the target gene(s) of *Sox3/SOX3*, either direct or indirect. By setting out to identify *Sox3* target genes we are likely to gain a greater understanding of the mechanisms involved in brain development. To tackle this gap in our knowledge microarray analysis was chosen as a tool to examine change in gene expression at 10.5 dpc in wild-type, *Sox3*-null and Extra-Sox3 mouse embryos, with the aim to identify potential *Sox3* target genes. As microarrays act as a tool, it is important to validate the data generated with an independent approach, in this case qPCR. Genes that are detected as being differentially expressed are validated by qPCR and subsequently these identified and confirmed differentially expressed gene(s) can be further analyzed for expression by *in situ* hybridization and immunohistochemistry.

A. FACS Does Not Yield Enough GFP+ Cells from *Sox3*-null 10.5 dpc Mouse Embryonic Heads

In order to examine the gene expression differences between the *Sox3*-null, Extra-*Sox3* and wild-type mice a microarray gene profiling approach was utilized. In this study, Illumina BeadChip glass microarrays were chosen over the previously used Affymetrix membrane arrays, as they offered a number of benefits including their ability to simultaneously analyze six different samples at once, improved image acquisition and analysis, and increased number of genes per array. The originally intended source of RNA was sorted GFP^+ cells from embryonic 10.5 dpc heads from the three *Sox3* transgenic strains using FACS. A similar study examined *Pax2*-regulated genes in mid-hindbrain patterning from E10.5 wild-type and $Pax2^{-/-}$ embryos carrying a $Pax2^{GFP}$ BAC transgene (Bouchard et al., 2005). The authors successfully identified genes, using cDNA microarray technology that depends on Pax2 function for their expression in the mid-hindbrain boundary region (Bouchard et al., 2005). However, adapting this method to the *Sox3* gene proved to be an insurmountable challenge to collect enough GFP^+ cells per embryo to extract enough RNA for microarray analysis. The required RNA minimum was 50ng for microarray hybridization.

As described in Chapter 1II Sox Family of Transcription Factors (p.50), Sox3 is expressed within the developing CNS. In the transgenic mouse models of altered Sox3 expression, GFP has been inserted in place of *Sox3* in *Sox3*-null mice. Using live GFP imaging I was able to determine which mice carry the transgene. However, live-GFP in these mice is not very intense. As reported by (Corish and Tyler-Smith, 1999) it is still debatable as to how accurately GFP fluorescence intensity is a reliable indicator of GFP levels in the cell. Corish and Tyler-Smith (1999) suggest that two factors may significantly affect the fluorescent properties of GFP, namely the requirement for post-translational oxidative fluorophore formation and the sensitivity to cellular pH. These could result in fluorescence intensities being lower than actual GFP concentration (Corish and Tyler-Smith, 1999). Analysis by western blot analysis has shown that a good correlation exists between fluorescence intensity and protein concentration (Li et al., 1998). It is likely that the low GFP fluorescence of these cells is contributing to the low numbers being collected through FACS.

I examined two methods of cell dissociation, one using trypsin and another using a combination of collagenase B and dispase II in Hank's Balanced Salt Solution. Both methods were trialed thrice and in all cases results showed that less than 0.1% of all cells per embryo head were sorted as GFP-positive cells. For the microarray, a minimum of 50ng RNA is required per group. To be able to collect enough cells to generate enough RNA to be collected, an extremely large number of embryos, and subsequently matings, would need to be set-up according to a schedule that would provide sufficient 10.5 dpc embryos on a single day for dissociating and sorting sufficient Sox3 cells (refer to 3III.A, p.108). In a similar study, Bouchard et al, 2005 found that 5,000 cells produced approximately 5ng RNA (Bouchard et al., 2005). Extrapolating this result to my RNA needs in order to obtain the required minimum 50ng RNA would require approximately 30 GFP^+ embryos per mouse line. As an alternative to sorting GFP^+ cells a different approach was taken. Briefly, I set about collecting 10.5 dpc embryonic heads (cut below the second branchial arch) from which total RNA was extracted and analyzed for integrity using the Agilent 2100 bioanalyzer (Adelaide Microarray Facility, University of Adelaide, Adelaide, South Australia, Australia). RNA samples were chosen based on their RNA integrity number (RIN), which assigns a numerical value (based on the amount of RNA degradation) for the quality of RNA. RNA was determined to be of high quality with RINs between the ranges of 7.5-10. For each transgenic *Sox3* mouse line a total of three samples were analyzed: two RNA samples from independent mouse embryos from two different litters and one pooled sample from four independent mouse embryos. The pooled and individual mouse embryo samples of RNA were used to help reduce individual variation, increase the emphasis on

specific variation caused by the loss of *Sox3* and increase the reproducibility of the experiment during statistical analysis. A similar experimental design approach has previously been utilized for the identification of *Rfx4v3* target genes involved in brain development in the mouse (Zhang et al., 2006). These authors successfully isolated RNA from 10.5 dpc wild-type and Rfx4vs-null embryonic mouse heads and identified differentially expressed genes between samples (Zhang et al., 2006). A similar study, examining differentially expressed genes in the developing hypothalamic region of E12.5 SIM1-null and wild-type mice, successfully identified both up- and down-regulated genes, using an oligonucleotide-based microarray (Caqueret et al., 2006). In this study, the anterior hypothalamus (AH) was isolated from embryos by first splitting the head on the midline and from the two halves the AH was bisected. Although this method collected and used a precise area, it has some disadvantages. Isolating the same precise region from each embryo is difficult, and is likely to include surrounding tissue that includes genes specific to that area. In turn, these will be detected in the microarray and could results in a higher false-positive identification. Nonetheless, the authors were able to focus in on known genes that act downstream of *Sim1* in the embryonic hypothalamus.

B. Microarray Analysis Validation

A comparison of all the statistical tests, SAM and t-test, revealed that a total of 45 genes were identified as down-regulated in *Sox3*-null mice. In contrast, only 18 genes were identified as down-regulated in *Sox3*-null mice using the LIMMA statistical method. The various statistical approaches resulted in some genes being detected as differentially expressed and others not. Here, RNA was extracted from whole embryonic mouse heads, rather than from the GFP^+ cells. Therefore, it is expected that there will be a higher false-positive discovery rate. It is evident that the genes known to be down-regulated are confirmed. As part of the validation process, my colleague Dale McAninch performed extensive validation on some of the known genes using both independent and microarray RNA samples. Briefly, he chose control genes *Sox3, GFP,* and *Xist* to examine by qPCR. He demonstrated that *Sox3* and GFP are only expressed in wild-type and *Sox3*-null samples, respectively, and *Xist* is only present in female samples; the expected outcomes (McAninch, 2008). Furthermore, the GFP ORF, which replaces the *Sox3* ORF is another positive control. In wild-type samples Sox3 should only be detectable whereas in *Sox3*-null samples only GFP. The microarray data detected Sox3 in wild-type samples but not in *Sox3*-null samples, however GFP was not detected in either wild-type or *Sox3*-null samples. The microarray GFP probe detects enhanced GFP (eGFP) that has approximately 30% silent base substitutions compared with GFP. Thus, this is the likely explanation for why the

microarray was unable to detect GFP in the *Sox3*-null samples. By using qPCR primers for GFP Dale was able to detect GFP in *Sox3*-null samples thereby demonstrating expression in *Sox3*-null but not wild-type samples. These results confirmed that some of the genes identified by microarray analysis were correct, as validated by qPCR. However, many of the genes identified by microarray and chosen by my colleague, Dale McAninch, for validation by qPCR were not confirmed.

While it remains unclear why there were such a high number of false positive genes within the microarray, there are a number of possibilities pertaining to the microarray process. These include the quality of RNA, array hybridization, data analysis and data validation (Morey et al., 2006).

RNA was extracted from the 10.5 dpc mouse embryonic heads and analyzed using the Agilent Bioanalyzer (Adelaide Microarray Facility, The University of Adelaide). The higher the quality of RNA, based on RIN higher than 8, is better suited for microarray and qPCR analysis (refer to Figure 3-3, p.114 and Chapter 2XIV.B Analysis of RNA Quality, p.93). All RNA samples used in the microarray were of the highest quality and are unlikely to have resulted in the variability seen. My colleague, Dale McAninch, analyzed a number of the microarray RNA samples by qPCR and the results showed identical gene expression to independent RNA and cDNA preparations (McAninch, 2008).

Microarray hybridization involves the incubation of each aRNA sample with one array, allowing binding to its corresponding probe. Bound RNA probes are washed and incubated with Cy3 conjugated streptavidin that is then followed by image acquisition using a fibre optic scanner that measures the fluorescence intensity (measures the absolute abundance of a transcript) of each bead. Array hybridization and data collection were performed by the AUSTRALIAN GENOME RESEARCH FACILITY (AGRF) and the quality of data was assessed by standard proprietary quality control measures; all passed. It is unlikely that an error here affected the identification of differentially expressed genes, given that all positive control genes were confirmed by qPCR (as detailed above).

One of the core goals of microarray data analysis is to identify the genes which were being differentially expressed. The major important goal is to select a statistic that will rank the genes in order of evidence for differential expression, from strongest to weakest. The primary importance of ranking genes arises from the fact that only a limited number of genes can be tested. By using the criteria outlined in Chapter 2XIV.F Criteria for the Identification of Differentially Expressed Genes (p.101) I was able to use this together with the three statistical methods (LIMMA, SAM, and t-test) to identify differentially expressed genes (refer to results section 3III.E Identification of Differentially Expressed

Genes, 120). As discussed above, the positive control genes, *Sox3, GFP* and *Xist* were identified correctly by the microarray and confirmed by qPCR. However, my colleague, Dale McAninch, was unable to confirm the gene set he had chosen. However, from those I selected (*Nfya, Ngn3, Sfrp1,* and *Nenf*) only *Ngn3* was confirmed down-regulated by qPCR (Figure 3-9, p.131) (discussed below). It appears that many of the genes identified as being differentially expressed appear to have some evidence of expression within the developing brain. Perhaps the false positive data represents inaccuracies in the measurement of absolute levels of these genes. It is therefore probable that real changes in gene expression due to the loss of *Sox3* are present. Nevertheless, to detect them would require the analysis of all genes identified by the microarray, technically possible but expensive and time consuming.

C. Microarray Analysis and qPCR Validation Reveal Ngn3 as a Likely Target Gene of *Sox3*

Of the genes I selected (*Nfya, Ngn3, Sfrp1,* and *Nenf*) from the microarray results, that were expressed within the developing hypothalamus, for validation by qPCR, only *Ngn3* was down-regulated in *Sox3*-null mice (Figure 3-8 and Figure 3-9, p.131). In Extra-Sox3 10.5 dpc mice *Ngn3* was not significantly up-regulated, this may be due to *Ngn3* requiring a cofactor at higher levels. This was not examined further but requires validation (Figure 3-8, p.130).

Ngn3, a bHLH transcription factor and a member of the neurogenin family (of which there are two additional members, Ngn1 and Ngn2), plays a critical role in the specification of endocrine cells in the pancreatic Islets of Langerhans (Gradwohl et al., 2000) and is expressed in the developing hypothalamus of zebrafish (Wang et al., 2001). Specifically, *Ngn3*-expressing cells in the pancreas have been shown to be progenitor cells that are fated to give rise to islet endocrine cells (Gradwohl et al., 2000). However, little is known about *Ngn3*/Ngn3 expression and function in the hypothalamus. Furthermore, previous reports have only described Ngn3 expression at various stages in the pancreas (Burlison et al., 2008; Gradwohl et al., 2000; Murtaugh, 2007; Schwitzgebel et al., 2000) with limited detail pertaining to its characterization in the hypothalamus (Wang et al., 2001).

Here, I identified expression of the *Ngn3* RNA transcripts at 10.5 dpc and protein during hypothalamic development in mice between 10.5-14.5 dpc (discussed below). Interestingly, this is the first study to have identified *Ngn3* as a potential target gene of *Sox3* in the developing hypothalamus, in mice. I define a dramatic and previously unnoticed gap in developmental Ngn3 expression in the hypothalamus; limited studies

have examined the role of Ngn3 in the developing hypothalamus, in mice (Raverot et al., 2005; Wang et al., 2001). The results presented within this body of work shows that both Ngn3 and *Sox3* transcript and protein expression occur during early development at 10.5 dpc, and that Ngn3 expression is not detected at 15.5 dpc (data not shown). It is tempting to speculate that Ngn3 expression within the hypothalamus plays a critical role in the specification of hypothalamic endocrine cells.

From previous studies in the pancreas we know that Ngn3 commits the fates of pancreatic progenitors to endocrine cell types (Baeyens et al., 2006; Gasa et al., 2004; Gradwohl et al., 2000; Huang et al., 2000; Lee et al., 2001; Mellitzer et al., 2006; Petri et al., 2006; Villasenor et al., 2008). Targeted inactivation of *Ngn3* leads to complete absence of all four differentiated endocrine cell types, in the pancreas (Gradwohl et al., 2000). Mice homozygous for the Ngn3 null mutation develop diabetes and die 1-3 days after birth (Gradwohl et al., 2000); the hypothalamus of these mice has not been examined. Ngn3-positive ($Ngn3^+$) cells are present in all embryonic stages between E9 and E18.5 in the developing mouse pancreas (Apelqvist et al., 1999; Jensen et al., 2000a; Jorgensen et al., 2007; Schwitzgebel et al., 2000). Hitherto each pancreatic cell only transiently expresses Ngn3 in a shorter-than-48-hour time frame (Gu et al., 2002; Schwitzgebel et al., 2000). Thus, there are three distinct aspects of Ngn3 expression that require tight regulation. Firstly, the number of $Ngn3^+$ cells needs to be controlled to ensure that there is a balance between islet cell differentiation and progenitor cell proliferation (Apelqvist et al., 1999; Jensen et al., 2000b). Second, the expression of Ngn3 must reach a threshold level to activate endocrine differentiation (Wilson et al., 2002). Third, Ngn3 expression must be down-regulated for endocrine differentiation to become switched on.

The known target genes of *Ngn3*, detected in pancreatic tissue, are NEUROD1, NKX2.2, PAX4, insulinoma-associated 1 (IA1) and myelin transcription factor 1 (Myt1) (Huang et al., 2000; Mellitzer et al., 2006; Smith et al., 2003). Only Myt1 was detected as down-regulated in *Sox3*-null embryonic heads, by all three statistical tests with a fold change greater than 2, in the microarray study (refer to Appendices - Microarray DATA showing differentially expressed genes, p.210). *Neurod1,* although not detected by microarray, is expressed within the developing hypothalamus. Recently, a study identified, by chromatin immunoprecipitation, a zinc-finger transcription factor, OVO homolgue-like 1 (OVOL1) as a direct target of Ngn3 (Vetere et al., 2010). OVOL1 belongs to a family of evolutionarily conserved genes found in *C. elegans*, Drosophila, mice and humans, and regulates the development of epithelial tissues and germ cells (Dai et al., 1998; Oliver et al., 1987). In mice, *Ovol1* expression is limited in its cellular distribution to skin, testis and

kidneys (Dai et al., 1998; Li et al., 2005; Nair et al., 2006). *Ovol1* was not detected by microarray.

D. Expression Studies by Immunohistochemistry Reveal that Sox3 and Ngn3 are Co-expressed in the Developing Hypothalamus

Immunostaining and *in situ* hybridization (compare Figure 3-10, p.135 and Figure 3-12, p.137, respectively) was not conducted on consecutive sections from the same embryo, therefore I am unable to determine accurately whether *Ngn3* transcript is more wide-spread throughout the hypothalamic region than the protein, which was clearly restricted to individual scattered cells; in some of which the expression of Ngn3 overlapped that of Sox3. It is possible that *in situ* hybridization is more sensitive and therefore better at detecting low levels of *Ngn3*, than immunostaining. Moreover, these observations could be suggesting that post-transcriptional regulation may be important during endocrine differentiation. Certainly, this has been the case when examining *Ngn3* transcript and protein expression in the developing pancreas, in mice (Villasenor et al., 2008).

It was also observed that Ngn3-expressing cells contained variable levels of protein (Figure 3-11, p.136), as determined by immunostaining. It is likely possible that this high versus low expression correlates with the initial differentiation of hypothalamic endocrine cells. This transient expression has been shown to occur in pancreatic cells (Gu et al., 2002; Schwitzgebel et al., 2000; Villasenor et al., 2008). Interestingly, cells expressing high levels of Sox3 also express high levels of Ngn3, and are located in the mid-dorsal hypothalamic region. We know that the hypothalamic cells differentiate outside-in (lateral - medial), with the cells located more lateral being more differentiated (refer to the review by (Szarek et al., 2010)). Thereby, it is likely that those cells expressing high levels of both Ngn3 and Sox3 that are found more lateral are undergoing differentiation, whereas those found more medial are likely to have been differentiated. The exact fate of these cells remains unknown and warrants further investigation. Although we do not know for certain whether Ngn3 is a direct target of *Sox3*, it is likely to be an important downstream gene that shapes hypothalamic endocrine development and neurodifferentiation, an area poorly understood. In the examination of Ngn3 during neurodifferentiation in zebrafish, (Wang et al., 2001) found a region harboring ngn3 expression in the anterior hypothalamus (for a review please see (Rubenstein et al., 1998)). Interestingly, at 48-hour post fertilization, cells expressing ngn3 were juxtaposed to a domain of expression of SF-1-related ff1b (NR5A4). In zebrafish Ff1b, a member of the Ftz-F1 subfamily of orphan nuclear receptors,

has been established as the homolog of SF-1 (Mazilu et al., 2010; Quek and Chan, 2009). Ff1b has been proposed to alter hypothalamic and hypophysial function (Chai and Chan, 2000). In mice that lack SF-1 there is an almost complete ablation of the ventromedial hypothalamic nucleus. This region has been implicated in the regulation of GnRH neurons (Dellovade et al., 2000). In mice and rats, GnRH neurons, all born in the olfactory placode at E9.5, are found scattered in the medial septum, preoptic area and anterior hypothalamus (Jasoni et al., 2009). It remains a mystery as to how and why GnRH neurons end up in these forebrain regions. These results further suggest a potential role of Ngn3 in hypothalamic neuroendocrine cell differentiation, at least in mice and zebrafish. It remains unclear the function of Ngn3 in the developing neuroendocrine hypothalamus.

E. Conclusion and Future Directions

In conclusion, the experiments outlined were designed to further knowledge in the role Sox3 plays during brain development, with the hope of identifying key target genes. This study provides the first detailed analysis of gene expression in *Sox3*-null and Extra-Sox3 10.5 dpc mouse embryonic heads by microarray. This study demonstrated that the majority of genes determined to be down-regulated by microarray could not be confirmed by either qPCR or Northern blot analysis (McAninch, 2008) and accordingly the data may have contained many false-positive results. However, only one gene, *Ngn3*, was found to be down-regulated by both microarray and qPCR methods. Thus, these data provide a foundation for further studies, specifically in examining in more detail Ngn3, a potential downstream target gene in Sox3 signaling during brain development.

Another practicable path to successfully identify target genes of *Sox3* by microarray would be to use neurospheres generated from Sox3 expressing tissues (recently generated in the lab, Nick Rogers) or knockdown cell cultures or those over-expressing Sox3. Neurospheres and cell cultures would provide a more homogenous source material, however it is uncertain as to how the information obtained would reflect endogenous *Sox3* targets.

A different approach would be to perform Chromatin Immunoprecipitation (ChIP), a cost effective and technically accessible procedure. In brief, ChIP utilizes cells of interest that are cross-linked and would thereby bind protein and DNA. For this procedure, cells need to be fragmented by sonication, followed by sonication of the DNA into fragments that are suitable for PCR. With the use of a specific antibody, in this case SOX3, DNA/protein complexes are precipitated from solution. The DNA retrieved is then analyzed by one of several methods currently available. For example, ChIP sequencing,

which allows sequencing of all DNA present in the sample, provides a robust catalogue of SOX3-bound DNA regions. This catalogue of sequences provides regulatory regions to which *Sox3* binds, thereby providing direct target gene identification. However, ChIP sequencing is not able to provide information on indirect targets because these are not directly bound. Cells for the use in ChIP can be obtained from two sources. Ideally, cells would be collected from 10.5 dpc mouse embryonic heads. Cells that express Sox3 would be obtained from age-matched wild-type embryos, whereas for negative control cells from age-matched *Sox3*-null embryos. In addition, *Sox3*-expressing neurospheres could also be utilized. For ChIP to be successful a specific antibody for Sox3 is required. There are currently two Sox3 specific antibodies commercially available, both have been successfully trialed in immunohistochemistry: one produced by R&D (this antibody was used in the immunostaining experiments within this body of work) and the second by GenWayBio (Catalog Number: 18-003-43230; CA, USA). Note: Even though an antibody may be successful in detecting the protein in sections by immunostaining, this does not necessarily indicate success for ChIP.

Aside from further experiments, a bioinformatics approach can be applied to identify differentially expressed genes, given that we know that Sox3 binds to the Sox Consensus Motif (AAC AAT). Many bioinformatics approaches and tools have been developed for comparative genomics analysis. Using these approaches one is able to find orthologous relationships of genes by analyzing their protein sequences as well as looking for transcription factor binding sites with these tools. Furthermore, by using known functional information about the gene of interest, one can use statistical models to discover novel targets. These include using motif-finding algorithms, such as MEME (Bailey and Elkan, 1995) and Gibbs Sampler (Lawrence et al., 1993), and promoter and gene finders, such as Twinscan (Korf et al., 2001). Together with microarray analysis and ChIP data, the use of statistical methods will significantly increase the analyzing power in discovering differentially expressed genes.

Given that Ngn3 was identified as down-regulated, by both microarray and qPCR, and has been previously detected to be co-expressed in Sox3 expressing cells, at least in spermatogonial cells (Raverot et al., 2005), it would be advantageous to examine this connection further. For example, taking advantage of the available transgenic mouse line expressing the *Cre*-recombinase gene under the control of the mouse *Ngn3* gene promoter to characterize the activity of *Ngn3* and tracing Ngn3 progeny during hypothalamic development (Yoshida et al., 2004)

We do know that Ngn3 is expressed from E9.5, in mice (Villasenor et al., 2008) and, from the results shown here, Ngn3 is not detected at 15.5 dpc (data not shown). Furthermore, I detected that Ngn3 is co-expressed in some, but not all, Sox3-expressing cells. This raises the question whether the expression is region specific and also whether there is an effect on timing. As shown at 10.5 dpc, there were more Sox3-expressing/Ngn3-expressing cells than when comparing to 14.5 dpc. Moreover, which neuroendocrine cells require Ngn3 for differentiation? To examine this further we can generate Nestin-*Cre* CNS-specific *Ngn3*-null mice and look for hypothalamic defects.

Overall, the results from this project provide important insights into the identification of *Sox3* target genes. Identification of a decreased expression of Ngn3 in the developing brain of *Sox3*-null mice is intriguing, but further work is required to determine its exact role and function during hypothalamic development. Further research into hypothalamic development is likely to have a considerable importance for human health. Genetic defects in the development of specific cell subtypes in the hypothalamus may directly lead to disorders of metabolism (already reported for congenital obesity (Holder et al., 2000)) and homeostasis.

4 Novel Dwarf Mouse Generated by ENU Mutagenesis

I. INTRODUCTION

Dysfunction of the hypothalamic-pituitary axis (HP) axis occurs in approximately 1 in 2,200 live births (Pescovitz and Eugster, 2004) and is associated with a range of common disease states including short stature, infertility, hypogonadism, poor stress management and slow metabolism. While several genes involved in common disease states have been identified the genetic cause in many patients remains unknown.

Growth-deficient mice provide an invaluable model with which to elucidate the molecular mechanisms involved in the physiological regulation of growth and the genetic influence. Various growth-retarded mouse models have been generated from spontaneous gene mutations that have resulted in dwarfism and have provided an extremely useful system with which to elucidate the mechanisms of GH regulation and transcription factor interplay. However, dwarfism is not limited to disorders that affect the pituitary gland (e.g. GH1) and/or hypothalamus (GHRHR) (refer to Chapter 1IV.A Growth-Hormone and Growth Hormone-Releasing Factor, p.59). In this study I identified and further examined a

novel recessive mouse mutant, *Tukku*[7], exhibiting dwarfism. The mouse was generated by N-ethyl-N-nitrosourea (ENU) mutagenesis at The Australian Phenomics Centre (APC, Canberra, ACT, Australia). The mutation was identified to be a point mutation of leucine to proline, at residue 30 in the ORF, in the *Wars* gene (*Wars*^{L30P}). Although the identification of the mutation was not made apparent until further into the characterization of the dwarfism phenotype, I would like to provide a very brief introduction to this gene.

Wars, or tryptophanyl-tRNA synthetase, belongs to a large family of enzymes, the aminoacyl-tRNA synthetase (AARS) family of enzymes. AARSs are large enzymes that have evolved from two different active sites, gradually incorporating additional domains (Ribas de Pouplana and Geslain, 2008). There are 20 cytoplasmic AARSs in vertebrates, each specific for one amino acid. AARS enzyme are named after their single letter amino acid code and followed by 'ARS'. For example, the ARS for tryptophan (amino acid code W) is known as WARS (also known as TrpRS, whereby Trp is for tryptophan). AARSs have a broad repertoire of functions beyond translation, including transcriptional and translational regulation as well as cell signaling (Martinis et al., 1999). AARSs also have canonical functions, which is the specific aminoacylation of tRNAs with their cognate amino acids. Aminoacylated tRNAs are then used by the ribosome for transmission of codon information into protein sequence (Figure 4-1, p.153). Importantly, AARS have been linked to regulating the noncanonical activity of angiogenesis (the formation of new capillaries from preexisting vasculature by migration and proliferation of endothelial cells) (Otani et al., 2002; Wakasugi, 2010; Wakasugi and Schimmel, 1999; Wakasugi et al., 2002b).

II. AIMS

The overall aims of this study were to:

- Characterize the primary pathology of the dwarfism phenotype that links the function of the mutation to dwarfism by focusing on altered regulation of the GH axis (*Aim 1*);
- Confirm the mutation by sequencing (*Aim 2*);
- Examine the expression of the mutant protein, specifically focusing on the HP axis (*Aim 3*).

[7] Tukku, meaning 'small' in Kaurna Aboriginal language. For simplicity the homozygous *Tukku* mouse with the Wars^{L30P} mutation will be referred to as 'dwarf' or '*Wars*^{l30P}' dwarf throughout this work.

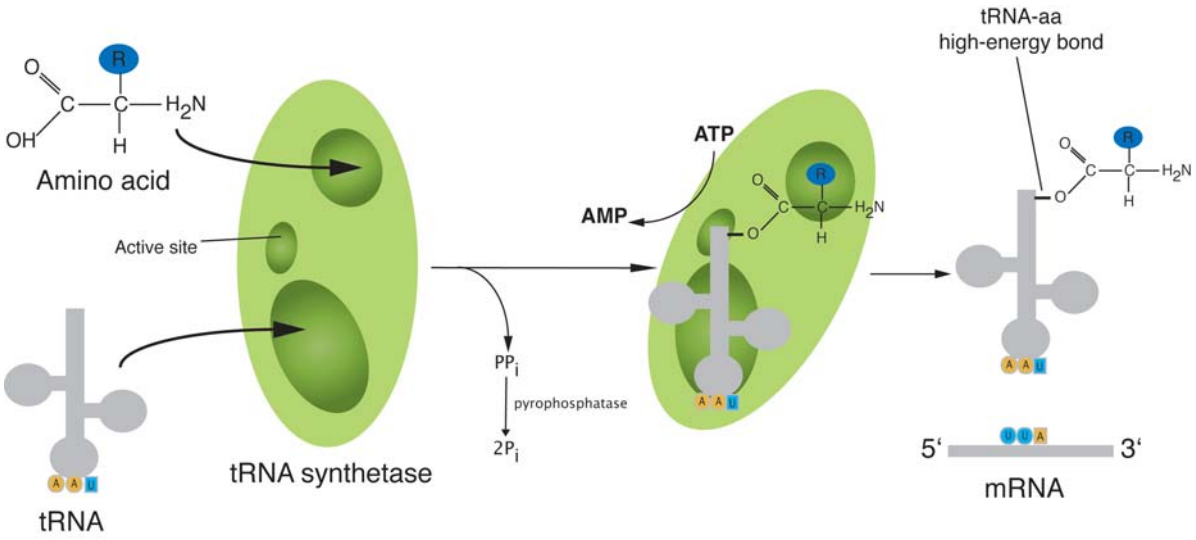

Figure 4-1 Aminoacylation of tRNA

Amino acids are covalently linked to tRNAs by aminoacyl-tRNA synthetases (AARS). Each AARS recognizes one kind of amino acid (aa) and all the cognate tRNAs that recognize codons for that aa. The process occurs in two steps. Firstly, AARS forms an aminoacyl-AMP complex using energy from the hydrolysis of ATP. The equilibrium of the reaction favors the synthetase complexed with the aminoacyl-AMP because the pyrophosphate (PPi) is converted to inorganic phosphate (2Pi) by a pyrophosphatase. Secondly, the aminoacyl moiety is transferred to the 3′ terminal adenosine of the cognate tRNA; tRNA-aa high-energy bond.

III. RESULTS

AIM 1: CHARACTERIZE THE PRIMARY PATHOLOGY OF THE DWARFISM PHENOTYPE THAT LINKS THE FUNCTION OF THE MUTATION TO DWARFISM BY FOCUSING ON ALTERED REGULATION OF THE GH AXIS

A. Dwarf Mice Show a Reduced and Sustained Decrease in Weight and Growth

To characterize the growth phenotype of dwarf mice, body weight was measured over a 4-month period (at 10 day intervals, post-weaning), and at pre-weaning (postnatal days (P) 1, 7 and 14). Body length was measured in 8-week old mice (male and female).

Strikingly, growth curves showed that dwarf mice weighed considerably less than their corresponding wild-type littermates by the time of weaning (Figure 4-2 A and B; p.155). There was no difference between wild-type and heterozygous mice. Consequently, the remaining analysis was performed on wild-type and homozygous dwarf mice[8]. The difference in body weight was not obvious during the first 3 postnatal weeks (P1, P7, and P14; Figure 4-2 C and D) but became significant when mice reached weaning age (P21-29). On average, adult dwarf mice weighed 30-40% less than their wild-type littermates. Dwarf mice exhibited reduced longitudinal growth, displaying a dwarf-like appearance (Figure 4-2 B). Specifically, adult dwarf mice were 10% shorter than their control littermates (Figure 4-2 E).

[8] Herein, for simplicity, when referring to homozygous dwarf mice the term dwarf will be used, unless otherwise stated.

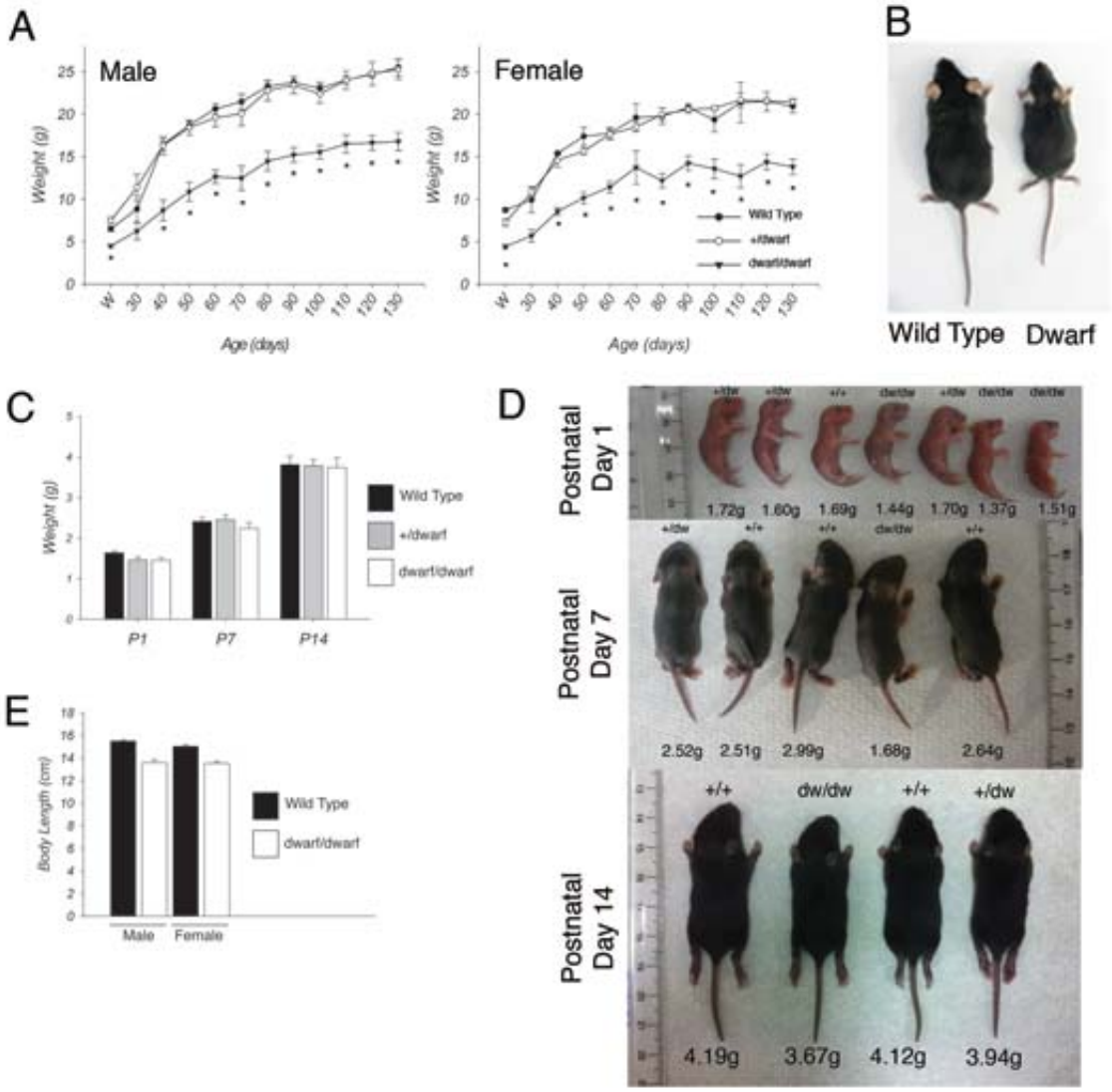

Figure 4-2 Body weight and length of dwarf and control littermates

(A) Growth curves of dwarf (homozygous dwarf (dwarf/dwarf; solid triangle), heterozygous mice (+/dwarf; open square) and their wild-type littermates (solid circle). Pups were weighted at weaning (W) (21-29 days postnatal), again at day 30, and every 10 days thereafter. Homozygous dwarf mice weighed significantly less than their control littermates. Wild-type (female: n=4; male: n=6), heterozygous (female: n=8; male: n=7), and homozygous dwarf (female: n=5; male: n=7) mice. (B) Physical appearance of a representative dwarf and control mouse (Female littermates, 8-weeks). (C) Bar graph showing the weights of homozygous dwarf (dwarf/dwarf) heterozygous (+/dwarf) mice and their wild-type littermates (male and female) from 3 litters per time point, postnatal day 1 (P1), 7 (P7) and 14 (P14). Number of pups/genotype/sex are as follows-P1: wild-type female (n=4), male (n=4); +/dwarf female (n=3), male (n=1); dwarf/dwarf female (n=4), male (n=3). P7: wild-type female (n=4), male (n=4); +/dwarf female (n=5), male (n=4); dwarf/dwarf female (n=2), male (n=2). P14: wild-type female (n=3), male (n=1); +/dwarf female (n=2), male (n=4); dwarf/dwarf female (n=3), male (n=1). Due to low number per sex results were pooled and bar graph represents data from both female and male/genotype. No significant differences were noted at each time point. (D) Physical appearance of representative postnatal pups from one of the three litters at P1, P7 and P14 showing weights (g) and genotype. (E) Body length of wild-type and dwarf mice (8-week; male and female). No significant differences were noted. Measurements show the distance from the tip of the nose to the base of the tail. Data are given as mean±SEM. *, $P < 0.05$, as compared with the corresponding wild-type group.

B. Dwarf Mice Show Decreased Pituitary GH and Serum IGF-1 Levels

To explore the mechanisms underlying the dwarf phenotype displayed I measured the level of GH in whole pituitary extracts and the serum levels of the key hormone involved in somatic growth, IGF-1. Pituitary GH levels were significantly reduced in dwarf mice compared to wild-type littermates (Figure 4-5 A, p.162). GH is released into the blood stream from the anterior pituitary and binds to specific receptors in the liver, where it triggers the secretion of IGF-1. Circulating IGF-1 is considered the major factor that mediates the stimulatory effects of GH on longitudinal growth (Nilsson et al., 2005; Yakar et al., 2002). Consistent with the whole pituitary GH levels observed, dwarf mice showed a striking reduction in the serum levels of IGF-1 (Figure 4-5 B). It is therefore likely that the observed decreases in GH levels and serum IGF-1 in dwarf mice are responsible for the observed growth deficit.

C. Dwarf Mice Show a Pronounced Hypoplasia of the Anterior Pituitary Gland

The morphology of the pituitary gland, where GH and several other important hormones are synthesized and stored, was examined for anatomical alterations. The pituitary gland of dwarf mice was significantly smaller than that of their wild-type littermates (Figure 4-5 C). The anterior pituitary of dwarf mice was disproportionally smaller than in wild-type. Figure 4-5 D shows that the pituitary glands from dwarf mice weighed 30-40% less than those of wild-type mice. In contrast, brains from wild-type and dwarf mice were not noticeably different in size at 8-weeks (Figure 4-5 E). However, the total brain weight was significantly lower in dwarf mice (Figure 4-5 F). Figure 4-5 G indicates that the pituitary hypoplasia displayed by dwarf mice was primarily caused by a dramatic decrease in the size of the anterior pituitary (the size of posterior pituitary appeared essentially unchanged). Besides the pituitary hypoplasia displayed by the dwarf mice, there was no noticeable differences in overall brain morphology between the dwarf and wild-type mice (Figure 4-5 E and also refer to Section D, p.157).

To examine the morphology of pituitary glands from dwarf mutant mice and wild-type littermates in greater detail, pituitary gland sections were prepared and stained with an antibody directed against GH (Figure 4-5 G). The size of the posterior pituitary, which stores and releases only two major hormones, AVP and OT, was similar in dwarf and wild-type mice (compare also Figure 4-5 C). In striking contrast, the size of the anterior pituitary gland/area of GH staining was greatly reduced in the dwarf mice compared with

wild-type littermates (Figure 4-5 G). Note that 40-50% of anterior pituitary cells are GH-secreting somatotropes (refer Table 1-1, p.30) (Lin et al., 1993).

D. Histopathology of the Dwarf Mouse Brain

Analysis of adult (8-week) dwarf pituitaries revealed marked hypoplasia (Figure 4-5, p.162) of the anterior lobe (which contains GH-secreting somatotropes). This phenotype is typical of mice with GH deficiency due to a hypothalamic-pituitary GH axis dysfunction (Alba and Salvatori, 2004). Together with the detection of significantly lower serum IGF-I levels (Figure 4-5, p.162), results indicate that the dwarf *Wars*^{L30P} mutation compromises the hypothalamic-pituitary-somatotrope axis. This defect may perhaps arise from abnormal development of the hypothalamus, the anterior pituitary or the portal vasculature that conveys hypothalamic peptides (such as GHRH) to their pituitary target cells (e.g. somatotropes). In wild-type mice, the number of hypothalamic neurons in the ARC producing GHRH, and the total GHRH mRNA and protein levels, steadily increases during postnatal development and plateaus once adulthood is reached (Bartke, 1965; Garcia-Tornadu et al., 2006; Sinha et al., 1975). Conversely, mice with congenital GH deficiency, due to a primary defect in GH-secreting cells of the anterior pituitary, have a deficiency in GH-mediated negative feedback, which results in overstimulation of the hypothalamus. Subsequently leading to excessive numbers of GHRH neurons, producing abnormally high *Ghrh* mRNA levels (McGuinness et al., 2003; Phelps and Hurley, 1999). In contrast, the GH inhibitory peptide Sst is abnormally low in the hypothalamus of mice with a defect in pituitary GH. Pituitary hypoplasia/GH deficiency that results from the defective development of the hypothalamus has the opposite phenotype (i.e. decrease(↓) GHRH:increase(↑) Sst levels). Thus, guided by this information I firstly performed histological analysis (using H&E staining) of the hypothalamus at 8-weeks in male and female wild-type and dwarf mice. Sagittal and coronal sections were carefully inspected for structural abnormalities focusing primarily on areas implicated in growth regulation (ARC and ventromedial hypothalamus (VMH)). Secondly, I examined mRNA levels of *Ghrh* and *Sst.* These results are presented in the proceeding section (Section E, p.160).

Brain sections were stained with H&E in the sagittal (Figure 4-3 A and B, p.158) and the coronal Figure 4-3 C and D) orientation of wild-type and dwarf 8-week old mice (male and female). Only male sections are shown (Figure 4-14), as there was no observable difference between the males and females. Figure 4-3 A shows the representative photomicrographs of the brain, sectioned in the sagittal plane. Figure 4-3 B shows higher power representative photomicrographs of the ARC and lateral hypothalamus (LH). There

was no distinct pathological difference between wild-type and dwarf mice. Figure 4-3 C shows the representative photomicrographs of the brain, sectioned in the coronal plane. Figure 4-3 D shows the representative photomicrographs of ARC, VMH and median eminence. Panels from wild-type and dwarf are from regions as closely matching as possible. There was an observed variation in cell density within the VMH in dwarf (when comparing nuclei staining; dark purple/blue) compared to wild-type mice. Additionally, there appears a decrease in cell density within the ARC in dwarf compared to wild-type mice. Altogether, sections from 4 wild-type and 4 dwarf mice were examined. All sections examined showed the same phenotype; there was no difference between males and female mice. Importantly, the ARC houses GHRH neurons (Suhr et al., 1989).

Figure 4-3 Gross brain morphology of dwarf and wild-type littermates

(A) Representative sagittal brain sections (H&E stained) from a wild-type (Left) and a dwarf mouse (Right). Sections are from 8-week-old males. Altogether, sections from 4 wild-type and 4 dwarf mice were examined. (B) Higher magnification of H&E stained sections from wild-type (*i*) and dwarf (*ii*) mice. No obvious differences in brain morphology or in the HP axis were observed. (C) Representative coronal brain sections (H&E stained) from a wild-type (Left) and a dwarf mouse (Right). Sections are from 8-week-old males. Altogether, sections from 4 wild-type and 4 dwarf mice were examined. (D) Higher magnification of H&E stained sections from wild-type (*i* at x2.5 magnification; *ii* at x10 magnification) and dwarf (*iii* at x2.5 magnification; *iv* at x10 magnification) mice. No obvious differences in hypothalamic morphology were observed. Note: panels from wild-type and dwarf are from regions as closely matching as possible. Variation is observed when trying to match regions between sections. In *iv* cell density appears less than that of *ii*. Abbreviations: VM, ventromedial hypothalamus; LH, lateral hypothalamus; OX, optic chiasm; Pe, periventricular hypothalamic nuclei; CC, corpus callosum; DM, dorsomedial hypothalamic nuclei; ME, median eminence; Arc, arcuate nucleus; VMH, ventromedial hypothalamus.

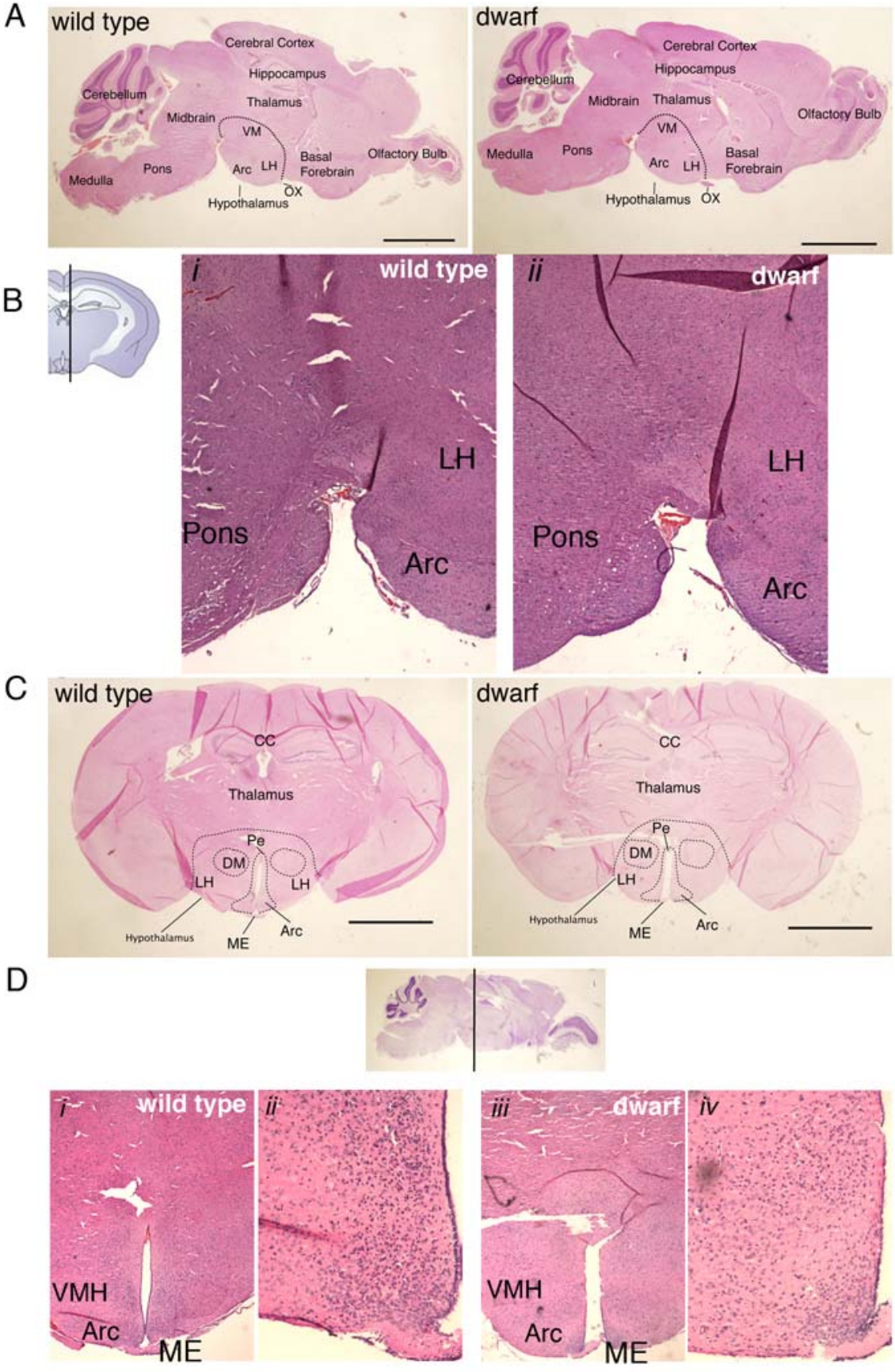
A
wild type
Cerebral Cortex
Hippocampus
Cerebellum
Thalamus
Midbrain
VM
Basal
Forebrain
Olfactory Bulb
Pons
Arc
LH
Medulla
OX
Hypothalamus
dwarf
Cerebral Cortex
Hippocampus
Cerebellum
Midbrain
Thalamus
Olfactory Bulb
VM
Medulla
Pons
Arc
LH
Basal
Forebrain
Hypothalamus
OX
B
i
wild type
LH
Pons
Arc
ii
dwarf
LH
Pons
Arc
C
wild type
CC
Thalamus
Pe
DM
LH
LH
Hypothalamus
ME
Arc
dwarf
CC
Thalamus
Pe
DM
LH
Hypothalamus
ME
Arc
D
i
wild type
VMH
Arc
ME
ii
iii
dwarf
VMH
Arc
ME
iv

E. Hypothalamic GHRH and Somatostatin Levels Are Significantly Reduced in Dwarf Mice

The anterior pituitary, which is not of neuronal origin, is derived from the oral ectoderm, as detailed in the introduction (Chapter 1I.B Vertebrate Pituitary Development, p.26) (Cohen and Radovick, 2002). As a result of the GH and IGF-1 assay results, as well as the histological evidence suggesting that there is a low density of neurons within the arcuate nucleus (region where GHRH nuclei are found (Suhr et al., 1989)) (refer to previous histological data in the above section (D Histopathology of the Dwarf Mouse Brain, p.157), it is tempting to speculate that the defect leading to the hypoplasia of the anterior pituitary in dwarf-mice may not reside in the pituitary itself but involve other brain regions, namely the hypothalamus. The hypothalamus synthesizes several hormones that are known to stimulate the proliferation of specific cell types of the anterior pituitary. Studies with mice lacking hypothalamic GHRH neurons or that have been subjected to manipulations impairing the function of these neurons shows that GHRH stimulates the proliferation of GH-expressing cells (somatotropes) of the anterior pituitary (Frohman and Kineman, 2002b; Le Tissier et al., 2005). Since dwarf mice showed a reduction in pituitary GH levels, it is possible that the activity of hypothalamic GHRH neurons is compromised. In the mouse hypothalamus, GHRH is primarily expressed by specialized cells of the arcuate nucleus (Suhr et al., 1989).

To examine whether the GHRH-containing cells of the hypothalamus (contained within the ARC) were affected or altered, analysis of mRNA expression of *Ghrh* was undertaken by quantitative PCR (qPCR). In addition to examining the levels of *Ghrh*, I examined levels of *Sst*, produced by neurons in the periventricular nucleus (Giustina and Veldhuis, 1998). GHRH and GH release is regulated by the inhibitory actions of Sst that exerts its inhibitory effects on longitudinal growth (via the inhibition of GH release) (refer to Figure 1-14, p.61). If there is a *deficiency* in circulating GH then we expect to see an increase in GHRH; if there is an *increase* in circulating GH then we expect to see an increase in Sst as it is required to inhibit the secretion of more GH. Results, in Figure 4-4 (p.161), showed that both *Ghrh* and *Sst* were significantly decreased (greater than 60% reduction; $p<0.05$) in dwarf littermates compared with wild-type mice. Thus, it is possible that the decrease in hypothalamic *Sst* levels in dwarf mice is a compensatory mechanism that is activated by the reduction in peripheral GH and IGF-1 levels already shown in these mice.

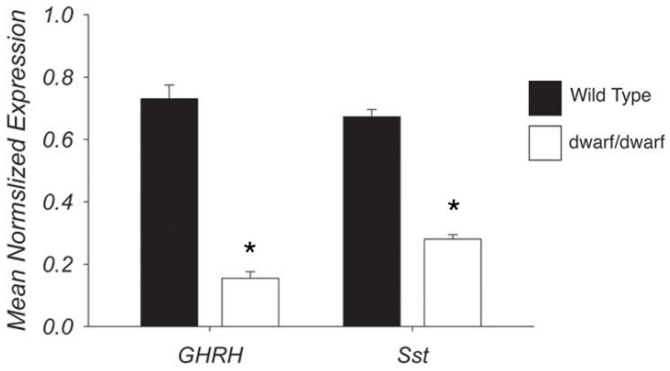

Figure 4-4 mRNA expression of *Ghrh* and *Sst* in wild-type and dwarf hypothalamic extracts
Mean normalized expression levels of *Ghrh* and *Sst* were compared between wild-type and homozygous dwarf mouse hypothalamic extracts at 8-weeks (male and female pooled, n=3). Transcripts were measured by quantitative-PCR using appropriate primers and normalized to *β-actin* mRNA levels. Values are expressed as the mean±SEM and are expressed as mean normalized expression based on fold change. * $p<0.05$.

Figure 4-5 Whole-pituitary GH and serum IGF-1 levels including pituitary gland weight and expression of GH in wild-type and dwarf littermates

(A) GH levels from whole pituitary extracts (8-week-old males and females; n=3 per group). (B) Serum IGF-1 levels. Hormone levels were measured by ELISA (in 8-week-old males and females; n=3 per group). (C) Gross morphology of pituitary glands. Representative glands from adult male dwarf and wild-type mice (there was no size difference between males and females). (D) Total weight of pituitary glands (8-week-old males and females; n=10 per group). (E) Gross morphology of brains. Representative brains from adult male dwarf and wild-type mice are shown. (F) Total brain weights (8-week-old males and females; n=10 per group). (G) GH immunostaining of pituitary sections shown in (C). Pituitary glands from dwarf and wild-type littermates (8-week-old males) were sectioned and incubated with the mouse GH antibody as described in Materials and Methods. Pink arrow in *i* point to auto-fluorescence that is likely attributed by over staining with secondary antibody or by over-fixation in 4% PFA during tissue processing. Note the pronounced hypoplasia of the anterior pituitary of dwarf mice (*ii*), compared to wild-type (*i*). AP, anterior pituitary; I, intermediate lobe; PP, posterior pituitary. Data are given as mean±SEM. * $P<0.05$ as compared with the corresponding wild-type group. Immufluorescent images shown in G were colored using AxioVision software when taking images. Magnification x2.5 in G *i* and *iv*, and x20 in G *ii, iii, v* and *vi.*

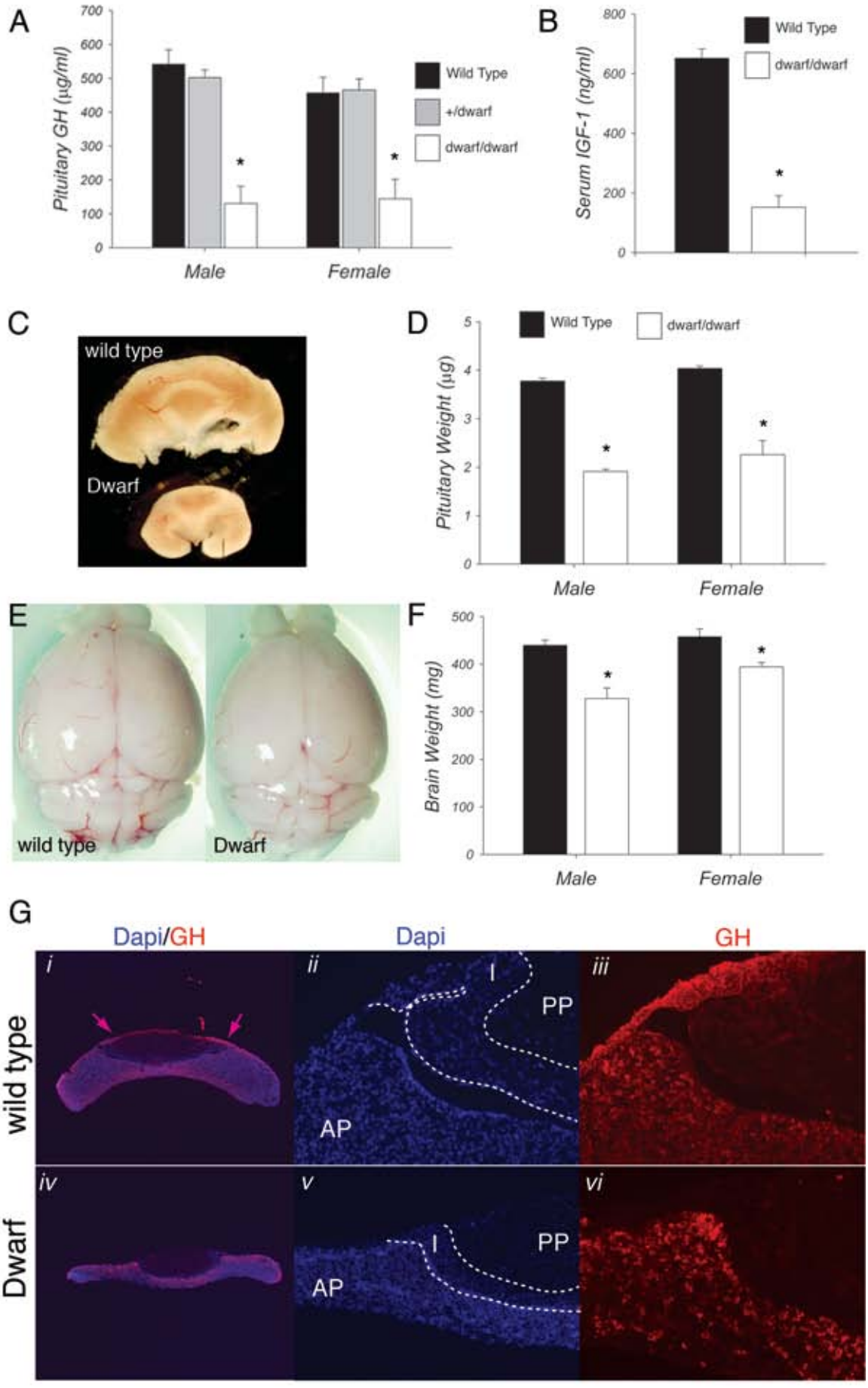
A
Pituitary GH (µg/ml)
700
600
500
400
300
200
100
0
Wild Type
+/dwarf
dwarf/dwarf
*
*
Male
Female
B
Serum IGF-1 (ng/ml)
800
600
400
200
0
Wild Type
dwarf/dwarf
*
C
wild type
Dwarf
D
Pituitary Weight (µg)
5
4
3
2
1
0
Wild Type
dwarf/dwarf
*
*
Male
Female
E
wild type
Dwarf
F
Brain Weight (mg)
500
400
300
200
100
0
*
*
Male
Female
G
Dapi/GH
Dapi
GH
wild type
Dwarf
i
ii
iii
iv
v
vi
I
PP
AP
I
PP
AP

AIM 2: CONFIRM THE MUTATION BY SEQUENCING

F. The Dwarf Mutation is a Non-Conservative Substitution of Leucine to Proline in the Gene Tryptophanyl-tRNA Synthetase

The dwarf mutation was generated, by ENU mutagenesis, on a C57Bl/6 genetic background at the APC (Canberra, ACT, Australia); the generation of these mice is detailed in Materials and Methods, Chapter 2II.B.2 Dwarf Mouse Line Generated by ENU Mutagenesis (p.74).

The dwarf mutation was mapped to a 7Mb region on mouse chromosome 12 (mChr12). Markers D12Mit7 and D12Mit79 flanked this 7Mb region, which was refined through mapping with SNP markers to a 2.5Mb interval between rs3663596 and D12Mit79 containing 85 genes (Figure 4-6 A, p.165). The identification of the specific gene causing dwarfism was performed by the APC (Canberra, ACT, Australia) in parallel to the physiological studies of the dwarf mouse (outlined in the preceding sections). 85 genes were identified within the dwarf critical region, mChr12:107606131-110275931 (Table 4-1, p166). Re-sequencing analysis, performed by APC (Canberra, ACT, Australia), of these genes revealed one mutation identified to be the dwarf mutation in the tryptophanyl-tRNA synthetase (*Wars*) gene (ENSMUSG00000021266). There was no other coding or splice site mutation identified in any other gene within the 2.5Mb region. Thus, confirming that the mutation in *Wars* was causing the dwarfism phenotype in these mice.

The *Wars*^{L30P} mutation was independently sequenced and confirmed by myself from mice in the Adelaide colony. As shown in Figure 4-6 B (p.165) the mutation in *Wars* is located in exon 2 (ENSMUSE00000116158 of transcript ENSMUST00000078788) and is a thymidine (**T**) to cytosine (**C**) substitution of bp220, resulting in a change of amino acid (aa) 30 from C**T**C (leucine, Leu) to C**C**C (proline, Pro). The mutation results in a non-conservative substitution of Leu for a Pro, in the ORF.

The Leu at residue 30 is highly conserved across species (Figure 4-7 A, p.168) and is located in the first alpha helix (Figure 4-7 B (*i*)). WARS proteins are conserved in the chordate lineage and in the WHEP domains of all mammalian AARs. The WHEP domain is present in five AARSs: WARS, HARS, and EPARS (for which the domain is named) and also in GARS and MARS, but not in any non-AARs proteins (Park et al., 2008). This is shown in Figure 4-7 C. The substitution of Leu to Pro, in the *Wars*^{L30P} dwarf mutant, is likely to result in disruption of the alpha helical structure due to Proline's unique cyclic (imino acidic) structure (Figure 4-7 D).

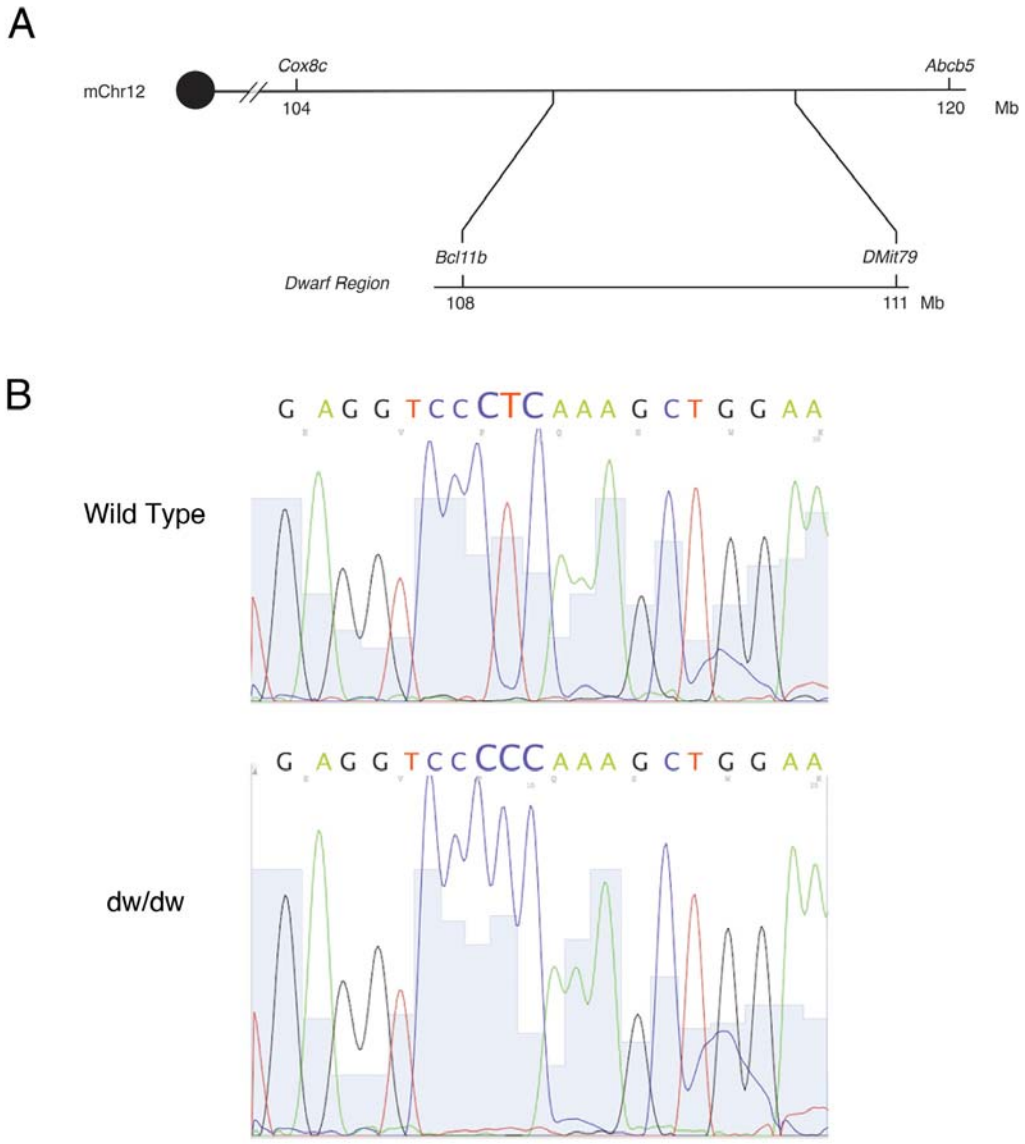

Figure 4-6 The dwarf region showing sequence confirmation

(A) Map of the region of mouse chromosome 12. The dwarf-critical region is indicated. Note that the first gene, RIKEN cDNA 3110018I06 gene [Source: MarkerSymbol;Acc:MGI:1920410] at 107Mb, in the dwarf region is not marked. (B) Sequencing of the *Wars* gene in a dwarf and wild-type littermate. Sequence identification of the $Wars^{L30P}$ mutation. Direct sequence of exon 2 PCR products in (A) a wild-type littermate and (B) dwarf (homozygous; dw/dw), showing substitution of T (leucine, CTC) to C (proline, CCC) at nucleotide position 220.

Table 4-1 Candidate genes in the dwarf critical region

85 genes are shown and are located between mChr12: 107606131-110275931. The corresponding human gene is also given, where applicable.

	Mouse		Human		
Name	Ensembl Gene ID	Description	Chr	Chr Start	Chr End
-	ENSMUSG00000059313	-	8	97150365	97151085
3110018I06Rik	ENSMUSG00000060375	RIKEN cDNA 3110018I06 gene			
Bcl11b	ENSMUSG00000048251	B-cell leukemia/lymphoma 11B	14	98705377	98807575
A130014H13Rik	ENSMUSG00000072842	RIKEN cDNA A130014H13 gene			
Setd3	ENSMUSG00000056770	SET domain containing 3	14	98933857	99016979
Ccnk	ENSMUSG00000021258	cyclin K	14	99017492	99047604
Q3UEX2_MOUSE	ENSMUSG00000072840	Adult retina cDNA, hypothetical protein, full insert sequence			
668158	ENSMUSG00000071162	-	14	99051336	99140049
1600002O04Rik	ENSMUSG00000021260	RIKEN cDNA 1600002O04 gene	14	99181233	99215466
Cyp46a1	ENSMUSG00000021259	cytochrome P450, family 46, subfamily a, polypeptide 1	14	99220407	99263390
	ENSMUSG00000058070	-	14	99329498	99478146
Evl	ENSMUSG00000021262	Ena-vasodilator stimulated phosphoprotein	14	99601504	99680325
mmu-mir-342	ENSMUSG00000065436	mmu-mir-342			
Degs2	ENSMUSG00000021263	degenerative spermatocyte homolog 2 (Drosophila), lipid desaturase	14	99682512	99695712
Yy1	ENSMUSG00000021264	YY1 transcription factor	14	99774855	99814557
Slc25a29	ENSMUSG00000021265	solute carrier family 25	14	99827213	99842613
mmu-mir-345	ENSMUSG00000065429	mmu-mir-345			
AI132487	ENSMUSG00000048856	epatocellular carcinoma down-regulated mitochondrial carrier homolog	14	99859428	99866467
Wars	ENSMUSG00000021266	tryptophanyl-tRNA synthetase	14	99869878	99912433
	ENSMUSG00000072839	WD repeat domain 25	14	99912563	100066361
Wdr25	ENSMUSG00000040877	WD repeat domain 25	14	99912563	100066361
BM948371	ENSMUSG00000040867	expressed sequence BM948371	14	100073243	100105884
Dlk1	ENSMUSG00000040856	delta-like 1 homolog (Drosophila)	14	100262917	100270986
Gtl2	ENSMUSG00000021268	GTL2, imprinted maternally expressed untranslated mRNA			
mmu-mir-770	ENSMUSG00000076451	mmu-mir-770 [Source:miRBase 9.0;Acc:MI0004203]			
mmu-mir-673	ENSMUSG00000076316	mmu-mir-673 [Source:miRBase 9.0;Acc:MI0004601]			
mmu-mir-337	ENSMUSG00000065526	mmu-mir-337 [Source:miRBase 9.0;Acc:MI0000615]			
mmu-mir-540	ENSMUSG00000072900	mmu-mir-540 [Source:miRBase 9.0;Acc:MI0003518]			
mmu-mir-665	ENSMUSG00000076313	mmu-mir-665 [Source:miRBase 9.0;Acc:MI0004171]			
Rtl1	ENSMUSG00000006551	retrotransposon-like 1 [Source:MarkerSymbol;Acc:MGI:2656842]			
mmu-mir-431	ENSMUSG00000070080	mmu-mir-431 [Source:miRBase 9.0;Acc:MI0001524]			
mmu-mir-433	ENSMUSG00000070072	mmu-mir-433 [Source:miRBase 9.0;Acc:MI0001525]			
mmu-mir-127	ENSMUSG00000070076	mmu-mir-127 [Source:miRBase 9.0;Acc:MI0000154]			
mmu-mir-434	ENSMUSG00000070133	mmu-mir-434 [Source:miRBase 9.0;Acc:MI0001526]			
mmu-mir-136	ENSMUSG00000070129	mmu-mir-136 [Source:miRBase 9.0;Acc:MI0000162]			
mmu-mir-341	ENSMUSG00000070101	mmu-mir-341 [Source:miRBase 9.0;Acc:MI0000625]			
mmu-mir-370	ENSMUSG00000065433	mmu-mir-370 [Source:miRBase 9.0;Acc:MI0001165]			
sno_14q_I_II	ENSMUSG00000064452	NOVEL [Source:RFAM;Acc:RF00181]			
sno_14q_I_II	ENSMUSG00000065039	NOVEL [Source:RFAM;Acc:RF00181]			
sno_14q_I_II	ENSMUSG00000064496	NOVEL [Source:RFAM;Acc:RF00181]			
sno_14q_I_II	ENSMUSG00000065013	NOVEL [Source:RFAM;Acc:RF00181]			
sno_14q_I_II	ENSMUSG00000064621	NOVEL [Source:RFAM;Acc:RF00181]			
sno_14q_I_II	ENSMUSG00000064417	NOVEL [Source:RFAM;Acc:RF00181]			
sno_14q_I_II	ENSMUSG00000064679	NOVEL [Source:RFAM;Acc:RF00181]			
sno_14q_I_II	ENSMUSG00000065757	NOVEL [Source:RFAM;Acc:RF00181]			
sno_14q_I_II	ENSMUSG00000065749	NOVEL [Source:RFAM;Acc:RF00181]			
sno_14q_I_II	ENSMUSG00000064487	NOVEL [Source:RFAM;Acc:RF00181]			
sno_14q_I_II	ENSMUSG00000065022	NOVEL [Source:RFAM;Acc:RF00181]			
sno_14q_I_II	ENSMUSG00000064545	NOVEL [Source:RFAM;Acc:RF00181]			
sno_14q_I_II	ENSMUSG00000064720	NOVEL [Source:RFAM;Acc:RF00181]			
sno_14q_I_II	ENSMUSG00000064726	NOVEL [Source:RFAM;Acc:RF00181]			
mmu-mir-379	ENSMUSG00000065498	mmu-mir-379 [Source:miRBase 9.0;Acc:MI0000796]			
mmu-mir-411	ENSMUSG00000065477	mmu-mir-411 [Source:miRBase 9.0;Acc:MI0001163]			
mmu-mir-299	ENSMUSG00000065550	mmu-mir-299 [Source:miRBase 9.0;Acc:MI0000399]			
mmu-mir-380	ENSMUSG00000065595	mmu-mir-380 [Source:miRBase 9.0;Acc:MI0000797]			
mmu-mir-323	ENSMUSG00000065617	mmu-mir-323 [Source:miRBase 9.0;Acc:MI0000592]			
mmu-mir-758	ENSMUSG00000076459	mmu-mir-758 [Source:miRBase 9.0;Acc:MI0004129]			
mmu-mir-329	ENSMUSG00000065577	mmu-mir-329 [Source:miRBase 9.0;Acc:MI0000605]			
mmu-mir-494	ENSMUSG00000070141	mmu-mir-494 [Source:miRBase 9.0;Acc:MI0003532]			
mmu-mir-679	ENSMUSG00000076145	mmu-mir-679 [Source:miRBase 9.0;Acc:MI0004638]			
mmu-mir-666	ENSMUSG00000076272	mmu-mir-666 [Source:miRBase 9.0;Acc:MI0004553]			

mmu-mir-543	ENSMUSG00000076241	mmu-mir-543 [Source:miRBase 9.0;Acc:MI0003519]
mmu-mir-495	ENSMUSG00000070105	mmu-mir-495 [Source:miRBase 9.0;Acc:MI0004639]
mmu-mir-667	ENSMUSG00000076396	mmu-mir-667 [Source:miRBase 9.0;Acc:MI0004196]
mmu-mir-376c	ENSMUSG00000076215	mmu-mir-376c [Source:miRBase 9.0;Acc:MI0003533]
mmu-mir-376b	ENSMUSG00000076006	mmu-mir-376b [Source:miRBase 9.0;Acc:MI0001162]
mmu-mir-376a	ENSMUSG00000076043	mmu-mir-376a [Source:miRBase 9.0;Acc:MI0000793]
mmu-mir-300	ENSMUSG00000065419	mmu-mir-300 [Source:miRBase 9.0;Acc:MI0000400]
mmu-mir-381	ENSMUSG00000065566	mmu-mir-381 [Source:miRBase 9.0;Acc:MI0000798]
mmu-mir-487b	ENSMUSG00000076219	mmu-mir-487b [Source:miRBase 9.0;Acc:MI0003534]
mmu-mir-539	ENSMUSG00000076063	mmu-mir-539 [Source:miRBase 9.0;Acc:MI0003520]
mmu-mir-382	ENSMUSG00000065428	mmu-mir-382 [Source:miRBase 9.0;Acc:MI0000799]
mmu-mir-134	ENSMUSG00000065426	mmu-mir-134 [Source:miRBase 9.0;Acc:MI0000160]
mmu-mir-668	ENSMUSG00000076350	mmu-mir-668 [Source:miRBase 9.0;Acc:MI0004134]
mmu-mir-485	ENSMUSG00000070128	mmu-mir-485 [Source:miRBase 9.0;Acc:MI0003492]
mmu-mir-154	ENSMUSG00000065448	mmu-mir-154 [Source:miRBase 9.0;Acc:MI0000176]
mmu-mir-496	ENSMUSG00000070136	mmu-mir-496 [Source:miRBase 9.0;Acc:MI0004589]
mmu-mir-377	ENSMUSG00000065438	mmu-mir-377 [Source:miRBase 9.0;Acc:MI0000794]
mmu-mir-541	ENSMUSG00000076052	mmu-mir-541 [Source:miRBase 9.0;Acc:MI0003521]
mmu-mir-409	ENSMUSG00000065478	mmu-mir-409 [Source:miRBase 9.0;Acc:MI0001160]
mmu-mir-412	ENSMUSG00000065570	mmu-mir-412 [Source:miRBase 9.0;Acc:MI0001164]
mmu-mir-369	ENSMUSG00000065561	mmu-mir-369 [Source:miRBase 9.0;Acc:MI0003535]
mmu-mir-410	ENSMUSG00000065497	mmu-mir-410 [Source:miRBase 9.0;Acc:MI0001161]
-	ENSMUSG00000057178	-

Figure 4-7 The WARS protein

(A) The mutated residue in dwarf mice is highly conserved. (B) (i) 3D schematic representation of the human WARS protein showing the WHEP domain and location of leucine residues (orange). The location of leucine at residue 26 is labeled with LEU (orange). (ii) Schematic representation of the 481 amino acid murine WARS protein showing N- terminal WHEP domain, catalytic core domain and position of mutation (*arrow*). (C) Dwarf mutation is located in the WHEP domain. BLAST alignments of mouse WARS WHEP domain protein sequence with other species WHEP containing ARS family members in human and mouse. The highly conserved residues in the domain are highlighted in red. The leucine at residue 30 (highlighted in blue) located in the WHEP domain is highly conserved across different species and also in other ARS enzyme that contain WHEP domain, EPRS, GARS, HARS and MARS. (D) Structure of leucine and proline. NB: 3D structure of the wars protein was obtained from RSC Protein Data Bank (1R6T) (Yang et al., 2003) and was produced using the UCSF Chimera package from the Resource for Biocomputing, Visualization, and Informatics at the University of California, San Francisco (supported by NIH P41 RR001081).

A

```
Dwarf L30P mouse      -QGELVRSPKAGNAPKDEIDSAVKMLL----------------
Mus musculus          -QGELVRSLKAGNAPKDEIDSAVKMLL----------------
Macaca mulata         -QGELVRSLKAGNASKDEIDSAVKMLL----------------
Rattis novergicus     --GELVRSLKAGNAPKDEIESAVKMLLS---------------
Gorilla gorilla       --GELVRSLKAGNASKDEIDSAVKMLVS---------------
Homo sapien           -QGELVRSLKAGNASKDEIDSAVKMLVSLKM------------
Gallus gallus         EQGEKVRALKAGKAPKDEIDAAVRLL-----------------
Takifugu rubreipes    -QGDQVRALKTAKSDKAEIDAAVQLLL----------------
Drosophila melanogester SQRRCIQARSFLPGLASRTAGTPSAT-----------------
Danio rerio           -QGETVRSIKAKKGSKV---SAVQVLLQMK-------------
Caenorhabditis elegans ----------GGGVQEDEEDRVTPWEV-----TTTKATGID--
Saccharomyces cerevisiae ----------------KEQVVTPWDVEGGVDEQGRAQNIDYD
```

B

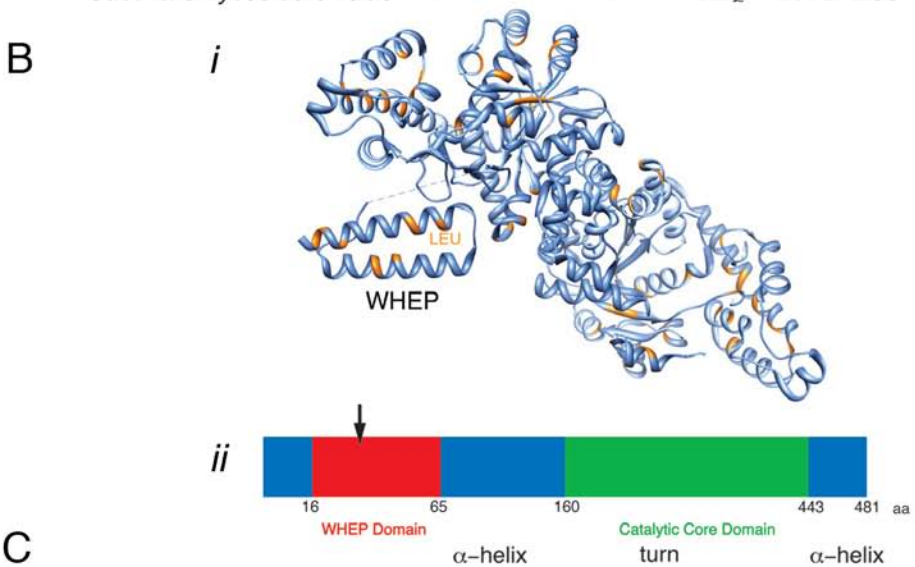

C

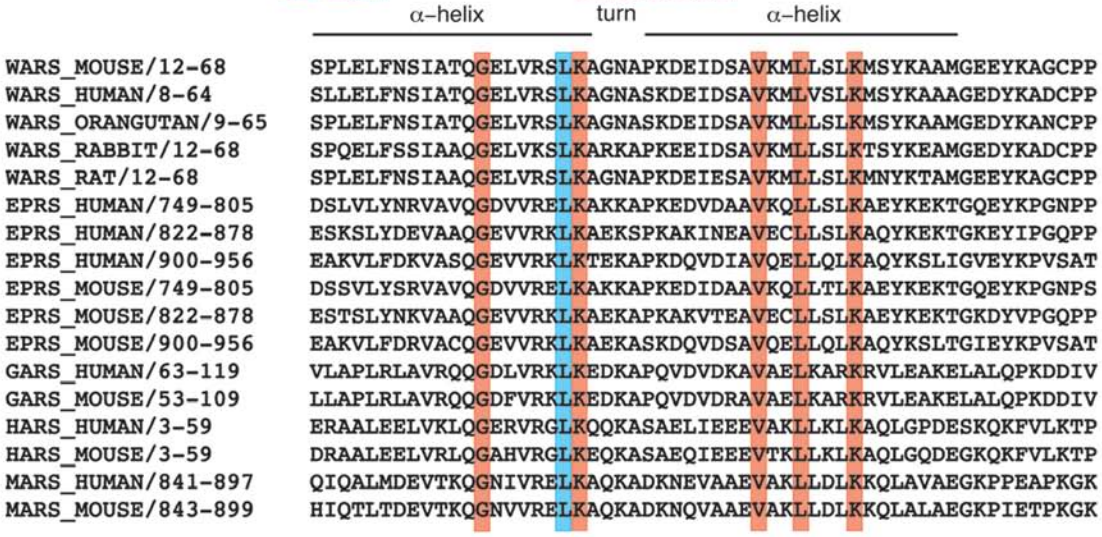

D

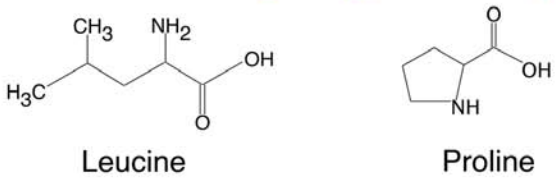

AIM 3: EXAMINE THE EXPRESSION OF THE MUTANT PROTEIN

Given that the mutation has been identified, I next set out to examine the expression of the protein in the pituitary. Wars, a member of the aminoacyl tRNA family of enzymes (AARS,) has been known to play a noncanonical role in angiogenesis, in zebrafish and in endothelial cell cultures (Fukui et al., 2009; Herzog et al., 2009; Ray and Fox, 2007; Wakasugi et al., 2002a; Wakasugi et al., 2002b). As the pituitary is a highly vascularized organ, I examined the pituitary of dwarf and wild-type littermates firstly to determine whether Wars was expressed in the pituitary vasculature, and secondly to determine whether there was a decrease in expression of the Wars protein. Although previous data (refer to Sections 4III.A - 4III.E, p.154-160) revealed that the primary defect might be hypothalamic, current data does not definitively show this. We know that the mutation is in *Wars*, it's protein is ubiquitously expressed and, importantly, has been linked to angiogenesis. With the pituitary being extensively vascularized examining Wars protein expression by immunostaining may provide useful information with respect to pituitary vasculature. The following sections examine the expression of Wars in pituitary vasculature and it's co-expression with vascular markers, platelet endothelial cell adhesion molecule (PECAM or CD31; an endothelial cell marker) and VE-Cadherin (or CD144), an endothelial specific, transmembrane protein, which clusters at adheren junctions where it promotes homotypic cell-cell adhesion (Carmeliet and Collen, 2000).

G. Wars is Expressed in Pituitary Vasculature

Figure 4-8 (p.171) shows the expression of Wars within the pituitary (anterior and posterior pituitary), in wild-type mice at 8-weeks. Specifically, Wars is expressed within all cells (it's canonical function is required for protein synthesis) but has higher expression within endothelial cells (detailed below) of the pituitary vasculature, both in the anterior and posterior lobes.

1. Wars is co-expressed with PECAM in pituitary vasculature

To examine further and confirm whether Wars is expressed in pituitary vasculature, immunostaining for PECAM was performed on wild-type and dwarf littermates, at 8-weeks (Figure 4-9, p.172). The normal anterior pituitary lobe has a dense vascular network, whereas cells in the intermediate lobe remain poorly vascularized. There was no marked decrease in vascular density in dwarf pituitaries, compared to wild-type littermates, nor was there a marked difference in the co-expression of PECAM and Wars. Both PECAM and Wars appeared co-expressed within the vascular wall. The expression of

Wars can also be seen expressed in some adjacent cells in the anterior and posterior pituitary, this is because it is a ubiquitously expressed protein.

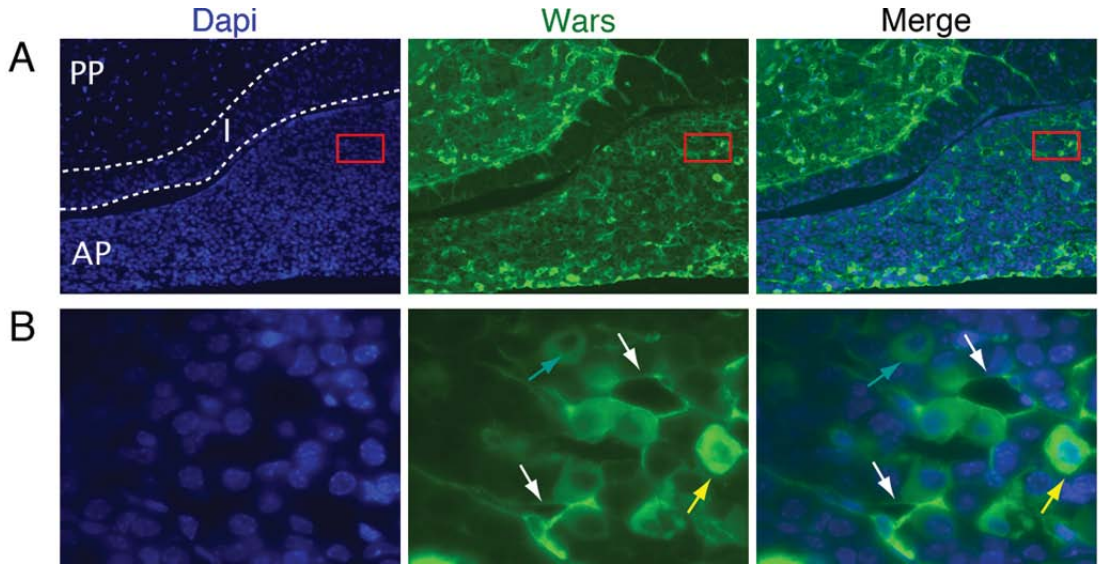

Figure 4-8 Expression of WARS in the mouse pituitary at 8-weeks

Low (A) and higher (B) magnification of pituitary region from a female mouse [showing the anterior pituitary (AP), intermediate lobe (I), and posterior pituitary (PP)] showing DAPI (nuclear chromosomal) and Wars immunostaining and merged (DAPI + Wars) images, as described in Materials and Methods. White arrows point to Wars expression in the vasculature. Wars is also seen expressed in some adjacent cells in anterior pituitary (yellow, high intensity; blue, low intensity), this is because it is a ubiquitously expressed protein. Images were colored using AxioVision software used when taking images. Low magnification: x10; high magnification: x20.

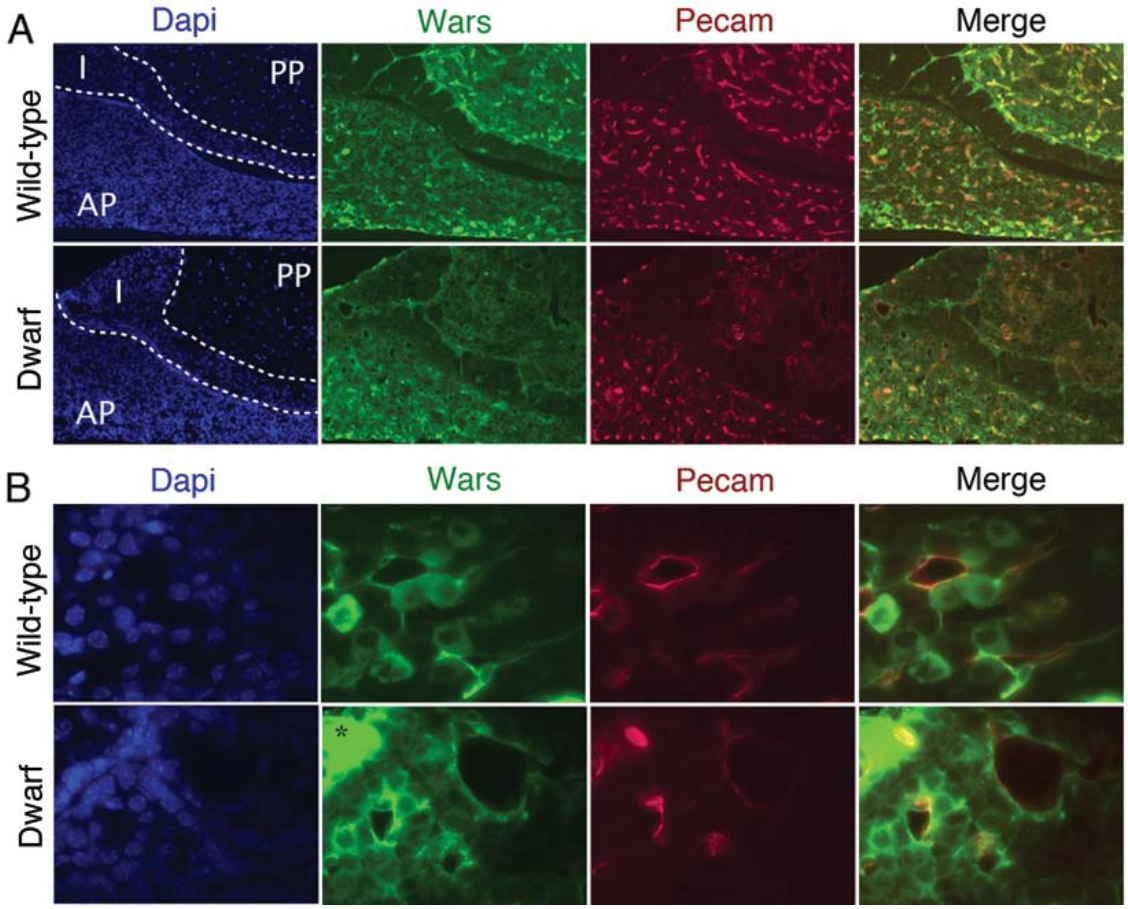

Figure 4-9 Expression of WARS and PECAM (CD-31) in female wild-type and dwarf mouse pituitary at 8 weeks

(A) Immunostaining of Wars and PECAM cells and merge (Wars + PECAM). Images were colored using AxioVision software used when taking images. (B) Unrelated high-resolution (x100) region from the same sections (region not shown) as in A. PECAM staining is present within the anterior and posterior lobe in both the wild-type and dwarf pituitaries; the intermediate lobe is devoid of it. P, posterior lobe; I, intermediate lobe; A, anterior lobe. * indicates overexposure. Magnification x20 in A, and x100 (oil) in B. The wild-type sections (also shown in Figure 4-8) were vertically flipped to align with the dwarf sections seen here.

2. *VE-Cadherin and Wars are expressed in pituitary vasculature*

In order to analyze in more detail the organization of the vascular system and the expression of Wars in pituitary vasculature, pituitary sections from 8-week old wild-type and dwarf mice were immunostained with Wars and VE-Cadherin. VE-Cadherin plays an important role during the angiogenesis pathway (refer to the VEGF:VE-Cadherin pathway Figure 1-10, p.49). Furthermore, WARS, in its truncated form, has been shown to interact with VE-Cadherin to inhibit angiogenesis (angiostasis) (Kapoor et al., 2008). Given that dwarf mice have a substitution mutation (*Wars*^{L30P}) it is tempting to speculate that the *Wars*^{L30P} mutation may be affecting its interaction with VE-Cadherin. We know that full length WARS is cleaved by a protease to release the WHEP domain forming a truncated WARS (T2-WARS) (Kapoor et al., 2008). This truncated WARS is able to bind with VE-Cadherin and inhibits angiogenesis (Figure 4-10, p.175). Perhaps the *Wars*^{L30P} mutation is affecting the helical structure of the WHEP domain, thereby the truncated version is not formed and subsequently is preventing angiogenesis (Figure 4-10, p.175)(Zhou et al., 2010).

Figure 4-11 (p.177) shows the expression of Wars and VE-Cadherin in pituitary sections of 8-week old male wild-type and dwarf mice (there was no detectable difference between male and female pituitaries) as detected by immunostaining. VE-Cadherin was not detected at low (x10) and medium (x20) magnifications. However, at high magnification (x100 oil) the expression of VE-Cadherin can be seen located in vasculature, together with Wars. Wars protein is also seen expressed within the cytoplasm of select cells. It is unknown what these cells are; likely to be hormone-secreting cells.

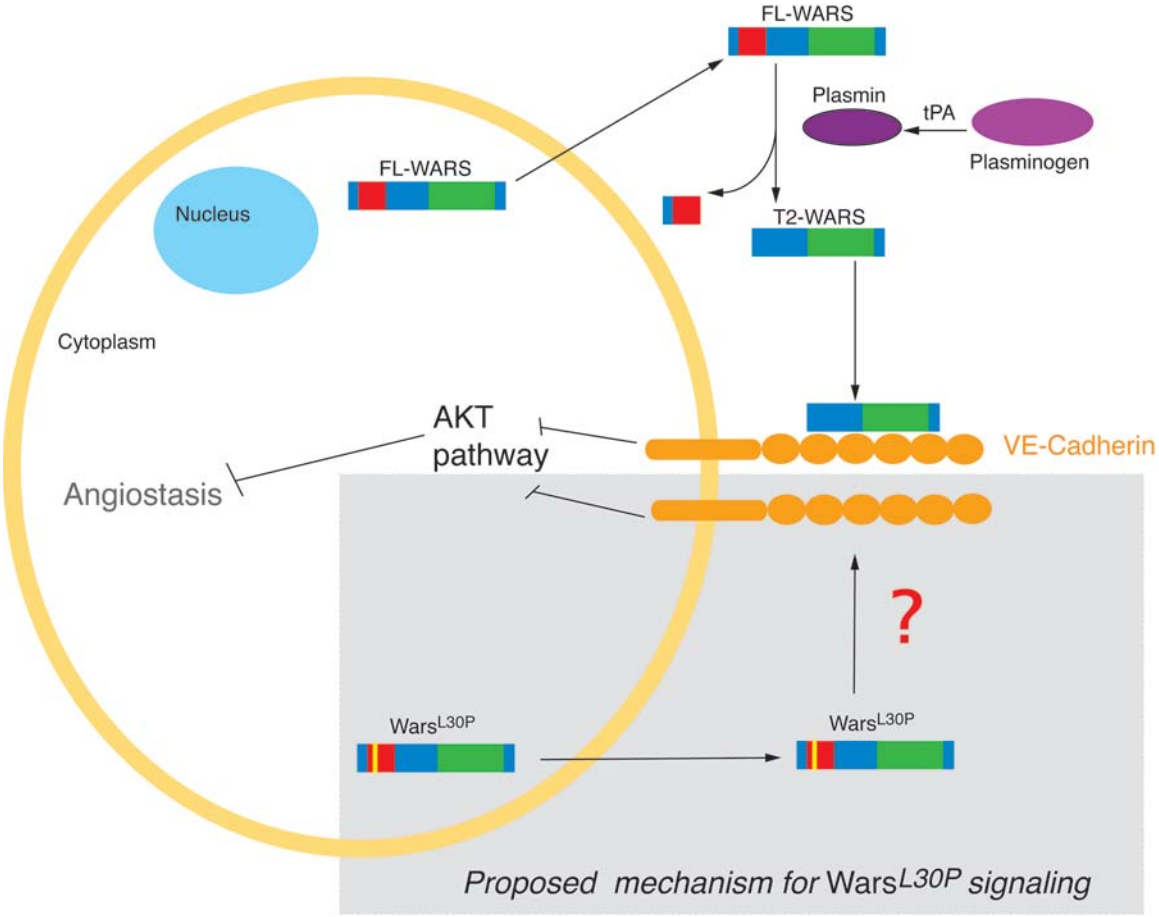
FL-WARS
Plasmin
tPA
Plasminogen
FL-WARS
Nucleus
T2-WARS
Cytoplasm
AKT
pathway
VE-Cadherin
Angiostasis
?
Wars L30P
Wars L30P
Proposed mechanism for Wars L30P signaling

Figure 4-10 Action of WARS on VE-Cadherin and proposed role of the Wars^{L30P} mutation during angiogenesis

Full length WARS (FL-WARS) is cleaved by protease to release the WHEP domain (red box region) and truncated WARS (T2-WARS) is generated. T2-WARS interacts with VE-Cadherin to inhibit angiogenesis (angiostasis). The *Wars*^{L30P} mutation (proposed signaling highlighted in grey) is likely to affect the helical structure of WHEP domain by relieving steric hindrance of the WHEP domain that normally prevents binding of FL-WARS to VE-Cadherin. This may potentially result in a decrease in blood vessel formation. Clearly, from immunostaining studies, vasculature is present within the pituitary, however the extent of this remains undetermined.

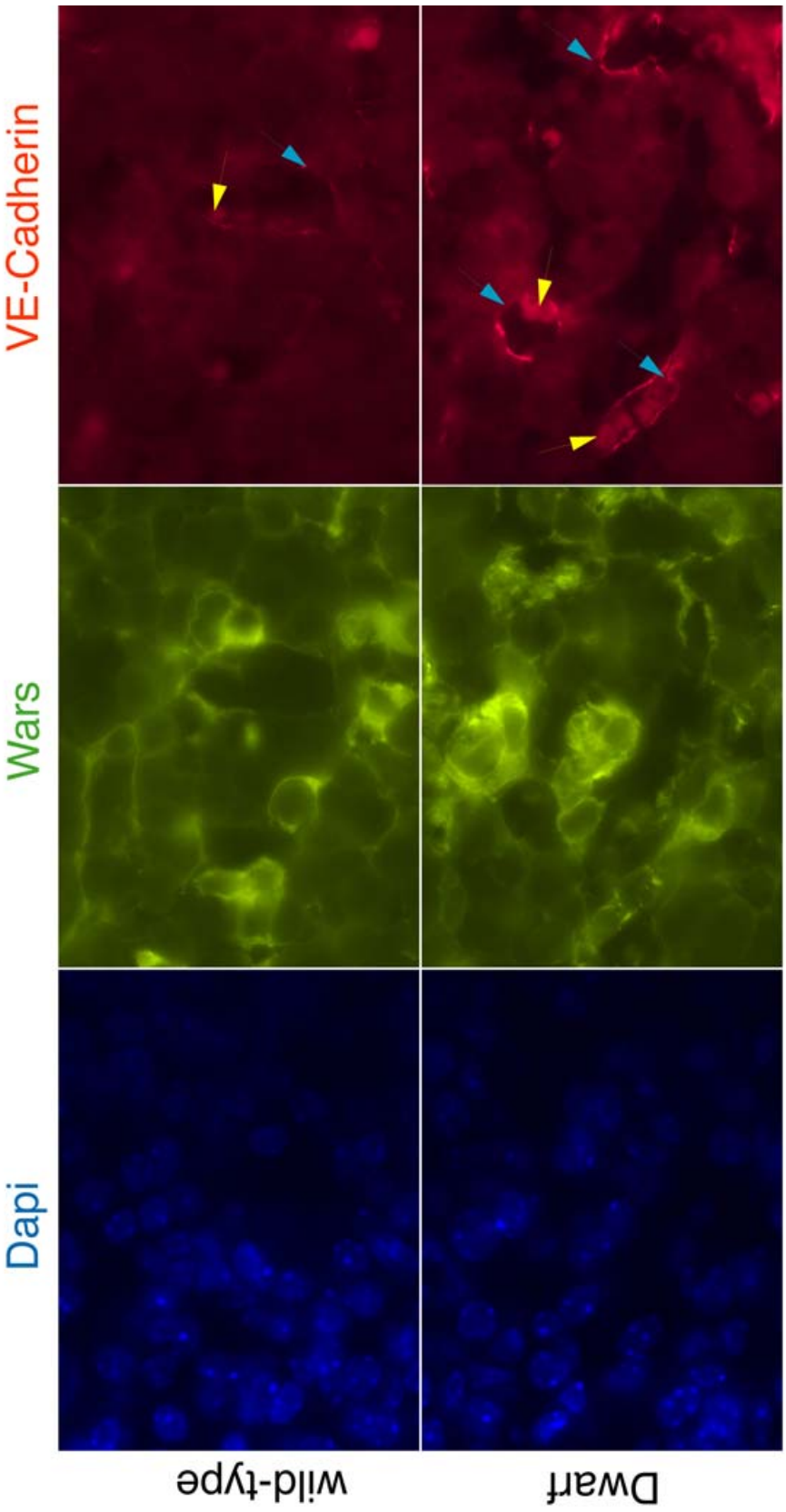
VE-Cadherin
Wars
Dapi
wild-type
Dwarf

Figure 4-11 Expression of VE-Cadherin and Wars in wild-type and dwarf mouse pituitary at 8 weeks.
Sections of the pituitary (male at 8 weeks) at high (x100 oil) magnification showing immunostaining of nuclei (DAPI), Wars, and VE-Cadherin. VE-Cadherin is detected lining blood vessels (blue arrows). Within blood vessels can be seen red blood cells (yellow arrow). There was no detectable difference between male and female pituitaries.

3. *Steady state level of Wars protein is not altered in the pituitary*

Wars is expressed in both wild-type and dwarf pituitaries, as determined by immunostaining, however, this technique was unable to determine whether there was a significant change in Wars protein level. Thus, to determine whether Wars protein was decreased in dwarf compared to wild-type pituitaries western-blot analysis, using SDS-PAGE gel electrophoresis, was performed. This experiment was performed by Chin T. Ng as part of her Honors thesis (Ng, 2010).

Western blot analysis used extracts of pituitary, brain and kidney tissues from wild-type and dwarf 5-month mice littermates (n=2 per organ/group) (Figure 4-12, below). These results indicate that Wars is strongly recognized at the expected molecular weights (53kDa) in pituitary, brain and kidney. There was no detectable difference in Wars protein levels between wild-type and dwarf in the pituitary, kidney or brain (data confirmation based on four repeats of this experiment). Wars protein expression was decreased in the kidney, in both wild-type and dwarf. Data suggests that the *Wars*^{L30P} mutation does not affect the stability of the Wars protein, although additional experiments that directly measure protein stability (e.g. pulse chase or immunoprecipitation analysis) should be performed for confirmation. These results also indicate that Wars protein has higher expression in the pituitary and brain compared to the kidney.

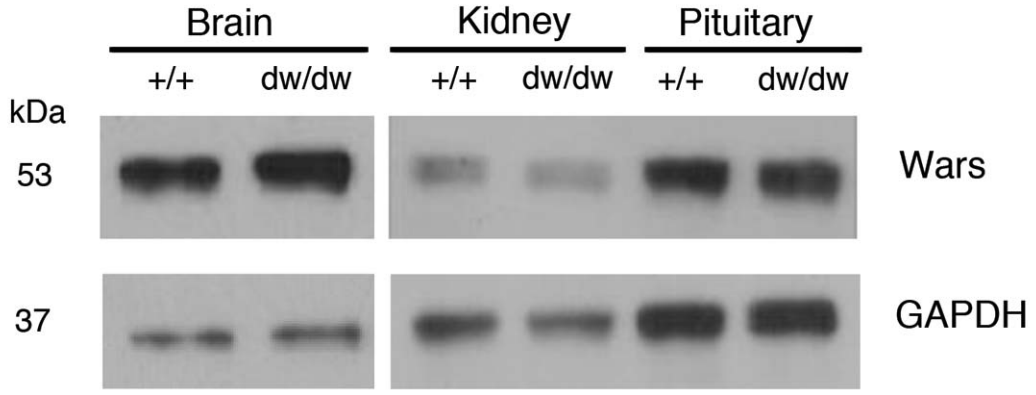

Figure 4-12 Western blot analysis of Wars expression in pituitaries, brains and kidney in wild-type and dwarf mice

Molecular weight standards indicated. GAPDH used to analyze ample load. Data collected by Chin Ng (Ng, 2010), figure re-constructed for the purpose of representation in this work. Abbreviations: +/+, wild-type; dw/dw, homozygous dwarf.

ADDITIONAL AND PRELIMINARY DATA

H. *Wars*^{L30P} Mutation Affects Angiogenesis

The following results summarize the findings presented by Chin T. Ng as part of her Honors thesis (Ng, 2010).

As mentioned briefly in the introduction to this chapter, AARS have been linked to regulating the noncanonical activity of angiogenesis (Otani et al., 2002; Wakasugi, 2010; Wakasugi and Schimmel, 1999; Wakasugi et al., 2002b). In humans, cells contain two distinct WARS isoforms, the full length WARS (FL-WARS; 471 aa) and mini-WARS (424 aa), the later arising by alternative mRNA splicing, naturally (Wakasugi, 2010). Furthermore, there exist two alternative mRNA spliced forms of WARS: T1-WARS and T2-WARS (refer to Figure 4-18, p.197). These have been implicated in the inhibition of angiogenesis (Tzima and Schimmel, 2006).

The angiostatic activity of human mini-WARS is well characterized, however truncated versions of the mouse protein (which is 89% identical across the entire ORF) have not been tested. Therefore, the aim of Chin's work was to perform angiogenesis assays using human mini-WARS (as the positive control), full-length human WARS (as the negative control), mouse mini-WARS (a likely positive control), full-length mouse WARS (a likely negative control) isoforms and comparing these with the *Wars*^{L30P} mutation.

1. Generation of Wars Isoforms

Three different Wars isoforms were cloned: full-length (FL-Wars), mini (mini-Wars) and T2-Wars, using the pET32a-TEV-Kpn1 expression vector. FL-Wars was used as template for the synthesis of *Wars*^{L30P} by site-directed mutagenesis. The construction and relationship of Wars and it's variants are shown Figure 4-13 A (p.180). Successful cloning of the Wars isoforms was confirmed by sequence analysis (Figure 4-13 , p.180; and refer to Ng, 2010). The cloning strategy employed for generating mouse Wars isoforms is described Appendices - Figure A 3 (p.234).

2. Angiostatic activity of WARS isoforms

3B11 cells were cultured (4-h) with murine FL-Wars, mini-Wars, T2-Wars and *Wars*^{L30P} in suramin (a blocker of growth factors that prevents binding to receptors), buffer alone, and VEGF. Tube formation was measured using rhodamine phalloidin staining. Treatment with suramin significantly impaired angiogenesis (Figure 4-14 a, p.188), consistent with previous results in human FL-Wars (Otani et al., 2002), whereas treatment

with buffer-only resulted in angiogenesis (Figure 4-14 b). Similarly, mouse FL-Wars showed comparable angiogenesis (Figure 4-14 c) to the buffer-only treatment. However, both mouse mini-Wars and T2-Wars slowed angiogenesis (Figure 4-14 d and e, respectively). Strikingly, *Wars*^{L30P}, like mini-Wars and T2-Wars, slowed angiogenesis (Figure 4-14 f). These results illustrate that the *Wars*^{L30P} mutation impairs angiogenesis (or has an angiostatic consequence), in 3B11 cells. In agreement with previous data (Otani et al., 2002; Wakasugi et al., 2002b), these preliminary results show that *Wars*^{L30P} mutation plays an influential role on vasculature development.

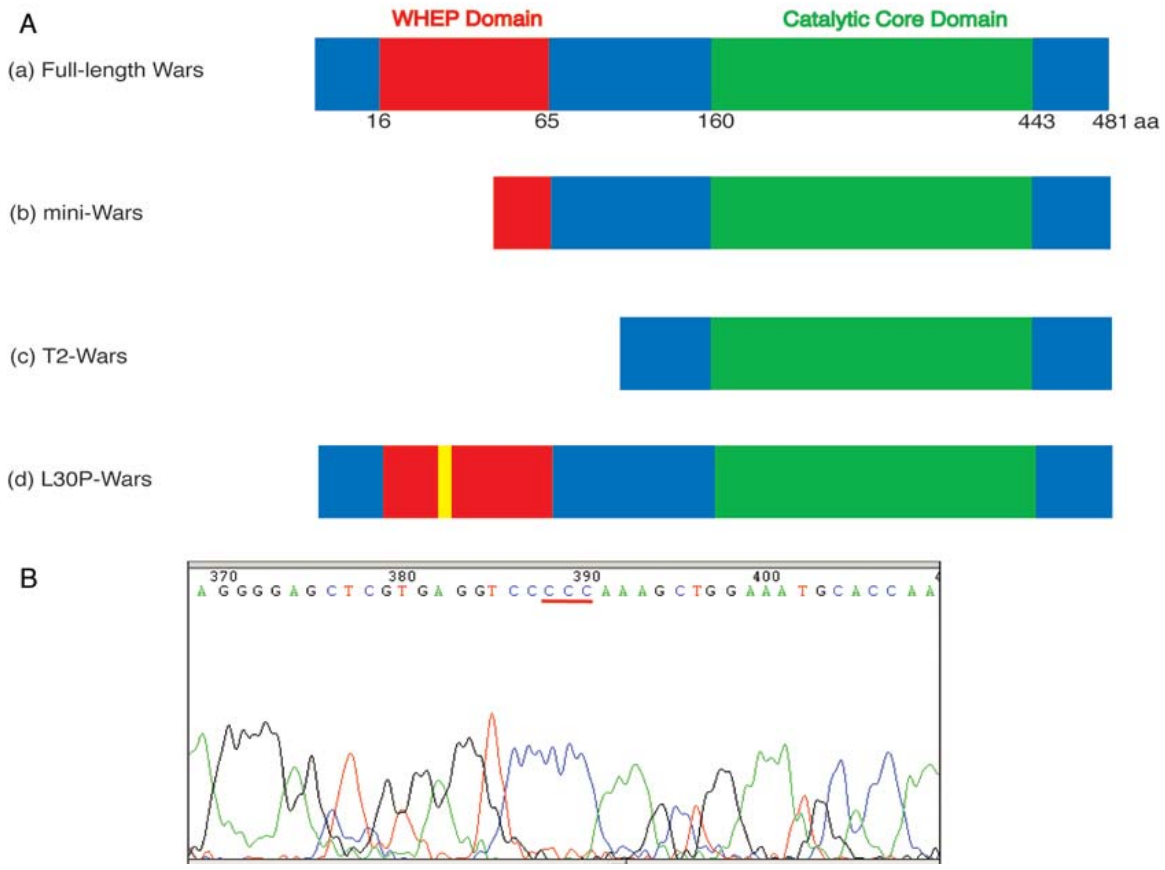

Figure 4-13 Schematic representation of the mouse tryptophanyl-tRNA (Wars) synthetase isoforms used in the tube-formation assay

(A) Full-length Wars (FL-Wars) (a), mini-Wars (b), T2-Wars (c) and L30P-Wars (d) isoforms are shown. L30P-Wars was generated using QuickChange Site-directed mutagenesis to generate a point mutation 220T>C (shown as yellow bar) using pET32a FL-Wars as a template. (B) DNA sequencing confirmed the success of mutagenesis 220T>C in the *Wars* gene. The mutated codon, CCC (encoding a Proline residue at position 30) is underlined in red. Isoforms and sequencing confirmation was performed by Chin Ng as part of her Honors thesis (Ng, 2010) and re-drawn by me for the purpose of this thesis.

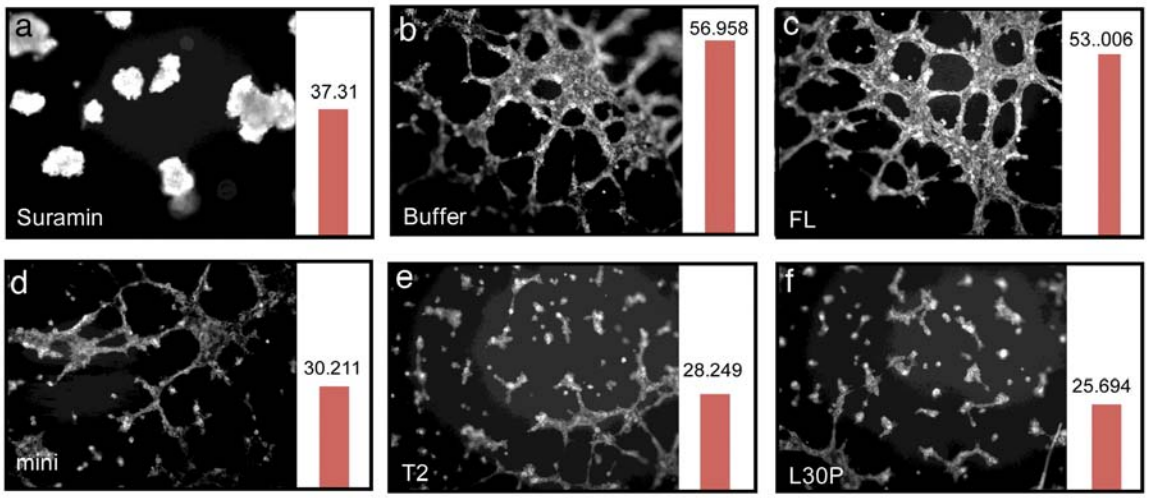

Figure 4-14 Preliminary data of tube-formation assay showing that the *Wars*^{L30P} mutation has angiostatic properties

3B11 cells were cultured (4-h) with murine FL-Wars, mini-Wars, T2-Wars and L30P-Wars in suramin (a; a blocker of growth factors; prevents binding to receptors), buffer alone (b), and VEGF (c-f). For each image the total area that was covered by vasculature in each image was calculated as the average number (μm^2) and is shown for each group, along with a representative image (n=1). Data was prepared and collected by Chin Ng (Ng, 2010).

I. Vascularity in the Mouse Brain and Pituitary

As outlined above, the dwarf phenotype may arise from abnormal development of the portal vasculature. To examine this possibility of the mutation affecting the vascular pattern, the mouse cerebral cortex surface, lateral hypothalamic region and pituitary anatomical localization was examined in 8-week old mice (male and female, n=4 per group) during routine dissection of the pituitaries and brains that were collected for other experiments. Only brains from male mice are shown in Figure 4-15 (p.182). The brains of wild-type animals exhibited branched vessels crossing and gathering radially to the surface (Figure 4-15 A *i*). All these vessels arborized to form a continuous network of small blood vessels. In contrast, the brains from dwarf animals exhibited a few deranged microvessels (Figure 4-15 A *iii*). There were fewer prominent vessel branch points on the cerebral cortical surface in dwarf mice compared to wild-type. Several discontinued vascular structures were observed and the radial patterns were lost (compare Figure 4-15 A *i* and *iii*, as indicated by arrows). Fewer prominent vessel branch points were seen on the ventral surface compared to wild-type (compare Figure 4-15 A *ii* and *iv* indicated by arrows). By contrast, the dwarf pituitary was surrounded by fewer vessels, as indicated by the pooling of blood within the pituitary/sphenoid bone region (Figure 4-15 B *i* and *iii; ii* and *iv*).

Figure 4-15 Vascular pattern in the cerebral cortical surface, lateral hypothalamus and pituitary from wild-type and dwarf brains and pituitary at 8-weeks

Representative brains (A) and corresponding pituitaries (B) from adult dwarf (homozygous) and wild-type male mice at 8-weeks. (A) The dwarf mouse brain had fewer prominent vessel branch points on the cerebral cortical surface compared to wild-type. Several discontinued vascular structures were observed and the radial patterns were lost (compare *i* and *iii*, as indicated by arrows). Fewer prominent vessel branch points were seen on the ventral surface compared to wild-type (compare *ii* and *iv* indicated by arrows). (B) The dwarf pituitary was surrounded by fewer vessels, as indicated by the pooling of blood within the pituitary/sphenoid bone region (arrow). Abbreviations: OB, olfactory bulb; Cb, cerebellum; OCh, optic chiasm; hyp, hypothalamus, LH, lateral hypothalamus.

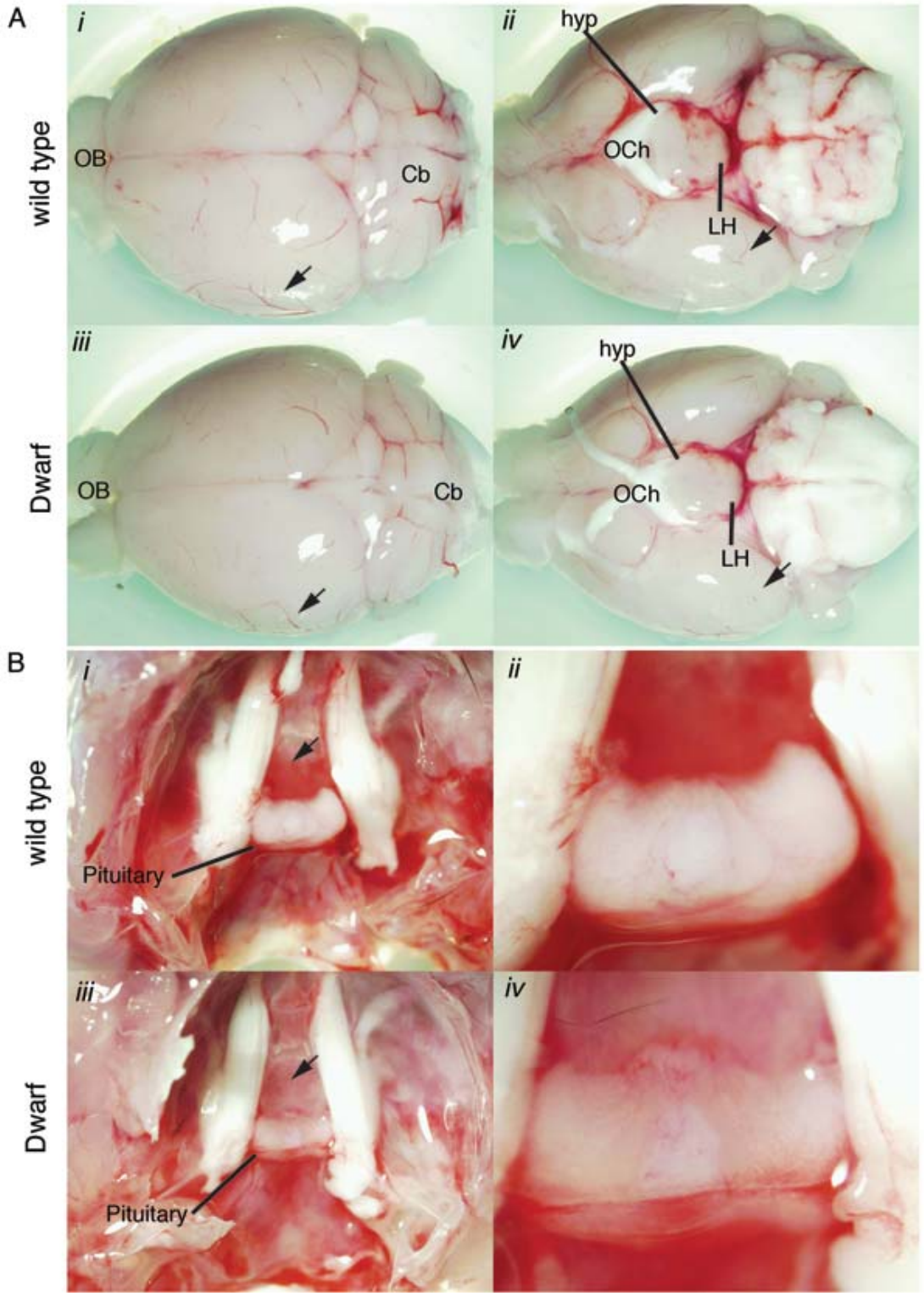
A
wild type
Dwarf
i
ii
iii
iv
OB
Cb
hyp
OCh
LH
B
Pituitary

J. Comparison of the Major Organs Reveals Proportionate Decrease in Size

Given that the pituitary and brains of dwarf mice were smaller (Figure 4-5, p.162) I extended my observation to the major organs (heart, kidney, adrenal, spleen, liver, ovary, testis) (Figure 4-16, p.186). Here I compared the size of these organs in 8-week old wild-type to dwarf mice (male and female, n=1 per group). Only data from females is shown; there was no difference in size between males and females (data not shown). Size comparison showed that dwarf mice exhibit proportionate dwarfing of all major organs: heart, kidney, adrenal, spleen, liver, ovary, testis, and brain (ovary and testis are shown later and in more detail in Figure 4-17, p.188); and disproportional dwarfing of the pituitary (as shown previously in Figure 4-5, p.162). The comparison between heart, kidney, adrenal, spleen, liver and brain is shown in Figure 4-16 (p.186). Weights of these organs were not obtained, as the primary focus of this project was the characterization of the dwarfism phenotype with respect to the somatotropic axis.

K. Dwarf Mice Show Delayed Gonadal Development and are Sub-fertile

The APC (Canberra, ACT, Australia), where the mice were created, observed that dwarf homozygous males and females did not produce offspring. This posed the question whether dwarf homozygous mice were infertile. Analysis of the gross morphology of the female (ovary) and male (testis) reproductive organs (Figure 4-17 A and C (p.188), respectively) revealed a decrease in size; the most striking decrease in size was between the wild-type and dwarf ovary. Histological examination (using H&E staining) of sections from the female 8-week ovary revealed an absence of the corpus lutea, compared with wild-type littermates. The absence of corpus lutea indicates that female dwarf mice, at 8-weeks (mice are fertile from 5- to 8-weeks (Fox, 2007)), are not ovulating like their wild-type littermates, suggesting that they have not yet developed reproductive fitness at this age. Histological examination (using the H&E morphology stain) of cross-sections of the 8-week old male testis did not reveal any gross abnormality (Figure 4-17 D), aside from the testis being proportionally smaller than the wild-type littermate. Using a masson trichome stain (nuclei stain black; collagen and mucus membrane stain blue; cytoplasm, keratin and muscle stain red) on adjacent sections for better visualization of the nuclear and cytomorphologic detail in the testis, again there was no gross abnormality. Given that there was no gross morphological abnormality in testis, spermatozoa morphology was examined to determine whether there was any defect, which may be preventing fertilization (Figure

4-17 E). Morphologically abnormal spermatozoa are less able to pass through the cervix (Hanson and Overstreet, 1981; Mortimer et al., 1982), the uterotuberal junction (de Boer et al., 1976; Krzanowska, 1974) and the oocyte vestments (Krzanowska and Lorenc, 1983). Comparison of wild-type and dwarf spermatozoa did not reveal any gross morphological defect, however, the tail of spermatozoa from dwarf mice showed the presence of a cytoplasmic droplet (Figure 4-17 E) indicating that these spermatozoa were undergoing maturation. Cytoplasmic droplets are a normal component of the mammalian spermatozoa maturation (Cooper et al., 2004). These results suggest that the compromised fertility of dwarf mice is not due to any gross morphological abnormality, but indicates that these mice are developing at a much slower rate then their wild-type littermates.

Given that dwarf mice are developing at a much slower rate I decided to examine their reproductive fitness. Specifically, I wanted to determine whether homozygous dwarf mice were able to reproduce and at what age they produce their first litter. To answer these questions I set up several combinations of breeder pairs; mated from the age of reproductive fitness (8-weeks). The breeders were as follows: (1) homozygous wild-type female x homozygous wild-type male (n=3); (2) heterozygous wild-type female x heterozygous wild-type male (n=3); (3) homozygous dwarf female x homozygous dwarf male (n=2); (4) homozygous dwarf female x homozygous wild-type male (n=1); and (5) homozygous wild-type female x homozygous dwarf male (n=1). The homozygous dwarf x wild-type matings were set up to ascertain whether the homozygous dwarf female or male were sub-fertile. The results are shown in Table 4-2 (below).

Table 4-2 Reproductive fitness of dwarf mice

Preliminary data for breeding methods set up between wild-type (+/+), heterozygous (+/dw) and dwarf homozygous (dw/dw) males and females. Males and females were placed together at 8-weeks (42 days) and allowed to breed normally. Breeders were separated when they reached 9 months of age. Breeder females and males were age matched from different litters, making sure the female was 8-weeks old.

Breeders		Number of breeders pairs	Female Age at First Litter (days)	Number of Litters per breeder pair	Average Pups per Litter
Female	Male				
+/+	+/+	3	68	6	8
+/dw	+/dw	3	69	6	8
dw/dw	dw/dw	2	165	4	5
dw/dw	+/+	1	No births recorded	-	-
+/+	dw/dw	1	No births recorded	-	-

Figure 4-16 Gross morphology of organs of 8-week old age matched wild-type and dwarf littermates
Images of organs from 8-week old female (n=1) wild-type and dwarf littermates. (A) Comparison of organ (heart, kidney, adrenal, spleen) sizes between wild-type and dwarf littermates. (B) Higher magnification images of heart (*i* and *v*), kidney (*ii* and *vi*), adrenal (*iii* and *vii*) and spleen (*iv* and *viii*), shown in A. All organs in the dwarf mouse are smaller than their wild-type littermates. However, there is a more profound decrease in size of the adrenal. (C) Comparison of liver sizes of wild-type and dwarf littermates. (D) Comparison of brain sizes of wild-type and dwarf littermates. (E) Higher magnification images of wild-type and dwarf brains. Outline of the structures of the brain in dorsal (*i*) and ventral (*ii*) view in the wild-type brain. The dorsal (*iii* and *iv*) and ventral (*v* and *vi*) view of the wild-type and dwarf mouse brain.

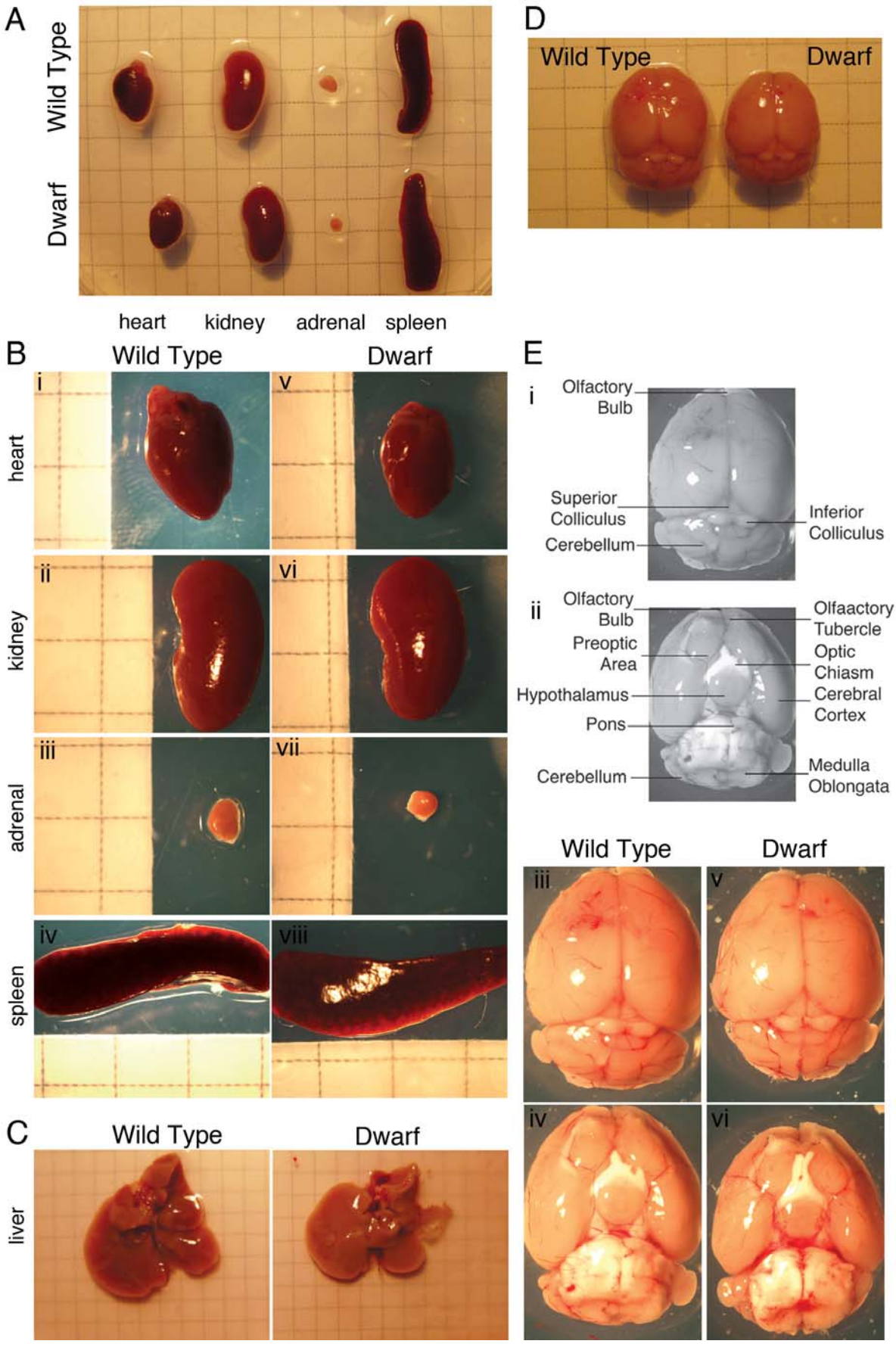
A
Wild Type
Dwarf
heart
kidney
adrenal
spleen
D
Wild Type
Dwarf
B
Wild Type
Dwarf
heart
kidney
adrenal
spleen
i
v
ii
vi
iii
vii
iv
viii
E
i
Olfactory Bulb
Superior Colliculus
Cerebellum
Inferior Colliculus
ii
Olfactory Bulb
Preoptic Area
Hypothalamus
Pons
Cerebellum
Olfaactory Tubercle
Optic Chiasm
Cerebral Cortex
Medulla Oblongata
Wild Type
Dwarf
iii
v
iv
vi
C
Wild Type
Dwarf
liver

Homozygous wild-type male and females, and heterozygous male and females, had their first litter when the female was 68 and 69 days old (12 - 13 days after being placed in a breeder pair), respectively and produced 6 litters over 9 months. In contrast, homozygous dwarf male and females had their first litter when the female was 165 days old (109 days, or 5 months, after being placed in a breeder pair) and produced 4 litters over 9 months. No litters were recorded for the homozygous dwarf x wild-type matings. It is unclear why no litters were produced, given that the homozygous dwarf female and male mating produced 4 litters over the 9-month period. Together, these preliminary results suggest that homozygous dwarf mice have slower reproductive maturation than wild-type littermates. A more extensive analysis would be needed to accurately assess the reproductive fitness and reproductive maturation, including a detailed examination of the female reproductive cycle. Furthermore, a greater number of homozygous dwarf x wild-type matings should be set-up.

Figure 4-17 Gross morphology and histology of reproductive organs from wild-type and dwarf mice
(A) Gross morphology of ovaries, showing the ovary and oviduct. Representative glands from adult dwarf and control mice (8-week-old females). (B) Sections through corresponding ovaries. Ovarian paraffin sections (5μm) were stained with hematoxylin and eosin (H&E); CL, Corpus Luteum; scale bar 50μm. Higher magnification of as shown by box. *, atretic follicles were observed in dwarf, but not wild-type, ovaries. (C) Gross morphology of testis. Representative glands from adult dwarf and wild-type mice (8-week-old males). (E) Sections through corresponding testis. Testis paraffin sections (5μm) were stained with H&E (a-d) and masson trichome (e-h). (a) and (b) show low magnification of seminiferous tubules lined by germline epithelium and enclosed by tunica propria. In the interstices are blood vessels and clumps of leydig (intersticial) cells. (c) and (d) show higher magnification of a single seminiferous tubule. (e) and (f) show low magnification of seminiferous tubules stained with masson trichome. (g) and (h) show a higher magnification of a single seminiferous tubule. Seminiferous tubules of dwarf mice (h) show a decrease sperm, as shown by density of sperm tails within the lumen, compared with wild-type littermates (g). Scale bar 0.1mm. (E) Sperm morphology. Sperm sample was obtained, during testis dissection, from the vas deferens emerging from the tail of the epididymis to examine sperm morphology (using H&E staining), from wild-type and dwarf mice. Dwarf mice showed no abnormal morphology, however, the presence of a cytoplasmic droplet on the tail region indicates immature development. Together results suggest that a slower maturation of both the male and reproductive tract takes place in dwarf mice. Scale bar in B and D = 50μm.

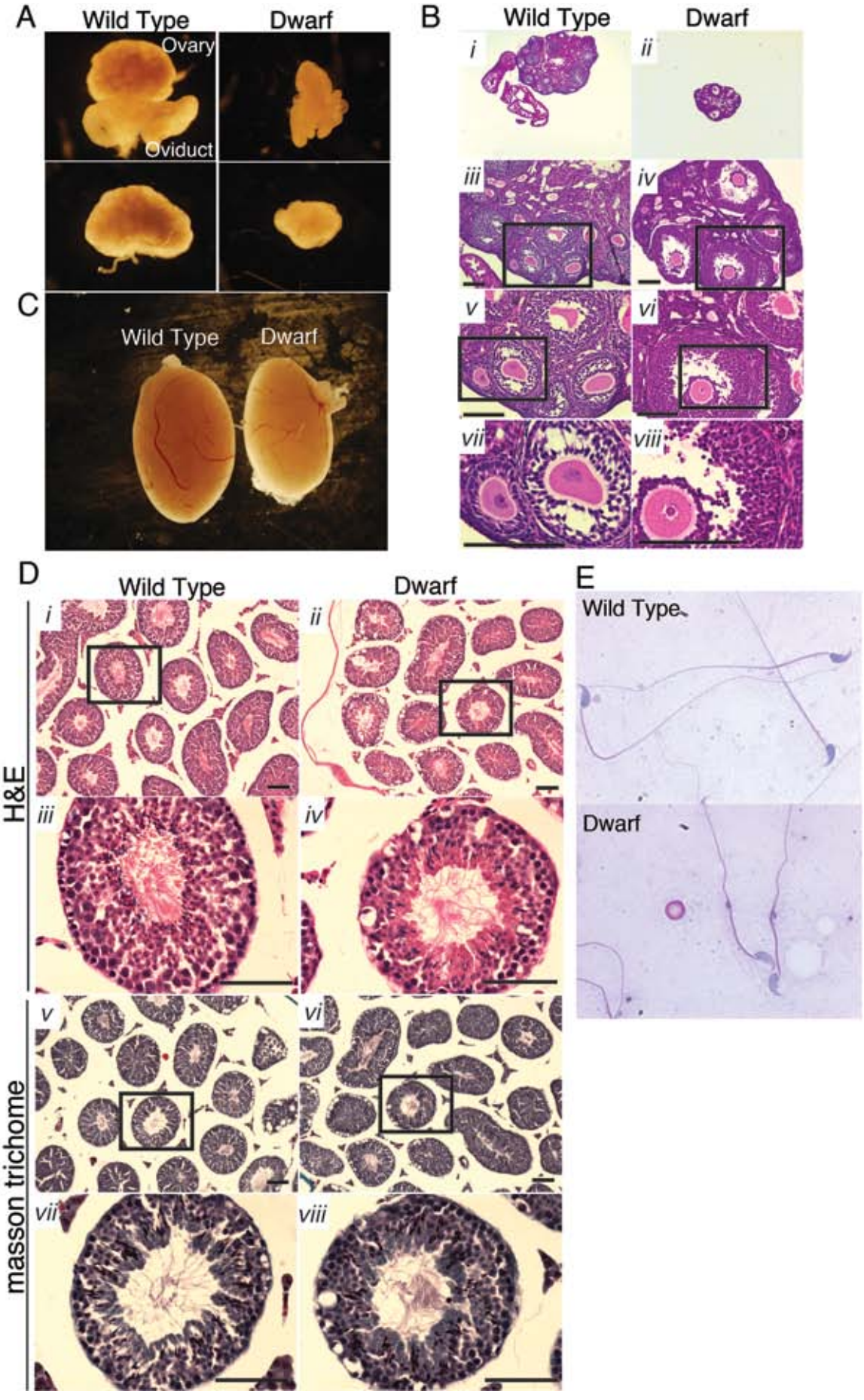
A
Wild Type
Dwarf
Ovary
Oviduct
B
Wild Type
Dwarf
i
ii
iii
iv
v
vi
vii
viii
C
Wild Type
Dwarf
D
Wild Type
Dwarf
H&E
masson trichome
i
ii
iii
iv
v
vi
vii
viii
E
Wild Type
Dwarf

IV. DISCUSSION

In the present study, a novel dwarfism mutation was identified in the *Wars* gene. Dwarf mice displayed dramatic hypoplasia of the anterior pituitary gland, associated with greatly reduced pituitary GH. Moreover, serum GH and IGF-1 levels, the major endocrine regulators of postnatal growth in mammals, were significantly decreased in these mutant mice, leading to greatly reduced longitudinal growth. The anterior pituitary, in contrast to the posterior pituitary, is not of neuronal origin but is derived from the oral ectoderm. However, Wars expression was shown in both the anterior and posterior lobes, specifically within cells lining the vessels. Furthermore, both GHRH and Sst were decreased in the hypothalamus. It is well established that GHRH, which is released from specific hypothalamic neurons, plays a key role in stimulating the proliferation of pituitary somatotrope cells (Frohman and Kineman, 2002b; Giustina and Veldhuis, 1998). It is therefore likely that the defect leading to anterior pituitary hypoplasia and the subsequent dwarfism phenotype is a result of a hypothalamic defect, most likely to be affecting hypothalamic neuron development (Figure 4-3, p.158 and Figure 4-15, p.182) and their connections with the hypophysial portal vasculature, the most important network of vessels and capillaries connecting hypothalamic neurons to the pituitary. *Wars*, and other members of the AARS family, has been known to play a role in angiogenesis, in zebrafish and in endothelial cell cultures (Fukui et al., 2009; Herzog et al., 2009; Ray and Fox, 2007; Wakasugi et al., 2002a; Wakasugi et al., 2002b). Although the other AARSs, YARS, WARS and EPRS, can regulate angiogenesis in cell culture, it is not fully understood whether AARSs contribute to the establishment of vascular patterning in vertebrates, including mice. In fact, the only known AARS mutations in mice are in GARS and YARS, and have been associated with dominant types of Charcot-Marie-Tooth (CMT) disease (a group of peripheral neuropathies characterized by sensory loss and poor motor function) in patients (Antonellis et al., 2003; Jordanova et al., 2006). Note, these two AARSs have *not* been shown to play a role in angiogenesis. Thus, it is tempting to speculate that a mutation in *Wars*, in mice, plays an important role during angiogenesis, and this is specifically important during development of the vascular connection between the hypothalamus and pituitary.

It was hypothesized that this novel *Wars*^{L30P} mutation in mice results from a hypothalamic defect, most likely in GHRH and/or Sst and that this is contributing to the dwarfism phenotype. GHRH neurons, located within the ARC, gradually increase during postnatal development and plateau when adulthood is reached. Mice with congenital GH deficiency, due to a deficiency in GH-secreting somatotropes, lack GH-mediated negative feedback, subsequently leading GHRH overstimulation and excessive GHRH neuron

number. In turn, the increase in GHRH neurons promotes an increase in the production of GHRH (McGuinness et al., 2003; Phelps and Hurley, 1999). However, given that the mutation has been identified in an AARS whereby other AARSs have been linked to noncanonical activities in vascular development, it is likely that the substitution mutation effects vasculature structure and/or communication between endothelial cells.

A. *Wars*^{L30P} Dwarf Mice are Proportionally Smaller with Pituitary Hypoplasia

One of the primary effects of the mutation is dwarfism. The aim of the work presented in this chapter was to investigate the cause of this dwarfism, in order to gain insight into the mechanism that underpins this phenotype. Characterization of the dwarfism phenotype revealed that homozygous dwarf mice are 30-40% smaller than both heterozygous and wild-type littermates, and this observation is seen throughout postnatal development and into adulthood (Figure 4-2, p.155). Longitudinal growth was also reduced in dwarf mice (Figure 4-2, p.155). Mice harboring mutations in other genes that result in dwarfism have similar phenotype characteristics (Alba et al., 2005; Bokryeon et al., 2009; Cheng et al., 1983; Lin et al., 1994; Schaiber and Gowen, 1961; Sinha et al., 1975; Snell, 1929). During these experiments the mutation had not yet been identified and I speculated that the dwarfism mutation could be a result of either a pituitary or hypothalamic defect. In both cases the secretion of GH from somatotropes would be decreased and subsequent downstream signaling in the somatotropic-axis would be compromised. Additionally, the size of littermates at birth would not differ. Examination of postnatal pups, at P1, 7 and 14, did not reveal any significant difference between weights, indicating that the growth defect becomes prominent later than P14, but is definitely observed between P21-29.

To further determine the extent of dwarfism, I next examined the pituitary, the key regulator of GH and other pituitary hormone secretion, and the brain, specifically the hypothalamus, for any abnormalities. Firstly, pituitaries were examined. Dwarf mice revealed pituitary hypoplasia, which was primarily caused by a dramatic decrease in the size of the anterior pituitary (the size of posterior pituitary appeared essentially unchanged). The anterior pituitary, in contrast to the posterior pituitary, is not of neuronal origin but is derived from the oral ectoderm. Therefore, it is likely that the mutation has an affect on the anterior, rather than posterior, pituitary. Secondly, the brain was examined and the hypothalamus examined for anatomical abnormalities. Besides the pituitary hypoplasia displayed in dwarf mice, there was no significant difference in overall brain morphology between the dwarf and wild-type. This suggests that the mutation is having a

profound affect on pituitary size, and likely resulting in a decrease in somatotropes, which in turn are not producing the correct concentration of GH essential for growth and development.

B. Pituitary GH and Serum IGF-1 are Reduced in *Wars*^{L30P} Dwarf Mice

To explore the mechanisms underlying the dwarf phenotype, I next examined whole pituitary extract levels of GH as well as serum levels of the key hormone IGF-1 that is involved in somatic growth. The serum levels of other important hormones (e.g. gherlin, a hormone that stimulates pituitary GH release via activation of central GH secretagogue receptors (Osterstock et al., 2010; Sun et al., 2004)) were not examined because the main focus point of this project was to analyze the somatotropic axis of the novel dwarf mouse line. Strikingly, dwarf mice showed a significant reduction in GH levels as well as IGF-1. GH is released into the blood from the anterior pituitary where it then binds to specific receptors in the liver, triggering the secretion of IGF-1. In turn, circulating IGF-1, considered the major factor that mediates the stimulatory effects of GH on longitudinal growth (Yakar et al., 2002), has an inhibitory (negative feedback) action on GHRH neurons located with the hypothalamus. Consistent with the observed decrease in GH levels, dwarf mice reveal a striking reduction in serum IGF-1. It is therefore likely that the observed decreases in both GH and serum IGF-1 levels in dwarf mice are responsible for the observed growth deficit.

C. Hypothalamic *Ghrh* and *Sst* Expression Levels are Reduced in *Wars*^{L30P} Dwarf Mice

Hypothalamic *Ghrh* as well as *Sst* levels were significantly reduced in dwarf mice. GHRH and GH release is controlled by the inhibitory control of Sst whereby Sst exerts its inhibitory effects on longitudinal growth by inhibiting the secretion of GH from pituitary somatotropes. It is pertinent to know that a subset of GHRH neurons located in the ARC expresses Sst receptors, and that expression and release of GHRH are inhibited by Sst (for review see (Bertherat et al., 1995). Conversely, Sst neurons of the periventricular area of the anterior hypothalamus are also stimulated by GHRH (Aguila and McCann, 1987). Thus, GH deficiency normally results in an overstimulation of GHRH and inhibition of Sst (Alba and Salvatori, 2004; Alba et al., 2005). Additionally, the observed decreased in *Sst* has also been observed in mice deficient in GH (Bartke, 2000; Hurley et al., 1997; Phelps et al., 1996). An absence of GH production has a marked negative effect on the differentiation and levels of the peptide expression in hypophysiotropic Sst neurons (Phelps et al., 1996), as well as *Sst* mRNA levels (Hurley et al., 1997). Importantly, an informative study that

examined *Sst* expression over time in the Ames dwarf and wild-type mice, found that a reduction of *Sst* in dwarf mice at 7 days of age suggests that GH production during embryonic or very early postnatal development is important for activating Sst transcription (Hurley et al., 1997). Mice with congenital GH deficiency, due to a primary defect in somatotropes, lack GH-mediated negative feedback thereby resulting in overstimulation of hypothalamic GHRH neurons (i.e. ↑GHRH:↓Sst) (Hurley et al., 1997; McGuinness et al., 2003). Whereas abnormally low Sst in the hypothalamus of mice with a *pituitary* GH defect. Therefore, pituitary hypoplasia and associated GH deficiency are due to a hypothalamic defect and have the opposite phenotype (i.e. ↑Sst:↓GHRH). Then how can the observed decrease in *both* GHRH and Sst, in these dwarf mice (i.e. ↓GHRH:↓Sst), be explained? A study in sheep examined GHRH and Sst secretion into hypophysial portal blood and relationship to GH secretion in peripheral blood (Bluet-Pajot et al., 1998). As expected, the majority of GH peaks were associated with an increased portal GHRH and a fall in Sst concentrations. Interestingly, a simultaneous increase in GHRH and Sst levels was observed in 18.5% of GH peaks while 12.9% of GH peaks occurred with a fall in Sst and no modification in GHRH concentrations. This data, although in sheep, indicate that the GHRH/Sst interplay is complex. Perhaps, in the dwarf mouse, we are seeing a decrease in *Sst* relative to *Ghrh*. Although *Sst* mRNA levels were decreased in dwarf mice, *Ghrh* was significantly more reduced. These results agree with previous dwarf data that the observed decrease in hypothalamic *Sst* is due to feedback inhibition triggered by low GH and IGF-1 levels (Giustina and Veldhuis, 1998).

D. Dwarf Mice Show Delayed Reproductive Development

Dwarf mice show delayed reproductive organ development and sub-fertility (Figure 4-17, p.188 and Table 4-2, p.185, respectively). Infertility has been observed in other dwarf phenotypes, for example, the Snell dwarf mouse show gonadal dysfunction arising from a lack of neuroendocrine axis activation (Bartke, 2000; Bartke and Lloyd, 1970). It is known that diminished GH levels lead directly to diminished circulating insulin and IGF-1, both of which are necessary for normal body size and aging in dwarfism mouse models, such as the Snell and Ames mice (Bartke, 2000). Therefore a decrease in these important hormones significantly reduces reproductive ability, and this is seen in most dwarf mouse models (Brown-Borg, 2009). Anatomical observation of the female and male reproductive organs revealed a decrease in size; the most striking decrease in size was between the wild-type and dwarf ovary. Histological examination (using the H&E staining) of sections from the female 8-week ovary revealed an absence of the corpus lutea, indicating that female dwarf mice were not fertile at 8-weeks (the normal reproductive age in mice is between 5-8

weeks (Fox, 2007)). Histological examination (using the H&E morphology stain and masson trichome stain) of the male testis of dwarf and wild-type littermates did not reveal any gross abnormality, aside from the testis being proportionally smaller in dwarf mice. Given that there was no gross morphological abnormality in testis, morphology of spermatozoa was examined to determine extent of defect, which may be preventing fertilization. Morphologically abnormal spermatozoa are less able to pass through the cervix (Hanson and Overstreet, 1981; Mortimer et al., 1982), the uterotuberal junction (de Boer et al., 1976; Krzanowska, 1974), and the oocyte vestments (Krzanowska and Lorenc, 1983). There was no gross morphological defect in spermatozoa, however, the tail of spermatozoa from dwarf mice contained a cytoplasmic droplet (a normal component of the mammalian spermatozoa) maturation (Cooper et al., 2004). These results suggest that the compromised fertility of dwarf mice does not stem from any gross morphological abnormality within the reproductive organs or within the spermatozoa. Simply dwarf mice have delayed reproductive development. As a preliminary study, wild-type and homozygous dwarf mice were mated from the age of reproductive fitness (8-weeks). The first birth of pups to homozygous dwarf parents was at 5-months of age. Although preliminary, these data support the anatomical data that dwarf mice had slower reproductive maturation. A more extensive analysis, using a larger sample size, would be needed to accurately assess the reproductive fitness and reproductive maturation, including a detailed examination of the female reproductive cycle.

Table 4-3 summarizes the phenotype of several dwarf mouse models including the novel *Wars*^{L30P} mouse mutant characterized within this work.

E. Wars is Expressed Within Blood Vessels of the Pituitary

The mutation was identified in the tryptophanyl-tRNA synthetase (*Wars*) gene (Figure 4-6, p.165). This enzyme has never been previously associated with a growth defect, nor has there existed a mouse model of this mutation, until now. Therefore, the generation of this novel *Wars*^{L30P} mutant mouse is an invaluable resource that will ultimately provide an insight into the mechanism of HP axis vascular development resulting from a single substitution mutation in this ubiquitously expressed AARS.

Table 4-3 Phenotypic characteristics comparing GH/IGF-1 long-living mutant mice with the L30P dwarf mouse

Adapted from (Brown-Borg, 2009). [1] Homozygous dwarf and wild-type mice were maintained for 2 years, after which time they were culled. There were no recorded deaths in either groups. It is likely these mice will have extended longevity; this test should be performed in the future. ND, not determined.

	Mouse Models							
Phenotype	**Ames (Prop1)**	**Snell (Pit1)**	**GHR/BP KO**	**IGF-1R +/-**	**LID (liver IGF1 mutant)**	**Little (GHRHR mutant)**	**Klotho**	**Tukkuburko (*Wars*^{L30P} dwarf)**
GH/IGF1/Insulin signalling	↓	↓	↓	↓	↓	↓	↓	↓
Body Size	↓	↓	↓	↓	↔	↓	↔	↓
Reproduction	↓	↓	↓	↔	↔	↓	↓	↓
Longevity	49-68% ↑	42% ↑	21-40% ↑	33% females ↑	↔	23-25% ↑	18-30% ↑	ND[1]

AARSs are large enzymes that have evolved from two different active sites, gradually incorporating additional domains (Ribas de Pouplana and Geslain, 2008). Their Noncanonical functions have been of considerable interest recently as they have been implicated in various disease states. Fragments of YARS stimulate angiogenesis, whereas those of WARS inhibit angiogenesis (Tzima and Schimmel, 2006). Notably, several additional AARSs have been involved in angiogenesis in different contexts (Table 4-4, p.196). Human AARSs have been involved in cell-signaling activity throughout evolution, arising through individual sequence adaptations and domain acquisitions. In the mammalian YARS there is an embedded tripeptide Glu-Leu-Arg motif essential for cell signaling (Wakasugi and Schimmel, 1999). This was conferred by introducing Glu-Leu-Arg motif into yeast YARS (Liu et al., 2002). The YARS-appended domain is able to stimulate mononuclear phagocyte chemotaxis and tumor necrosis factor-α production in a behavior

similar to that of the cytokine endothelial and monocyte-activating polypeptide II (Wakasugi and Schimmel, 1999). Thus, linking translation and cell signaling.

Human WARS, a close homologue of YARS, also participates in cell-signaling pathways (Wakasugi et al., 2002b) and catalyzes the aminoacylation of tRNA. In humans, cells contain two distinct WARS isoforms, the full length WARS (FL-WARS; 471 aa) and mini-WARS (424 aa) in which most of the N-terminal extension is absent, the later arising by alternative mRNA splicing, naturally (Wakasugi, 2010). There exist also two other isoforms of WARS: T1-WARS and T2-WARS (Figure 4-18, p.197) alternative mRNA spliced forms of WARS and are implicated in the inhibition of angiogenesis (Tzima and Schimmel, 2006). Expression of WARS and mini-WARS is robustly induced by interferon-gamma (IFN-γ), an antiproliferative cytokine (Fleckner et al., 1995; Liu et al., 2002; Tolstrup et al., 1995). While both the alternative splicing and IFN-γ induction has been known for several years, the importance was not well understood until it was confirmed that mini-WARS had antiangiogenic (or angiostatic) activities in assays (both *in vitro* and *in vivo*). For instance, mini-WARS can block VEGF-induced migration of human umbilical vein endothelial cells (Wakasugi et al., 2002b). Furthermore, mini-WARS and a closely related proteolytic variant, T2-WARS (Figure 4-18, p.197) both block VEGF-stimulated angiogenesis in chick cell adhesion molecule and mouse matrigel assays *in vivo* (Otani et al., 2002; Wakasugi et al., 2002b). However, FL-WARS does not have this effect (Otani et al., 2002; Wakasugi et al., 2002b). T2-WARS has also been shown to be a potent inhibitor of retinal angiogenesis in the neonatal mouse, where it was localized to retinal blood vessels. Together, this data suggest that blood vessel endothelial cells are likely a direct target of WARS.

Table 4-4 Noncanonical activities of AARSs in vascular development
Adapted from (Kawahara and Stainier, 2009)

AARS	Functions	Reference
Sars	Disruption of Sars leads to dilatation of the aortic arch vessels and aberrant branching of cranial and intersegmental vessels in zebrafish	(Fukui et al., 2009; Herzog et al., 2009)
YARS	N-terminal fragment of YARS functions as an angiogenic factor for endothelial cells in culture	(Wakasugi et al., 2002a)
WARS	N-terminal truncated form of WARS functions as an angiostatic factor for endothelial cells in culture	(Wakasugi et al., 2002b)
EPRS	EPRS is involved in the IFN-γ–mediated translational silencing of VEGF-A in culture	(Ray and Fox, 2007)

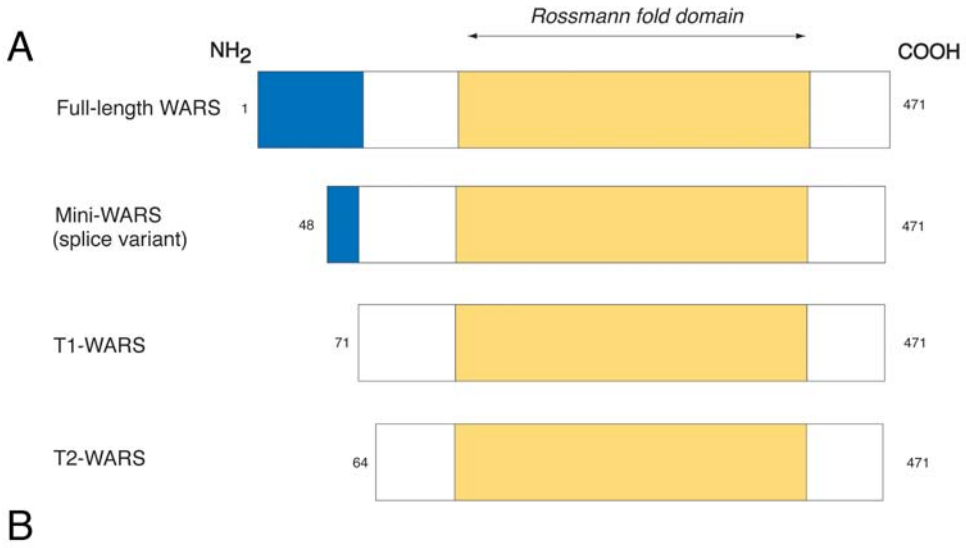

Figure 4-18 Schematic representation of the human full length and truncated WARS
(A) Schematic representation of human WARS, and variant constructs. Numbers on the left and right correspond to the NH_2- and COOH-terminal residues relative to the human full-length enzymes, respectively. Rossman fold catalytic domain is shaded yellow and the N-terminal is shaded blue. (B) Structure of the dimeric human WARS. Corresponding Rossman fold catalytic domain is shaded yellow and the N-terminal is shaded blue. Figure A modified and adapted from (Wakasugi, 2010); B modified and adapted from (Yang et al., 2003)

Endothelial cells of vessels are constantly subjected to mechanical forces that are a direct result of the hemodynamic forces of blood flow and include shear stress and pressure. These hemodynamic forces have profound effects on endothelial cell biology thereby playing a major role in vascular homeostasis and pathophysiology. Fluid shear stress plays an integral part of the mechanical stimulus experience by endothelial cells, whereby it helps to regulate migration, proliferation, and survival—key mechanisms involved in angiogenesis. Most importantly, fluid shear stress aids in the production of vasoactive mediators and expression of adhesion molecules, essential for regulating vasculature (Olsson et al., 2006). Angiogenesis plays a fundamental role in growth, survival, and function of normal and pathological tissues (Carmeliet, 2000a; Nicosia and

Villaschi, 1999). The process of angiogenesis requires intercellular junctions to loosen followed by extracellular matrix degradation by endothelial cells, migration of endothelial cells toward the angiogenic stimulus, sprout formation, lumen formation, and the joining of sprouts to form a capillary bed (refer to Introduction Chapter 1I.C.3 Angiogenesis, p.41, for a detailed description) (Carmeliet, 2000a; Carmeliet and Collen, 2000; Nicosia and Villaschi, 1999)

Wars, as mentioned above, has reported noncanonical functions in angiogenesis. To examine further the function of the *Wars*^{L30P} mutation I used immunostaining to localize the expression of Wars within the pituitary. Wars expression was localized to blood vessels of both the anterior and posterior pituitaries (Figure 4-7, p.171). Additionally, Wars was expressed within the cytoplasm of several cells. This is not unexpected, because Wars is a ubiquitously expressed protein; a result never previously shown. No significant difference in Wars protein expression was determined by immunostaining of pituitary sections from wild-type compared to dwarf mice at 8-weeks (Figure 4-9, p.172). To further determine whether there was a decrease or change in Wars expression in dwarf mouse pituitaries, a western blot was performed by my colleague Chin Ng (Chin Ng, 2010) on pituitary, brain and kidney extracts (Figure 4-12, p.178). There was no detectable difference in Wars steady state protein levels in pituitary, brain nor kidney. Thus, the *Wars*^{L30P} mutation does not result in a simple loss of protein. Similarly, this was also seen in GARS protein levels in Gars$^{G240R/+}$ heterozygous patients and *Gars*$^{C201R/+}$ heterozygous mouse brain homogenates (Achilli et al., 2009). However, the investigation of Wars protein expression was performed on pituitaries, brains and kidneys from 5-month old littermates. Given that we know that Wars plays a role in angiogenesis, it is likely that we will not see a difference in Wars protein expression at this age. The formation of blood vessels, in particular within the HP axis, occurs during development and early postnatally (as shown by the growth chart in Figure 4-2, p.155). At 5-months of age there may be compensatory up-regulation of Wars expression. Therefore, expression levels of Wars should be examined during embryogenesis, particularly during the crucial phase of pituitary development, between 10.5-17.5 dpc, the later time point being when pituitary cells have differentiated (refer Figure 1-4, p.35) and also during the first three weeks of postnatal development, a time when growth is rapid.

To confirm that Wars is expressed in pituitary blood vessels, immunostaining of important vessel proteins, PECAM and VE-Cadherin was performed. Wars was found to be expressed in pituitary vasculature, as shown by co-expression analysis with PECAM and VE-Cadherin, confirming that Wars is expressed within pituitary vasculature (Figure

4-9, p.172 and Figure 4-11, p.177). However, immunostaining was unable to determine whether VE-Cadherin was compromised. It has been hypothesized that T2-WARS binds to VE-Cadherin (refer to Figure 4-10, p.175) (Zhou et al., 2010) thus regulating angiogenesis. The question to ask here is whether the *Wars*^{L30P} mutation on the full length Wars protein is acting like the angiogenic T2-WARS or whether the point mutation has an alternate affect, possibly having an anti-angiogenic affect. Immunostaining of the blood vessels within the HP axis was not performed, primarily because immunostaining of the hypophysial portal vasculature is a difficult region to locate on corresponding sections. In particular, given that Wars is likely to have its affects during HP axis development and early postnatal growth, examination of vessels would be best completed utilizing recent novel technologies, as described in (Walls et al., 2008). Key vasculogenic and angiogenic events occur in the mouse embryo between E8.0 and E10.0, during which time the vasculature develops from a simple circulatory loop into a complex, fine structured, three-dimensional organ (see example in Appendices Figure A 2, p.231). Interpretation of vascular phenotypes exhibited by signaling pathway mutants has historically been hindered by an inability to comprehensively image the normal sequence of events that shape the basic architecture of the early mouse vascular system. To get around this hurdle, Walls et al (Walls et al., 2008) employed Optical Projection Tomography using frequency distance relationship-based deconvolution to image embryos immunostained with the endothelial specific marker PECAM to create a high resolution, three-dimensional atlas of mouse vascular development between E8.0 and E10.0 (5 to 30 somites). Analysis of the atlas has provided significant new information regarding normal development of intersomitic vessels, the perineural vascular plexus, the cephalic plexus and vessels connecting the embryonic and extraembryonic circulation. Although the authors did not look at vascular development postnatally, this technique has the potential to be applied at these stages; a potential avenue for examining vascular development in the *Wars*^{L30P} dwarf mouse. This atlas is freely available at http://www.mouseimaging.ca/research/mouse_atlas.html (Walls et al., 2008).

F. *Wars*^{L30P} Mutation Inhibits the Formation of New Vessels in Cell Culture

This is the first study to examine and document the expression of Wars and the novel *Wars*^{L30P} mutation, in mouse. Preliminary data have demonstrated that the *Wars*^{L30P} mutation, inhibits angiogenesis, in 3B11 cells (Chin Ng, 2010). This is supported by the preliminary anatomical data of the mouse cerebral cortex surface, lateral hypothalamic region and pituitary in 8-week old dwarf mice. (Figure 4-15, p.182). Here I showed that

brains from dwarf animals exhibited deranged microvessels with fewer prominent vessel branch points on the cerebral cortical surface and the dwarf pituitary was surrounded by fewer vessels. Although both these results are preliminary and require confirmation, they agree with other studies (outlined above), specifically those that have examined truncated WARS isoforms in cell culture; the extent of vascularization in brains *in vivo* remains unknown. Human FL-WARS has been shown to be inactive in angiostatic activity due to the steric hindrance of the WHEP domain blocking the interaction of WARS and VE-Cadherin (Wakasugi et al., 2002b; Zhou et al., 2010) Interestingly, analysis of *Wars*^{L30P} in endothelial cell tube formation assays demonstrated anti-angiogenic activity. The *Wars*^{L30P} mutation is most likely disrupting the helical structure of the WHEP domain in the Wars protein, thereby compromising its ability to block the interaction between Wars and VE-Cadherin, and resulting in a substantial decrease in endothelial cell tube formation. To confirm this the interaction between *Wars*^{L30P} and VE-Cadherin need to be examined. This can be accomplished by testing the binding of *Wars*^{L30P} to VE-Cadherin, using co-immunoprecipitation.

G. Conclusion and Future Directions

This study is the first to have identified a novel mouse strain, by ENU mutagenesis, with a point mutation (leucine to proline substitution) in the enzyme tryptophanyl-tRNA synthetase (*Wars*) that results in dwarfism, pituitary hypoplasia as well as GH and IGF-1 deficiency, indicating a defect in the HP axis. Preliminary data have also shown that the point mutation prevents the formation of new vessels (anti-angiogenic).

To further understand the function of Wars in regulating HP axis development and determine the impact of the *Wars*^{L30P} mutation on WARS activity the following key points need to be examined:

- Examine extent of hypothalamic dysfunction

  Perform qPCR to examine mRNA expression of all hypothalamic neurons, initially at 8-weeks. In addition, validate this data by section in situ hybridization and immunostaining using available probes/antibodies.

- Understand the developmental progression and functional impact of the *Wars*^{L30P} dwarf phenotype

  This can be examined using GHRH-EGFP (Balthasar et al., 2003) and/or GH-EGFP transgenic reporter mice (Magoulas et al., 2000), generated by Prof. Iain Robinson at the National Institute for Medical Research (London). In GHRH-EGFP mice, EGFP is targeted to the secretory vesicles of the GHRH neurons in the ARC and enables GHRH neurons to be identified for

developmental and electrophysiological studies. Generating homozygous dwarf GHRH-EGFP transgenic mice would allow the number, morphology, directionality and terminal structure of GHRH neuron axonal projections to be traced and identified across postnatal development (Balthasar et al., 2003). Furthermore, this model would allow patch clamp time-lapse as well as live imaging analysis of GHRH neurons. This would ultimately provide information regarding the impact of the Wars mutation on the electrophysiological properties as well as time-lapse analysis of GHRH neurons, respectively.

- Confirm the angiostatic assays

  In addition to confirming the angiostatic assay, perform an in vivo assay measuring the impact of the mutation on the development of mouse retinal vasculature. This can be done by injecting recombinant Wars protein into P8 retinas in vivo and harvesting them at p12. This method will allow for the scoring of vascular development via visual inspection.

- Assessment of vasculature

  To gain an insight into the structure of vasculature of dwarf mice, quantitative assessment of total vascular volume, tube length and diameter can be performed using reconstruction of optical sections (z-series) acquired using confocal microscopy. Furthermore, analysis of endothelial cell/vasculature ultrastructure in dwarf and wild-type tissue may also be performed with the use of transmission electron microscopy.

- Determine whether *WARS* mutations cause GH deficiencies in humans

  Many of the genes that have been associated with HP axis dysfunction in humans were originally identified as causative genes in mouse model of dwarfism (Dattani and Robinson, 2000). This gene has never been implicated in pituitary function thereby providing a strong case for further investigating its role in mice and examining its significance in human HP axis dysfunction. This can be done by sequencing the WARS gene in patient DNA, prioritizing the screen for patients with GH deficiency.

Overall, the results from this project have identified a novel dwarf mouse with a genetic determinant of HP axis function and provide novel insights into the role and function of the *Wars*^{L30P} mutation *in vivo*. Identification of this enzyme and its importance during angiogenesis provides an exciting opportunity to further this work by determining its exact role and function during vascular development, during embryogenesis and postnatally. Dysfunction of the HP axis is a significant clinical problem and, despite the significant contributions been made to this genetic etiology, the responsible gene(s) in many patients remain unknown. Further research is likely to have a considerable importance for human health and will contribute to understanding the key insights into the molecular pathology of HP axis dysfunction and the role of Wars in GH regulation. It is highly probably that ongoing research on newly discovered gene will open the possibility

for novel genetic screening tests and potential new treatments; early diagnosis of GH deficiencies are linked to a lower risk of adverse effects of the disease.

APPENDICES

PERL SCRIPT USED IN THE COLLATION OF MICROARRAY STATISTICAL DATA

The following PERL script was used to collate the microarray statistical results into one excel file for easy comparison between the three statistical methods used. Genes were sorted and compared using the ProbeID.

The script takes four input files: (1) limma, (2) sam, and (3) ttest, list of known genes. Each file contains a ProbeID, which is used to determine common genes between the three files (limma, sam & ttest). The ProbeID is used to determine whether the gene appears in all three tests, just two of the tests or is unique to an individual test. The 'FC' and 'pval' for each test is included in the output comparing the three tests. The list of known genes is to provide additional detail (accession, all-symbol and transcript).

```
#!/usr/bin/perl

my $lineSep = "\n";
my $result = 0;

if ($#ARGV == 5) {
   $result = main(@ARGV);
} else {
   print "Invalid arguments to $0$lineSep";
   print "Arguments$lineSep";
   print "1. limma file$lineSep";
   print "2. sam file$lineSep";
   print "3. ttest file$lineSep";
   print "4. probe details file$lineSep";
   print "5. file containing commonalities$lineSep";
   print "6. error file$lineSep";
}

exit $result;

# Read in three files to be compared ie. limma, sam & ttest.
# A fourth file read in provides additional details for the probe ids
# in the first three files. The output is written to a fifth file
# that lists the probe ids in the limma, sam & ttest files showing
# which are common between all three, common in two or unique.
#
# A sixth file details errors encountered while processing the input
# files.
sub main {
   my $infile1 = shift;
   my $infile2 = shift;
   my $infile3 = shift;
   my $infile4 = shift;
   my $outcommon = shift;
   my $errorFile = shift;
   my %lines1;
   my %lines2;
   my %lines3;
   my %lines4;
   my $tmp1;
   my $tmp2;
   my $tmp3;
   my $fh;
   my $fhe;
   my $error;

   open($fhe, ">", $errorFile) or
        die "Could not open file: $errorFile$lineSep";

   # Read in the four files - limma, sam, ttest & probe details
   ($error, $tmp1) = suckFile($infile1, \&getLimma, $fhe);
   %lines1 = %{ $tmp1 };
   if ($error == 0) {
      ($error, $tmp1) = suckFile($infile2, \&getSam, $fhe);
      %lines2 = %{ $tmp1 };
   }
   if ($error == 0) {
      ($error, $tmp1) = suckFile($infile3, \&getTtest, $fhe);
      %lines3 = %{ $tmp1 };
   }
```

```
   if ($error == 0) {
      ($error, $tmp1) = suckFile($infile4, \&getDetail, $fhe);
      %lines4 = %{ $tmp1 };
   }
   if ($error == 0) {
      # Open the common points file to be written to
      open($fh, ">", $outcommon) or
           die "Could not open file: $outcommon$lineSep";

      # Column headings
      print $fh "\t\t\t".
                "limma, sam & ttest\t".
                "limma & sam\t".
                "limma & ttest\t".
                "sam & ttest\t".
                "only in limma\t".
                "only in sam\t".
                "only in ttest\t\t\t\t\t\t\t$lineSep".
                "Accession\tall-symbol\tTranscript\t".
                "Probe Id\tProbe Id\tProbe Id\tProbe Id\t".
                "Probe Id\tProbe Id\tProbe Id\t".
                "Gene name\tlimma FC\tlimma p value\tsam FC\t".
                "sam p value\tttest FC\tttest p value$lineSep";

      # There are three calls to the 'common' function that checks
      # for common points between the files. The only need for the
      # third call is to report probe ids in the ttest that isn't
      # in the limma or sam.
      ($tmp1, $tmp2, $tmp3) = common($fh, \%lines1, \%lines2,
                                     \%lines3, 1, \%lines4);
      ($tmp2, $tmp1, $tmp3) = common($fh, \%{ $tmp2 }, \%,
                                     \%{ $tmp3 }, 2, \%lines4);
      ($tmp3, $tmp1, $tmp2) = common($fh, \%{ $tmp3 }, \%{ $tmp1 },
                                     \%{ $tmp2 }, 3, \%lines4);
      %lines1 = %{ $tmp1 };
      %lines2 = %{ $tmp2 };
      %lines3 = %{ $tmp3 };

      close($fh) or die "Could not close file: $outcommon$lineSep";
   }
   close($fhe) or die "Could not close file: $errorFile$lineSep";

   if ($error == 0) {
      unlink $errorFile;
   }

   return $error;
}

# Read in each line of a file and store the lines in a hash, the hash
# is then returned as the product of this function.
# Storing each line of the file in a hash where the key is the probe
# id provides a simple way to check for common data across the limma,
# sam & ttest.
sub suckFile {
   my $file = shift;
   my $lineParser = shift;
   my $fhe = shift;
   my $fh;
   my %lines;
   my $key;
```

```
   my $value;
   my $line;
   my $error;

   open($fh, "<", $file) or
        die "Could not open file: $file$lineSep";

   if (<$fh>) { # ignore first line
      chomp();
      $_ =~ /^[^\n]*$/;
   }
   while(<$fh>) {
      chomp();
      $line = $_;
      $line =~ s/\r$//;
      ($error, $key, $value) = &$lineParser($line);

      # this function needs to return hash ref so that error flag can
      # be returned
      if ($error == 1) {
         print $fhe "Error parsing line$lineSep";
         print $fhe "$file$lineSep";
         print $fhe "$line$lineSep";
         print $fhe "$key = $value$lineSep$lineSep";
      } elsif (exists($lines{$key})) {
         print $fhe "Duplicate probe id$lineSep";
         print $fhe "$file$lineSep";
         print $fhe "$line$lineSep";
         print $fhe "$key = $value$lineSep";
         print $fhe "First found: $lines{$key}$lineSep$lineSep";
         $error = 2;
      } else {
         $lines{$key} = $value;
      }
   }

   close($fh) or die "Could not close file: $file$lineSep";

   return ($error, \%lines);
}

sub getLimma {
   my $line = shift;
   my $error = 0;

   # $1 = probe id
   # $2 = gene name
   # $3 = fc
   # $4 = pval
   $line                                                                =~
/^([^\t]*)\t[^\t]*\t([^\t]*\t)[^\t]*\t([^\t]*\t)[^\t]*\t([^\t]*)/;
   $error = ($1 eq "" || $2 eq "" || $3 eq "" || $4 eq "");

   return ($error, $1, $2.$3.$4);
}

sub getSam {
   my $line = shift;
   my $error = 0;

   # $1 = probe id
```

```
    # $2 = gene name
    # $3 = fc & pval
    $line =~ /^([^\t]*)\t[^\t]*\t([^\t]*\t)[^\t]*\t([^\t]*\t[^\t]*)$/;
    $error = ($1 eq "" || $2 eq "" || $3 eq "");

    return ($error, $1, $2.$3);
}

sub getTtest {
    my $line = shift;
    my $error = 0;

    # $1 = probe id
    # $2 = gene name
    # $3 = fc & pval
    $line                                                                    =~
/^([^\t]*)\t[^\t]*\t([^\t]*\t)|([^\t]*\t[^\t]*)\t[^\t]*$/;
    $error = ($1 eq "" || $2 eq "" || $3 eq "");

    return ($error, $1, $2.$3);
}

sub getDetail {
    my $line = shift;
    my $error = 0;

    # $1 = probe id
    # $3 = accession & all-symbol
    # $2 = transcript
    $line                                                                    =~
/^[^\t]*\t[^\t]*\t([^\t]*)\t[^\t]*\t([^\t]*)\t([^\t]*\t[^\t]*\t)/;
    $error = ($1 eq "" || $2 eq "" || $3 eq "");

    return ($error, $1, $3.$2);
}

# Determine which files contain common points.
# When a common point is found delete the points from the hashes.
sub common {
    my $fh = shift;
    my %linesA = %{ shift @_ };
    my %linesB = %{ shift @_ };
    my %linesC = %{ shift @_ };
    my $round = shift;
    my %lines4 = %{ shift @_ };
    my @arr = keys %linesA;
    my $geneName;
    my $fcA;
    my $fcB;
    my $fcC;
    my $pvalA;
    my $pvalB;
    my $pvalC;
    my $extraDetail;

    foreach my $key (@arr) {
        ($geneName, $fcA, $pvalA) = deconstructLine(\%linesA, $key);
        ($geneName, $fcB, $pvalB) = deconstructLine(\%linesB, $key);
        ($geneName, $fcC, $pvalC) = deconstructLine(\%linesC, $key);
        $extraDetail = $lines4{$key};
```

```
      if (exists($linesB{$key}) && exists($linesC{$key})) {
         # In limma, sam & ttest
         print $fh "$extraDetail\t$key\t$key\t$key\t$key".
                   "\t\t\t\t$geneName\t$fcA\t$pvalA\t$fcB".
                   "\t$pvalB\t$fcC\t$pvalC$lineSep";

         delete $linesA{$key};
         delete $linesB{$key};
         delete $linesC{$key};
      } elsif (exists($linesB{$key})) {
         if ($round == 1) {
            # In limma & sam
            print $fh "$extraDetail\t\t$key\t\t\t\t\t\t$geneName".
                      "\t$fcA\t$pvalA\t$fcB\t$pvalB\t\t$lineSep";
         }

         delete $linesA{$key};
         delete $linesB{$key};
      } elsif (exists($linesC{$key})) {
         if ($round == 1) {
            # In limma & ttest
            print $fh "$extraDetail\t\t\t$key\t\t\t\t\t$geneName".
                      "\t$fcA\t$pvalA\t\t\t$fcC\t$pvalC$lineSep";
         } elsif ($round == 2) {
            # In sam & ttest
            print $fh "$extraDetail\t\t\t\t$key\t\t\t\t$geneName".
                      "\t\t\t$fcA\t$pvalA\t$fcC\t$pvalC$lineSep";
         }

         delete $linesA{$key};
         delete $linesC{$key};

      } else {
         if ($round == 1) {
            print $fh "$extraDetail\t\t\t\t\t$key\t\t\t$geneName".
                      "\t$fcA\t$pvalA\t\t\t\t$lineSep";
         } elsif ($round == 2) {
            print $fh "$extraDetail\t\t\t\t\t\t$key\t\t$geneName".
                      "\t\t\t$fcA\t$pvalA\t\t$lineSep";
         } elsif ($round == 3) {
            print $fh "$extraDetail\t\t\t\t\t\t\t$key\t$geneName".
                      "\t\t\t\t\t$fcA\t$pvalA$lineSep";
         }

         delete $linesA{$key};
      }
   }

   return (\%linesA, \%linesB, \%linesC);
}

sub deconstructLine {
    my %lines = %{ shift @_ };
    my $key = shift;
    my $geneName = "";
    my $fc = "";
    my $pval = "";

    if (exists($lines{$key})) {
       $lines{$key} =~ /^([^\t]*)\t([^\t]*)\t([^\t]*)$/;
       $geneName = $1;
```

```
            $fc = $2;
            $pval = $3;
        }

        return ($geneName, $fc, $pval);
}
```

MICROARRAY DATA SHOWING DIFFERENTIALLY EXPRESSED GENES

The list below shows all the genes from the microarray from the *Sox3*-null samples. *Sox3*-null microarray data was compared to wild-type data. LIMMA, SAM and t-test statistics were conducted and the fold change (FC) is shown for each together with the p-value. Values in red indicate a negative value and indicate that gene expression is down-regulated; values in black indicate a positive value and indicate gene expression is up-regulated.

		limma, sam & ttest		limma & sam	limma & ttest	sam & ttest	only in limma	only in sam	only in ttest							
Accession	all-symbol	Transcript	Probe Id	Probe Id	Probe Id	Probe Id	Probe Id	Probe Id	Probe Id	Gene name	limma FC	limma p value	sam FC	sam p value	ttest FC	ttest p value
AK018243	6330566F14Rik	ri|6330566F14|PX00044K09|AK018243|1273						104070736		ZW10 homolog (Drosophila), centromere/kinetochore protein			9.90	8.000E-04		
AK035122	9430091F09Rik	ri|9430091F09|F	105130184	105130184	105130184	105130184				zinc finger, MYM-type 6	1.63	1.735E-04	2.75	2.100E-03	2.75	0.000E+00
NM_175126.3	Zcchc3	scl0067917.2_176						4780278		zinc finger, CCHC domain containing 3			1.54	2.100E-03		
NM_175126.3	Zcchc3	scl0067917.1_135						1990035		zinc finger, CCHC domain containing 3			1.40	6.000E-04		
AK019056	2210039O17Rik	ri|2210039O17|ZX00079D03|AK019056|357						104780332		zinc finger protein 87			1.67	1.900E-03		
NM_182996.2	AI839920	scl41520.9.1_11						5340600		zinc finger protein 692			1.41	2.600E-03		
NM_178734.2	D030014N22Rik	scl31409.6.1_0						4150528		zinc finger protein 473			1.94	1.200E-03		
NM_020589	Zfp467	scl068910.1_219		100070364						zinc finger protein 467	0.85	9.327E-05	1.75	2.000E-03		
NM_173364	Zfp445	scl0235682.1_81						10610161		zinc finger protein 445			2.08	5.000E-04		
AK033090	8030405J07Rik	ri|8030405J07|PX00102P18|AK033090|2330					102230079			zinc finger protein 410	3.88	2.392E-04				
NM_027477.1	Zfp398	scl00272347.2_200		5390546						zinc finger protein 398	1.26	2.678E-04	2.38	1.200E-03		
NM_178364.3	Zfp369	scl00170936.1_203						4070458		zinc finger protein 369			2.44	1.400E-03		
AK077316	5330412A19Rik	ri|5330412A19|PX00643G15|AK077316|1745						106200390		zinc finger protein 365			3.27	2.700E-03		
NM_199304.1	Zfp341	scl0228807.33_9	520066	520066	520066	520066				zinc finger protein 341	1.84	2.000E-07	3.63	0.000E+00	3.63	0.000E+00
NM_145600.1	Zfp330	scl030932.2_33	1990504	1990504	1990504	1990504				zinc finger protein 330	1.29	2.183E-04	2.33	8.000E-04	2.33	0.000E+00
AK046006	B230333C16Rik	ri|B230333C16|PX00160D19|AK046006|2404					106100113			zinc finger protein 287	4.10	4.604E-04				
NM_028245.1	Zfp131	scl072465.7_112						510427		zinc finger protein 131			1.30	2.300E-03		
AK043258	Zfp276	ri|A730076O17|PX00151J21|AK043258|2225						104560358		zinc finger protein (C2H2 type) 276			1.75	1.000E-04		
NM_015753.2	Zfhx1b	scl024136.1_28				4150215				zinc finger E-box binding homeobox 2			2.30	8.000E-04	2.30	1.000E-04
AK038731	A230057M07Rik	ri|A230057M07|PX00128817|AK038731|3080						104540300		zinc finger and BTB domain containing 20			1.75	1.700E-03		
AK034574	Zfp288	ri|9430009A01|PX00108G09|AK034574|3503						107050402		zinc finger and BTB domain containing 20			1.83	1.100E-03		
NM_153566.1	BC023823	scl24984.5.1_10						2060047		yrdC domain containing (E.coli)			1.72	7.000E-04		
AK079300	9530095N04Rik	ri|9530095N04|PX00654M15|AK079300|940						102230390		WW domain binding protein 2			2.07	2.900E-03		
NM_009526.2	Wnt6	scl0022420.2_231							4570364	wingless-related MMTV integration site 6					2.60	1.110E-02
NM_009522.1	Wnt3a	scl40164.4.1_128						6350348		wingless-related MMTV integration site 3A			1.83	1.700E-03		
AK036186.1		scl0001602.1_506				104920288				Wilms' tumour 1-associating protein			5.79	1.000E-04	5.79	4.000E-04
XM_135109	9430077D24Rik	scl36519.9_127	106510133	106510133	106510133	106510133				WD repeat domain containing 82	3.22	2.304E-06	8.75	0.000E+00	8.75	0.000E+00
NM_134139.1	5730436H21Rik	scl0107071.9_36						3140315		WD repeat domain 74			1.44	1.100E-03		
NM_021322.1	Wdr4	scl0001639.1_26						1850368		WD repeat domain 4			1.67	1.000E-04		
XM_128578.2	Wfikkn1	scl50174.1.1_122	2350731	2350731	2350731	2350731				WAP, FS, Ig, KU, and NTR-containing protein 1	3.04	2.338E-05	9.05	1.000E-04	9.05	2.200E-03
NM_134222.1	V1ri5	scl12338.1.1_252					3940369			vomeronasal 1 receptor, I5	2.05	5.016E-04				
NM_021284	Kras2	scl016653.1_47	2060170	2060170	2060170	2060170				v-Ki-ras2 Kirsten rat sarcoma viral oncogene homolog	1.19	2.537E-08	2.28	0.000E+00	2.28	0.000E+00
NM_153786.1	Vgll2	scl38936.3.1_27		7040142						vestigial like 2 homolog (Drosophila)	1.32	2.086E-04	2.63	2.300E-03		
NM_153786.1	Vgll2	scl0003769.1_81						3940148		vestigial like 2 homolog (Drosophila)			2.99	2.600E-03		
NM_016794.2	Vamp8	scl28865.3.1_49				1190139				vesicle-associated membrane protein 8			2.34	2.000E-04	2.34	0.000E+00
AK032794	6720453O12Rik	ri|6720453O12|PX00059O09|AK032794|4226						106020286		versican			2.39	2.500E-03		
NM_011912.1	Vax2	scl29835.3.141_2						5130377		ventral anterior homeobox containing gene 2			2.53	5.000E-04		
NM_175137.3	Vars2l	scl0068915.2_30	4210270	4210270	4210270	4210270				valyl-tRNA synthetase 2, mitochondrial (putative)	1.55	3.205E-09	2.92	0.000E+00	2.92	0.000E+00
NM_175137	Vars2l	scl49980.28_299							103840575	valyl-tRNA synthetase 2, mitochondrial (putative)					49.30	0.000E+00
NM_173443	5730538E15Rik	scl16998.3_89	105420735	105420735	105420735	105420735				valosin containing protein (p97)/p47 complex interacting protein 1	5.13	2.128E-09	10.63	1.000E-04	53.27	0.000E+00
NM_147153.2	Vps39	scl0269338.1_1						50332		vacuolar protein sorting 39 (yeast)			2.41	9.000E-04		
NM_030724.1	AA407809	scl000973.1_27						5420048		uridine-cytidine kinase 2			1.40	1.800E-03		
NM_009477.1	Upp1	scl41842.10.1_70		3850358						uridine phosphorylase 1	0.60	1.639E-04	1.50	1.200E-03		
BC011039	Ung	scl0003983.1_83						107100348		uracil DNA glycosylase			2.19	1.300E-03		
NM_009464.2	Ucp3	scl32314.7_159						4210148		uncoupling protein 3 (mitochondrial, proton carrier)			3.64	1.300E-03		
AK087777	E330019N15Rik	ri|E330019N15|PX00211M04|AK087777|1733						103140364		unc-45 homolog A (C. elegans)			2.82	2.400E-03		
NM_133806.2	Uap1	scl15961.15.1_3	3060093	3060093	3060093	3060093				UDP-N-acetylglucosamine pyrophosphorylase 1	2.63	2.197E-08	5.70	0.000E+00	5.70	0.000E+00
NM_080445.2	B3galt6	scl00117592.2_262							50195	UDP-Gal:betaGal beta 1,3-galactosyltransferase, polypeptide 6					3.74	0.000E+00
NM_011674.2	Ugt8	scl21552.7_36						3710128		UDP galactosyltransferase 8A			2.09	2.800E-03		
AK049649	Usp23	ri|C530015C05|PX00081A16|AK049649|1970						101850301		ubiquitin specific peptidase 21			2.08	1.000E-04		
NM_011670.1	Uchl1	scl27752.9.1_0		1230066						ubiquitin carboxy-terminal hydrolase L1	0.56	7.035E-05	1.48	1.000E-04		
NM_023053.1	Twsg1	scl0065960.1_26	4570736	4570736	4570736	4570736				twisted gastrulation homolog 1 (Drosophila)	1.06	1.457E-05	2.08	1.000E-04	2.08	0.000E+00
NM_178589	Tnfrsf21	scl50710.7_436		104810504						tumor necrosis factor receptor superfamily, member 21	2.10	1.864E-05	4.14	0.000E+00		
NM_009451.3	Tubb4	scl49746.4_205						5310681		tubulin, beta 4			1.44	2.400E-03		
NM_026481.2	2700055K07Rik	scl34402.5.1_27						2470148		tubulin polymerization-promoting protein family member 3			1.51	3.600E-03		
AK079510	A130090M16Rik	ri|A130090M16|PX00316O07|AK079510|2675						104480347		TSC22 domain family 4			1.57	1.600E-03		
AK049383	C430002D13Rik	ri|C430002D13|I	100780280	100780280	100780280	100780280				tropomyosin 4	1.27	1.693E-05	2.39	0.000E+00	2.39	0.000E+00
NM_016712	Tmod4	scl0001984.1_38						2360021		tropomodulin 4			3.27	0.000E+00		

		limma, sam & ttest		limma & sam	limma & ttest	sam & ttest	only in limma	only in sam	only in ttest							
Accession	all-symbol	Transcript	Probe Id	Probe Id	Probe Id	Probe Id	Probe Id	Probe Id	Probe Id	Gene name	limma FC	limma p value	sam FC	sam p value	ttest FC	ttest p value
NM_016712.1	Tmod4	scl0002067.1_49						4590722		tropomodulin 4			2.54	1.000E-04		
NM_016712.1	Tmod4	scl22890.10.1_51						5910520		tropomodulin 4			2.10	5.000E-04		
NM_199033.1	AU067695	scl0381802.12_9		1940204						tRNA splicing endonuclease 2 homolog (SEN2, S. cerevisiae)	0.76	1.584E-04	1.70	6.000E-04		
NM_178110.2	6330414G21Rik	scl24927.7_348				4760451				tripartite motif-containing 62			3.22	2.700E-03	3.22	0.000E+00
NM_201373.1	Trim56	scl0384309.1_171		1580528						tripartite motif-containing 56	1.96	4.097E-05	3.64	1.000E-04		
NM_053167.1	Trim9	scl0094090.1_135						6450687		tripartite motif protein 9			2.65	2.600E-03		
NM_053168.1	Trim11	scl094091.6_116							2570162	tripartite motif protein 11					3.44	5.000E-04
NM_011552.1	Tcof1	scl0021453.2_208		2680086						Treacher Collins Franceschetti syndrome 1, homolog	0.86	3.051E-04	1.82	5.000E-04		
NM_144805.1	9030407H20Rik	scl28522.14.1_1						5550286		transmembrane protein 40			1.90	4.400E-03		
NM_173446.1	AW121567	scl35118.3_474							7100519	transmembrane protein 28					2.33	8.000E-04
AK081890	C130085D15Rik	ri|C130085D15|PX00666B08|AK081890|2974						100940441		transmembrane protein 164			1.31	3.600E-03		
NM_183311.1	B930076A02	scl32933.15.1_222						6020348		transmembrane protein 145			1.98	3.000E-03		
NM_027992	2310036D22Rik	scl30378.11_478						104810195		transmembrane protein 1068			4.49	7.000E-04		
NM_172476.2	Tmc7	scl00209760.1_40						5290253		transmembrane channel-like gene family 7			1.38	7.000E-04		
AK015068	4930403O06Rik	ri|4930403O06|PX00029B22|AK015068|1185						104050068		transmembrane and coiled-coil domains 1			1.89	2.300E-03		
NM_138599	Tomm70a	scl49022.13_219						103930369		translocase of outer mitochondrial membrane 70 homolog A (yeast)			1.45	1.100E-03		
NM_172609.2	Tomm22	scl00223696.2_2	1240142	1240142	1240142	1240142				translocase of outer mitochondrial membrane 22 homolog (yeast)	6.95	4.367E-13	111.62	0.000E+00	111.62	0.000E+00
NM_013899.1	Timm13a	scl20689.4.1_4						2450601		translocase of inner mitochondrial membrane 10 homolog (yeast)			1.50	1.600E-03		
AK077331	5330423N11Rik	ri|5330423N11|PX00643A18|AK077331|1561		102510594						transient receptor potential cation channel, subfamily M, member 3	3.23	1.555E-05	8.85	0.000E+00		
AK005144	Trrp1	ri|1500004E04|ZX00042E15|AK005144|2064						100770181		transient receptor potential cation channel, subfamily C, member 1			1.47	3.500E-03		
AK037910	A130062D16Rik	ri|A130062D16|PX00123L08|AK037910|944						103130563		transforming, acidic coiled-coil containing protein 1			1.86	1.000E-04		
AK087834	Trp53	ri|E330026I23|PX00675H12|AK087834|2901						103120537		transformation related protein 53			2.91	2.400E-03		
NM_020601	Tbl1x	scl54819.15_251						100450452		transducin (beta)-like 1 X-linked			1.59	2.000E-04		
NM_031183.1	Sp6	scl0083395.1_307							60484	trans-acting transcription factor 6					2.21	4.800E-03
NM_031183.1	Sp6	scl13960.1.1_83							510452	trans-acting transcription factor 6					3.60	1.450E-02
NM_026708.1	0610007A15Rik	scl068385.4_14						6840438		TLC domain containing 1			1.38	1.400E-03		
NM_009426.1	Trh	scl28676.3_567							5050576	thyrotropin releasing hormone					2.36	3.850E-02
NM_010241.1	Fts	scl0014339.2_163		6350575						thymoma viral proto-oncogene 1 interacting protein	1.10	2.910E-06	2.14	0.000E+00		
AK021335	D730042P09Rik	ri|D730042P09|PX00091I15|AK021335|776		102970280						thymocyte nuclear protein 1	1.35	1.234E-04	2.61	2.000E-04		
NM_172444.1	B230114P05Rik	scl35747.13.1_171							6040037	thrombospondin, type I, domain containing 4					2.11	0.000E+00
NM_023719	Txnip	scl22856.7_28						102640017		thioredoxin interacting protein			1.69	3.400E-03		
NM_025920	Thap4	scl16458.7.1_28						7040181		THAP domain containing 4			5.16	6.000E-04		
NM_152817.2	2610511O17Rik	scl50495.21.3_143							1090280	tetratricopeptide repeat domain 27					7.90	0.000E+00
NM_183106.1	Ttc17	scl074569.1_282						2470440		tetratricopeptide repeat domain 17			1.33	3.100E-03		
AK031605	6030458P06Rik	ri|6030458P06|PX00057I09|AK031605|2390				104070717				tetratricopeptide repeat domain 14			2.22	1.400E-03	2.22	0.000E+00
NM_025978.2	Ttc14	scl0067120.1_59						6200114		tetratricopeptide repeat domain 14			1.80	2.300E-03		
NM_027880.1	1200003M09Rik	scl50188.17.10_:	4850047	4850047	4850047	4850047				TEL2, telomere maintenance 2, homolog (S. cerevisiae)	1.22	2.381E-05	2.34	0.000E+00	2.34	0.000E+00
NM_009347.1	Tecta	scl35982.24.1_47		2570372						tectorin alpha	1.31	1.069E-04	2.35	1.000E-03		
NM_009346.1	Tead1	scl32176.16.1_1						2470551		TEA domain family member 1			2.32	1.500E-03		
NM_016921.2	Tcirg1	scl53436.18.1_9		6900619						T-cell, immune regulator 1, ATPase, H+ transporting, lysosomal V0 protein A3	0.65	1.152E-04	1.58	2.000E-04		
NM_011537	Tbx5	scl27300.10.1_99						106840364		T-box 5			2.63	1.500E-03		
NM_146252.1	Tbc1d13	scl21096.14_260		870010						TBC1 domain family, member 13	0.75	3.024E-04	1.68	4.000E-04		
AK080913	B430206N15Rik	ri|B430206N15|PX00071K10|AK080913|3194						106770184		tankyrase, TRF1-interacting ankyrin-related ADP-ribose polymerase			2.58	1.200E-03		
NM_011430.1	Sncg	scl45723.1.148_13							3120725	synuclein, gamma					2.43	1.000E-04
AK040413	Sntb2	ri|A430092J05|PX00138P22|AK040413|1157						100630112		syntrophin, basic 2			1.30	4.200E-03		
NM_018804.2	Syt11	scl21963.5_3		630433						synaptotagmin XI	0.50	2.115E-04	1.41	1.300E-03		
NM_011428	Snap25	scl20231.9_372							103190138	synaptosomal-associated protein 25					2.01	7.000E-04
NM_009304.1	Syngr2	scl0020973.1_244		6130348						synaptogyrin 2	0.62	5.322E-05	1.55	2.000E-03		
NM_031842	Smarcd1	scl0002509.1_27						3060193		SWI/SNF related, matrix associated, actin dependent regulator of chromatin,			1.57	1.400E-03		
NM_198160.1	5930405J04Rik	scl068094.2_112		130368						SWI/SNF related, matrix associated, actin dependent regulator of chromatin, subfamily c, member 2	0.61	2.360E-04	1.50	4.100E-03		
NM_172205	Sbsn	scl0073733.1_231						6900239		suprabasin			1.37	3.900E-03		
NM_080843	Socs4	scl46405.2_247						101850064		suppressor of cytokine signaling 4			1.66	1.300E-03		
AK086878	E030007H10Rik	ri|E030007H10|PX00204L24|AK086878|1352						103800706		superoxide dismutase 1, soluble			1.54	2.200E-03		

			limma, sam & ttest		limma & ttest		sam & ttest	only in limma	only in sam	only in ttest							
Accession	all-symbol	Transcript	Probe Id	limma & sam Probe Id	Probe Id	sam & ttest Probe Id	Probe Id	Probe Id	Probe Id	Gene name	limma FC	limma p value	sam FC	sam p value	ttest FC	ttest p value
NM_026151.1	2610528A15Rik	sc43496.27.1_1							5360215	superkiller viralicidic activity 2-like 2 (S. cerevisiae)			1.39	3.700E-03		
AK037389	A130013J22Rik	ri|A130013J22|PX00121O18|AK037389|2703							104520072	sulfatase 1			2.89	2.500E-03		
NM_018754.1	Sfn	sc8055948.2_144							7510608	stratifin			1.56	1.200E-03		
NM_009291.1	Stra6	sc36890.23.1_31							4070592	stimulated by retinoic acid gene 6			1.56	1.900E-03		
NM_009293.1	Sts	sc30020905.1_329							630632	steroid sulfatase			2.91	2.100E-03		
NM_020611.3	Srd5a2l	sc27696.10_114	670403	670403	670403	670403			6220390	steroid 5 alpha-reductase 2-like	1.77	2.001E-06	3.50	0.000E+00	3.50	0.000E+00
NM_177272	E130306A17Rik	sc38216.3_182							103850020	sterile alpha motif domain containing 5			2.11	5.000E-04		
NM_177225	A830034I09Rik	sc47202.3_616								sterile alpha motif domain containing 12	0.99	1.751E-04	2.43	1.900E-03		
NM_009133.2	Stmn3	sc020262.2_8	2690692						106130132	stathmin-like 3			1.50	1.800E-03		
AK043202	Scgn10	ri|A730069C18|PX00151U08|AK043202|3414								stathmin-like 2			1.78	2.100E-03		
NM_199018.1	Stard8	sc02360.20.7_41	1780047						107000673	START domain containing 8	0.83	1.904E-04	1.41	3.300E-03		
AK087634	E230029F23Rik	ri|E230029F23|PX00675P17|AK087634|2138							2640368	stabilin 1			5.54	1.000E-03		
NM_009177.2	Siat4a	sc00020442.2_266								ST3 beta-galactoside alpha-2,3-sialyltransferase 1			2.12	1.100E-03	2.12	2.000E-04
NM_011447.1	Sox8	sc050179.2_171				580026				SRY-box containing gene 8	5.94	1.855E-09	44.09	0.000E+00	44.09	0.000E+00
NM_009237.1	Sox3	sc054200.1.223_1	4570537	4570537	4570537	4570537			103120364	SRY-box containing gene 3	1.69	2.800E-04	1.77	8.000E-04		
XM_284529.2	Sox14	Gl_38050018								SRY-box containing gene 14			3.19	8.000E-04		
NM_035232.2	Spred2	sc800114726.1_17		540195		100130082				sprouty-related, EVH1 domain containing 2			2.12	1.100E-03	2.12	5.000E-04
AK051703	D130066L18Rik	ri|D130066L18|PX00185V15|AK051703|1637								spliceing factor 3a, subunit 1			2.12	1.100E-03		
NM_027141.1	Tce1	sc050999.7.56_7:	1740239	1740239	1740239	1740239				sphA/ryanodine receptor domain and SOCS box containing 3	1.20	1.430E-06	2.26	1.000E-04	2.26	0.000E+00
NM_172287.2	Spire2	sc813206.16.1_107	450088						103206707	spire homolog 2 (Drosophila)	0.73	3.977E-05	1.64	5.000E-04		
NM_028035.2	Snx10	sc836048.11_144	3800035							sorting nexin 10	0.55	1.431E-04	1.47	1.500E-03		
NM_148933.1	Slco4a1	sc119788.13_0	1090176							solute carrier organic anion transporter family, member 4a1	0.62	2.474E-04	1.54	7.000E-04		
NM_177870.2	Slc5a6	sc26744.20.688_4							2570438	solute carrier family 5 (sodium-dependent vitamin transporter), member 6			1.47	2.300E-03		
NM_053248	Slc5a5	sc34686.15_590							106590070	solute carrier family 5 (sodium iodide symporter), member 5			1.75	6.000E-04		
NM_173774.3	Slc45a1	Gl_75709221							2470477	solute carrier family 45, member 1			2.28	4.500E-03		
NM_134135.1	Slc39a3	sc810694?.1_49							3990397	solute carrier family 39 (zinc transporter), member 3			1.35	4.300E-03		
NM_144808.1	Slc39a14	sc800213053.1_19							1400093	solute carrier family 39 (zinc transporter), member 14			2.48	2.100E-03		
AK028984	Slc37a1	ri|4732478E03|PX00052A23|AK028984|2945							100060707	solute carrier family 37 (glycerol-3-phosphate transporter), member 2			2.90	4.300E-03		
NM_153139.3	Slc36a1	sc814540.14.201_30		5080242						solute carrier family 36 (proton/amino acid symporter), member 1	2.00	5.956E-05	3.93	1.000E-04		
NM_028756.2	Slc35e5	sc800741?2.2_20		4480546						solute carrier family 35, member A5	1.04	2.539E-04	2.02	1.000E-03		
NM_009508	Vlait	sc119993.2_312							6200278	solute carrier family 32 (GABA vesicular transporter), member 1					2.41	7.700E-03
NM_011773	Slc30a3	sc80227B4.1_270							100380017	solute carrier family 30 (zinc transporter), member 3			1.90	2.100E-03		
NM_026232.1	Slc25a30	sc80067554.2_226							6840707	solute carrier family 25, member 30			1.50	2.500E-03		
NM_021551	Slc22a17	sc800354.1_6							4200253	solute carrier family 22 (organic cation transporter), member 17			3.22	1.700E-03		
NM_0114012	Slc2a3	sc02843B.14_163		1990377						solute carrier family 2 (facilitated glucose transporter), member 3	0.81	2.134E-04	1.78	1.600E-03		
NM_021544	Scn5a	sc835220.27_681							103450671	sodium channel, voltage-gated, type V, alpha			1.36	2.400E-03		
NM_010831.1	Snf1lk	sc856075.14_101	6110403	6110403	6110403	6110403				SNF1-like kinase	1.89	1.552E-05	3.59	0.000E+00	3.59	0.000E+00
NM_178719	AI452372	sc847731.8_425	105550487	105550487	105550487	105550487				Smith-Magenis syndrome chromosome region, candidate 7-like (human)	3.54	9.241E-12	11.36	0.000E+00	11.36	0.000E+00
AK078494	6820416H03Rik	ri|6820416H03|PX00049J20|AK078494|997							100070161	SMC hinge domain containing 1			2.80	1.700E-03		
NM_144838.1	Sgtb	sc44443.11_211		460170						small glutamine-rich tetratricopeptide repeat (TPR)-containing, beta	1.46	1.770E-04	2.90	5.000E-04		
NM_172218.1	Rutbc2	sc826197.25_374							1500647	small G protein signaling modulator 1			1.63	5.000E-04		
AK051262	D130026C08Rik	ri|D130026C08|PX00183J24|AK051262|2483							103120687	SLIT-ROBO Rho GTPase activating protein 3			5.01	2.200E-03		
AK035727	Slit3	ri|9530096H22|PX00115O01|AK035727|2203							106650441	slit homolog 3 (Drosophila)			1.76	1.300E-03		
AK084012	Slit2	ri|D130076F04|PX00186D03|AK084012|3209				101390064				slit homolog 2 (Drosophila)			3.46	2.900E-03	3.46	1.500E-03
AK053145	Slit2	ri|E030015M03|PX00204O04|AK053145|3015							106400110	slit homolog 2 (Drosophila)			2.93	3.900E-03		
NM_011377.1	Sim2	sc843846.11.1_43							2100044	single-minded homolog 2 (Drosophila)			1.70	1.600E-03		
NM_009275.2	Srpr1b	sc820818.5_51		1500138						signal recognition particle receptor, B subunit	0.73	6.900E-06	1.65	1.000E-04		
NM_012058	Srp9	sc827658.3_76							3170053	signal recognition particle 9					2.94	5.400E-03
AK088947	E430033B07Rik	ri|E430033B07|PX00100N08|AK088947|1082							106660195	SH3-domain GRB2-like (endophilin) interacting protein 1			2.37	1.000E-04		
AK035372	Posh-pending	ri|9530028H17|PX00111B16|AK035372|1665							104570019	SH3 domain containing ring finger 1			1.61	1.000E-03		
AK029392	4833429C11Rik	ri|4833429C11|PX00028N11|AK029392|2557							100070435	SH3 domain binding glutamic acid-rich protein like 2			1.53	9.000E-04		

		limma, sam & ttest		limma & sam	limma & ttest	sam & ttest	only in limma	only in sam	only in ttest							
Accession	all-symbol	Transcript	Probe Id	Probe Id	Probe Id	Probe Id	Probe Id	Probe Id	Probe Id	Gene name	limma FC	limma p value	sam FC	sam p value	ttest FC	ttest p value
AK042261	A630076G18Rik	ri|A630076G18|PX00147I02|AK042261|2711							105270390	SH3 and PX domains 2B					7.06	1.000E-04
AK043324	A730085F06Rik	ri|A730085F06|PX00152D24|AK043324|2660							105050068	SH3 and PX domains 2B					3.01	3.100E-03
NM_177364	G431001E03Rik	scl41723.13_180						106660487		SH3 and PX domains 2B			1.59	9.000E-04		
NM_009762	Smyd1	scl28887.12_50						104060465		SET and MYND domain containing 1			2.63	1.600E-03		
NM_019442.2	Stk19	scl0001697.1_9						6620300		serine/threonine kinase 19			1.42	3.300E-03		
AK014004	Srpk2	ri|3110005M20|ZX00070F21|AK014004|1962						105700176		serine/arginine-rich protein specific kinase 2			2.70	4.200E-03		
NM_175229.2	Srrm2	scl075956.6_20		6350253						serine/arginine repetitive matrix 2	0.78	1.518E-04	1.70	3.000E-04		
AK030668	37865	ri|5430412N19|PX00102B18|AK030668|1883						105860451		septin 3			1.71	1.900E-03		
AK042751	Sema6a	ri|A730020P05|PX00149A22|AK042751|3226						102350112		sema domain, transmembrane domain (TM), and cytoplasmic			1.92	8.000E-04		
NM_009154.1	Sema5a	scl0020356.1_23	6520435	6520435	6520435	6520435				sema domain, seven thrombospondin repeats (type 1 and type 1-like), transmembrane domain (TM) and short cytoplasmic domain, (semaphorin) 5A	3.75	1.774E-11	13.32	0.000E+00	13.32	0.000E+00
NM_013834.1	Sfrp1	scl020377.12_22				6980315				secreted frizzled-related protein 1			3.58	3.000E-04	3.58	0.000E+00
AK090280	G630034H08Rik	ri|G630034H08|	101690040	101690040	101690040	101690040				scratch homolog 2, zinc finger protein (Drosophila)	1.64	1.300E-04	2.83	1.800E-03	2.83	0.000E+00
NM_175303.2	Sall4	scl0003130.1_110							2100528	sal-like 4 (Drosophila)					3.13	3.440E-02
NM_007444	Amd2	scl0011703.1_132						6770551		S-adenosylmethionine decarboxylase 2			2.81	2.200E-03		
NM_016661	Ahcy	scl18466.10_8	106130025	106130025	106130025	106130025				S-adenosylhomocysteine hydrolase	1.37	6.513E-05	2.61	1.000E-04	2.61	0.000E+00
AK083781.1		scl0002702.1_3805						103130204		runt-related transcription factor 1; translocated to, 1 (cyclin D-related)			1.83	3.900E-03		
NM_016759.1	Rapzip	scl40861.10.1_1		4810132						RUN domain containing 3A	0.79	1.606E-04	1.75	5.000E-04		
NM_009088	Rpo1-4	scl020019.27_27	2570082	2570082	2570082	2570082				RNA polymerase 1-4	4.78	2.269E-06	4.73	1.400E-03	0.00	0.000E+00
AK031689	Rpo1-4	ri|6030490M24|PX00058J03|AK031689|3196						106940019		RNA polymerase 1-4			5.41	1.400E-03		
AK012265	Rbpms	ri|2700019M19|ZX00063I13|AK012265|1040		106650070						RNA binding protein gene with multiple splicing	0.93	1.385E-05	1.90	1.000E-04		
AK012586	Rbpms	ri|2700088L14|ZX00056J10|AK012586|1040		104120592						RNA binding protein gene with multiple splicing	0.85	1.913E-04	1.83	1.100E-03		
NM_026453.1	2600016B03Rik	scl34969.6.1_9						4230528		RNA binding motif protein 13			1.50	1.800E-03		
NM_024242.2	Riok1	scl44884.17.178_	1980079	1980079	1980079	1980079				RIO kinase 1 (yeast)	1.54	2.580E-04	2.97	1.100E-03	2.97	6.000E-04
NM_146218.2	BC027246	scl00234736.1_63						6350484		ring finger and WD repeat domain 3			1.49	7.000E-04		
AK042822	A730027E01Rik	ri|A730027E01|PX00150I13|AK042822|1946						104060603		RIKEN cDNA E130319B15 gene			1.67	2.300E-03		
NM_001033781.	LOC434147	GI_85702092	6420433	6420433	6420433	6420433				RIKEN cDNA D930028M14 gene	1.15	5.986E-05	2.13	5.000E-04	2.13	0.000E+00
AK037550	A130026C10Rik	ri|A130026C10|PX00121P09|AK037550|2970		103800687						RIKEN cDNA D730035F11 gene	1.26	5.110E-06	2.40	0.000E+00		
NM_207274.1	D630004N19Rik	scl0402747.1_104						6760021		RIKEN cDNA D630004N19 gene			4.98	6.000E-04		
NM_175514.1	D430039N05Rik	scl00241520.2_184				1190022				RIKEN cDNA D430039N05 gene			3.81	4.000E-04	3.81	0.000E+00
XM_149840.2	D330027H18Rik	scl29214.5.1_30	580736	580736	580736	580736				RIKEN cDNA D330027H18 gene	3.59	9.794E-09	8.92	0.000E+00	14.78	0.000E+00
NM_177391.2	C920005C14Rik	scl0338368.2_77						7040411		RIKEN cDNA C920005C14 gene			1.54	1.700E-03		
NM_175461	C030014K22Rik	scl14351.1.1_75						10870632		RIKEN cDNA C030014K22 gene			1.81	3.900E-03		
AK046764	B630019A10Rik	ri|B630019A10|PX00072K02|AK046764|2407						102810736		RIKEN cDNA B630019A10 gene			2.90	3.100E-03		
AK050558	C820017N15Rik	ri|C820017N15|PX00088K23|AK050558|2742					102480112			RIKEN cDNA A930011G23 gene	2.14	3.671E-04				
AK088897	E430030L01Rik	ri|E430030L01|PX00100P23|AK088897|3500						102260605		RIKEN cDNA A430108E01 gene			1.93	1.000E-04		
AK039293	A330017A19Rik	ri|A330017A19|PX00131K13|AK039293|1191						10637034B		RIKEN cDNA A330017A19 gene			1.85	4.200E-03		
NM_026739.1	9530077C05Rik	scl37201.7.1_109		1170066						RIKEN cDNA 9530077C05 gene	0.58	1.974E-04	1.49	1.000E-03		
NM_026633.1	9530058B02Rik	scl50172.5.1_49	6100670	6100670	6100670	6100670				RIKEN cDNA 9530058B02 gene	1.10	2.790E-04	2.24	1.300E-03	2.24	1.800E-03
AK035350	9530020O07Rik	ri|9530020O07|PX00111H12|AK035350|1983						104670706		RIKEN cDNA 9530020O07 gene			1.56	2.300E-03		
NM_178746.3	9130023D20Rik	scl00268706.2_1	1230195	1230195	1230195	1230195				RIKEN cDNA 9130023D20 gene	1.10	5.265E-05	2.10	4.000E-04	2.10	0.000E+00
AK011615	2610029J22Rik	ri|2610029J22|ZX00034M23|AK011615|1095						10635071		RIKEN cDNA 9030624J02 gene			1.76	4.100E-03		
NM_133733	9030425E11Rik	scl37065.9_216		104210196						RIKEN cDNA 9030425E11 gene	1.06	1.325E-04	1.98	1.900E-03		
AK034042	9330151E04Rik	ri|9330151E04|PX00105A03|AK034042|2469						10704042		RIKEN cDNA 9030409G11 gene			1.58	2.200E-03		
NM_028982	8430419L09Rik	scl29431.12_3		104120671						RIKEN cDNA 8430419L09 gene	0.66	8.713E-05	1.58	4.000E-04		
NM_172600.2	6720456H20Rik	scl00218989.1_168						4570075		RIKEN cDNA 6720456H20 gene			1.52	4.000E-04		
NM_029545	6530401N04Rik	scl42480.4.1_11		100610168						RIKEN cDNA 6530401N04 gene	1.15	2.076E-05	2.20	1.000E-04		
NM_029530.1	6330527O06Rik	scl20236.5.1_61	3610398	3610398	3610398	3610398				RIKEN cDNA 6330527O06 gene	1.92	5.969E-05	3.44	3.000E-04	3.44	0.000E+00
NM_176962.2	6330416L07Rik	GI_31342475						106450088		RIKEN cDNA 6330416L07 gene			1.44	7.000E-04		
NM_177177	5930403N24Rik	scl39021.4.1_52						103520372		RIKEN cDNA 5930403N24 gene			4.14	2.000E-04		
NM_144877.1	5630401D24Rik	scl071449.1_103						770722		RIKEN cDNA 5630401D24 gene			1.57	2.500E-03		
XM_134954	5430433E21Rik	scl35693.1.688_266		104280408						RIKEN cDNA 5430433E21 gene	0.91	3.882E-05	1.92	1.600E-03		
NM_028963.1	4933427D14Rik	scl39973.20.1_51		3170121						RIKEN cDNA 4933427D14 gene	1.01	2.025E-05	2.00	1.000E-04		
AK016936	4933426K21Rik	ri|4933426K21|PX00020B07|AK016936|1368						106020014		RIKEN cDNA 4933426K21 gene			1.59	2.000E-03		
AK028507	4933407H18Rik	ri|4632410K16|PX00012D18|AK028507|3237						101660575		RIKEN cDNA 4933407H18 gene			1.40	2.000E-03		
AK044023	A830081I03Rik	ri|A830081I03|PX00155N02|AK044023|3789						10007007		RIKEN cDNA 4932442K08 gene			1.40	2.300E-03		
AK031527	6030447G11Rik	ri|6030447G11|PX00057O19|AK031527|3758						102320193		RIKEN cDNA 4932432K03 gene			2.11	1.900E-03		
NM_026358.1	4930583H14Rik	scl22188.5_6		5570142						RIKEN cDNA 4930583H14 gene	0.89	1.391E-04	1.83	1.000E-04		
NM_134041.1	4930427A07Rik	scl42718.7.1116_1							6110685	RIKEN cDNA 4930427A07 gene					2.05	1.790E-02
AK081262	C030034J23Rik	ri|C030034J23|PX00665J16|AK081262|2599							101190358	RIKEN cDNA 4921533L14 gene					2.65	1.820E-02

Accession	all-symbol	limma, sam & ttest		limma & sam	limma & ttest	sam & ttest	only in limma	only in sam	only in ttest									
		Transcript	Probe Id	Probe Id	Probe Id	Probe Id	Probe Id	Probe Id	Probe Id	Gene name	limma FC	limma p value	sam FC	sam p value	ttest FC	ttest p value
NM_178141.1	3830406C13Rik	sc446626.7_218						2650632		RIKEN cDNA 3830406C13 gene			1.40	3.600E-03		
AK076179	3830402D07Rik	n|3830402D07|PX00636M14|AK076179|4438	100060322							RIKEN cDNA 3830402D07 gene	3.92	3.157E-08	15.13	0.000E+00		
XM_132047.3	3110047P20Rik	sc27788.8.2924_41						3130017		RIKEN cDNA 3110047P20 gene			1.61	7.000E-04		
NM_178399.2	3110035E14Rik	sc118174.5_252							5670494	RIKEN cDNA 3110035E14 gene					2.08	9.000E-04
NM_026534	3110003A22Rik	sc25703.8_76						10470364		RIKEN cDNA 3110003A22 gene			2.18	7.000E-04		
AK013928	3100003A19Rik	n|3100003M19|	101340746	101340746	101340746					RIKEN cDNA 3100003M19 gene	1.80	7.462E-08	3.50	0.000E+00	3.50	0.000E+00
NM_026515.1	2810417H13Rik	sc36799.4_9	4830091							RIKEN cDNA 2810417H13 gene	0.88	7.137E-05	1.83	2.000E-04		
XM_133597.3	2810406K13Rik	sc32327.9.1_32	2450010	2450010	2450010	2450010				RIKEN cDNA 2810406K13 gene	1.82	3.163E-04	2.82	3.500E-03	2.82	0.000E+00
AK012908	2810404L04Rik	n|2810404L04|ZX00065F19|AK012908|943						102470164		RIKEN cDNA 2810404L04 gene			1.29	3.400E-03		
NM_026529.2	2700062G07Rik	sc0068046.2_0	60372							RIKEN cDNA 2700062G07 gene	0.66	5.762E-05	1.58	1.000E-03		
NM_175184.3	2610528K11Rik	sc119423.12_9	5900325							RIKEN cDNA 2610528K11 gene	0.77	1.319E-04	1.71	1.200E-03		
AK002569.1		sc00001651.1_229						102340735		RIKEN cDNA 2610110G12 gene			1.58	3.100E-03		
AK053253	E130001M03Rik	n|E130001M03|PX00207D14|AK053253|2760						104150136		RIKEN cDNA 2510009E07 gene			1.96	9.000E-04		
NM_029759.2	2410166O05Rik	sc21686.4_28						3850427		RIKEN cDNA 2410166O05 gene			1.46	4.000E-03		
NM_175245.2	2410129H14Rik	sc00076789.1_86						5910131		RIKEN cDNA 2410129H14 gene			1.94	4.000E-04		
XM_485688	2310043G07Rik	sc27121.5.1_46		102230139						RIKEN cDNA 2310043G07 gene	0.88	3.536E-04	1.79	1.000E-03		
NM_178618.2	2310040G09Rik	sc00696402_311		780377						RIKEN cDNA 2310040G09 gene	1.26	1.516E-04	2.52	1.400E-03		
NM_178618	2310040G09Rik	sc414462.6_709		103130735	103130735	103130735				RIKEN cDNA 2310040G09 gene	1.25	2.042E-04	2.46	1.500E-03	2.46	2.800E-03
NM_028834	2210009G21Rik	sc20229.12_66		103850095						RIKEN cDNA 2210009G21 gene	1.29	4.747E-05	2.46	2.000E-04		
AK048948	C230084O16Rik	n|C230084O16Rik|PX00177B21|AK048948|785						10290270		RIKEN cDNA 2010011I20 gene			1.75	3.600E-03		
NM_021437.1	1700123O20Rik	sc446298.1_54						6350725		RIKEN cDNA 1700123O20 gene					0.04	1.080E-02
NM_053216.1	1700102P08Rik	sc364713.1_3						5670180		RIKEN cDNA 1700102P08 gene			1.80	4.500E-03		
NM_138581.1	1700088E04Rik	sc027660.1_217						1050288		RIKEN cDNA 1700088E04 gene			1.40	4.500E-03		
AK079686	A430015E08Rik	n|A430015E08|PX00133F12|AK079686|884						104050091		RIKEN cDNA 1700049G17 gene			1.58	1.700E-03		
NM_029338	1700027N10Rik	sc458876.5.1_70		1050093						RIKEN cDNA 1700027N10 gene	0.59	1.291E-04	1.50	1.900E-03		
NM_027081.1	1700027J05Rik	sc0069440.1_122						2850131		RIKEN cDNA 1700027J05 gene			1.31	3.500E-03		
NM_025892.1	1500031J02Rik	sc459245.4_458						2760037		RIKEN cDNA 1500031J02 gene			1.32	2.500E-03		
NM_026886	1500001A10Rik	sc058955.1_4						1570373		RIKEN cDNA 1500001A10 gene			1.51	2.000E-03		
AK081939	C030038O19Rik	n|C030038O19Rik|PX00172E17|AK081939|2520						103780433		RIKEN cDNA 1200015N20 gene			2.60	1.500E-03		
NM_028773.2	1200013B08Rik	sc54952.8_631	520519							RIKEN cDNA 1200013B08 gene	1.78	9.506E-05	3.41	1.000E-04		
AK035834.1		sc00001676.1_649						106270411		RIKEN cDNA 1110012J17 gene			4.16	2.300E-03		
AK050411	C730046C01Rik	n|C730046C01|PX00087H11|AK050411|2898	105900017							ribosome binding protein 1	0.83	3.888E-05	1.78	1.000E-04		
NM_199447.2	AA408556	sc01070941_210						6130731		ribosomal RNA processing 12 homolog (S. cerevisiae)			1.42	1.660E-03		
NM_170669.2	Rps15a	sc00267019.1_256			1170180					ribosomal protein S15a	4.54	5.176E-07			55.59	0.000E+00
NM_026533	Rps13	sc30771.2_110	102970711	102970711	102970711	102970711				ribosomal protein S13	2.28	1.032E-04	3.58	2.000E-03	3.58	0.000E+00
NM_025938.1	Rpp14	sc446641.9_62						7040014		ribonuclease P 14 subunit (human)			1.80	2.000E-04		
AK077549	5730445E20Rik	n|5730445E20|PX00644C06|AK077549|3271						101500253		ribonuclease III, nuclear			3.62	5.000E-04		
AK035683	Lbcl1	n|9530068N01|PX00113D02|AK035683|3187						102650082		rho/rac guanine nucleotide exchange factor (GEF) 2			1.48	6.000E-04		
XM_149562.4	Arhgef16	sc23452.14.1_29	3990372							Rho guanine nucleotide exchange factor (GEF) 16	1.31	7.851E-05	2.51	8.000E-04		
NM_008113.2	Arhgdig	sc50150.4.1_163					5130338			Rho GDP dissociation inhibitor (GDI) gamma	0.61	3.198E-04				
NM_028810.1	Rhoe	sc0741941_11	940504	940504	940504	940504				Rho family GTPase 3	6.96	4.088E-04	26.65	0.000E+00	711.98	0.000E+00
NM_009053.1	Rfng	sc00019719.2_122						6290086		RFNG O-fucosylpeptide 3-beta-N-acetylglucosaminyltransferase			1.39	2.500E-03		
NM_024233.2	Smfn	sc00035421_12	1580338							REX2, RNA exonuclease 2 homolog (S. cerevisiae)	1.86	9.666E-05	2.04	2.000E-04		
NM_009030	Rbbp4	sc21784.13_65	106230239							retinoblastoma binding protein 4	1.70	1.266E-05	2.91	7.000E-04		
NM_009029.1	Rb1	sc45319.27_70	5900338							retinoblastoma 1	0.61	9.827E-05	1.54	3.000E-04		
NM_028879.1	Rpgrip1	sc00079845.1_177				2690142				retinitis pigmentosa GTPase regulator interacting protein 1			16.65	0.000E+00	16.65	0.000E+00
NM_018739.1	Rpl9n	sc936111.9.1_0						4050739		retinitis pigmentosa 9 (human)			1.57	1.800E-03		
XM_489103	A230057G18Rik	sc26213.1.3_304							101850070	retinal noncoding RNA 2					2.02	3.000E-04
NM_013648.4	Rtn2	sc020167.10_162						4480538		reticulon 2 (Z-band associated protein)			1.42	4.000E-03		
NM_023396.3	Reprimo	sc119271.1.36_133	1580706							reprimo, TP53 dependent G2 arrest mediator candidate	0.56	2.726E-04	1.47	1.000E-03		
NM_145923.1	AA536743	sc00100522_66	4540746							RET-like 1	0.88	9.013E-05	1.86	3.000E-04		
NM_145840.2	Rgs9bp	sc0243923.1_215	840047							regulator of G-protein signalling 9 binding protein	1.05	2.424E-04	2.09	1.400E-03		
NM_026380.2	6530413N01Rik	sc117360.1.193_85						6760440		regulator of G-protein signalling 8			1.52	2.400E-03		
NM_011880.1	Rgs7	sc115892.18.1_65						3390044		regulator of G-protein signaling 7			1.89	3.700E-03		
NM_053271.1	Rims2	sc00116838.2_281						670725		regulating synaptic membrane exocytosis 2			1.43	2.000E-03		
AK037671	A130035O14Rik	n|A130035O14|PX00122H19|AK037671|1567						102850066		radixin			3.51	1.000E-04		
NM_009041	Rdx	sc0159684.7_10	4260039							radial spokehead-like 2A	0.66	2.328E-04	1.58	7.000E-04		
NM_025789.2	Rsh12	sc51156.10.1_24	6110014							radial spokehead-like 2A	0.75	3.009E-07	1.68	0.000E+00		
BC019118	Rab6	sc000310_17	106200110							RAB6, member RAS oncogene family	0.69	4.097E-05	1.62	6.000E-04		

		limma, sam & ttest		limma & sam	limma & ttest	sam & ttest	only in limma	only in sam	only in ttest							
Accession	all-symbol	Transcript	Probe Id	Probe Id	Probe Id	Probe Id	Probe Id	Probe Id	Probe Id	Gene name	limma FC	limma p value	sam FC	sam p value	ttest FC	ttest p value
NM_024287.2	Rab6	scl00072.1_32	4780731	4780731	4780731	4780731				RAB6, member RAS oncogene family	1.23	3.812E-05	2.24	1.200E-03	2.24	0.000E+00
AK010874	2500004H21Rik	ri|2500004H21|ZX00052O06|AK010874|1261						10604071		RAB43, member RAS oncogene family			1.70	4.000E-04		
NM_031874.3	Rab3d	scl36130.5_341	4210253	4210253	4210253	4210253				RAB3D, member RAS oncogene family	1.05	4.364E-07	2.08	0.000E+00	2.08	0.000E+00
AK052775.1		scl0001689.1_10						102570280		RAB11 family interacting protein 3 (class II)			1.89	1.200E-03		
NM_133686.1	Qprt	scl30662.5.1_110		670270						quinolinate phosphoribosyltransferase	1.39	2.231E-07	2.63	0.000E+00		
NM_021888.1	Qtrt1	scl37224.9.157_21					1340162			queuine tRNA-ribosyltransferase 1	2.73	4.234E-04				
NM_024221.2	Pdhb	scl0068263.1_19	610086	610086	610086	610086				pyruvate dehydrogenase (lipoamide) beta	1.88	4.054E-05	3.59	0.000E+00	3.59	0.000E+00
NM_023217.2	Pgpep1	scl066522.1_109		2650739						pyroglutamyl-peptidase I	0.61	7.650E-05	1.52	2.800E-03		
NM_133993.1	2310058A11Rik	scl38607.15_418					3800301			PWP1 homolog (S. cerevisiae)	5.89	5.234E-04				
AK044496	Ppfibp1	ri|A930016N13|	105860440	105860440	105860440	105860440				PTPRF interacting protein, binding protein 1 (liprin beta 1)	3.93	5.962E-06	3.51	9.000E-04	77.65	0.000E+00
NM_018785	Fnbp3	scl4489.1.1_30	102900619	102900619	102900619	102900619				PRP40 pre-mRNA processing factor 40 homolog A (yeast)	2.73	6.154E-06	6.52	0.000E+00	6.52	0.000E+00
NM_175485.2	A230098A12Rik	scl00235472.2_7	4540403	4540403	4540403	4540403				protogenin homolog (Gallus gallus)	2.49	2.633E-04	5.85	3.000E-04	5.85	5.600E-03
NM_175485	A230098A12Rik	scl36723.20_445				100840609				protogenin homolog (Gallus gallus)			2.78	2.300E-03	2.78	9.700E-03
NM_053128.1	Pcdhb3	scl52072.1.185_54						450725		protocadherin beta 3			2.59	4.300E-03		
NM_011215.1	Ptprn2	scl019276.23_1						2450110		protein tyrosine phosphatase, receptor type, N polypeptide 2			2.01	2.900E-03		
AK053271	Ptprg	ri|E130003N22|PX00207G04|AK053271|2596		103170377						protein tyrosine phosphatase, receptor type, G	1.97	1.879E-05	3.74	0.000E+00		
NM_013643.1	Ptpn5	scl31333.17.1_37						2350161		protein tyrosine phosphatase, non-receptor type 5			1.51	5.000E-04		
XM_129160	4930428J16Rik	scl53270.6_364		104010538						protein prenyltransferase alpha subunit repeat containing 1	1.97	2.169E-05	4.18	4.000E-04		
NM_026447	2810423O19Rik	scl067905.1_18						5270279		protein phosphatase 1M			1.53	2.000E-03		
NM_027982.1	Ppp2cz	scl22768.2.1_26		5340193						protein phosphatase 1J	0.70	1.282E-04	1.60	8.000E-04		
AK076943	Piasg-pending	ri|4930568A14|PX00314K01|AK076943|1189						105550577		protein inhibitor of activated STAT 4			1.93	3.600E-03		
AK013364	2810458H16Rik	ri|2810458H16|ZX00067O24|AK013364|1814		104250138						protection of telomeres 1B	1.14	2.057E-04	2.18	6.000E-04		
NM_133949.1	Ptov1	scl084113.2_12						4230025		prostate tumor over expressed gene 1			1.76	1.400E-03		
NM_153565.1	Pcsk9	scl24041.13_589						3120044		proprotein convertase subtilisin/kexin type 9			1.45	4.400E-03		
AK014139	3110038B19Rik	ri|3110038B19|ZX00071F15|AK014139|1148		100870601						proline-rich coiled-coil 1	1.14	6.389E-05	2.21	3.000E-04		
NM_008865.2	Csh2	scl44966.5.170_12		2260463						prolactin family 3, subfamily b, member 1	1.49	3.057E-05	2.63	1.000E-04		
NM_028829	1700019B16Rik	scl18131.5_291						10860538		progestin and adipoQ receptor family member VIII			1.42	1.200E-03		
NM_011961	Plod2	scl36619.20_240	3360427	3360427	3360427	3360427				procollagen lysine, 2-oxoglutarate 5-dioxygenase 2	2.17	9.281E-06	4.28	0.000E+00	4.28	0.000E+00
NM_172832.1	C630049M13	scl51357.6.1_32						4810692		prenylcysteine oxidase 1 like			1.69	3.800E-03		
NM_025823	Pcyox1	scl28753.6_75						10572057S		prenylcysteine oxidase 1			1.41	3.100E-03		
AK036131	9630038C08Rik	ri|9630038C08|PX00116O10|AK036131|3133							103870239	predicted gene, OTTMUSG00000001284					4.05	1.500E-03
AK045810	B230311P14Rik	ri|B230311P14|PX00159K19|AK045810|2703						101940286		predicted gene, ENSMUSG00000074940			1.99	3.300E-03		
AK051399	D130046C19Rik	ri|D130046C19|PX00184D09|AK051399|1407		100630142						predicted gene, ENSMUSG00000072635	2.26	8.573E-07	4.70	0.000E+00		
AK081107	Gpld1	ri|B930088F07|PX00166D08|AK081107|2893		101240601						predicted gene, ENSMUSG00000055849	0.60	4.385E-05	1.52	1.000E-04		
AK079848	A430092C21Rik	ri|A430092C21|PX00135C19|AK079848|1098						10536006S		predicted gene, ENSMUSG00000052368			2.37	1.300E-03		
AK046228	B230354O11Rik	ri|B230354O11|PX00161G02|AK046228|3253						100770333		predicted gene, EG668468			1.47	6.000E-04		
AK085082	D430034L15Rik	ri|D430034L15|PX00194F12|AK085082|3853		100130139						predicted gene, EG546150	3.52	6.923E-08	5.26	5.000E-04		
AK007723	1810037J08Rik	ri|1810037J08|ZX00051K09|AK007723|534						102810044		predicted gene, EG434402			1.41	1.200E-03		
NM_008783.1	Pbx1	scl0018514.2_78	6660301	6660301	6660301	6660301				pre B-cell leukemia transcription factor 1	1.45	1.092E-05	2.69	0.000E+00	2.69	0.000E+00
NM_001003825	Kcnq2	scl18216.17.1_43							105670300	potassium voltage-gated channel, subfamily Q, member 2					2.53	2.000E-04
AK015907	Kcnj9	ri|4930526L21|PX00034C20|AK015907|1557						10407061S		potassium inwardly-rectifying channel, subfamily J, member 9			2.74	1.300E-03		
NM_199251.1	Kcnk12	scl0210741.1_194						4070072		potassium channel, subfamily K, member 12			2.01	5.000E-04		
NM_030229.2	Polr3h	scl078929.1_104		1980369						polymerase (RNA) III (DNA directed) polypeptide H	1.26	6.931E-06	2.39	1.000E-04		
NM_009632.2	Adprtl2	scl000341.1_0	6510097	6510097	6510097	6510097				poly (ADP-ribose) polymerase family, member 2	2.45	2.961E-04	5.57	0.000E+00	5.57	0.000E+00
NM_013807.1	Plk3	scl23942.14.1_32						2640592		polo-like kinase 3 (Drosophila)			1.41	3.400E-03		
AK038943	A230077I10Rik	ri|A230077I10|PX00129O18|AK038943|1086						10312016S		podocalyxin-like 2			1.78	3.200E-03		
NM_009434	Phlda2	scl30454.4.1_68						4810494		pleckstrin homology-like domain, family A, member 2			3.39	8.000E-04		
AK041857	Phip	ri|A630042G05|	105570292	105570292	105570292	105570292				pleckstrin homology domain interacting protein	1.17	3.839E-08	2.25	0.000E+00	2.25	0.000E+00
AK082118	C230009C22Rik	ri|C230009C22|PX00666N04|AK082118|5148						105890156		pleckstrin homology domain containing, family B (evectins) member 2			1.89	1.200E-03		
NM_008872	Plat	scl33993.13_72						6860128		plasminogen activator, tissue			1.46	2.600E-03		
NM_026163.1	Pkp2	scl49390.9.3_12						1990068		plakophilin 2			1.77	1.500E-03		
AK079680	Phkg2	ri|A430010P18|PX00133J08|AK079680|1428		100510673						phosphorylase kinase, gamma 2 (testis)	1.12	1.414E-04	2.11	1.600E-03		
NM_172285.1	Plcg2	scl33269.35.1_230							5720008	phospholipase C, gamma 2					2.48	1.700E-02
AK007777	1810044J04Rik	ri|1810044J04|ZX00042P12|AK007777|1541						100510735		phosphoinositide-3-kinase adaptor protein 1			2.24	4.000E-04		
NM_025951.1	Pi4k2b	scl0004021.1_968						2480215		phosphatidylinositol 4-kinase type 2 beta			1.58	3.000E-04		

		limma, sam & ttest		limma & sam	limma & ttest	sam & ttest	only in limma	only in sam	only in ttest							
Accession	all-symbol	Transcript	Probe Id	Probe Id	Probe Id	Probe Id	Probe Id	Probe Id	Probe Id	Gene name	limma FC	limma p value	sam FC	sam p value	ttest FC	ttest p value
AK050333	C730038E05Rik	ri|C730038E05|PX00087M20|AK050333|4745		104850070						phosphatidylinositol 3 kinase, regulatory subunit, polypeptide 4, p150	1.39	3.170E-04	2.60	2.000E-04		
NM_008819.2	Pemt	scl40150.13.1_57						1230292		phosphatidylethanolamine N-methyltransferase			1.79	2.600E-03		
NM_024274.1	Fars1	scl44903.11.3_96		5340575						phenylalanine-tRNA synthetase 2 (mitochondrial)	0.68	5.400E-05	1.61	1.000E-04		
NM_026737.1	Phf5a	scl46929.4_12						2690519		PHD finger protein 5A			1.41	4.000E-04		
NM_172303.3	Phf17	scl0001927.1_147						4280066		PHD finger protein 17			8.26	9.000E-04		
NM_145610	Ppan	scl37238.1_20	540398	540398	540398	540398				peter pan homolog (Drosophila)	2.47	4.903E-09	5.25	0.000E+00	5.25	0.000E+00
NM_022889.2	Pes1	scl0064934.1_269						2470427		pescadillo homolog 1, containing BRCT domain (zebrafish)			1.62	1.900E-03		
NM_023041.2	Pex19	scl019298.8_30		3140037						peroxisome biogenesis factor 19	0.72	7.921E-05	1.66	9.000E-04		
AK030565	5330432H08Rik	ri|5330432H08|PX00054F14|AK030565|2751						106180347		peroxisomal biogenesis factor 6			1.53	3.000E-04		
NM_027275.2	2810422B04Rik	scl28877.24.1_45	5860632	5860632	5860632	5860632				pentatricopeptide repeat domain 3	3.30	1.776E-05	3.00	1.400E-03	219.72	0.000E+00
NM_033602	Peli2	scl46390.1.1_198						105360528		pellino 2			1.72	1.000E-04		
NM_054088	Adpn	scl47673.9_482						5050551		patatin-like phospholipase domain containing 3			2.49	6.000E-04		
AK031487	6030439I24Rik	ri|6030439I24|PX00057M11|AK031487|2398						102680025		par-3 partitioning defective 3 homolog B (C. elegans)			1.95	2.400E-03		
NM_018809	Pef1a	scl21240.2.1_45						6450377		pancreas specific transcription factor, 1a			2.41	2.000E-04		
AK052579	Pmx2b	ri|D530038E02|PX00089K24|AK052579|1177						103130093		paired-like homeobox 2b			2.06	0.000E+00		
NM_008780.1	Pax1	scl018503.6_182		3360253						paired box gene 1	2.05	3.542E-06	3.99	0.000E+00		
NM_178939.1	Pdrg1	scl068559.1_22							5340592	p53 and DNA damage regulated 1					0.01	0.000E+00
NM_145525	Osbpl6	scl099031.19_30						102650735		oxysterol binding protein-like 6			1.55	8.000E-04		
AK040881	Oxr1	ri|A530033P13|PX00140N10|AK040881|2763		106660603						oxidation resistance 1	1.92	3.223E-08	3.74	0.000E+00		
AK037468	Odf2	ri|A130020I08|PX00121D09|AK037468|1550						104150039		outer dense fiber of sperm tails 2			1.63	4.100E-03		
NM_010953.1	Oc90	scl47131.15.1_20		1740392						otoconin 90	1.15	3.644E-05	2.18	7.000E-04		
NM_008753	Oaz1	scl018245.5_1						110181		ornithine decarboxylase antizyme			1.28	3.200E-03		
NM_026480.1	2410146L05Rik	scl33573.3.1_114	2630333	2630333	2630333	2630333				oocyte expressed protein homolog (dog)	2.49	9.982E-10	5.65	0.000E+00	5.65	0.000E+00
NM_008262.2	Onecut1	scl0015379.2_121						6450136		one cut domain, family member 1			3.64	9.000E-04		
NM_016968.2	Olig1	scl48883.1.23_254							1660594	oligodendrocyte transcription factor 1					7.82	0.000E+00
NM_146596	Olfr703	scl32231.1.1_325						1500546		olfactory receptor 703			1.71	1.000E-03		
NM_146536	Olfr313	scl41514.1.1_155						5050100		olfactory receptor 313			3.40	7.000E-04		
NM_173777.2	A030009A06Rik	scl36161.8.1_55						730154		olfactomedin 2			1.57	2.700E-03		
AK078102	6330444G18Rik	ri|6330444G18|PX00315G03|AK078102|3345		101190040						OCIA domain containing 1	0.93	3.965E-05	1.90	0.000E+00		
NM_023429.2	Asrij	scl27722.12.1_0	2940132	2940132	2940132	2940132				OCIA domain containing 1	1.40	3.616E-06	2.67	1.000E-04	2.67	0.000E+00
AK089939	G430008M12Rik	ri|G430008M12|PH00001B21|AK089939|1270				105360487				NUF2, NDC80 kinetochore complex component, homolog (S. cerevisiae)			3.58	9.000E-04	3.58	0.000E+00
NM_153561.1	Nudt6	scl22226.9.1_81		2650020						nudix (nucleoside diphosphate linked moiety X)-type motif 6	1.44	1.419E-05	2.22	1.000E-04		
NM_029385.1	2310041H06Rik	scl35414.1_2						4540504		nudix (nucleoside diphosphate linked moiety X)-type motif 16			1.36	1.300E-03		
NM_008723.1	Npm3	scl29824.1.5_102		3610300						nucleoplasmin 3	0.85	4.257E-05	1.81	1.000E-04		
NM_010880.2	Ncl	scl16520.16_184						4540279		nucleolin			1.42	9.000E-04		
NM_133800.2	C78541	scl0002568.1_14		6020324						nucleolar protein 12	0.91	9.081E-07	1.88	1.000E-04		
AK054118	E230020O17Rik	ri|E230020O17|PX00209H07|AK054118|2704						10645040		nucleolar protein 11			1.35	3.400E-03		
NM_010913	Nfya	scl49828.11_159	103450017	103450017	103450017	103450017				nuclear transcription factor-Y alpha	1.52	3.626E-05	2.63	7.000E-04	2.63	0.000E+00
NM_010264.2	Nr6a1	scl19350.14_370				4010347				nuclear receptor subfamily 6, group A, member 1			2.55	2.200E-03	2.55	6.100E-03
NM_010881.1	Ncoa1	scl0017977.2_208						3610438		nuclear receptor coactivator 1			1.47	1.100E-03		
NM_144847.1	BC011468	scl0223649.1_255						6350397		nuclear receptor binding protein 2			1.73	2.200E-03		
NM_010908.3	Nfkbib	scl31572.8.1_327						2260167		nuclear factor of kappa light chain gene enhancer in B-cells inhibitor, beta			2.42	1.900E-03		
AK052726	Nfkb1	ri|D630036B16|PX00197N10|AK052726|1253						102340039		nuclear factor of kappa light chain gene enhancer in B-cells 1, p105			1.39	3.000E-03		
AK011168	Nudel-pending	ri|2600006O07|ZX00060D03|AK011168|1653						102120044		nuclear distribution gene E-like homolog 1 (A. nidulans)			4.22	6.000E-04		
NM_175263.2	5730593N15Rik	scl40626.1.1_194						3520450		notum pectinacetylesterase homolog (Drosophila)			2.54	7.000E-04		
NM_013864	Ndrg2	scl45598.20_218	450403	450403	450403	450403				N-myc downstream regulated gene 2	2.65	1.267E-04	6.04	0.000E+00	6.04	0.000E+00
NM_010822.2	Mpg	scl41728.5_44			2760021					N-methylpurine-DNA glycosylase	2.32	2.764E-04			3.26	0.000E+00
NM_133787	C87860	scl23088.16_137	103940707	103940707	103940707	103940707				NMD3 homolog (S. cerevisiae)	2.58	5.909E-07	5.72	0.000E+00	5.72	0.000E+00
NM_144955.1	Nkx6-1	scl26314.4.1_182						6040731		NK6 transcription factor related, locus 1 (Drosophila)			1.38	1.600E-03		
NM_011848.1	Nek3	scl35027.16.1_147						6650035		NIMA (never in mitosis gene a)-related expressed kinase 3			1.46	6.000E-04		
NM_021607.2	Ncstn	scl000060.1_19						940601		nicastrin			3.04	1.100E-03		
AK030358	Nrp	ri|5330401L20|PX00053A17|AK030358|2575						102760168		neuropilin 1			1.64	3.400E-03		
AK045259	B130052F17Rik	ri|B130052F17|PX00158C20|AK045259|2394		106940014						neuron-glia-CAM-related cell adhesion molecule	0.97	3.370E-05	1.93	4.000E-04		
AK077465	Nnat	ri|5730414I02|PX00643J18|AK077465|774						103990551		neuronatin			1.89	3.700E-03		
AK050957	Npas3	ri|D630044N15|PX00180H08|AK050957|2983						104230059		neuronal PAS domain protein 3			1.99	2.700E-03		

		limma, sam & ttest		limma & sam	limma & ttest	sam & ttest	only in limma	only in sam	only in ttest							
Accession	all-symbol	Transcript	Probe Id	Probe Id	Probe Id	Probe Id	Probe Id	Probe Id	Probe Id	Gene name	limma FC	limma p value	sam FC	sam p value	ttest FC	ttest p value
NM_025424.1	1110060M21Rik	scl15766.4.1_27	4210731	4210731	4210731	4210731				neuron derived neurotrophic factor	4.00	2.937E-11	16.55	0.000E+00	16.55	0.000E+00
NM_009719.4	Neurog3	scl38863.2.1_137						6980451		neurogenin 3			2.54	0.000E+00		
NM_009718.2	Neurog2	scl22640.2_1							5420278	neurogenin 2					2.37	4.000E-04
NM_007789.2	Cspg3	scl021811.1_58	3870239	3870239	3870239	3870239				neurocan	1.44	1.680E-04	2.34	4.100E-03	2.34	0.000E+00
NM_172544.1	Nrxn3	scl0002402.1_134							1400546	neurexin III					4.53	1.000E-04
NM_010947.2	Ntn3	scl0018209.1_327		5270593						netrin 2-like (chicken)	0.51	4.057E-05	1.43	2.000E-04		
NM_028721	Nphp3	scl36533.8.1_27						106550551		nephronophthisis 3 (adolescent)			8.22	1.100E-03		
NM_016743.1	Nell2	scl0054003.1_330		4280301						NEL-like 2 (chicken)	0.73	2.052E-04	1.63	3.000E-03		
NM_025383	1110005F07Rik	scl23602.11_383		6200048						NECAP endocytosis associated 2	0.91	7.200E-08	1.87	0.000E+00		
NM_022565	Ndst4	scl0645801_9						5080017		N-deacetylase/N-sulfotransferase (heparin glucosaminyl) 4			2.56	1.800E-03		
NM_194059.1	Nanos3	scl0244551.2_35					4200204			nanos homolog 3 (Drosophila)	5.61	1.175E-04				
NM_172529.1	AU067744	scl00214505.2_7		3140176						N-acetylglucosamine-1-phosphotransferase, gamma subunit	0.52	1.745E-04	1.44	1.600E-03		
XM_203352.2	0610034P02Rik	scl40723.11.1_29				3710168				NA			2.66	0.000E+00	2.66	0.000E+00
	1110004M10Rik	scl20611.1.1_291						100730398		NA			1.42	3.300E-03		
	1110029I05Rik	scl36592.1.563_:	105570433	105570433	105570433	105570433				NA	1.03	1.353E-07	2.03	1.000E-04	2.03	0.000E+00
	1110030E23Rik	scl30677.2_0		103450176						NA	0.87	4.365E-05	1.85	2.000E-04		
	1190002F15Rik	scl0381822.1_19						105290494		NA			1.50	1.600E-03		
	1190004M23Rik	scl783.1.1_90						102060079		NA			1.56	3.000E-03		
XM_144634.1	1300006M19Rik	scl25791.15_62						2370040		NA			2.32	1.700E-03		
XM_484092	1500005I02Rik	scl39353.3_240						100380193		NA			1.90	2.300E-03		
XM_203453.1	1500005K14Rik	GI_25057085		106900132						NA	1.90	4.617E-07	3.63	0.000E+00		
XM_486262	1500005N04Rik	scl36454.7.1_119						102970372		NA			2.18	2.500E-03		
NM_173366.1	1500010G04Rik	scl0068965.1_205						5050403		NA			1.55	2.600E-03		
XM_485969	1700008D07Rik	scl30956.5.1_91	103120026	103120026	103120026	103120026				NA	1.13	1.441E-04	2.19	0.000E+00	2.19	0.000E+00
XM_131683.2	1700018D18Rik	scl23864.14.1_204		1400594						NA	0.59	5.156E-05	1.51	5.000E-04		
XM_355444.1	1700021C14Rik	scl21980.4.1_109						540041		NA			1.50	2.300E-03		
XM_133916.4	1700071K18Rik	scl076612.10_1						1090400		NA			2.65	1.000E-03		
	1700072N11Rik	scl50199.1.16_11		102030600						NA	3.22	6.243E-06	6.92	4.000E-04		
	1810006K23Rik	scl066259.1_113	103390746	103390746	103390746	103390746				NA	1.33	2.014E-06	2.44	1.000E-04	2.44	0.000E+00
	1810015C11Rik	scl0069102.1_328						102970647		NA			1.96	6.000E-04		
	1810018P12Rik	scl074170.1_145						107000132		NA			2.42	1.400E-03		
NM_025472.2	1810032O08Rik	scl40700.5_96		4070672						NA	0.97	8.121E-05	1.93	2.000E-03		
	1810044D09Rik	scl29745.2.1_5		104670142						NA	0.81	3.185E-04	1.77	4.000E-04		
XM_126676.3	1810057P16Rik	scl39291.6_426						6350739		NA			1.72	1.300E-03		
	1810059M14Rik	scl23475.1.1_110		102650487						NA	1.00	1.041E-04	2.03	1.000E-04		
	2010010M04Rik	scl0066546.1_59						103170075		NA			1.39	2.000E-03		
XM_356097.1	2210011C24Rik	scl34573.4.1_45		3710551						NA	4.04	1.508E-04	5.41	1.500E-03		
	2210410E06Rik	scl30406.1.1_4	106520398	106520398	106520398	106520398				NA	2.86	7.456E-06	6.07	0.000E+00	6.07	0.000E+00
XM_147000.1	2300004C15Rik	scl36894.13.1_20		1450338						NA	0.73	1.117E-05	1.66	3.000E-04		
	2300009N04Rik	scl069477.2_5						103440735		NA			2.24	1.300E-03		
	2310005C01Rik	scl27316.1.344_21						103940088		NA			2.18	2.200E-03		
	2310005L22Rik	scl24876.1.45_10		105910273						NA	0.74	1.894E-04	1.64	1.000E-03		
	2310028O11Rik	scl23626.6_138						103710014		NA			1.48	1.800E-03		
	2310038D14Rik	scl078495.2_180	100990672	100990672	100990672	100990672				NA	2.74	3.290E-05	4.61	1.000E-03	4.61	0.000E+00
	2310050P20Rik	scl16845.1.1_2						104050041		NA			2.32	5.000E-04		
	2310061G22Rik	scl4670.1.1_55						101780348		NA			1.73	2.000E-04		
XM_149067.1	2410088K16Rik	scl17681.2.1_40						6520619		NA			3.30	1.300E-03		
	2410133F24Rik	scl076794.1_1						101400204		NA			2.85	4.000E-04		
	2410137F16Rik	scl26142.1.2316_58						103840450		NA			2.08	1.400E-03		
	2510022D24Rik	scl066567.4_14			1980538					NA	1.63	1.149E-04			9.79	0.000E+00
XM_485010	2510042P03Rik	scl19112.1.2271_33						106650142		NA			3.81	1.800E-03		
XM_355816.1	2510047L19Rik	GI_38085260		104540408						NA	1.34	3.308E-05	2.60	2.000E-04		
	2600009P04Rik	scl066572.1_0						104780440		NA			1.62	2.000E-03		
	2610007B07Rik	scl54879.1.1_117						104120647		NA			12.69	1.500E-03		
	2610037P13Rik	scl7880.1.1_99		101090619						NA	0.71	2.042E-04	1.65	3.000E-04		
XM_131857	2610109H07Rik	scl23524.7_137				106590050				NA			2.85	0.000E+00	2.85	0.000E+00
	2610203C22Rik	scl072481.2_13		107040706						NA	0.96	2.113E-05	1.91	2.000E-04		
	2700024H10Rik	scl00108913.1_324		100770176						NA	0.87	1.398E-04	1.83	1.000E-04		
XM_489058	2700033B16Rik	scl072602.2_41		103140091						NA	1.10	1.146E-05	2.12	2.000E-04		
	2700078K13Rik	scl0078326.1_28						100460538		NA			1.42	3.800E-03		
	2810017I02Rik	scl069967.2_48		105360020						NA	0.83	3.395E-04	1.77	2.000E-04		
	2810410D24Rik	scl3938.1.1_28						106100706		NA			1.44	1.200E-03		

		limma, sam & ttest		limma & sam	limma & ttest	sam & ttest	only in limma	only in sam	only in ttest								
Accession	all-symbol	Transcript	Probe Id	Probe Id	Probe Id	Probe Id	Probe Id	Probe Id	Probe Id	Gene name	limma FC	limma p value	sam FC	sam p value	ttest FC	ttest p value
	2810423A18Rik	sc01566.1.1_41	102810273	102810273	102810273	102810273				NA	4.45	4.116E-05	9.37	1.000E-04	9.37	0.000E+00
XM_131155.3	2810453I12Rik	sc22650.20.1_0	4070162	4070162	4070162	4070162				NA	1.26	3.190E-07	2.39	0.000E+00	2.39	0.000E+00
	2900009G24Rik	sc25297.1.2_23:	103140050	103140050	103140050	103140050				NA	1.49	1.490E-04	2.71	3.000E-04	2.71	0.000E+00
	2900011I18Rik	sc43531.1.1_35	104780278							NA	0.86	3.940E-05	1.82	2.000E-04		
	2900037O03Rik	sc0072907.1_70						101050075		NA			1.34	2.600E-03		
	2900052N06Rik	sc0073028.1_125						102850577		NA			1.32	3.400E-03		
	2900063K03Rik	sc26306.1.1_82				105050601				NA			2.05	3.200E-03	2.05	1.000E-04
	2900084I15Rik	sc28397.1.1_37						102060390		NA			1.68	2.000E-04		
XM_149833.1	3010022N22Rik	sc068069.1_6	6160706							NA	1.66	5.208E-05	3.00	1.000E-04		
	3110021A11Rik	sc29574.1.666_27	105220711							NA	1.34	5.110E-05	2.55	0.000E+00		
XM_484036	3110043A19Rik	sc40128.1.3_246						101780398		NA			1.95	3.900E-03		
	3110045A19Rik	sc47576.1.1_118	103690100							NA	1.36	1.135E-04	2.57	1.000E-04		
XM_148118.1	4122402O22Rik	sc0001884.1_59						2630398		NA			1.49	7.000E-04		
XM_196130.3	4432411E13Rik	sc47278.57_323						1780605		NA			1.80	3.000E-04		
NM_175422.2	4631423B10Rik	sc28530.1.1_256						1740368		NA			1.63	1.600E-03		
	4732460O03Rik	sc0058894.2_274						106040600		NA			1.44	2.800E-03		
	4833411C07Rik	sc071624.3_33					100380066			NA	4.91	3.595E-04				
	4833424C13Rik	sc075770.2_292						104730019		NA			1.56	2.300E-03		
	4833424O12Rik	sc075765.1_328						104730440		NA			1.70	4.000E-04		
AK029468	4833442A19Rik	ri\4833442A19|PKO0313P13|AK029468|1260						103120204		NA			4.84	0.000E+00		
XM_135150.3	4930411J02Rik	GI_38050081	106520168	106520168	106520168	106520168				NA	1.14	3.378E-06	2.21	1.000E-04	2.21	0.000E+00
XM_148429.1	4930455C21Rik	sc48481.81_48	3800288	3800288	3800288	3800288				NA	1.55	4.299E-05	2.89	3.000E-04	2.89	0.000E+00
	4930456A14Rik	sc074676.2_114						103870358		NA			1.77	2.300E-03		
	4930522J14Rik	sc078020.3_12						101980300		NA			1.52	5.000E-04		
	4930524A08Rik	sc111029.1.1_237							100360279	NA					2.03	7.000E-03
	4930563A19Rik	sc50892.1.1_13		101450575						NA						
AK029665	4932411G08Rik	ri\4932411G08|PKO0017I15|AK029665|3917						100460576		NA			1.80	8.000E-04		
XM_359229	4932416N17Rik	sc49438.28_389	101170121	101170121	101170121	101170121				NA	1.49	3.349E-06	2.71	1.000E-04	2.71	0.000E+00
	4933411D12Rik	sc34058.1.1_81						105910739		NA			1.33	1.400E-03		
	4933428F06Rik	sc071245.8_9						100820372		NA			1.65	1.400E-03		
	4933437G19Rik	sc026082.1.1_192						104730044		NA			5.35	9.000E-04		
XM_139743.5	5033403D15	GI_38081841		102760577						NA	2.33	1.073E-05	4.88	0.000E+00		
	5330403D14Rik	sc16838.2_356		100620750						NA	0.78	2.054E-04	1.71	4.000E-04		
	5330409N07Rik	sc42170.1.1419_8						101090204		NA			3.35	3.600E-03		
	5330423I13Rik	sc37146.1.1_205						104830537		NA			1.57	2.000E-04		
XM_149959.1	5430400N05Rik	sc31136.1.434_8						3840706		NA			1.35	4.500E-03		
	5430404G13Rik	sc48438.1.1_22:	100380605	100380605	100380605	100380605				NA	4.32	2.715E-07	19.40	0.000E+00	19.40	0.000E+00
	5530400B01Rik	sc071434.1_160						103830551		NA			1.59	2.300E-03		
	5530401I12Rik	sc071377.1_15						103130541		NA			3.24	1.000E-04		
XM_126359.2	5730409G07Rik	sc040311.8.1_101				6660440				NA			2.81	6.000E-04	2.81	0.000E+00
NM_175297.2	5730427M17Rik	sc098314.1_180						6590538		NA			1.50	2.400E-03		
	5730480H06Rik	sc070592.4_117		100450750						NA	1.03	6.561E-05	1.95	1.800E-03		
	5930418K15Rik	sc0077106.1_295						104850273		NA			1.44	3.000E-04		
	5930420B01Rik	sc018996.1.1_237						102650044		NA			1.46	6.000E-04		
XM_126912.4	6030408C04Rik	sc0217558.10_30				6520059				NA			2.07	1.000E-03	2.07	0.000E+00
XM_358537.1	6330405I19	sc27465.5_88						4210176		NA			2.65	1.400E-03		
	6330415B21Rik	sc22832.1.1_31:	102230095	102230095	102230095	102230095				NA	1.27	2.374E-04	2.53	2.000E-04	2.53	0.000E+00
NM_177872.1	6330442E01Rik	sc26400.5.1_12						4730372		NA			3.91	4.200E-03		
XM_358602.1	6330562C20Rik	sc076193.1_200		2830446						NA	0.55	2.151E-04	1.46	6.000E-04		
XM_131537.4	6430559E15Rik	sc0068180.6_62		2030114						NA	0.80	1.806E-04	1.73	5.000E-04		
	6720403M19Rik	sc29361.1.617_238								NA	0.97	3.576E-04	1.93	3.000E-04		
XM_133272	6720407G21Rik	sc0077733.1_129		106110204		103450288				NA			5.02	4.100E-03	443.64	0.000E+00
	6720411N02Rik	sc0077728.1_328						101940044		NA			1.50	9.000E-04		
	6720422N22Rik	sc099946.1_47		104590600						NA	1.01	2.358E-04	1.94	2.300E-03		
AK032904	6720470G16Rik	ri\6720470G16|PKO0060817|AK032904|3670						105550050		NA			2.11	6.000E-04		
	6720477C19Rik	sc28484.1.1_30						104920239		NA			1.90	3.800E-03		
	6720494G13Rik	sc35446.1.1_167		102900388						NA	1.89	6.989E-08	3.66	0.000E+00		
AK032984	6720484O09Rik	ri\6720484O09|PKO0060K23|AK032984|1856						105270435		NA			2.31	3.000E-04		
XM_144310.3	6820424J24Rik	GI_38081984						103060121		NA			1.95	2.000E-04		
AK078781	8030481K01Rik	ri\8030481K01|PKO0060P24|AK078781|4107						103870170		NA			1.54	7.000E-04		
XM_354623.1	8430405D05Rik	GI_38091464						105340735		NA			1.59	1.400E-03		
	8430408G09Rik	sc027430.1.1_166	105690180	105690180	105690180	105690180				NA	1.60	6.398E-05	2.90	4.000E-04	2.90	0.000E+00
	8430413D17Rik	sc045977.1.1097_1						100960292		NA			5.43	4.000E-04		

		limma, sam & ttest		limma & sam	limma & ttest	sam & ttest	only in limma	only in sam	only in ttest							
Accession	all-symbol	Transcript	Probe Id	Probe Id	Probe Id	Probe Id	Probe Id	Probe Id	Probe Id	Gene name	limma FC	limma p value	sam FC	sam p value	ttest FC	ttest p value
	8430426K15Rik	scl16101.1.1002_	106450725	106450725	106450725	106450725				NA	1.52	9.171E-06	3.13	6.000E-04	3.13	3.500E-03
XM_484173	9030205A07Rik	scl42844.21.1_76		103440301						NA	1.16	2.880E-04	2.15	6.000E-04		
	9030218A15Rik	scl11828.1.1_189						102850053		NA			7.35	3.600E-03		
	9030607L20Rik	scl20066.1.1_26(	106020102	106020102	106020102	106020102				NA	1.16	1.981E-04	2.20	1.000E-04	2.20	0.000E+00
XM_126185.3	9130006A14Rik	GI_38091345						105420563		NA			2.31	3.000E-03		
AK078992	9230103K20Rik	ri|9230103K20|PX00316E01|AK078992|990						103170403		NA			1.84	2.000E-03		
XM_110546.2	9230115A19Rik	scl0338522.1_21						1400114		NA			1.78	1.300E-03		
AK033900	9330112I12Rik	ri|9330112I12|PX00104P17|AK033900|1392						100670348		NA			2.42	3.000E-03		
	9330161A03Rik	scl00320285.1_191							106180528	NA					2.48	1.000E-04
NM_178781.2	9330186A19Rik	scl0320365.12_9		1500091						NA	0.79	2.264E-05	1.72	1.000E-04		
	9430022A07Rik	scl077283.1_27						100430500		NA			1.39	3.000E-03		
	9430067K09Rik	scl0320341.3_114		105220053						NA	0.83	3.269E-04	1.76	1.800E-03		
	9430085L16Rik	scl46149.1.1_123						102370164		NA			4.09	1.000E-04		
	9430091N11Rik	scl47347.1.1_38	106200156	106200156	106200156	106200156				NA	1.97	1.364E-04	3.47	3.000E-04	3.47	0.000E+00
XM_485965	9530051K01Rik	scl31019.5_264						106760017		NA			2.03	9.000E-04		
AK035585	9530071H01Rik	ri|9530071H01|PX00113D12|AK035585|1520						104540068		NA			1.64	3.200E-03		
AK035591	9530073A13Rik	ri|9530073A13|PX00114K21|AK035591|3548						103140541		NA			1.43	2.400E-03		
	9630023C09Rik	scl41662.1_144							100940315	NA					2.24	7.600E-03
	9630045H20Rik	scl41911.1_404						106660088		NA			1.46	6.000E-04		
AK037153	A030001L21Rik	ri|A030001L21|PX00063K01|AK037153|2376						101940463		NA			1.62	2.400E-03		
	A130010C12Rik	scl33270.1.1_296						104920039		NA			1.61	8.000E-04		
	A130038I17Rik	scl45268.2.964_222						101780010		NA			1.76	1.000E-04		
	A130075O10Rik	scl16349.1.869_32						100670433		NA			1.54	4.500E-03		
	A230058F20Rik	scl54973.1.1243_164						100450735		NA			1.45	4.400E-03		
	A530028O18	scl45755.1.2_39						103360088		NA			2.28	2.200E-03		
AK040847	A530030B07Rik	ri|A530030B07|PX00140J07|AK040847|1127						100940128		NA			2.15	2.900E-03		
XM_203596	A530050D06Rik	scl42735.15_218		104070037						NA	1.61	1.789E-04	2.80	7.000E-04		
AK041877	A630043I21Rik	ri|A630043I21|PX00145M08|AK041877|1117						106840546		NA			5.45	1.900E-03		
XM_194983.2	A730032D07Rik	scl46883.13_90						4780551		NA			1.66	3.000E-03		
AK043124	A730058G16Rik	ri|A730058G16|PX00150N06|AK043124|2300						103290112		NA			2.18	9.000E-04		
NM_177156.2	A730089K16Rik	scl0320411.1_266						5690039		NA			1.58	4.000E-03		
AK080623	A830029A02Rik	ri|A830029A02|PX00661B04|AK080623|456							103130471	NA					215.26	7.000E-04
XM_130065.4	A930008K15Rik	scl21141.20.1_28		5340132						NA	1.02	1.247E-04	2.07	1.000E-04		
	A930009K04Rik	scl50058.1.1_22	102360673	102360673	102360673	102360673				NA	1.89	4.515E-05	3.66	0.000E+00	3.66	0.000E+00
	A930015D03Rik	scl077810.1_87						102320372		NA			3.14	1.000E-04		
	A930015N15Rik	scl0077957.1_7						105050593		NA			1.59	2.300E-03		
	A930039N10Rik	scl0320303.1_35						105860672		NA			1.34	2.000E-03		
XM_359298	AI661311	scl0106633.27_163		103440239						NA	2.79	2.033E-05	4.15	1.000E-04		
NM_175182.2	Atf7ip	scl072488.1_25						6770021		NA			1.98	2.000E-03		
	Atp1b1	scl16016.7_39						103710546		NA			1.46	3.200E-03		
NM_177836.2	AW046396	scl0329173.1_142		7000484						NA	0.94	1.594E-04	1.88	5.000E-04		
NM_198307.1	AW107703	scl35434.19.159_3		4760086						NA	0.92	1.046E-04	1.84	2.500E-03		
	B130021B11Rik	scl47377.1_418						104010471		NA			2.14	6.000E-04		
AK045144	B130040C13Rik	ri|B130040C13|PX00157D13|AK045144|2217						100940112		NA			2.43	4.400E-03		
	B230107H12Rik	scl9799.1.1_301						103060138		NA			1.45	3.200E-03		
	B230107K20Rik	scl4434.1.1_13		100380040						NA	0.87	4.654E-06	1.82	1.000E-04		
	B230202K19Rik	scl0078602.1_265						103440215		NA			2.03	1.100E-03		
	B230308P20Rik	scl20572.1.93_142						103440278		NA			2.19	1.800E-03		
AK045942	B230325I23Rik	ri|B230325I23|PX00160A05|AK045942|1893						103170279		NA			1.59	4.000E-04		
AK046037	B230337C21Rik	ri|B230337C21|PX00160G21|AK046037|1609						104570551		NA			1.42	2.600E-03		
XM_148123.1	B430305P08Rik	GI_20892692	103390731	103390731	103390731	103390731				NA	1.34	2.787E-05	2.50	1.000E-04	2.50	0.000E+00
AK047124	B930024A20Rik	ri|B930024A20|PX00163G08|AK047124|2490						105220088		NA			1.82	3.800E-03		
	B930032C10Rik	scl36914.1.1_39						101410528		NA			2.99	3.600E-03		
AK047419	B930059J09Rik	ri|B930059J09|PX00164P14|AK047419|2089						102370402		NA			1.73	4.500E-03		
AK047526	B930083E23Rik	ri|B930083E23|PX00166G18|AK047526|4126							101940100	NA					15.55	0.000E+00
	B930093H17Rik	scl34643.1.1_311						101450670		NA			1.51	3.000E-03		
XM_144541	BC023744	scl27327.5_269		103830204						NA	0.97	6.095E-05	1.98	4.000E-04		
XM_130696.2	BC028278	scl0003169.1_64		6290273						NA	1.64	1.490E-05	3.07	1.000E-04		
XM_196119	BC036313	scl46282.36.1_17						100050400		NA			1.59	7.000E-04		
	BC037704	scl6186.1.1_212						105360156		NA			1.50	2.400E-03		
NM_198170.2	BC059842	scl23919.20.1_50						1090300		NA			1.51	2.700E-03		
	C030013C21Rik	scl077417.1_158						105130601		NA			1.90	1.100E-03		
	C030014C12Rik	scl43324.1.1_319						104590121		NA			2.46	6.000E-04		

			limma, sam & ttest	limma & sam	limma & ttest	sam & ttest	only in limma	only in sam	only in ttest							
Accession	all-symbol	Transcript	Probe Id	Probe Id	Probe Id	Probe Id	Probe Id	Probe Id	Probe Id	Gene name	limma FC	limma p value	sam FC	sam p value	ttest FC	ttest p value
	C130065N10Rik	scl13693.1.1_207						102340390		NA			2.03	2.300E-03		
	C130080N23Rik	scl0226829.2_26							107000398	NA					2.05	1.850E-02
	C230037E05Rik	scl30422.1.1_0						101500541		NA			1.40	2.000E-03		
	C230052J16Rik	scl0320066.1_45						105670497		NA			1.38	3.200E-03		
	C230053D17Rik	scl36328.1.1_139						104060452		NA			5.54	1.000E-04		
NM_175351	C330008L01Rik	scl49868.1.1_330		7100452						NA	1.00	3.214E-04	2.00	1.100E-03		
XM_131189.4	C330027G06Rik	scl068280.6_0		5910707						NA	1.46	2.904E-07	2.73	0.000E+00		
	C530036F05Rik	scl25696.1.1_219						104570338		NA			1.58	1.000E-04		
	C530044C16Rik	scl30055.6_520		100460168						NA	1.78	2.192E-05	3.27	3.000E-04		
	C530050I23Rik	scl45236.1_85						104560091		NA			5.66	3.600E-03		
AK050029	C730004I03Rik	ri|C730004I03|PX00086I18|AK050029|1504		100730435						NA	2.50	1.051E-04	3.29	1.300E-03		
	C730009D12	scl51859.1.3752_6						102680632		NA			1.45	9.000E-04		
AK050083	C730013O11Rik	ri|C730013O11|PX00086H23|AK050083|2881						101780373		NA			2.63	1.000E-04		
XM_358863	Cblb	scl49037.1.1_264						106520066		NA			1.52	5.000E-04		
XM_356367.1	Cdkl5	scl53651.15.1_42						2450070		NA			1.88	1.700E-03		
XM_489839	Cecr2	scl00330409.1_0						100130039		NA			1.66	1.300E-03		
XM_123188.1	Cox7a2l	scl020463.2_41							1500142	NA					3.27	2.780E-02
XM_489496	Crebbp	scl0012914.1_86						106590601		NA			2.86	3.000E-03		
XM_358301	Crsp3	scl39078.31_431						104570497		NA			1.44	1.600E-03		
AK050771	D030018H12Rik	ri|D030018H12|PX00179M07|AK050771|2374						103830286		NA			3.23	1.900E-03		
AK083690	D030067L12Rik	ri|D030067L12|PX00181K23|AK083690|1985						101170273		NA			1.98	5.000E-04		
	D0Kist3	scl0027492.1_262						106020161		NA			1.49	8.000E-04		
AK083827	D130017D19Rik	ri|D130017D19|PX00182L09|AK083827|3639						101990497		NA			1.71	1.000E-04		
	D130043N08Rik	scl0103250.1_3						104200215		NA			1.47	2.700E-03		
AK083927	D130064A21Rik	ri|D130064A21|PX00185A16|AK083927|3523						101940400		NA			1.99	1.200E-03		
	D130086K05Rik	scl00319882.1_22		100110095						NA	1.36	8.628E-06	2.51	2.000E-04		
	D15Bwg0759e	scl052877.1_143						100870373		NA			1.58	1.500E-03		
	D1Ertd471e	scl14355.1.1_113							106420008	NA					2.67	1.160E-02
AK051848	D230009O13Rik	ri|D230009O13|PX00187L08|AK051848|2469						103190746		NA			3.44	2.400E-03		
	D230016O17	scl44414.1.1_179		107000288						NA	0.80	4.133E-06	1.74	1.000E-04		
AK051900	D230017B08Rik	ri|D230017B08|PX00188J17|AK051900|1932						106380079		NA			1.46	2.900E-03		
AK051902	D230017C05Rik	ri|D230017C05|PX00188N16|AK051902|1673						102450170		NA			1.40	1.300E-03		
AK084320	D230023E14Rik	ri|D230023E14|PX00188D01|AK084320|2990		102370747						NA	0.94	2.024E-04	1.92	5.000E-04		
AK051990	D230032H14Rik	ri|D230032H14|PX00189J17|AK051990|2210						101570484		NA			2.08	1.500E-03		
AK084442	D230047F17Rik	ri|D230047F17|PX00189J18|AK084442|2755						103610400		NA			2.61	1.200E-03		
XM_283282	D330001F17Rik	scl00223658.1_328						104850538		NA			1.50	5.000E-04		
AK084991	D430021P20Rik	ri|D430021P20|PX00194K01|AK084991|3702						102480242		NA			5.85	0.000E+00		
AK085184	D430050H21Rik	ri|D430050H21|PX00195J19|AK085184|1293						101240398		NA			1.65	1.500E-03		
XM_485743	D630045J12Rik	scl0330286.2_10	105420576	105420576	105420576	105420576				NA	1.33	4.178E-05	2.63	4.000E-04	2.63	5.000E-04
	D6Ertd245e	scl00269774.1_129		104610292						NA	1.11	1.894E-04	2.07	1.600E-03		
	D6Ertd245e	scl28743.1.6_282		104810494						NA	1.89	2.530E-05	3.45	0.000E+00		
	D730035F11Rik	scl35255.1_653						101400121		NA			5.18	3.000E-04		
AK052952	D930002M03Rik	ri|D930002M03|PX00200H23|AK052952|1695						102060452		NA			1.79	2.700E-03		
	D930014N22Rik	scl0320689.1_82				102640221				NA			2.14	1.000E-04	2.14	0.000E+00
	Dlc1	scl050768.1_330						1090632		NA			2.17	6.000E-04		
XM_129566	Dusp23	scl15914.2_382		6100632						NA	0.78	2.825E-04	1.71	8.000E-04		
AK087310	E030043F19Rik	ri|E030043F19|PX00206F09|AK087310|1815		103440484						NA	3.86	8.168E-05	8.52	7.000E-04		
XM_488964	E130013N09Rik	scl20000.1_138						104730114		NA			1.65	1.900E-03		
XM_484476	E130113K22Rik	scl00239510.1_118						102690113		NA			1.49	2.900E-03		
	E130115I21Rik	scl53151.1.226_33						106550603		NA			1.55	2.400E-03		
	E230012J19Rik	scl24673.1.660_178				106590528				NA			3.31	1.000E-04	3.31	0.000E+00
AK087579	E230013N04Rik	ri|E230013N04|PX00210I14|AK087579|3262		100940148						NA	1.92	2.146E-05	3.64	1.000E-04		
AK054368	E330020G21Rik	ri|E330020G21|PX00211P24|AK054368|2866						102510373		NA			1.63	7.000E-04		
AK089149	E530016P10Rik	ri|E530016P10|PX00319A22|AK089149|1281						102630717		NA			1.42	3.000E-03		
AK089567	F830002E14Rik	ri|F830002E14|PL00004M15|AK089567|1280				105550685				NA			3.82	4.100E-03	3.82	1.000E-04
AK031454	Fbln1	ri|6030434L12|PX00056N16|AK031454|4019						102320164		NA			1.49	3.000E-04		
	Gcap3	scl0014483.1_1						6130148		NA			1.59	2.500E-03		
NM_182695.1	Ggn	scl32846.3.1_64						5290170		NA			2.11	8.000E-04		
XM_355574.1	Gnai1	scl014677.2_17						4560390		NA			4.01	3.000E-04		
	Gtf3a	scl26973.9_90						104540524		NA			1.62	1.500E-03		
NM_144513	Gtl2	scl42789.1.791_155						102340154		NA			2.63	2.400E-03		
AK031353	Gukmi1	ri|6030411A16|PX00056D06|AK031353|3346						103450315		NA			1.85	2.300E-03		
NM_010396	H2-T17	scl015032.1_236		6100440						NA	0.74	8.060E-05	1.68	1.000E-04		

		limma, sam & ttest		limma & sam	limma & ttest	sam & ttest	only in limma	only in sam	only in ttest							
Accession	all-symbol	Transcript	Probe Id	Probe Id	Probe Id	Probe Id	Probe Id	Probe Id	Probe Id	Gene name	limma FC	limma p value	sam FC	sam p value	ttest FC	ttest p value
AK036620	Hbb-b1	ri|9830142B20|PX00119K03|AK036620|3219						101660435		NA			1.63	4.300E-03		
XM_133622.3	Hbxap	scl32346.12_306							1580097	NA					2.71	1.100E-03
XM_145005.2	Iqsec3	scl28446.23_488						3360278		NA			3.02	5.000E-04		
	Klfc5b	scl0094117.1_67						5690121		NA			2.40	9.000E-04		
	Lin28	scl24855.1.1_97						100430373		NA			10.81	3.000E-04		
XM_139845.1	LOC207695	GI_20899653						101660463		NA			5.63	1.000E-03		
XM_146954.1	LOC208943	GI_20891290						101170725		NA			2.03	1.300E-03		
XM_142222.2	LOC209203	GI_38086810		104200717						NA	2.59	7.847E-06	5.27	1.000E-04		
XM_140186.2	LOC210245	GI_38082965						105570286		NA			5.43	1.000E-04		
XM_148086.4	LOC224137	GI_38079936	104010070	104010070	104010070	104010070				NA	1.95	8.767E-08	3.84	0.000E+00	3.84	0.000E+00
XM_130476.4	LOC228730	GI_38075147		106420056						NA	0.55	1.546E-04	1.46	9.000E-04		
XM_124173.2	LOC229810	GI_38077071	103130451	103130451	103130451	103130451				NA	1.28	9.225E-08	2.42	0.000E+00	2.42	0.000E+00
XM_144090.1	LOC230805	GI_20846743						106400037		NA			5.23	7.000E-04		
XM_144267.2	LOC231118	GI_38079663						104210364		NA			4.04	3.200E-03		
XM_124826.2	LOC232606	GI_38083743							102570242	NA					2.16	9.000E-03
XM_133360.2	LOC233038	GI_38086184						107100301		NA			10.03	2.000E-04		
XM_134273.2	LOC234413	GI_38089326						106860044		NA			2.98	3.000E-04		
XM_134917.5	LOC235497	GI_38089906	100730132	100730132	100730132	100730132				NA	1.58	2.879E-08	2.98	0.000E+00	2.98	0.000E+00
XM_142547.2	LOC235979	GI_38090853						105670433		NA			9.06	6.000E-04		
XM_138275.5	LOC238403	GI_38073759							103800288	NA					2.24	9.600E-03
XM_138902.2	LOC238943	GI_38075578						106860112		NA			1.53	1.300E-03		
XM_196027.3	LOC268393	GI_38091589	106760253	106760253	106760253	106760253				NA	6.07	3.025E-12	67.07	0.000E+00	67.07	0.000E+00
XM_193262.3	LOC269251	GI_38074596						106100465		NA			1.83	8.000E-04		
XM_194140.2	LOC269533	GI_38078308						102480711		NA			3.66	1.200E-03		
XM_203663.2	LOC277193	GI_38080876				100780154				NA			2.22	4.000E-04	2.22	0.000E+00
XM_285291.1	LOC329032	GI_28551257					101850546			NA	5.61	1.552E-04				
XM_149644.3	LOC380617	GI_38081863						102470168		NA			1.43	1.800E-03		
XM_358457.1	LOC380895	GI_38076058						104200056		NA			4.61	1.700E-03		
XM_358459.1	LOC380908	GI_38076347						106220373		NA			1.88	2.000E-03		
XM_354894.1	LOC380983	GI_38077453				106100520				NA			2.40	4.300E-03	2.40	1.000E-04
XM_354909.1	LOC380998	GI_38077645						101050487		NA			3.58	1.800E-03		
XM_355042.1	LOC381125	GI_38083286						102190110		NA			1.51	4.200E-03		
XM_355045.1	LOC381127	GI_38083390						102060041		NA			2.03	8.000E-04		
XM_355201.1	LOC381259	GI_38049517	103840750	103840750	103840750	103840750				NA	1.96	1.336E-07	3.87	0.000E+00	3.87	0.000E+00
XM_355213.1	LOC381270	GI_38049568						102450619		NA			2.38	1.700E-03		
XM_355233.1	LOC381292	GI_38073326	102320070	102320070	102320070	102320070				NA	1.39	1.029E-08	2.62	0.000E+00	2.62	0.000E+00
XM_355317.1	LOC381352	GI_38074568						10604041		NA			1.57	8.000E-04		
XM_358596.1	LOC381483	GI_38077274					104480273			NA	6.05	1.534E-04				
XM_358643.1	LOC381697	GI_38081745		10840487						NA	1.95	6.817E-05	3.48	2.000E-04		
XM_355753.1	LOC381758	GI_38083938						103120438		NA			2.33	1.500E-03		
XM_355797.1	LOC381795	GI_38084949	104560131	104560131	104560131	104560131				NA	1.15	5.265E-06	2.25	0.000E+00	2.25	0.000E+00
XM_355822.1	LOC381820	GI_38085360	103440402	103440402	103440402	103440402				NA	1.52	3.796E-06	2.88	0.000E+00	2.88	0.000E+00
XM_358678.1	LOC381922	GI_38087419						106650079		NA			3.50	2.100E-03		
XM_358706.1	LOC382098	GI_38090020		104560195						NA	0.88	3.666E-06	1.85	0.000E+00		
XM_356285.1	LOC382182	GI_38094076		101660706						NA	1.28	5.728E-05	2.36	7.000E-04		
XM_356781.1	LOC382972	GI_38076992						102900706		NA			1.43	3.900E-03		
XM_357101.1	LOC383514	GI_38049590						106650647		NA			1.51	1.500E-03		
XM_357160.1	LOC383619	GI_38074144						104920368		NA			2.13	2.200E-03		
XM_357442.1	LOC384129	GI_38079355					102650161			NA	4.81	2.538E-04				
XM_357563.1	LOC384313	GI_38082401						105720010		NA			2.20	2.000E-03		
XM_357564.1	LOC384315	GI_38082430						104850086		NA			1.70	1.200E-03		
XM_357740.1	LOC384607	GI_38086640		104010040						NA	1.38	2.321E-05	2.71	5.000E-04		
XM_357896.1	LOC384842	GI_38089332		105340647						NA	1.45	1.289E-05	2.68	1.000E-04		
XM_357995.1	LOC385019	GI_38088704						105890148		NA			2.60	1.000E-04		
XM_359066.1	LOC386091	GI_38081137						104060687		NA			4.63	1.700E-03		
XM_130308.2	Lrp2	scl19172.21_467						3290706		NA			1.52	1.700E-03		
NM_013597	Mef2a	scl31226.15_497						106400685		NA			1.46	2.100E-03		
NM_198619.1	MGC67181	scl0075615.1_61				5270066				NA			2.66	4.000E-04	2.66	0.000E+00
NM_198619.1	MGC67181	scl00242747.1_237						6650520		NA			1.94	3.000E-03		
XM_485570	Mll5	scl0069188.1_256							104540338	NA					12.10	8.100E-03
XM_128594.4	Ndufb10	scl50198.3.1_17			5900576					NA	3.27	6.820E-05			51.77	0.000E+00
XM_355517.1	Ndufs5	scl0170658.2_22						4010692		NA			1.31	3.700E-03		
AK077830	Neo1	ri|5930405G04|PX00646ED7|AK077830|2792		102900152						NA	2.46	3.316E-04	5.13	1.000E-04		

Accession	all-symbol	limma, sam & ttest		limma & sam	limma & ttest	sam & ttest	only in limma	only in sam	only in ttest								
		Transcript	Probe Id	Probe Id	Probe Id	Probe Id	Probe Id	Probe Id	Probe Id	Gene name	limma FC	limma p value	sam FC	sam p value	ttest FC	ttest p value
	Nme7	sc000061.1_90						106940632		NA			1.42	1.000E-03		
XM_128363.1	Chf28	sc48205.2_588						940184		NA			2.23	1.600E-03		
XM_148364.1	Parn	sc48742.24.1_21						3840129		NA			1.34	2.500E-03		
XM_134863.3	Parp6	sc36871.20.1_240		3290332						NA	0.77	9.821E-05	1.69	4.000E-04		
NM_008556.1	Pxa15	sc115925.5_61						4590685		NA			1.33	1.000E-03		
XM_135820.3	Pfc	sc54357.9.1_59						2100619		NA			1.43	1.800E-03		
XM_484060	Pprn1e	sc93758.7_531						102480465		NA			1.37	1.400E-03		
NM_012022.1	Pprnr	sc53007.3.1_70						2940138		NA			1.71	4.000E-04		
XM_131309.2	Prdm13	sc245674_95						1430022		NA			1.74	4.100E-03		
XM_484024	Rapgef6	sc93192786.10_13						102470537		NA			2.38	5.000E-04		
XM_289906.2	Ribp2	Gi_38084937						100550044		NA			1.81	6.000E-04		
NM_011248	Robo3	sc9196492_21				6550408				NA			3.52	2.400E-03	3.52	0.000E+00
AK037457	Sin3a	ri|A130020A06|PX00121023|AK037457|3936	105720707							NA	3.67	2.973E-08	12.45	0.000E+00		
XM_147213.1	Slc15a2	sc48560.72_173							1780538	NA					2.22	1.110E-02
XM_128634.4	Slc35b1	sc50680.6_424		7000735						NA	0.65	5.621E-05	1.56	1.700E-03		
	Tcra	sc92147.3_14					101850040			NA	8.05	1.790E-07				
XM_130797	Tnik	sc21325.34_214						100430148		NA			1.87	1.000E-04		
	Zfp125	sc80022651.1_9							101230408	NA					2.84	2.830E-02
XM_147215.1	Zfp288	sc80056490.1_199							5720450	NA					2.14	2.500E-03
XM_111053	Zfx11	sc80195018.6_13						106180398		NA			1.87	3.000E-04		
		sc80001671.1_105						102510520		NA			3.21	1.000E-03		
		sc80003389.1_16						107040315		NA			1.98	6.000E-04		
		sc8000826.1_68						101580142		NA			3.53	3.000E-04		
		mtDNA_ND4L						104480538		NA			3.40	9.000E-04		
		sc80002397.1_19						102810746		NA			3.04	1.700E-03		
		sc80003138.1_13						100870347		NA			2.08	2.000E-04		
		28S_rRNA_X06525_656						106250039		NA			3.99	4.000E-04		
		NeoR							104060685	NA					0.09	0.000E+00
NM_177619.2	Myo1e	sc139693.17_117							4540494	MYST histone acetyltransferase 2					2.16	2.000E-04
NM_028860.1	Ntmr3	sc80074302.1_179		1050314						myotubularin related protein 3	0.86	1.884E-04	1.78	3.000E-04		
AK088715	E430024E16Rik	ri|E430024E16|PX00109824|AK088715|3095						100610075		myotubularin related protein 10			1.48	3.800E-03		
NM_080728.1	Myh7	sc80014078.1_330							6220398	myosin, heavy polypeptide 7, cardiac muscle, beta					5.67	3.740E-02
NM_019914.2	Af389462	sc8056772.1_0		5080278						myeloid/lymphoid or mixed-lineage leukemia (trithorax homolog, Drosophila); translocated to, 11	0.69	3.554E-04	1.58	4.500E-03		
NM_008665.2	Myl1	GI_23346428	6770524	6770524	6770524	6770524				myelin transcription factor 1	1.18	6.902E-05	2.14	1.200E-03	2.14	0.000E+00
NM_008628.1	Mjh2	sc50397.16.1_24						6180273		mut5 homolog 2 (E. coli)			3.12	1.000E-03		
AK037967	Nkiin1	ri|A130067M19|PX00124195|AK037967|3636	105080390							muskelin 1, intracellular mediator containing kelch motifs	0.81	1.477E-04	1.73	5.000E-04		
NM_008624.2	Nras	sc8017532.3_105						2030524		muscle and microspikes RAS			1.35	2.000E-03		
NM_001001979	3000002B06Rik	sc115160.1.1_303						103120132		multiple EGF-like-domains 10			1.50	2.500E-03		
NM_134160.1	Mcoln3	sc8017166.12_30		2850398						mucolipin 3	0.85	3.325E-05	1.80	2.000E-04		
NM_028832.1	1700007D05Rik	sc137671.3.1_35						4810594		MTERF domain containing 3			2.23	4.000E-03		
NM_008622.1	Npv17	sc8017527.1_149						1190133		Mpv17 transgene, kidney disease mutant			1.34	2.200E-03		
NM_172778.1	Maob	sc54377.16.1_8		2970520						monoamine oxidase B	0.63	6.686E-05	1.55	1.300E-03		
NM_145571.1	Mob4b	sc80023157.2_1	4810373	4810373	4810373	4810373				MO81, Mps One Binder kinase activator-like 1B (yeast)	1.41	2.752E-09	2.66	0.000E+00	2.66	0.000E+00
AK078977	9130604K18Rik	ri|9130604K18|PX00651P17|AK078977|1002	103940237							mitogen-activated protein kinase-activated protein kinase 3	2.77	3.285E-04	3.40	1.000E-03		
NM_013871.2	Mapk12	sc80002436.1_22						450022		mitogen-activated protein kinase 12			1.86	9.000E-04		
NM_009006	Mapk12	sc52873.29_9						106550112		mitogen activated protein kinase kinase kinase 2			1.63	3.200E-03		
NM_027115.1	2310009E07Rik	sc80536.3_403						460372		mitogen activated protein kinase 1 interacting protein 1			1.84	2.900E-03		
AK010766	2410112C06Rik	ri|2410112C06|i:	102450601	102450601	102450601	102450601				mitochondrial translational initiation factor 2	2.42	4.618E-05	3.90	1.600E-03	3.90	0.000E+00
NM_173757.2	Mrps27	sc44467.12_5	4850546	4850546	4850546	4850546				mitochondrial ribosomal protein S27	3.34	3.501E-10	10.77	0.000E+00	10.77	0.000E+00
NM_025544	1500003E24Rik	sc80072204.1_2						102450138		mitochondrial ribosomal protein S15			1.98	2.300E-03		
NM_183086	Mrps10	sc8064657.6_146	4880300	4880300	4880300	4880300				mitochondrial ribosomal protein S10	2.90	1.162E-04	4.33	2.900E-03	4.33	0.000E+00
NM_025430.1	Mrp35	sc8066223.2_69			3980671					mitochondrial ribosomal protein L35	2.47	1.299E-04			37.99	0.000E+00
NM_027436.1	Mpep	sc870478.15_14	6370497	6370497	6370497	6370497				mitochondrial intermediate peptidase	2.96	2.936E-05	7.80	0.000E+00	7.80	0.000E+00
NM_144898.1	BC008103	sc219957.9.1_32						2030026		mitochondrial ribosomal protein L41			1.41	4.000E-04		
AK039532	A330055K22Rik	ri|A330055K22|PX00132C01|AK039532|2339			103830193					microtubule-associated protein 2			2.57	7.000E-04	2.57	0.000E+00
NM_019946.3	Mgst1	sc29413.4.6_35		6020605						microsomal glutathione S-transferase 1	2.84	1.292E-06	5.97	1.600E-04		
NM_028557.1	Mbd3l1	sc137257.3.1_106						2940162		methyl-CpG binding domain protein 3-like 1			3.57	8.000E-04		

		limma, sam & ttest		limma & sam	limma & ttest	sam & ttest	only in limma	only in sam	only in ttest							
Accession	all-symbol	Transcript	Probe Id	Probe Id	Probe Id	Probe Id	Probe Id	Probe Id	Probe Id	Gene name	limma FC	limma p value	sam FC	sam p value	ttest FC	ttest p value
NM_145569	Mat2a	scl0232087.1_5		4070026						methionine adenosyltransferase II, alpha	1.73	1.653E-05	3.39	3.000E-04		
NM_013603.1	Mt3	scl017751.1_8		1450537						metallothionein 3	1.56	3.393E-08	2.98	0.000E+00		
NM_008636.2	Mtf1	scl017764.4_33						2340364		metal response element binding transcription factor 1			2.38	9.000E-04		
AK044963	Mgea5	ri|B130016G05|PX00157C10|AK044963|2499						103170079		meningioma expressed antigen 5 (hyaluronidase)			1.64	4.000E-04		
NM_010367	Baiap1	scl28654.30_30		104540242						membrane associated guanylate kinase, WW and PDZ domain containing 1	0.82	4.265E-05	1.78	6.000E-04		
NM_023061.1	Mcam	scl37042.16_496						6620577		melanoma cell adhesion molecule			1.38	2.400E-03		
NM_008627.1	Mrg2	scl33055.5.1_62		4850450						Meis homeobox 3	0.42	1.936E-04	1.34	1.200E-03		
AK032947	Meis1	ri|6720477P20|PX00060C14|AK032947|2638						102190563		Meis homeobox 1			1.55	5.000E-04		
NM_008613.1	Mns1	scl36733.11.1_17						5690528		meiosis-specific nuclear structural protein 1			1.54	1.300E-03		
NM_026042.2	Ixl	scl31581.5.1_37						2630100		mediator complex subunit 29			1.63	1.500E-03		
NM_013634.1	Pparbp	scl0001273.1_3109		4280131						mediator complex subunit 1	0.99	2.055E-04	2.03	5.000E-04		
NM_010751	Mad	scl28748.1.533_163		100110433						MAX dimerization protein 1	3.59	2.887E-04	6.02	3.000E-04		
NM_024263	1200013A08Rik	scl074761.10_0	7100411	7100411	7100411	7100411				matrix-remodelling associated 8	1.76	2.519E-05	2.94	1.000E-03	2.94	0.000E+00
AK021409.1		scl0001284.1_18				106400100				matrix-remodelling associated 7			7.21	0.000E+00	7.21	0.000E+00
NM_010808	Mmp24	scl20046.9_689						106450368		matrix metallopeptidase 24			1.90	4.600E-03		
NM_172948.2	GnT-IX	scl026851O.16_30					2570364			mannoside acetylglucosaminyltransferase 5, isoenzyme 8	6.18	3.551E-04				
NM_010795.2	Mgat3	scl47733.1_175	2260593	2260593	2260593	2260593				mannoside acetylglucosaminyltransferase 3	2.11	1.141E-07	4.35	0.000E+00	4.35	0.000E+00
NM_011746.1	Mkrn3	scl31260.1.18_287						1340270		makorin, ring finger protein, 3			1.37	3.800E-03		
NM_008600.2	Mip	scl38292.4_242		6520333						major intrinsic protein of eye lens fiber	0.98	1.680E-04	2.05	1.400E-03		
AK007898	1810058M03Rik	ri|1810058M03|ZX00043C08|AK007898|384						103140195		major facilitator superfamily domain containing 11			1.62	3.000E-04		
NM_011837.1	Ly6h	scl023934.2_19						5340332		lymphocyte antigen 6 complex, locus H			1.44	9.000E-04		
NM_148939.1	Ly6g5b	scl49997.2.1_244						6110129		lymphocyte antigen 6 complex, locus G5B			2.39	5.000E-04		
NM_008529	Ly6e	scl017069.4_4		5050538						lymphocyte antigen 6 complex, locus E	0.49	1.015E-04	1.41	4.000E-04		
NM_172947	2600001B17Rik	scl39516.6_65	10648004S	10648004S	10648004S	10648004S				LSM12 homolog (S. cerevisiae)	1.38	2.052E-04	2.45	2.000E-04	2.45	0.000E+00
NM_008514.1	Lrp6	scl016974.1_230						5130064		low density lipoprotein receptor-related protein 6			2.36	6.000E-04		
AK019846	Lipe	ri|4931402D16|PX00015P13|AK019846|2760						101580288		lipase, hormone sensitive			1.66	4.300E-03		
NM_022964.2	Wbscr5	scl25940.13_350						5340440		linker for activation of T cells family, member 2			1.52	3.100E-03		
NM_145833.1	Lin28	scl23699.4_5						6590672		lin-28 homolog (C. elegans)			3.15	2.000E-04		
NM_175548	Lsamp	scl49109.9_489						10485044I		limbic system-associated membrane protein			1.52	7.000E-04		
AK090339	Lhx6	ri|G630055O13|PL00013O12|AK090339|1552						101990373		LIM homeobox protein 6			2.44	1.100E-03		
NM_008499.2	Lhx5	scl016873.7_45		2350097						LIM homeobox protein 5	0.71	6.650E-05	1.65	2.000E-04		
NM_008498	Lhx1	scl39807.6_296				104010706				LIM homeobox protein 1			3.34	2.500E-03	3.34	0.000E+00
NM_008498.1	Lhx1	scl0016869.2_138				1690100				LIM homeobox protein 1			2.77	4.200E-03	2.77	0.000E+00
AK045341	B130066H02Rik	ri|B130066H02|PX00158P04|AK045341|4142		103140048						LIM domain containing preferred translocation partner in lipoma	0.68	2.548E-04	1.59	1.100E-03		
AK077424	5730406F04Rik	ri|5730406F04|PX00643N15|AK077424|1751				106760368				ligand dependent nuclear receptor corepressor			2.05	1.700E-03	2.05	2.000E-04
NM_176920.2	A930016D02Rik	scl0319476.2_26						3390039		leucine-rich repeats and transmembrane domains 1			2.39	2.000E-03		
NM_144556.2	Lgi4	scl32801.8.1_2						1570577		leucine-rich repeat LGI family, member 4			1.39	3.400E-03		
NM_144945	Lgi2	scl26588.10.546_100						106840075		leucine-rich repeat LGI family, member 2			1.91	1.000E-03		
NM_024194.2	2610040E16Rik	scl22421.15_321						870685		leucine rich repeat containing 40			1.65	1.300E-03		
NM_198119.1	6430402H13Rik	scl0378937.1_229						6650193		leucine rich repeat containing 24			2.90	1.000E-04		
NM_172528.2	Lrrc1	scl0003577.1_294		6180746						leucine rich repeat containing 1	0.73	7.104E-05	1.65	4.000E-04		
NM_011150.1	Lgals3bp	scl39273.6_263		840692						lectin, galactoside-binding, soluble, 3 binding protein	2.67	1.768E-05	3.84	1.100E-03		
AK017509	5730406O13Rik	ri|5730406O13|PX00002C05|AK017509|2803						106130102		Leber congenital amaurosis 5 (human)			1.42	2.300E-03		
NM_010638.2	Bteb1	scl53274.2_128		3840022						Kruppel-like factor 9	0.79	7.828E-05	1.73	8.000E-04		
NM_133922.2	A930040G15Rik	scl0001018.1_24						540671		KRAB-A domain containing 1			2.74	2.500E-03		
NM_008443.2	Kif3a	scl0016568.1_42	6650079	6650079	6650079	6650079				kinesin family member 3A	2.38	2.523E-05	3.95	1.000E-03	3.95	0.000E+00
NM_033073.2	Krt2-7	scl47481.12.1_2	3610273	3610273	3610273	3610273				keratin 7	1.05	3.857E-05	2.11	6.000E-04	2.11	2.000E-04
NM_182782.1	BC027373	scl0207952.3_242							4780193	kelch-like 25 (Drosophila)					2.12	4.500E-03
AK052765	D630046D15Rik	ri|D630046D15|PX00197J14|AK052765|3577						102690164		kelch domain containing 5			7.90	2.000E-04		
NM_153572.1	Katnal1	scl25750.10.1_14			1570538					katanin p60 subunit A-like 1	1.02	3.704E-04			2.18	1.360E-02
NM_133727.1	Kptn	scl33059.9.1_10	3520487	3520487	3520487	3520487				kaptin	1.22	3.378E-07	2.31	1.000E-04	2.31	0.000E+00
NM_008940.1	Prss19	scl32740.6.1_76						2340440		kallikrein related-peptidase 8			1.87	2.300E-03		
AK008164	2010009J12Rik	ri|2010009J12|ZX00043L22|AK008164|1175						105080458		jumonji, AT rich interactive domain 1B (Rbp2 like)			1.37	1.700E-03		
NM_028680	Esrrbl1	scl49050.9.1_23						2360292		intraflagellar transport 57 homolog (Chlamydomonas)			1.53	2.200E-03		
AK014712	Aabp3-pending	ri|4833416M03|PX00028O22|AK014712|934		102340139						interleukin-1 receptor-associated kinase 1 binding protein 1	0.80	2.544E-04	1.73	2.000E-03		
NM_010531.1	Il18bp	scl30953.4_24		3450128						interleukin 18 binding protein	3.10	1.918E-05	3.82	3.000E-04		

Accession	all-symbol	Transcript	limma, sam & ttest Probe Id	limma & sam Probe Id	limma & ttest Probe Id	sam & ttest Probe Id	only in limma Probe Id	only in sam Probe Id	only in ttest Probe Id	Gene name	limma FC	limma p value	sam FC	sam p value	ttest FC	ttest p value
NM_133871.1	A430056A10Rik	sc00019672.1_19						6320102		interferon-induced protein 44			2.83	1.600E-03		
NM_008394.2	Ifgf3g	sc000304.1_6						3190131		interferon regulatory factor 9			2.83	3.800E-03		
NM_018738.2	Ifgp	sc0016145.5_111						2570056		interferon gamma induced GTPase			1.54	1.400E-03		
NM_010494.1	Icam2	sc039447.7.1_219						6400113		intercellular adhesion molecule 2			1.41	1.800E-03		
NM_172471.1	Itih5	sc21298.12.88_101						1720064		inter-alpha (globulin) inhibitor H5			2.21	7.000E-04		
NM_013565.2	Itga3	sc39694.29_139					4570427			integrin alpha 3	0.82	2.166E-04				
AK035769		9930002P13Rik r|9930002P13|PX00114015|AK035769|3477						105290592		integrator complex subunit 9			1.55	1.000E-03		
AK040147		A430070A22Rik r|A430070A22|PX00138M21|AK040147|2230						103390706		integrator complex subunit 3			1.37	3.200E-03		
NM_018741	Igfbpl1	sc24366.5_218						2510685		insulin-like growth factor binding protein-like 1			1.67	2.700E-03		
AK030096	Igf2bp3	r|4932441J09|PX00019A23|AK030096|4154						103130605		insulin-like growth factor 2 mRNA binding protein 3			1.37	7.000E-04		
NM_173027.1	D830007E07Rik	sc50139.6.1_395						4730358		inositol hexaphosphate kinase 3			2.64	1.700E-03		
NM_053261.1	Impa2	sc00114463.2_25						1980070		inositol (myo)-1(or 4)-monophosphatase 2			1.40	9.000E-04		
AK030841		5830420C15Rik r|5830420C15|f	107050025	107050025	107050025	107050025				inner membrane protein, mitochondrial	1.02	1.131E-04	2.06	5.000E-04	2.06	0.000E+00
NM_133345.1	Ing4	sc028019.8_226						5290706		inhibitor of growth family, member 4			1.33	3.400E-03		
NM_009349	Tkmt	sc28971.3_6	2320020	2320020	2320020	2320020				indolethylamine N-methyltransferase	1.74	5.845E-05	3.54	3.000E-04	3.54	1.700E-03
NR_001463.2	Xist	sc002137421_1	104280446	104280446	104280446	104280446				inactive X specific transcripts	-4.57	1.445E-04	30.09	0.000E+00	30.09	1.000E-04
NM_012043.2	Idr	sc026968.1_121						6450368		immunoglobulin superfamily containing leucine-rich repeat			1.54	9.000E-04		
NM_053262.2	Dhrs8	sc0114664.1_62						4540239		hydroxysteroid (17-beta) dehydrogenase 11			1.55	1.400E-03		
NM_133943	Hsd3b7	sc3063.3.2.1_192						103320619		hydroxy-delta-5-steroid dehydrogenase, 3 beta- and steroid			2.09	6.000E-04		
NM_026897	Haghl	sc50175.2.2489_38						101980112		hydroxyacylglutathione hydrolase-like			1.43	3.000E-03		
AK050856		D030036I11Rik r|D030036I11|PX00179A05|AK050856|1070						104200358		hydroxyacyl-A-coenzyme A dehydrogenase/3-ketoacyl-Coenzyme A			1.31	4.400E-03		
NM_019986	Habp4	sc0036541.13_2		840487						hyaluronic acid binding protein 4	1.78	1.570E-06	3.71	2.000E-04		
NM_008316.2	Hus1	sc0155574.1_13						3440494		Hus1 homolog (S. pombe)			2.17	4.000E-04		
NM_019752.2	Prss25	sc28806.5.1_108		1400025						HtrA serine peptidase 2	0.67	1.161E-04	1.60	3.000E-04		
NM_019752.2	Prss25	sc0001172.1_55						130048		HtrA serine peptidase 2			1.57	3.000E-04		
AK003784		1110018K11Rik r|1110018K11|f	103850021	103850021	103850021	103850021				HOP homeobox	5.69	1.415E-06	40.52	0.000E+00	40.52	0.000E+00
NM_010468.1	Hoxd3	sc0154342_98		6450154						homeo box D3	3.37	2.078E-04	8.04	1.000E-04		
NM_130432.1	Hox62	sc0103889.1_67		6450592						homeo box B2	0.83	5.490E-05	1.79	2.000E-04		
NM_010451.1	Hoxa2	sc29068.2.1_47						2120121		homeo box A2			1.46	5.000E-04		
NM_178592.2	Bat5	sc50792.22.1_75						5720687		HLA-B associated transcript 5			1.40	3.500E-03		
NM_144919.1	Hdac11	sc29747.11_233						2510242		histone deacetylase 11			1.40	3.300E-03		
NM_175657	Hist1h4m	sc00319161.1_8							6900092	histone cluster 1, H4m					2.01	4.440E-02
NM_175656	Hist1h4i	sc44225.1.12_219		106550022						histone cluster 1, H4i	2.56	1.057E-04	8.15	1.800E-03		
NM_175653.1	Hist1h3c	sc111507.1.1_324		730204						histone cluster 1, H3c	0.57	2.285E-04	1.48	2.600E-03		
NM_010399	H2-T9	sc00150051.1_246		7040044						histocompatibility 2, T region locus 9	0.63	2.164E-04	1.54	6.000E-04		
NM_023124	H2-Q8	sc01150193_96					3140093			histocompatibility 2, Q region locus 8	3.81	3.258E-06				
NM_008199.1	H2-Bl	sc00149631_90	1450373	1450373	1450373	1450373				histocompatibility 2, blastocyst	6.44	7.075E-07	58.17	0.000E+00	58.17	0.000E+00
NM_175074.1	Hmgn3	sc335436.17	4210541	4210541	4210541	4210541				high mobility group nucleosomal binding domain 3	1.79	7.915E-09	3.41	0.000E+00	3.41	0.000E+00
AK002970.1		sc00013556.1_11		103170021						high mobility group nucleosomal binding domain 3	1.01	7.667E-05	1.97	1.100E-03		
BC064076.1		sc0015365.1_6		104150390						high mobility group AT-hook 2, pseudogene 1	3.09	1.763E-05	6.65	1.000E-04		
NM_080846.1	2310056K19Rik	sc460852.4.1_7						2630088		HIG1 domain family, member 1B			1.49	1.900E-03		
NM_019424.1	Hps1	sc52469.21.1_7						2510026		Hermansky-Pudlak syndrome 1 homolog (human)			1.36	3.600E-03		
AK011016	Hbb-b1	r|2510028J08|ZX00060D20|AK011016|628							104560707	hemoglobin, beta adult major chain					3.96	3.950E-02
AK011053	Hbb-b1	r|2510039D09|ZX00056I15|AK011053|630				102230086				hemoglobin, beta adult major chain			5.62	1.660E-03	5.62	2.020E-02
AK011067	Hbb-b1	r|2510043007|ZX00060E20|AK011067|627							102510156	hemoglobin, beta adult major chain					4.52	2.440E-02
NM_133984.1	Hemk1	sc33377.113_104		5860253						HemK methyltransferase family member 1	0.67	9.509E-05	1.59	1.000E-04		
NM_013546.1	Help1	sc22295.6.1_86	6100279	6100279	6100279	6100279				heme binding protein 1	1.37	8.666E-06	2.57	1.000E-04	2.57	0.000E+00
AK044226		A930002F06Rik r|A930002F06|PX00065L01|AK044226|3749						106020139		helicase with zinc finger domain			1.60	4.000E-04		
NM_008302.2	Hspcb	sc00015516.2_144							6040093	heat shock protein 90kDa alpha (cytosolic), class B member 1					2.13	7.000E-04
AK032066	Osp94	r|6130569N16|PX00335O21|AK032066|1997						105570671		heat shock protein 4 like			1.48	1.200E-03		
NM_175199	Hspa12a	sc852332.22_483						103440592		heat shock protein 12A			1.46	2.200E-03		
NM_010477.2	Hspd1	sc015510.1_74						2030451		heat shock protein 1 (chaperonin)			1.44	1.400E-03		
NM_026812.1	1110033O09Rik	sc00686895.1_100							4230017	HD domain containing 3					3.55	2.250E-02
NM_021429.1	Hs1bp3	sc00582402.2_223	5050390							HCLS1 binding protein 3	0.77	2.708E-04	1.70	2.200E-03		
AK020478		9430068D06Rik r|9430068D06|PX00109P12|AK020478|1151						106840279		H3 histone, family 3B			1.87	2.700E-03		
NM_016750.1	H2afz	sc00517881.1_27	1470168	1470168	1470168	1470168				H2A histone family, member Z	3.43	5.150E-06	10.70	0.000E+00	10.70	0.000E+00
AK053579	Ghr	r|E130111P21|PX00091I18|AK053579|3795						100360095		growth hormone receptor			1.59	1.300E-03		
NM_020040.2	Gfer	sc50203.3_209		6450333						growth factor, erv1 (S. cerevisiae)-like (augmenter of liver regeneration)	0.81	9.042E-05	1.75	3.000E-04		

		limma, sam & ttest		limma & sam	limma & ttest	sam & ttest	only in limma	only in sam	only in ttest							
Accession	all-symbol	Transcript	Probe Id	Probe Id	Probe Id	Probe Id	Probe Id	Probe Id	Probe Id	Gene name	limma FC	limma p value	sam FC	sam p value	ttest FC	ttest p value
AK012646	Grb10	ri|2810002M10|ZX00053I11|AK012646|830				104560736				growth factor receptor bound protein 10			2.54	1.100E-03	2.54	3.000E-04
AK037997	A130070G01Rik	ri|A130070G01|PX00125K11|AK037997|2219						101230019		GRIP1 associated protein 1			1.66	8.000E-04		
NM_011824.1	Grem1	scl18860.2_108						3940180		gremlin 1			2.88	4.000E-04		
AK089856	AB041568	ri|F830033L24|PL00007A19|AK089856|4767				106760687				golgi autoantigen, golgin subfamily a, 7			10.17	0.000E+00	10.17	0.000E+00
NM_011821	Gpc6	scl023888.1_39						101090072		glypican 6			4.90	8.000E-04		
NM_010327.1	Gp1bb	scl014724.1_74						3780075		glycoprotein ib, beta polypeptide			1.70	7.000E-04		
XM_485455	2810043G13Rik	scl23691.3_135					103520100			glycine/arginine rich protein 1	0.79	2.998E-04				
NM_025638.1	2610020H15Rik	scl39769.10_186						2360524		glycerophosphodiester phosphodiesterase domain containing 1			1.38	4.300E-03		
AK033435	Gss	ri|9030204A06|PX00060F04|AK033435|3256						104850288		glutathione synthetase			1.93	1.700E-03		
NM_053108	Glrx1	scl093692.3_322							3520471	glutaredoxin					0.04	3.360E-02
NM_008168	Grik5	scl31642.18_0						3710717		glutamate receptor, ionotropic, kainate 5 (gamma 2)			1.63	2.000E-03		
NM_013540.1	Gria2	scl0014800.2_192							5080088	glutamate receptor, ionotropic, AMPA2 (alpha 2)					2.33	1.900E-03
NM_008165.2	Gria1	GI_34328127						100580563		glutamate receptor, ionotropic, AMPA1 (alpha 1)			2.18	3.500E-03		
NM_020619.2	Gcs1	scl29846.4_459						1740603		glucosidase 1			1.45	2.300E-03		
NM_031184	Glis2	scl083396.6_33						4810170		GLIS family zinc finger 2			1.83	4.000E-04		
NM_010279.2	Gfra1	scl014585.2_30		3610152						glial cell line derived neurotrophic factor family receptor alpha 1	0.64	3.225E-04	1.56	3.000E-04		
NM_175335.1	Gtf2a1	scl0083602.1_4						5390110		general transcription factor II A, 1			2.67	2.200E-03		
NM_001009950.	Gm587	GI_57977292		1090343						gene model 587, (NCBI)	0.97	1.330E-04	1.99	6.000E-04		
XM_140607.1	LOC240539	GI_20887520						103190014		gene model 336, (NCBI)			3.13	2.200E-03		
XM_357972.1	LOC384985	GI_38090184							106900441	gene model 1476, (NCBI)					36.62	0.000E+00
NM_139304.1	C430014D17Rik	scl00229542.2_217						6650195		GATA zinc finger domain containing 2B			1.62	2.500E-03		
NM_019439	Gabbr1	scl50737.21_416						101780504		gamma-aminobutyric acid (GABA-B) receptor, 1			1.96	1.300E-03		
NM_008071	Gabrb3	scl32600.10_229		105080440						gamma-aminobutyric acid (GABA-A) receptor, subunit beta 3	0.77	9.152E-05	1.68	2.600E-03		
NM_008065.2	Gabpa	scl0000109.1_23						4780301		GA repeat binding protein, alpha			2.45	1.300E-03		
AK019886.1		scl0002088.1_1						104570131		G protein-coupled receptor 177			5.47	9.000E-04		
NM_153394.2	Gpr156	scl0239845.10_235		6350609						G protein-coupled receptor 156	1.06	1.666E-04	2.03	1.500E-03		
XM_132089.2	Gpr125	scl26598.18_80	6380025	6380025	6380025	6380025				G protein-coupled receptor 125	3.51	6.194E-10	10.77	0.000E+00	10.77	0.000E+00
NM_019988.2	Gbl	scl50208.9_12						2120161		G protein beta subunit-like			1.27	3.400E-03		
AK009138	2310004H21Rik	ri|2310004H21|;	101990441	101990441	101990441	101990441				furry homolog-like (Drosophila)	1.07	1.629E-05	2.08	1.000E-04	2.08	0.000E+00
NM_010244.2	Fv1	scl0014349.2_37		2230102						Friend virus susceptibility 1	2.85	1.736E-04	5.21	3.000E-04		
AK080898	Fmr1	ri|B430202I01|PX00071A05|AK080898|1337		104920563						fragile X mental retardation syndrome 1 homolog	0.84	1.535E-05	1.78	1.000E-04		
AF114382	Fhl3	scl0002754.1_85		2650017						four and a half LIM domains 3	2.29	1.156E-04	3.37	2.000E-04		
NM_010213.1	Fhl3	scl24989.2.50_2						1090369		four and a half LIM domains 3			3.15	9.000E-04		
AK013585	Fmn2	ri|2900024F01|ZX00068N11|AK013585|1536		103390014						formin 2	3.14	2.908E-06	4.87	3.000E-04		
NM_010230.1	Fmn	scl20471.26.1_268		3520136						formin 1	2.67	6.518E-04	3.67	1.100E-03		
AK083529	D030041G07Rik	ri|D030041G07|PX00180A08|AK083529|3073						107050112		forkhead box P4			1.71	3.000E-04		
NM_028767.1	Foxp4	scl49834.18_361		6290022						forkhead box P4	0.62	8.082E-05	1.54	4.000E-04		
NM_008046.1	Fst	scl014313.3_29				1110600				follistatin			2.28	1.100E-03	2.28	1.200E-03
NM_029798.1	2810417J12Rik	scl50230.5.1_81		3360152						FLYWCH family member 2	0.73	1.691E-05	1.66	1.000E-04		
NM_183178.1	Fsd1	scl50605.12.1_93						6940576		fibronectin type 3 and SPRY domain-containing protein			1.30	3.400E-03		
NM_026218.1	Fgfr1op2	scl067529.7_122				60538				FGFR1 oncogene partner 2			2.26	6.000E-04	2.26	0.000E+00
NM_145583.1	Frag1	scl000187.1_133		2030092						FGF receptor activating protein 1	1.73	1.082E-04	2.98	2.000E-04		
NM_145583.1	Frag1	scl00233575.1_0		1050504						FGF receptor activating protein 1	0.90	1.168E-05	1.87	1.000E-04		
NM_009146	Sdfr2	scl22689.16.1_37	6370692	6370692	6370692	6370692				ferric-chelate reductase 1	1.95	6.097E-10	3.85	0.000E+00	3.85	0.000E+00
AK051779	D130078K04Rik	ri|D130078K04|PX00186I14|AK051779|3130						106620056		FERM domain containing 4B			1.56	7.000E-04		
NM_010185.2	Fcer1g	scl15940.5.1_15							5550020	Fc receptor, IgE, high affinity I, gamma polypeptide					92.12	0.000E+00
NM_173401.1	Fbxo44	scl23522.8_437	4760372	4760372	4760372	4760372				F-box protein 44	1.57	8.664E-05	2.94	0.000E+00	2.94	0.000E+00
NM_030236.1	Fbxo34	scl078938.5_60						6450026		F-box protein 34			1.76	6.000E-04		
AK076521	4833438J18Rik	ri|4833438J18|PX00638B20|AK076521|1966						102690373		F-box protein 21			1.57	8.000E-04		
AK032079	Faah	ri|6330576B15|PX00315A12|AK032079|1927						104480373		fatty acid amide hydrolase			1.91	2.300E-03		
AK046935	Fto	ri|B930005B09|PX00162P21|AK046935|1770						100060538		fat mass and obesity associated			1.56	3.400E-03		
NM_134469	Fdps	scl21952.1_54						102360463		farnesyl diphosphate synthetase			1.83	0.000E+00		
AK035488	Fanoc	ri|9530056E08|PX00113G06|AK035488|2921		100050528						Fanconi anemia, complementation group C	0.72	1.743E-04	1.63	1.800E-03		
NM_007985.1	Fanoc	scl0014088.2_59		2060022						Fanconi anemia, complementation group C	0.69	1.190E-04	1.62	1.200E-03		
NM_198860.1	AI646023	scl0192734.1_109						3940519		expressed sequence AI646023			1.43	3.500E-03		
NM_001033210.	AI427122	Gi_85986576		630114						expressed sequence AI427122	1.32	1.073E-04	2.41	5.000E-04		
NM_028042.1	Ckn1	scl071991.11_21		1240300						excision repaiross-complementing rodent repair deficiency, complementation group 8	4.03	1.189E-07	3.58	8.000E-04		

Accession	all-symbol	Transcript	limma, sam & ttest		limma & sam		limma & ttest		sam & ttest		only in limma		only in sam		only in ttest							
			Probe Id		Probe Id		Probe Id		Probe Id		Probe Id		Probe Id		Probe Id	Gene name	limma FC	limma p value	sam FC	sam p value	ttest FC	ttest p value
AK019693	4930523M17Rik	ri|4930523M17|PX00033016|AK019693|2820											101450168			eukaryotic translation initiation factor 4 gamma, 3			3.50	2.500E-03		
NM_133916.1	Eif3i9	sci27050.15.6_2											2030068			eukaryotic translation initiation factor 3, subunit B	1.47	8.000E-04				
NM_026030	Eif2s2	sci18467.8_28	2810487	2810487	2810487	2810487										eukaryotic translation initiation factor 2, subunit 2 (beta)	1.80	3.205E-08	3.52	0.000E+00	3.52	0.000E+00
NM_010120.3	Eif1a	sci51993.3_190		5080100												eukaryotic translation initiation factor 1A	0.53	2.999E-04	1.44	2.500E-03		
NM_007959.1	Etsrp71	sci31515.6.1_57							3520195							ets variant gene 2	6.39	2.100E-03				
NM_019585.2	Espn	sci23466.19.1_1		1990022												espin	1.69	6.654E-05	3.30	4.000E-04		
NM_133362	Erdr1	sci01709421_210											5890184			erythroid differentiation regulator 1					3.09	0.000E+00
NM_133362.1	Erdr1	sci00170942.1_90											6370142			erythroid differentiation regulator 1					2.04	1.510E-02
AK079301	9530095P18Rik	ri|9530095P18|PX00654M17|AK079301|2730														erythrocyte protein band 4.1-like 5	1.91	1.900E-03				
NM_145506.2	Epb41l5	sci16379.27.1_6											106450471			erythrocyte protein band 4.1-like 5	2.03	1.900E-03				
NM_026346.2	Epb41l	sci33135.23.1_86		5900300									4060440			EPS8-like 1	1.93	2.935E-04	3.80	0.000E+00		
AK017630	Ephb2	ri|5730443P23|P	103190181		103190181		103190181									Eph receptor B2	1.32	2.182E-04	2.62	3.000E-04	2.62	0.000E+00
AK086762	Echs1	ri|D930049N01|PX00203F08|AK086762|4090											101690372			enoyl Coenzyme A hydratase, short chain, 1, mitochondrial			1.39	2.500E-03		
NM_024208.3	Echdc3	sci19720.5_23											360725			enoyl Coenzyme A hydratase domain containing 3	2.16	1.200E-03				
NM_026421.1	2310057D15Rik	sci27541.6_227											840725			enolase-phosphatase 1	2.75	3.000E-04				
NM_199307	Ece1	sci00027221.1_25	3870093	3870093	3870093	3870093										endothelin converting enzyme 1	1.30	2.593E-05	2.59	7.000E-04	2.59	1.100E-03
NM_010104.2	Edn1	sci44852.5-1_6				1720047										endothelin 1			2.46	6.000E-04	2.46	7.000E-04
NM_010330.2	Emb	sci01372.9_219	610270	610270	610270	610270										embigin	2.94	7.714E-06	2.73	1.900E-03	50.95	0.000E+00
NM_148941.1	Elovl4	sci35539.6_411	5220333	5220333	5220333	5220333										elongation of very long chain fatty acids (FEN1/Elo2, SUR4/Elo3, yeast)-like 4	2.45	9.184E-11	5.44	0.000E+00	5.44	0.000E+00
AK048572	C130078D09Rik	ri|C130078D09|PX00171J01|AK048572|3060														ELMO domain containing 2			3.11	1.200E-03		
NM_010487.1	Elavl3	sci01557.1_35											100060139			ELAV (embryonic lethal, abnormal vision, Drosophila)-like 3 (Hu antigen C)			1.53	4.500E-03		
NM_033612.1	Ela1	sci46716.10.1_32											2850014			elastase 1, pancreatic			2.68	1.100E-03		
NM_053255.2	Elac1	GI_31981496		105910142									3390167			elaC homolog 1 (E. coli)	2.99	3.622E-04	4.99	1.000E-04		
NM_028133.1	Egfl6	sci01124O7.1_41											1660484			EGL nine homolog 3 (C. elegans)			1.85	7.000E-04		
NM_133222.1	Eted1	sci22460.17_298											3120086			EGF, latrophilin seven transmembrane domain containing 1			1.80	9.000E-04		
NM_032003.1	Enpp5	sci50698.5_378													1780338	ectonucleotide pyrophosphatase/phosphodiesterase 5					60.45	0.000E+00
AK089553	ENPP3	ri|F830001C18|PL0000HE13|AK089553|1749											100630707			ectonucleotide pyrophosphatase/phosphodiesterase 3	1.68	5.000E-04				
NM_0100952	Ebf2	sci46147.17_118											940324			early B-cell factor 2	1.33	3.600E-03				
AK075684	1110070O15Rik	ri|1110070O15|ZA00008E02|AK075684|303											106590341			E2F transcription factor 6	2.28	9.000E-04				
NM_177733.2	E2f2	sci0242705.6_30											5570377			E2F transcription factor 2	1.55	2.500E-03				
NM_029297.1	Dnc2lh	sci33281.4.1_129							6370471							dynein light chain roadblock-type 2	2.02	3.300E-03	2.02	3.300E-03	2.02	0.000E+00
NM_026302.2	Dctn4	sci06766.1_0											3390010			dynactin 4	1.55	3.800E-03				
XM_140740.3	LOC240672	GI_38085196				104060746										dual specificity phosphatase 5	1.06	3.421E-04			2.26	1.470E-02
NM_025869.1	2310043D21Rik	sci33938.5-1_209											1170593			dual specificity phosphatase 26 (putative)			2.47	1.500E-03		
NM_053090	Dctn6la	sci0344652.1_47							60647							down-regulated by Ctnnb1, a			5.96	3.500E-03	5.96	2.900E-03
NM_027539.3	6330415M09Rik	sci21998.21_151											2510291			E2F transcription factor 2			1.42	3.800E-03		
NM_019978.1	Dcamkl1	sci0013179.1_273									2690092					doublecortin-like kinase 1	0.64	2.447E-04				
NM_010025.2	Dcx	sci0011193.1_96				7050673										doublecortin	1.24	2.712E-04			2.10	0.000E+00
NM_007873.2	Doc2b	sci39929.9-1_88											2190021			double C2, beta			3.36	1.000E-04		
NM_016672.1	Ddc	sci0011395.2_156				670408										dopa decarboxylase	0.58	2.458E-04	1.50	2.000E-04		
NM_013739.1	Dok3	sci0003688.1_14											130347			docking protein 3			1.85	4.400E-03		
NM_007837.2	Ddit3	sci38324.4.1_0											780373			DNA-damage inducible transcript 3			1.55	2.200E-03		
AK052464	D430030C18Rik	ri|D430030C18|PX00194L13|AK052464|1287											104920377			DNA segment, Chr 6, Wayne State University 116, expressed			2.31	1.000E-03		
NM_144553.1	Dlg7	sci45647.18.1_84		3120041												discs, large homolog 7 (Drosophila)	4.94	1.616E-04	11.29	2.000E-04		
NM_198618.1	Dlgap3	sci0242667.10_106											4540113			discs, large (Drosophila) homolog-associated protein 3			1.70	3.400E-03		
NM_007584.1	Ddr1	sci45983.22_274		5220180		5220180		5220180					2340301			discoidin domain receptor family, member 1	2.43	6.711E-10	5.34	0.000E+00	5.34	0.000E+00
NM_177259.2	C630028C02Rik	sci32607.6.3_58											2640270			disabled homolog 1 (Drosophila)			2.93	8.000E-04		
NM_145217.2	Diras1	sci0208666.1_329													10473066	DIRAS family, GTP-binding RAS-like 1			1.38	2.300E-03		
NM_009955	Dpysl2	sci45397.1_353														dihydropyrimidinase-like 2					2.31	0.000E+00
AK028513	4632413C10Rik	ri|4632413C10|PX00012E03|AK028513|3156											105080373			dimyristoylphosphatidic acid acyltransferase (tEA component of 4			1.33	3.200E-03		
NM_010022	Dbt	sci23692.12_249		106180717	106180717		106180717		106180717							dihydrolipoamide branched chain transacylase E2	7.10	1.088E-10	15.45	1.000E-04	0.00	0.000E+00
NM_019670.1	Dap3	sci00056419.2_241				430692										diaphanous homolog 3 (Drosophila)	1.87	1.868E-05	3.50	0.000E+00		
NM_010046.2	Dgat1	sci47041.10.1_18											1850538			diacylglycerol O-acyltransferase 1			1.35	3.100E-03		
AK003639	Dguok	ri|1110012E08|ROO003617|AK003639|760				102340377										deoxyguanosine kinase	1.01	9.253E-05	1.95	1.400E-03		
NM_152915.1	Dner	sci16535.14_269		3610170	3610170		3610170		3610170							delta/notch-like EGF-related receptor	1.65	2.116E-04	2.56	4.100E-03	2.56	0.000E+00

		limma, sam & ttest		limma & sam	limma & ttest	sam & ttest	only in limma	only in sam	only in ttest							
Accession	all-symbol	Transcript	Probe Id	Probe Id	Probe Id	Probe Id	Probe Id	Probe Id	Probe Id	Gene name	limma FC	limma p value	sam FC	sam p value	ttest FC	ttest p value
AK014376	3300002N10Rik	ri|3300002N10|ZX00035N20|AK014376|2067						10060541		CASK interacting protein 1			2.60	4.000E-04		
NM_027937	Caskin1	scl0000101.1_564		3710500						CASK interacting protein 1	2.00	1.330E-05	3.98	0.000E+00		
NM_027937	Caskin1	scl0268932.5_13				580035				CASK interacting protein 1			2.05	0.000E+00	2.05	0.000E+00
AK031617	Csnk2a1-rs3	ri|6030461M12|PX00057P23|AK031617|1359						10105018		casein kinase 2, alpha 1 polypeptide			1.83	2.400E-03		
NM_053200.1	Ces3	scl34490.14.1_30						5050167		carboxylesterase 3			1.62	9.000E-04		
NM_007621.1	Cbr2	scl39222.8.1_55						3800102		carbonyl reductase 2			1.82	2.000E-03		
NM_178396	Car12	scl36787.11_464	5290048	5290048	5290048	5290048				carbonic anyhydrase 12	1.28	2.250E-06	2.39	0.000E+00	2.39	0.000E+00
NM_021715.1	Chst7	scl55027.2.1_78						2760066		carbohydrate (N-acetylglucosamino) sulfotransferase 7			4.11	3.000E-04		
NM_007598.2	Cap1	scl012331.2_166	2650278	2650278	2650278	2650278				CAP, adenylate cyclase-associated protein 1 (yeast)	1.84	2.664E-04	3.48	1.000E-04	3.48	0.000E+00
NM_023160.1	Cmll1	scl28759.2_148						6520500		camello-like 1			3.90	5.000E-04		
NM_009904	Clgn	scl33608.15_606		103440128						calmegin	1.16	1.332E-06	2.21	1.000E-04		
AK044660	A930030J18Rik	ri|A930030J18|PX00067E22|AK044660|3139						104230037		calcium/calmodulin-dependent protein kinase kinase 2, beta			1.68	3.000E-04		
AK086018.1		scl0002022.1_2978						103830020		calcium/calmodulin-dependent protein kinase II, delta			1.86	1.900E-03		
AK017525	5730408I11Rik	ri|5730408I11|PX00002P17|AK017525|937		100460075						calcium homeostasis endoplasmic reticulum protein	4.32	8.596E-09	19.85	0.000E+00		
NM_133189	Cacng7	scl081904.2_65						4780369		calcium channel, voltage-dependent, gamma subunit 7			2.95	1.700E-03		
NM_026908.2	Cab39l	scl46231.15_279						5670040		calcium binding protein 39-like			1.58	3.000E-04		
NM_198656.1	Gm1010	scl0381409.15_27						4590270		cadherin-like 26			2.37	1.100E-03		
NM_080437.1	Celsr3	scl0107934.22_249						7100082		cadherin EGF LAG seven-pass G-type receptor 3			1.66	1.300E-03		
NM_007666.1	Cdh6	scl47372.13.1_82	4730541	4730541	4730541	4730541				cadherin 6	1.44	6.476E-07	2.71	0.000E+00	2.71	0.000E+00
NM_201646	Btbd6	scl0399566.4_97	110088	110088	110088	110088				BTB (POZ) domain containing 6	1.40	1.501E-04	2.57	1.100E-03	2.57	1.200E-03
NM_145534.1	Btbd3	scl00228662.1_125						4200746		BTB (POZ) domain containing 3			2.07	9.000E-04		
NM_175235.3	Brunol6	scl36874.14_424						6840373		bruno-like 6, RNA binding protein (Drosophila)			2.84	2.800E-03		
NM_029815.1	Bcas1	scl0076960.2_269		2030711						breast carcinoma amplified sequence 1	1.43	7.423E-08	2.72	0.000E+00		
NM_009755.2	Bmp1	scl000373.1_361		380594						bone morphogenetic protein 1	0.69	2.437E-05	1.60	1.200E-03		
NM_027444	Bbx	scl48409.23_594						10109060		bobby sox homolog (Drosophila)			2.37	1.600E-03		
NM_027444	Bbx	scl0070508.2_288							6520112	bobby sox homolog (Drosophila)					2.04	1.900E-03
NM_029792.1	B3gat1	scl0076898.1_65						3840048		beta-1,3-glucuronyltransferase 1 (glucuronosyltransferase P)			1.61	1.200E-03		
AK051623	D130060L11Rik	ri|D130060L11|PX00185D11|AK051623|1733						103450484		BCL2-associated athanogene 4			1.57	4.000E-03		
AK041391	A630006J20Rik	ri|A630006J20|PX00144C02|AK041391|1960						104560056		BAT2 domain containing 1			1.63	2.200E-03		
AK082487	C230055K21Rik	ri|C230055K21|PX00176A15|AK082487|1881						102260400		BAT2 domain containing 1			1.73	1.700E-03		
NM_175325.2	Bbs4	scl35765.18_440	4280592	4280592	4280592	4280592				Bardet-Biedl syndrome 4 homolog (human)	2.03	3.547E-04	3.53	6.000E-04	3.53	0.000E+00
NM_153287.2	Axud1	scl35215.8_496						1230053		AXIN1 up-regulated 1			2.92	6.000E-04		
NM_153583	Apg4d	scl37228.10_481		106400086						autophagy-related 4D (yeast)	1.19	5.219E-05	2.22	1.000E-04		
NM_153583.8	Apg4d	scl00235040.2_157		3290176						autophagy-related 4D (yeast)	0.95	1.095E-06	1.92	1.000E-04		
AK081952	Abcd3	ri|C130089K18|PX00172G15|AK081952|639						106760373		ATP-binding cassette, sub-family D (ALD), member 3			1.62	1.000E-03		
NM_013850.1	Abca7	scl38697.44.1_55						6900364		ATP-binding cassette, sub-family A (ABC1), member 7			1.52	2.000E-04		
NM_013855	Abca3	scl51018.32_4						102570673		ATP-binding cassette, sub-family A (ABC1), member 3			1.43	2.500E-03		
NM_153389.2	Atp10d	scl27730.23_48						4850139		ATPase, class V, type 10D			2.92	1.000E-04		
NM_009727	Atp8a1	scl26522.39_597		101340369						ATPase, aminophospholipid transporter (APLT), class I, type 8A, member 1	1.97	1.529E-05	3.98	0.000E+00		
NM_025983.2	Atp5e	scl18252.2_52						4120411		ATP synthase, H+ transporting, mitochondrial F1 complex, epsilon subunit			1.73	1.900E-03		
NM_133884.1	AI838661	scl24858.5.1_216		6980537						ATP binding domain 1 family, member B	1.03	1.233E-05	1.99	5.000E-04		
NM_012055.1	Asns	scl29294.14.1_194		7100687						asparagine synthetase	0.81	5.451E-05	1.74	2.000E-04		
NM_178220.2	Arrb1	scl0109689.7_23		2690195						arrestin, beta 1	1.67	2.263E-04	2.73	4.000E-04		
NM_178220.2	Arrb1	scl0007.1_62		2650670						arrestin, beta 1	2.55	1.997E-04	5.18	8.000E-04		
AK033014	ARP2	ri|6820402C04|PX00023B16|AK033014|2090						106350184		ARP2 actin-related protein 2 homolog (yeast)			1.93	3.000E-04		
NM_009687	Apex1	scl46370.4_89	3190519	3190519	3190519	3190519				apurinic/apyrimidinic endonuclease 1	2.83	4.980E-05	7.13	0.000E+00	7.13	0.000E+00
AK005934	1700013A01Rik	ri|1700013A01|ZX00036P08|AK005934|1139						10640068		apoptosis, caspase activation inhibitor			1.67	1.800E-03		
AK077789	Trb	ri|5830465M17|PX00040J21|AK077789|1995						106510088		apoptosis antagonizing transcription factor			1.41	5.000E-04		
NM_177820.2	9130218O11Rik	scl47012.4_666						780731		apolipoprotein L 10b			3.02	4.300E-03		
NM_007469.2	Apoc1	scl31674.3.1_6						5900066		apolipoprotein C-I			2.02	1.500E-03		
NM_013474.1	Apoa2	scl011807.2_4						6510364		apolipoprotein A-II			4.71	1.100E-03		
NM_175270.2	5730467H21Rik	scl26364.1.722_12						6130064		ankyrin repeat domain 56			2.30	2.400E-03		
NM_019683.2	Gbif	scl36214.3_394		780102						ankyrin repeat domain 49	0.65	9.817E-05	1.56	7.000E-04		
AK032990	6720486H14Rik	ri|6720486H14|PX00060K10|AK032990|1965						105900100		ankyrin repeat and sterile alpha motif domain containing 6			1.52	2.300E-03		

		limma, sam & ttest		limma & sam	limma & ttest	sam & ttest	only in limma	only in sam	only in ttest							
Accession	all-symbol	Transcript	Probe Id	Probe Id	Probe Id	Probe Id	Probe Id	Probe Id	Probe Id	Gene name	limma FC	limma p value	sam FC	sam p value	ttest FC	ttest p value
NM_178910.1	Ankmy2	scl00217473.2_274						780600		ankyrin repeat and MYND domain containing 2			1.78	1.800E-03		
NM_181394.1	Anapc13	scl069010.2_129	3800446	3800446	3800446	3800446				anaphase promoting complex subunit 13	1.23	5.774E-06	2.23	6.000E-04	2.23	0.000E+00
AK087459	E130216C05Rik	ri|E130216C05|PX00092N04|AK087459|1156				101410136				amyloid beta (A4) precursor-like protein 2			2.52	3.000E-04	2.52	0.000E+00
NM_009597.1	Accn2	scl47526.10_548						6450465		amiloride-sensitive cation channel 2, neuronal			1.59	1.200E-03		
NM_172935	5730457F11Rik	scl50218.10.128_2		6860338						amidohydrolase domain containing 2	0.66	2.942E-04	1.58	1.100E-03		
NM_019496.2	Ammecr1	scl0056068.2_195							3800435	Alport syndrome, mental retardation, midface hypoplasia and elliptocytosis					2.14	1.350E-02
NM_181569.1	Mare	scl0017168.2_280						4010044		alpha globin regulatory element containing gene			1.56	4.400E-03		
AK043530	Aldh1a3	ri|A830006C10|PX00153E12|AK043530|1201				105700162				aldehyde dehydrogenase family 1, subfamily A3			3.19	2.300E-03	3.19	8.700E-03
NM_198608.1	Aarsl	GI_38348461						102450609		alanyl-tRNA synthetase 2, mitochondrial (putative)			3.98	1.000E-03		
AK045987	Aebp2	ri|B230331G24|PX00160H17|AK045987|2925		106550154						AE binding protein 2	1.01	5.376E-06	1.99	3.000E-04		
AK045838	Aebp2	ri|B230313N05|PX00159L17|AK045838|2923		102450048						AE binding protein 2	0.88	7.602E-06	1.84	1.000E-04		
NM_013460.1	Adra1d	scl4115.1.1_51						380035		adrenergic receptor, alpha 1d			2.80	1.100E-03		
AK048763	C230050J15Rik	ri|C230050J15|PX00175G04|AK048763|1546						102970520		adrenergic receptor kinase, beta 2			1.65	3.800E-03		
NM_182994.1	2810410P22Rik	scl0075423.2_59							1410446	ADP-ribosylation factor-like 5A					0.07	0.000E+00
NM_019718.2	Arl3	scl52400.3.8_10						5690725		ADP-ribosylation factor-like 3			1.66	1.000E-03		
NM_145760.2	Arfgap1	scl0003246.1_27						5390358		ADP-ribosylation factor GTPase activating protein 1			1.36	4.500E-03		
AK052985	D930008G03Rik	ri|D930008G03|PX00200E12|AK052985|1245						102570092		ADP-ribosylation factor GTPase activating protein 1			1.36	4.400E-03		
NM_028121.1	Adpgk	scl0072141.1_1		4200164						ADP-dependent glucokinase	0.60	2.634E-04	1.51	1.700E-03		
NM_025748.2	Deadc1	scl39143.6.1_8		1820367						adenosine deaminase, tRNA-specific 2, TAD2 homolog (S. cerevisiae)	0.59	2.156E-04	1.52	1.800E-03		
NM_007456	Ap1m1	scl33678.12.1_84		2480706						adaptor-related protein complex AP-1, mu subunit 1	0.68	6.345E-06	1.60	1.000E-04		
AK088080	E430003J01Rik	ri|E430003J01|PX00096H08|AK088080|1227						105080725		adaptor protein, phosphotyrosine interaction, PH domain and			2.00	1.300E-03		
NM_007381.2	Acadl	scl000906.1_50					6860025			acyl-Coenzyme A dehydrogenase, long-chain	3.93	4.961E-04				
NM_019426.2	Atf7ip	scl054343.15_6	2690176	2690176	2690176	2690176				activating transcription factor 7 interacting protein	2.06	1.299E-09	4.15	0.000E+00	4.15	0.000E+00
NM_009716	Atf4	scl0002504.1_31	1740195	1740195	1740195	1740195				activating transcription factor 4	5.81	9.792E-07	5.64	8.000E-04	0.02	0.000E+00
NM_009610.1	Actg2	scl28794.10.1_120						4780180		actin, gamma 2, smooth muscle, enteric			1.69	4.500E-03		
NM_027373	2600003E23Rik	scl27894.1.960_198						105700605		actin filament associated protein 1			1.39	1.400E-03		
NM_008553.2	Ascl1	scl37654.3_4						6650100		achaete-scute complex homolog-like 1 (Drosophila)			1.41	4.300E-03		
NM_029631	1810013B01Rik	scl36510.4_431						3800068		abhydrolase domain containing 14b			1.63	2.700E-03		
AK084708	D330034M21Rik	ri|D330034M21|PX00192M02|AK084708|3849						107050687		abhydrolase domain containing 10			4.64	3.100E-03		
NM_017476.1	Akap8l	scl054194.1_276						5290452		A kinase (PRKA) anchor protein 8-like			1.35	2.400E-03		
NM_009648.1	Akap1	scl0011640.2_184						110148		A kinase (PRKA) anchor protein 1			1.35	1.100E-03		
AK035797	9630005B22Rik	ri|9630005B22|PX00114P06|AK035797|3399						103710133		a disintegrin-like and metallopeptidase (reprolysin type) with			2.72	3.000E-04		
NM_172126.2	Adam1a	scl26094.1.1040_51						3800022		a disintegrin and metallopeptidase domain 1a			2.87	3.300E-03		
AK035283	2010013E09Rik	ri|9530009I20|PX00112C23|AK035283|2209						105360059		5',3'-nucleotidase, mitochondrial			2.18	2.900E-03		
NM_146256.2	BC034099	scl23947.1.22_246		3120609						4-hydroxyphenylpyruvate dioxygenase-like	1.00	3.341E-05	2.05	1.100E-03		
NM_175177.3	Bdh	scl0071911.2_148						2850390		3-hydroxybutyrate dehydrogenase, type 1			1.46	1.700E-03		
NM_011933.1	Decr2	scl0001610.1_0		6520280						2,4-dienoyl-Coenzyme A reductase 2, peroxisomal	2.72	2.851E-04	6.31	0.000E+00		
AK037239	Bpgm	ri|A030012J18|PX00063H17|AK037239|1862						101190538		2,3-bisphosphoglycerate mutase			3.77	1.500E-03		
NM_026792.2	D8Ertd319e	scl34022.8_400				4670113				1-acylglycerol-3-phosphate O-acyltransferase 5			4.25	8.000E-04	4.25	0.000E+00

THREE-DIMENSIONAL CEREBRAL VASCULATURE OF THE CBA MOUSE BRAIN: CIRCLE OF WILLIS

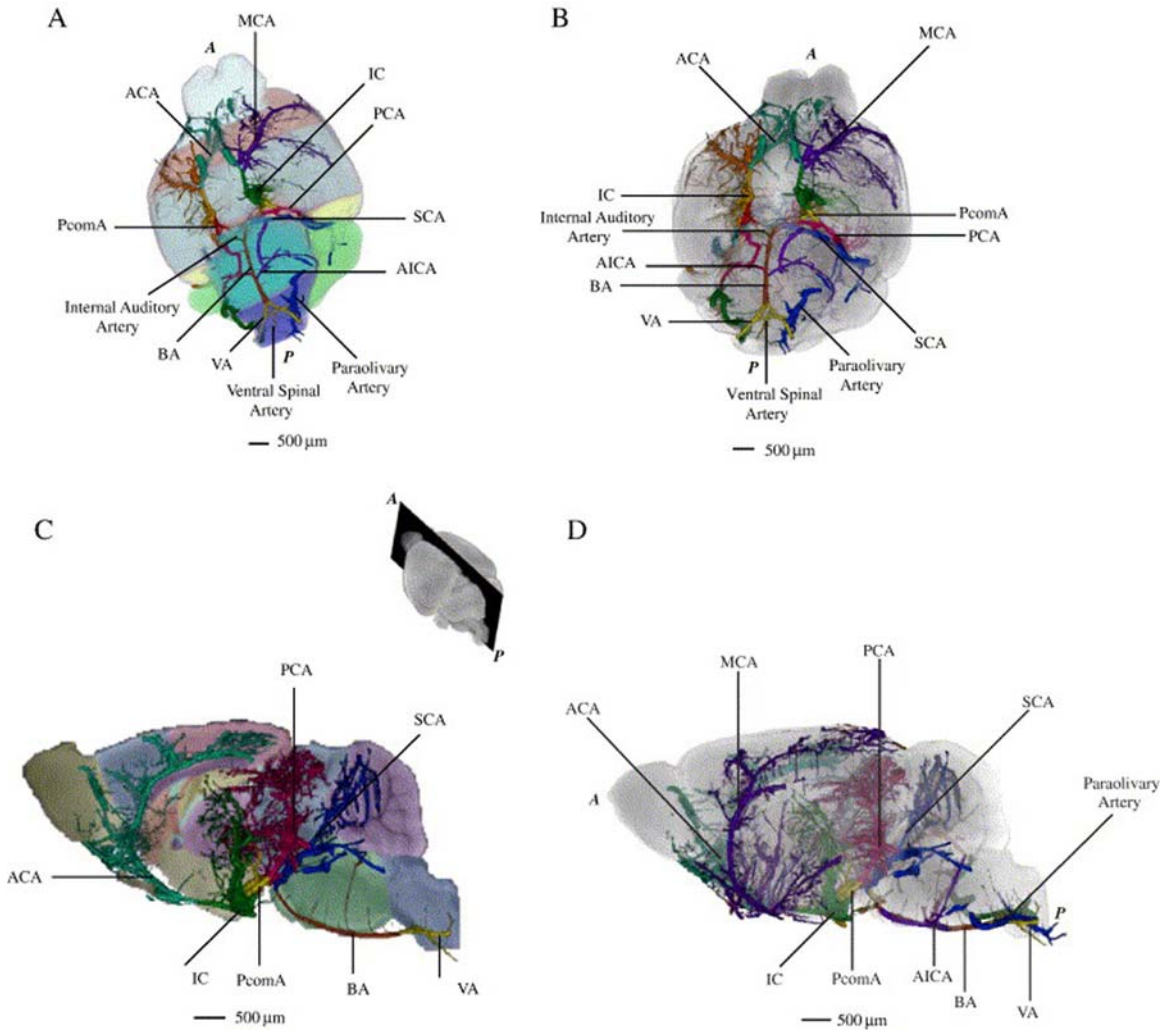

Figure A 1 Circle of Willis on mouse brain surface and all arteries on brain surface and a slice plane
(A) Circle of Willis on mouse brain surface with lobar regions depicted. The brain is shown from the inferior view at a small angle, enabling the best view possible of all arteries involved in the Circle of Willis. (B) Circle of Willis on semi-transparent mouse surface, also viewed inferiorly from an angle. (C) Arteries superimposed on a sagittal slice, midline. Insert represents the level at which the slice was taken. The MCA is excluded to allow better viewing of the internal arteries. (D) All major cerebral arteries with a semi-transparent mouse brain surface, left view. Refer to Dorr et al for a description of procedures and also abbreviations for the terms shown in this figure. Adapted from (Dorr et al., 2007).

THREE-DIMENSIONAL ANALYSIS OF VASCULAR DEVELOPMENT IN THE MOUSE EMBRYO

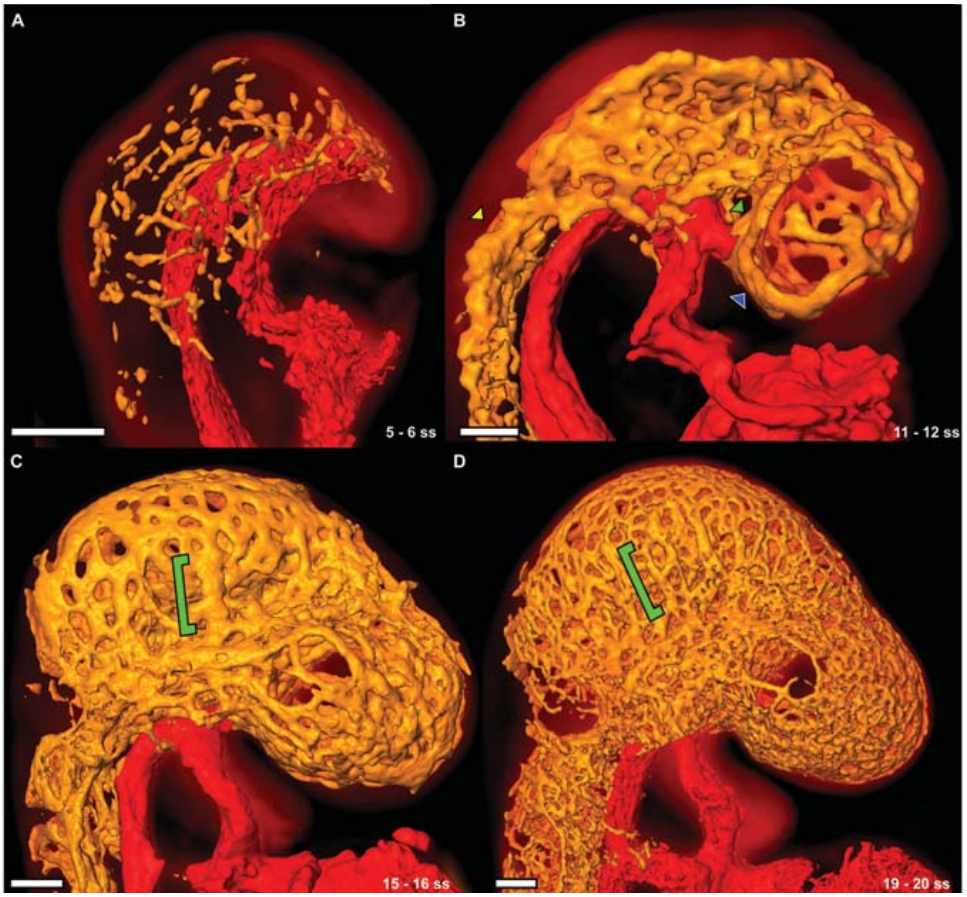

Figure A 2 Development of the cephalic plexus between the 5 and 20 somite in the mouse embryo
(A) The vasculature in the 5-somite mouse embryo is a series of disconnected clusters of PECAM-1-expressing cells. The DA and the heart are surface rendered red, PECAM-1 expression throughout the cephalic mesenchyme is surface rendered orange, and the autofluorescence of the mouse embryo is volume rendered with a hot metal colourmap. (B) By 11 somites, the cells have aggregated into a rudimentary vascular plexus. Larger vessels such as the PHV (blue arrowhead), the PMA (yellow arrowhead) and the ICA (green arrowhead) are visible (see also Supplemental Video S1). The PHV at this stage is a single large vessel that runs in an anterior-posterior direction starting from the cephalic flexure down to the first intersegmental vessel. (C) The cephalic plexus has remodeled into a more stereotypic pattern by 15 somites. The cephalic veins are easily distinguishable (green bracket). (D) At 19 somites the cephalic plexus has become more refined into recognizable structures. The cephalic veins are still visible at this stage (green bracket). All scale bars represent 100 microns. Figure and description from Walls et al, 2008.

MICROARRAY VALIDATION BY QPCR

Table A 1 Genes used in the validation of microarray data

Nestin, Notch1, Pax6 and *Sox2* were not detected by microarray but were used as positive controls. This table summarizes the results presented by Dale McAninch (McAninch, 2008). WT, wild-type; NA, not applicable.

Table A 2 Average intensity values for *Xist*, *Sox3*, *β-Actin* and *Gapdh*

Samples represented by number 1, 2 or 3. Background value of approximately 30. All *Sox3*-null (KO) samples were male, thus no expression of *Xist* was detected; whereas wild-type (WT) samples 1 and 3 were female and showed high intensity values, WT sample 2 is the pooled sample containing 3 males and 1 female giving a low intensity reading. *Sox3* shows no expression in KO samples and expression in WT samples. Both *β-Actin* and *Gapdh* show consistent readings for all samples (McAninch, 2008).

	KO				
Gene	1	2	3	4	Mean
Xist	23.82	30.86	22.55	20.2	24.35
Sox3	39.21	5.85	17.97	15.45	19.62
Beta Actin	24252.18	24953.72	17289.38	18489.24	21246.13
Gapdh	23912.19	26501.04	18702.12	23964.81	23270.04

	WT						
Gene	1	2	3	4	5	6	mean
Xist	940.08	924.29	167.15	204.43	793.34	934.86	660.69
Sox3	882.67	831.22	894.2	844.26	504.6	650.42	767.9
Beta Actin	19394.9	24051.75	22999.13	22470.25	17838.74	17426.17	20696.82
Gapdh	20751.11	25356.47	26182.25	23038.77	20015.15	24658.99	23333.79

GENERATIOIN OF MOUSE WARS ISOFORMS

The following method outline of the generation of Wars isoforms is extracted from Chin Ng's Honors thesis (Ng, 2010). Please refer to this body of work for detailed information.

The cloning strategy is outlined in the Figure A 3. First, the expression vector, pET32a-TEV-Kpn1 and pGEM-T Easy vector containing the inserts (either FL-Wars, mini-Wars, or T2-Wars) were digested with *Kpn1* and *EcoR1* enzymes. This isolated the insertswhich were then ligated into pET32a-TEV-Kpn1 vector. Digestion of pET32a vectors with *Kpn1* and *EcoR1* confirmed the ligation of *Wars* inserts. All the constructs were sequenced and confirmed that the pET32a vector contained the relevant *Wars* isoforms; in frame with the N-terminal His6 tag with no PCR-induced errors.

In order to investigate the effect of the $Wars^{L30P}$ mutation on WARS protein activity, the *Wars* coding region, containing the 220T>C mutation, was generated by site-directed mutagenesis (QuickChange™ Site-directed Mutagenesis). Site directed mutagenesis was performed using the pET32a-FL Wars as plasmid template. Sequencing results confirmed successful mutagenesis where the codon CTC encoding Leucine at residue 30 was substituted with CCC encoding a Proline. The sequencing results did not show any random mutations that may have been introduced during PCR.

NOTE:
This figure is included on page 235 of the print copy of the thesis held in the University of Adelaide Library.

Figure A 3 Cloning strategy used for generating mouse *Wars* isoforms

Cloning of different Wars isoforms insert (full length, mini and T2- Wars) into pET32a-TEV-Kpn1 expression vector that is restricted by Kpn1 and EcoR1. Successful cloning of the Wars isoforms was confirmed by sequencing. The full length Wars was then used as template for the synthesis of L30P Wars in the site-directed mutagenesis (Ng, 2010).

REFERENCES

Acevedo-Arozena, A., Wells, S., Potter, P., Kelly, M., Cox, R.D., Brown, S.D., 2008. ENU mutagenesis, a way forward to understand gene function. Annu Rev Genomics Hum Genet 9, 49-69.

Achilli, F., Bros-Facer, V., Williams, H.P., Banks, G.T., AlQatari, M., Chia, R., Tucci, V., Groves, M., Nickols, C.D., Seburn, K.L., Kendall, R., Cader, M.Z., Talbot, K., van Minnen, J., Burgess, R.W., Brandner, S., Martin, J.E., Koltzenburg, M., Greensmith, L., Nolan, P.M., Fisher, E.M., 2009. An ENU-induced mutation in mouse glycyl-tRNA synthetase (GARS) causes peripheral sensory and motor phenotypes creating a model of Charcot-Marie-Tooth type 2D peripheral neuropathy. Dis Model Mech 2, 359-373.

Adair, T.H., Gay, W.J., Montani, J.P., 1990. Growth regulation of the vascular system: evidence for a metabolic hypothesis. Am J Physiol 259, R393-404.

Agarwal, G., Bhatia, V., Cook, S., Thomas, P.Q., 2000. Adrenocorticotropin deficiency in combined pituitary hormone deficiency patients homozygous for a novel PROP1 deletion. J Clin Endocrinol Metab 85, 4556-4561.

Aguila, M.C., McCann, S.M., 1987. Evidence that growth hormone-releasing factor stimulates somatostatin release in vitro via beta-endorphin. Endocrinology 120, 341-344.

Aigner, B., Rathkolb, B., Herbach, N., Hrabe de Angelis, M., Wanke, R., Wolf, E., 2008. Diabetes models by screen for hyperglycemia in phenotype-driven ENU mouse mutagenesis projects. Am J Physiol Endocrinol Metab 294, E232-240.

Alatzoglou, K., Kelberman, D., Dattani, M., 2008. The role of SOX proteins in normal pituitary development. J Endocrinol.

Alatzoglou, K.S., Dattani, M.T., 2009. Genetic forms of hypopituitarism and their manifestation in the neonatal period. Early Hum Dev 85, 705-712.

Alatzoglou, K.S., Dattani, M.T., 2010. Genetic causes and treatment of isolated growth hormone deficiency-an update. Nat Rev Endocrinol 6, 562-576.

Alba, M., Salvatori, R., 2004. A mouse with targeted ablation of the growth hormone-releasing hormone gene: a new model of isolated growth hormone deficiency. Endocrinology 145, 4134-4143.

Alba, M., Schally, A.V., Salvatori, R., 2005. Partial reversibility of growth hormone (GH) deficiency in the GH-releasing hormone (GHRH) knockout mouse by postnatal treatment with a GHRH analog. Endocrinology 146, 1506-1513.

Alberts, B., Johnson, A., Lewis, J., Raff, M., Roberts, K., Walter, P., 2002. Molecular Biology of the Cell, 4th edition. Garland Science, New York, USA.

Ambrosetti, D.C., Basilico, C., Dailey, L., 1997. Synergistic activation of the fibroblast growth factor 4 enhancer by Sox2 and Oct-3 depends on protein-protein interactions facilitated by a specific spatial arrangement of factor binding sites. Mol Cell Biol 17, 6321-6329.

Ambrosetti, D.C., Scholer, H.R., Dailey, L., Basilico, C., 2000. Modulation of the activity of multiple transcriptional activation domains by the DNA binding domains mediates the synergistic action of Sox2 and Oct-3 on the fibroblast growth factor-4 enhancer. J Biol Chem 275, 23387-23397.

Antonellis, A., Ellsworth, R.E., Sambuughin, N., Puls, I., Abel, A., Lee-Lin, S.Q., Jordanova, A., Kremensky, I., Christodoulou, K., Middleton, L.T., Sivakumar, K., Ionasescu, V., Funalot, B., Vance, J.M., Goldfarb, L.G., Fischbeck, K.H., Green, E.D., 2003. Glycyl tRNA synthetase mutations in Charcot-Marie-Tooth disease type 2D and distal spinal muscular atrophy type V. Am J Hum Genet 72, 1293-1299.

Apelqvist, A., Li, H., Sommer, L., Beatus, P., Anderson, D.J., Honjo, T., Hrabe de Angelis, M., Lendahl, U., Edlund, H., 1999. Notch signalling controls pancreatic cell differentiation. Nature 400, 877-881.

Asa, S.L., Kovacs, K., Horvath, E., Losinski, N.E., Laszlo, F.A., Domokos, I., Halliday, W.C., 1988. Human fetal adenohypophysis. Electron microscopic and ultrastructural immunocytochemical analysis. Neuroendocrinology 48, 423-431.

Aubert, J., Stavridis, M.P., Tweedie, S., O'Reilly, M., Vierlinger, K., Li, M., Ghazal, P., Pratt, T., Mason, J.O., Roy, D., Smith, A., 2003. Screening for mammalian neural genes via fluorescence-activated cell sorter purification of neural precursors from Sox1-gfp knock-in mice. Proc Natl Acad Sci U S A 100 Suppl 1, 11836-11841.

Avilion, A.A., Nicolis, S.K., Pevny, L.H., Perez, L., Vivian, N., Lovell-Badge, R., 2003. Multipotent cell lineages in early mouse development depend on SOX2 function. Genes Dev 17, 126-140.

Baeyens, L., Bonne, S., German, M.S., Ravassard, P., Heimberg, H., Bouwens, L., 2006. Ngn3 expression during postnatal in vitro beta cell neogenesis induced by the JAK/STAT pathway. Cell Death Differ 13, 1892-1899.

Bailey, T.L., Elkan, C., 1995. The value of prior knowledge in discovering motifs with MEME. Proc Int Conf Intell Syst Mol Biol 3, 21-29.

Balthasar, N., Mery, P.F., Magoulas, C.B., Mathers, K.E., Martin, A., Mollard, P., Robinson, I.C., 2003. Growth hormone-releasing hormone (GHRH) neurons in GHRH-enhanced green fluorescent protein transgenic mice: a ventral hypothalamic network. Endocrinology 144, 2728-2740.

Bancroft, J.D., Gamble, M., 2007. Theory and Practice of Histological Techniques, 6th Edition. Churchhill Livingstone, PA, USA.

Bani-Yaghoub, M., Tremblay, R.G., Lei, J.X., Zhang, D., Zurakowski, B., Sandhu, J.K., Smith, B., Ribecco-Lutkiewicz, M., Kennedy, J., Walker, P.R., Sikorska, M., 2006. Role of Sox2 in the development of the mouse neocortex. Dev Biol 295, 52-66.

Baritaki, S., Sifakis, S., Huerta-Yepez, S., Neonakis, I.K., Soufla, G., Bonavida, B., Spandidos, D.A., 2007. Overexpression of VEGF and TGF-beta1 mRNA in Pap smears correlates with progression of cervical intraepithelial neoplasia to cancer: implication of YY1 in cervical tumorigenesis and HPV infection. Int J Oncol 31, 69-79.

Barth, K.A., Wilson, S.W., 1995. Expression of zebrafish nk2.2 is influenced by sonic hedgehog/vertebrate

hedgehog-1 and demarcates a zone of neuronal differentiation in the embryonic forebrain. Development 121, 1755-1768.

Bartke, A., 1965. The response of two types of dwarf mice to growth hormone, thyrotropin, and thyroxine. Gen Comp Endocrinol 5, 418-426.

Bartke, A., 2000. Delayed aging in Ames dwarf mice. Relationships to endocrine function and body size. Results Probl Cell Differ 29, 181-202.

Bartke, A., Lloyd, C.W., 1970. Influence of prolactin and pituitary isografts on spermatogenesis in dwarf mice and hypophysectomized rats. J Endocrinol 46, 321-329.

Bellorini, M., Lee, D.K., Dantonel, J.C., Zemzoumi, K., Roeder, R.G., Tora, L., Mantovani, R., 1997. CCAAT binding NF-Y-TBP interactions: NF-YB and NF-YC require short domains adjacent to their histone fold motifs for association with TBP basic residues. Nucleic Acids Res 25, 2174-2181.

Bergstrom, D.E., Young, M., Albrecht, K.H., Eicher, E.M., 2000. Related function of mouse SOX3, SOX9, and SRY HMG domains assayed by male sex determination. Genesis 28, 111-124.

Bertherat, J., Bluet-Pajot, M.T., Epelbaum, J., 1995. Neuroendocrine regulation of growth hormone. Eur J Endocrinol 132, 12-24.

Beverdam, A., Koopman, P., 2006. Expression profiling of purified mouse gonadal somatic cells during the critical time window of sex determination reveals novel candidate genes for human sexual dysgenesis syndromes. Hum Mol Genet 15, 417-431.

Bluet-Pajot, M.T., Epelbaum, J., Gourdji, D., Hammond, C., Kordon, C., 1998. Hypothalamic and hypophyseal regulation of growth hormone secretion. Cell Mol Neurobiol 18, 101-123.

Bokryeon, L., Kano, K., Young, J., John, S.W., Nishina, P.M., Naggert, J.K., Naito, K., 2009. A novel ENU-induced mutation, peewee, causes dwarfism in the mouse. Mamm Genome.

Boles, M.K., Wilkinson, B.M., Maxwell, A., Lai, L., Mills, A.A., Nishijima, I., Salinger, A.P., Moskowitz, I., Hirschi, K.K., Liu, B., Bradley, A., Justice, M.J., 2009. A mouse chromosome 4 balancer ENU-mutagenesis screen isolates eleven lethal lines. BMC Genet 10, 12.

Bolstad, B.M., Irizarry, R.A., Astrand, M., Speed, T.P., 2003. A comparison of normalization methods for high density oligonucleotide array data based on variance and bias. Bioinformatics 19, 185-193.

Bouchard, M., Grote, D., Craven, S.E., Sun, Q., Steinlein, P., Busslinger, M., 2005. Identification of Pax2-regulated genes by expression profiling of the mid-hindbrain organizer region. Development 132, 2633-2643.

Bowles, J., Schepers, G., Koopman, P., 2000. Phylogeny of the SOX family of developmental transcription factors based on sequence and structural indicators. Dev Biol 227, 239-255.

Bradeen, H.A., Eide, C.A., O'Hare, T., Johnson, K.J., Willis, S.G., Lee, F.Y., Druker, B.J., Deininger, M.W., 2006. Comparison of imatinib mesylate, dasatinib (BMS-354825), and nilotinib (AMN107) in an N-ethyl-N-nitrosourea (ENU)-based mutagenesis screen: high efficacy of drug combinations. Blood 108, 2332-2338.

Breier, G., Breviario, F., Caveda, L., Berthier, R., Schnurch, H., Gotsch, U., Vestweber, D., Risau, W., Dejana, E., 1996. Molecular cloning and expression of murine vascular endothelial-cadherin in early stage development of cardiovascular system. Blood 87, 630-641.

Breier, G., Clauss, M., Risau, W., 1995. Coordinate expression of vascular endothelial growth factor receptor-1 (flt-1) and its ligand suggests a paracrine regulation of murine vascular development. Dev Dyn 204, 228-239.

Brennan, J., Lu, C.C., Norris, D.P., Rodriguez, T.A., Beddington, R.S., Robertson, E.J., 2001. Nodal signalling in the epiblast patterns the early mouse embryo. Nature 411, 965-969.

Brinkmeier, M.L., Davis, S.W., Carninci, P., MacDonald, J.W., Kawai, J., Ghosh, D., Hayashizaki, Y., Lyons, R.H., Camper, S.A., 2009. Discovery of transcriptional regulators and signaling pathways in the developing pituitary gland by bioinformatic and genomic approaches. Genomics 93, 449-460.

Brinkmeier, M.L., Potok, M.A., Cha, K.B., Gridley, T., Stifani, S., Meeldijk, J., Clevers, H., Camper, S.A., 2003. TCF and Groucho-related genes influence pituitary growth and development. Mol Endocrinol 17, 2152-2161.

Brinkmeier, M.L., Potok, M.A., Davis, S.W., Camper, S.A., 2007. TCF4 deficiency expands ventral diencephalon signaling and increases induction of pituitary progenitors. Dev Biol 311, 396-407.

Brown-Borg, H.M., 2009. Hormonal control of aging in rodents: the somatotropic axis. Mol Cell Endocrinol 299, 64-71.

Brunelli, S., Silva Casey, E., Bell, D., Harland, R., Lovell-Badge, R., 2003. Expression of Sox3 throughout the developing central nervous system is dependent on the combined action of discrete, evolutionarily conserved regulatory elements. Genesis 36, 12-24.

Burlison, J.S., Long, Q., Fujitani, Y., Wright, C.V., Magnuson, M.A., 2008. Pdx-1 and Ptf1a concurrently determine fate specification of pancreatic multipotent progenitor cells. Dev Biol 316, 74-86.

Bustin, S.A., 2005. Real-time, fluorescence-based quantitative PCR: a snapshot of current procedures and preferences. Expert Rev Mol Diagn 5, 493-498.

Bylund, M., Andersson, E., Novitch, B.G., Muhr, J., 2003. Vertebrate neurogenesis is counteracted by Sox1-3 activity. Nat Neurosci 6, 1162-1168.

Caqueret, A., Boucher, F., Michaud, J.L., 2006. Laminar organization of the early developing anterior hypothalamus. Dev Biol 298, 95-106.

Carmeliet, P., 2000a. Mechanisms of angiogenesis and arteriogenesis. Nat Med 6, 389-395.

Carmeliet, P., 2000b. VEGF gene therapy: stimulating angiogenesis or angioma-genesis? Nat Med 6, 1102-1103.

Carmeliet, P., Collen, D., 2000. Molecular basis of angiogenesis. Role of VEGF and VE-cadherin. Ann N Y Acad Sci 902, 249-262; discussion 262-244.

Carmeliet, P., Ferreira, V., Breier, G., Pollefeyt, S., Kieckens, L., Gertsenstein, M., Fahrig, M., Vandenhoeck, A., Harpal, K., Eberhardt, C., Declercq, C., Pawling, J., Moons, L., Collen, D., Risau, W., Nagy, A., 1996.

Abnormal blood vessel development and lethality in embryos lacking a single VEGF allele. Nature 380, 435-439.

Carmeliet, P., Lampugnani, M.G., Moons, L., Breviario, F., Compernolle, V., Bono, F., Balconi, G., Spagnuolo, R., Oosthuyse, B., Dewerchin, M., Zanetti, A., Angellilo, A., Mattot, V., Nuyens, D., Lutgens, E., Clotman, F., de Ruiter, M.C., Gittenberger-de Groot, A., Poelmann, R., Lupu, F., Herbert, J.M., Collen, D., Dejana, E., 1999. Targeted deficiency or cytosolic truncation of the VE-cadherin gene in mice impairs VEGF-mediated endothelial survival and angiogenesis. Cell 98, 147-157.

Causton, H.C., Quackenbush, J., Brazma, A., 2003. A Beginner's Guide Microarray Gene Expression Data Analysis. Blackwell Publishing, London, UK.

Cha, K.B., Douglas, K.R., Potok, M.A., Liang, H., Jones, S.N., Camper, S.A., 2004. WNT5A signaling affects pituitary gland shape. Mech Dev 121, 183-194.

Chai, C., Chan, W.K., 2000. Developmental expression of a novel Ftz-F1 homologue, ff1b (NR5A4), in the zebrafish Danio rerio. Mech Dev 91, 421-426.

Charles, M.A., Mortensen, A.H., Potok, M.A., Camper, S.A., 2008. Pitx2 deletion in pituitary gonadotropes is compatible with gonadal development, puberty, and fertility. Genesis 46, 507-514.

Charles, M.A., Saunders, T.L., Wood, W.M., Owens, K., Parlow, A.F., Camper, S.A., Ridgway, E.C., Gordon, D.F., 2006. Pituitary-specific Gata2 knockout: effects on gonadotrope and thyrotrope function. Mol Endocrinol 20, 1366-1377.

Charles, M.A., Suh, H., Hjalt, T.A., Drouin, J., Camper, S.A., Gage, P.J., 2005. PITX genes are required for cell survival and Lhx3 activation. Mol Endocrinol 19, 1893-1903.

Cheng, T.C., Beamer, W.G., Phillips, J.A., 3rd, Bartke, A., Mallonee, R.L., Dowling, C., 1983. Etiology of growth hormone deficiency in little, Ames, and Snell dwarf mice. Endocrinology 113, 1669-1678.

Chew, J.L., Loh, Y.H., Zhang, W., Chen, X., Tam, W.L., Yeap, L.S., Li, P., Ang, Y.S., Lim, B., Robson, P., Ng, H.H., 2005. Reciprocal transcriptional regulation of Pou5f1 and Sox2 via the Oct4/Sox2 complex in embryonic stem cells. Mol Cell Biol 25, 6031-6046.

Chiang, C., Litingtung, Y., Lee, E., Young, K.E., Corden, J.L., Westphal, H., Beachy, P.A., 1996. Cyclopia and defective axial patterning in mice lacking Sonic hedgehog gene function. Nature 383, 407-413.

Cogan, J.D., Wu, W., Phillips, J.A., 3rd, Arnhold, I.J., Agapito, A., Fofanova, O.V., Osorio, M.G., Bircan, I., Moreno, A., Mendonca, B.B., 1998. The PROP1 2-base pair deletion is a common cause of combined pituitary hormone deficiency. J Clin Endocrinol Metab 83, 3346-3349.

Cohen, L.E., Radovick, S., 2002. Molecular basis of combined pituitary hormone deficiencies. Endocr Rev 23, 431-442.

Cohen, S.N., Chang, A.C., Hsu, L., 1972. Nonchromosomal antibiotic resistance in bacteria: genetic transformation of Escherichia coli by R-factor DNA. Proc Natl Acad Sci U S A 69, 2110-2114.

Collignon, J., Sockanathan, S., Hacker, A., Cohen-Tannoudji, M., Norris, D., Rastan, S., Stevanovic, M., Goodfellow, P.N., Lovell-Badge, R., 1996. A comparison of the properties of Sox-3 with Sry and two related genes, Sox-1 and Sox-2. Development 122, 509-520.

Conlon, F.L., Lyons, K.M., Takaesu, N., Barth, K.S., Kispert, A., Herrmann, B., Robertson, E.J., 1994. A primary requirement for nodal in the formation and maintenance of the primitive streak in the mouse. Development 120, 1919-1928.

Cooper, T.G., Yeung, C.H., Fetic, S., Sobhani, A., Nieschlag, E., 2004. Cytoplasmic droplets are normal structures of human sperm but are not well preserved by routine procedures for assessing sperm morphology. Hum Reprod 19, 2283-2288.

Corish, P., Tyler-Smith, C., 1999. Attenuation of green fluorescent protein half-life in mammalian cells. Protein Eng 12, 1035-1040.

Dai, X., Schonbaum, C., Degenstein, L., Bai, W., Mahowald, A., Fuchs, E., 1998. The ovo gene required for cuticle formation and oogenesis in flies is involved in hair formation and spermatogenesis in mice. Genes Dev 12, 3452-3463.

Dasen, J.S., O'Connell, S.M., Flynn, S.E., Treier, M., Gleiberman, A.S., Szeto, D.P., Hooshmand, F., Aggarwal, A.K., Rosenfeld, M.G., 1999. Reciprocal interactions of Pit1 and GATA2 mediate signaling gradient-induced determination of pituitary cell types. Cell 97, 587-598.

Dasen, J.S., Rosenfeld, M.G., 1999. Signaling mechanisms in pituitary morphogenesis and cell fate determination. Curr Opin Cell Biol 11, 669-677.

Dasen, J.S., Rosenfeld, M.G., 2001. Signaling and transcriptional mechanisms in pituitary development. Annu Rev Neurosci 24, 327-355.

Dattani, M.T., Robinson, I.C., 2000. The molecular basis for developmental disorders of the pituitary gland in man. Clin Genet 57, 337-346.

Davis, J.A., Reed, R.R., 1996. Role of Olf-1 and Pax-6 transcription factors in neurodevelopment. J Neurosci 16, 5082-5094.

Davis, S.W., Camper, S.A., 2007. Noggin regulates Bmp4 activity during pituitary induction. Dev Biol.

Davis, S.W., Castinetti, F., Carvalho, L.R., Ellsworth, B.S., Potok, M.A., Lyons, R.H., Brinkmeier, M.L., Raetzman, L.T., Carninci, P., Mortensen, A.H., Hayashizaki, Y., Arnhold, I.J., Mendonca, B.B., Brue, T., Camper, S.A., 2010. Molecular mechanisms of pituitary organogenesis: In search of novel regulatory genes. Mol Cell Endocrinol 323, 4-19.

de Boer, P., van der Hoeven, F.A., Chardon, J.A., 1976. The production, morphology, karyotypes and transport of spermatozoa from tertiary trisomic mice and the consequences for egg fertilization. J Reprod Fertil 48, 249-256.

Dejana, E., 1996. Endothelial adherens junctions: implications in the control of vascular permeability and angiogenesis. J Clin Invest 98, 1949-1953.

Dejana, E., 1997. Endothelial adherens junctions: implications in the control of vascular permeability and angiogenesis. J Clin Invest 100, S7-10.

Dellovade, T.L., Young, M., Ross, E.P., Henderson, R., Caron, K., Parker, K., Tobet, S.A., 2000. Disruption of the gene encoding SF-1 alters the distribution of hypothalamic neuronal phenotypes. J Comp Neurol 423, 579-589.

Deshmukh, S.R., Purohit, S.G., 2007. Microarray Data: Statistical Analysis Using R. Alpha Science International Ltd, Oxford, UK.

Dor, Y., Keshet, E., 1997. Ischemia-driven angiogenesis. Trends in Cardiovascular Medicine 7, 189-194.

Dorr, A., Sled, J.G., Kabani, N., 2007. Three-dimensional cerebral vasculature of the CBA mouse brain: a magnetic resonance imaging and micro computed tomography study. Neuroimage 35, 1409-1423.

Dubois, P.M., el Amraoui, A., Heritier, A.G., 1997. Development and differentiation of pituitary cells. Microsc Res Tech 39, 98-113.

Dubois, P.M., Elamraoui, A., 1995. Embryology of the pituitary gland. Trends Endocrinol Metab 6, 1-7.

Dvorak, H.F., Brown, L.F., Detmar, M., Dvorak, A.M., 1995. Vascular permeability factor/vascular endothelial growth factor, microvascular hyperpermeability, and angiogenesis. Am J Pathol 146, 1029-1039.

Ekonomou, A., Kazanis, I., Malas, S., Wood, H., Alifragis, P., Denaxa, M., Karagogeos, D., Constanti, A., Lovell-Badge, R., Episkopou, V., 2005. Neuronal migration and ventral subtype identity in the telencephalon depend on SOX1. PLoS Biol 3, e186.

Ellsworth, B.S., Butts, D.L., Camper, S.A., 2008. Mechanisms underlying pituitary hypoplasia and failed cell specification in Lhx3-deficient mice. Dev Biol 313, 118-129.

Fauquier, T., Lacampagne, A., Travo, P., Bauer, K., Mollard, P., 2002. Hidden face of the anterior pituitary. Trends Endocrinol Metab 13, 304-309.

Ferrara, N., Carver-Moore, K., Chen, H., Dowd, M., Lu, L., O'Shea, K.S., Powell-Braxton, L., Hillan, K.J., Moore, M.W., 1996. Heterozygous embryonic lethality induced by targeted inactivation of the VEGF gene. Nature 380, 439-442.

Ferrara, N., Davis-Smyth, T., 1997. The biology of vascular endothelial growth factor. Endocr Rev 18, 4-25.

Ferrara, N., Keyt, B., 1997. Vascular endothelial growth factor: basic biology and clinical implications. EXS 79, 209-232.

Ferraro, B., Cruz, Y.L., Coppola, D., Heller, R., 2009. Intradermal delivery of plasmid VEGF(165) by electroporation promotes wound healing. Mol Ther 17, 651-657.

Ferri, A.L., Cavallaro, M., Braida, D., Di Cristofano, A., Canta, A., Vezzani, A., Ottolenghi, S., Pandolfi, P.P., Sala, M., DeBiasi, S., Nicolis, S.K., 2004. Sox2 deficiency causes neurodegeneration and impaired neurogenesis in the adult mouse brain. Development 131, 3805-3819.

Ferte, C., Massard, C., Moldovan, C., Desruennes, E., Loriot, Y., Soria, J.C., 2009. Wound healing delay after central venous access following DCF/VEGF-trap therapy. Invest New Drugs.

Figdor, M.C., Stern, C.D., 1993. Segmental organization of embryonic diencephalon. Nature 363, 630-634.

Fleckner, J., Martensen, P.M., Tolstrup, A.B., Kjeldgaard, N.O., Justesen, J., 1995. Differential regulation of the human, interferon inducible tryptophanyl-tRNA synthetase by various cytokines in cell lines. Cytokine 7, 70-77.

Fleige, S., Pfaffl, M.W., 2006. RNA integrity and the effect on the real-time qRT-PCR performance. Mol Aspects Med 27, 126-139.

Fox, J.G., 2007. The Mouse in biomedical research, 2nd [upd. and rev.] ed. Academic Press, Amsterdam ; New York.

Frank, S., Hubner, G., Breier, G., Longaker, M.T., Greenhalgh, D.G., Werner, S., 1995. Regulation of vascular endothelial growth factor expression in cultured keratinocytes. Implications for normal and impaired wound healing. J Biol Chem 270, 12607-12613.

French, M.B., Moor, B.C., Lussier, B.T., Kraicer, J., 1991. Growth hormone-releasing factor does not activate protein kinase C in somatotrophs. Mol Cell Endocrinol 79, 139-146.

Frohman, L.A., Kineman, R.D., 2002a. Growth hormone-releasing hormone and pituitary development, hyperplasia and tumorigenesis. Trends Endocrinol Metab 13, 299-303.

Frohman, L.A., Kineman, R.D., 2002b. Growth hormone-releasing hormone and pituitary somatotrope proliferation. Minerva Endocrinol 27, 277-285.

Frontini, M., Imbriano, C., diSilvio, A., Bell, B., Bogni, A., Romier, C., Moras, D., Tora, L., Davidson, I., Mantovani, R., 2002. NF-Y recruitment of TFIID, multiple interactions with histone fold TAF(II)s. J Biol Chem 277, 5841-5848.

Fukui, H., Hanaoka, R., Kawahara, A., 2009. Noncanonical activity of seryl-tRNA synthetase is involved in vascular development. Circ Res 104, 1253-1259.

Gage, P.J., Suh, H., Camper, S.A., 1999. Dosage requirement of Pitx2 for development of multiple organs. Development 126, 4643-4651.

Garcia-Tornadu, I., Rubinstein, M., Gaylinn, B.D., Hill, D., Arany, E., Low, M.J., Diaz-Torga, G., Becu-Villalobos, D., 2006. GH in the dwarf dopaminergic D2 receptor knockout mouse: somatotrope population, GH release, and responsiveness to GH-releasing factors and somatostatin. J Endocrinol 190, 611-619.

Gasa, R., Mrejen, C., Leachman, N., Otten, M., Barnes, M., Wang, J., Chakrabarti, S., Mirmira, R., German, M., 2004. Proendocrine genes coordinate the pancreatic islet differentiation program in vitro. Proc Natl Acad Sci U S A 101, 13245-13250.

Gavard, J., Gutkind, J.S., 2006. VEGF controls endothelial-cell permeability by promoting the beta-arrestin-dependent endocytosis of VE-cadherin. Nat Cell Biol 8, 1223-1234.

Gaylinn, B.D., Dealmeida, V.I., Lyons, C.E., Jr., Wu, K.C., Mayo, K.E., Thorner, M.O., 1999. The mutant growth hormone-releasing hormone (GHRH) receptor of the little mouse does not bind GHRH. Endocrinology 140, 5066-5074.

Gerber, H.P., Hillan, K.J., Ryan, A.M., Kowalski, J., Keller, G.A., Rangell, L., Wright, B.D., Radtke, F., Aguet, M., Ferrara, N., 1999. VEGF is required for growth and survival in neonatal mice. Development 126, 1149-1159.

Gilbert, S.F., 2000. Developmental Biology, 6th edition. Sinauer Associates Inc., Sunderland, Massachusetts, USA.

Giustina, A., Veldhuis, J.D., 1998. Pathophysiology of the neuroregulation of growth hormone secretion in experimental animals and the human. Endocr Rev 19, 717-797.

Gradwohl, G., Dierich, A., LeMeur, M., Guillemot, F., 2000. neurogenin3 is required for the development of the four endocrine cell lineages of the pancreas. Proc Natl Acad Sci U S A 97, 1607-1611.

Gu, G., Dubauskaite, J., Melton, D.A., 2002. Direct evidence for the pancreatic lineage: NGN3+ cells are islet progenitors and are distinct from duct progenitors. Development 129, 2447-2457.

Gubbay, J., Collignon, J., Koopman, P., Capel, B., Economou, A., Munsterberg, A., Vivian, N., Goodfellow, P., Lovell-Badge, R., 1990. A gene mapping to the sex-determining region of the mouse Y chromosome is a member of a novel family of embryonically expressed genes. Nature 346, 245-250.

Gumbiner, B.M., 1996. Cell adhesion: the molecular basis of tissue architecture and morphogenesis. Cell 84, 345-357.

Hagge-Greenberg, A., Snow, P., O'Brien, T.P., 2001. Establishing an ENU mutagenesis screen for the piebald region of mouse Chromosome 14. Mamm Genome 12, 938-941.

Hanahan, D., Folkman, J., 1996. Patterns and emerging mechanisms of the angiogenic switch during tumorigenesis. Cell 86, 353-364.

Hanson, F.W., Overstreet, J.W., 1981. The interaction of human spermatozoa with cervical mucus in vivo. Am J Obstet Gynecol 140, 173-178.

Hauptmann, G., Gerster, T., 1996. Complex expression of the zp-50 pou gene in the embryonic zebrafish brain is altered by overexpression of sonic hedgehog. Development 122, 1769-1780.

Heaney, A.P., Melmed, S., 2004. Molecular targets in pituitary tumours. Nat Rev Cancer 4, 285-295.

Herzog, W., Muller, K., Huisken, J., Stainier, D.Y., 2009. Genetic evidence for a noncanonical function of seryl-tRNA synthetase in vascular development. Circ Res 104, 1260-1266.

Holder, J.L., Jr., Butte, N.F., Zinn, A.R., 2000. Profound obesity associated with a balanced translocation that disrupts the SIM1 gene. Hum Mol Genet 9, 101-108.

Huang, H.P., Liu, M., El-Hodiri, H.M., Chu, K., Jamrich, M., Tsai, M.J., 2000. Regulation of the pancreatic islet-specific gene BETA2 (neuroD) by neurogenin 3. Mol Cell Biol 20, 3292-3307.

Huber, W., von Heydebreck, A., Sultmann, H., Poustka, A., Vingron, M., 2002. Variance stabilization applied to microarray data calibration and to the quantification of differential expression. Bioinformatics 18 Suppl 1, S96-104.

Hurley, D.L., Wee, B.E., Phelps, C.J., 1997. Hypophysiotropic somatostatin expression during postnatal development in growth hormone-deficient Ames dwarf mice: mRNA in situ hybridization. Neuroendocrinology 65, 98-106.

Hynes, R.O., 1992. Specificity of cell adhesion in development: the cadherin superfamily. Curr Opin Genet Dev 2, 621-624.

Ideker, T., Thorsson, V., Siegel, A.F., Hood, L.E., 2000. Testing for differentially-expressed genes by maximum-likelihood analysis of microarray data. J Comput Biol 7, 805-817.

Ihaka, R., Gentleman, R., 1996. R: A language for data anlysis and graphics. Journal of Computational and Graphical Statistics 5, 299-314.

Ikeda, H., Suzuki, J., Sasano, N., Niizuma, H., 1988. The development and morphogenesis of the human pituitary gland. Anat Embryol (Berl) 178, 327-336.

Illig, R., Stahl, M., Henrichs, I., Hecker, A., 1971. Growth hormone release during slow-wave sleep. Comparison with insulin and arginine provocation in children with small stature. Helv Paediatr Acta 26, 655-672.

Illumina Inc, 2010. Illumina Data Sheer: Array-Based Gene Expression Analysis, San Diego, CA, USA.

Jasoni, C.L., Porteous, R.W., Herbison, A.E., 2009. Anatomical location of mature GnRH neurons corresponds with their birthdate in the developing mouse. Dev Dyn 238, 524-531.

Jensen, J., Heller, R.S., Funder-Nielsen, T., Pedersen, E.E., Lindsell, C., Weinmaster, G., Madsen, O.D., Serup, P., 2000a. Independent development of pancreatic alpha- and beta-cells from neurogenin3-expressing precursors: a role for the notch pathway in repression of premature differentiation. Diabetes 49, 163-176.

Jensen, J., Pedersen, E.E., Galante, P., Hald, J., Heller, R.S., Ishibashi, M., Kageyama, R., Guillemot, F., Serup, P., Madsen, O.D., 2000b. Control of endodermal endocrine development by Hes-1. Nat Genet 24, 36-44.

Jordanova, A., Irobi, J., Thomas, F.P., Van Dijck, P., Meerschaert, K., Dewil, M., Dierick, I., Jacobs, A., De Vriendt, E., Guergueltcheva, V., Rao, C.V., Tournev, I., Gondim, F.A., D'Hooghe, M., Van Gerwen, V., Callaerts, P., Van Den Bosch, L., Timmermans, J.P., Robberecht, W., Gettemans, J., Thevelein, J.M., De Jonghe, P., Kremensky, I., Timmerman, V., 2006. Disrupted function and axonal distribution of mutant tyrosyl-tRNA synthetase in dominant intermediate Charcot-Marie-Tooth neuropathy. Nat Genet 38, 197-202.

Jorgensen, M.C., Ahnfelt-Ronne, J., Hald, J., Madsen, O.D., Serup, P., Hecksher-Sorensen, J., 2007. An illustrated review of early pancreas development in the mouse. Endocr Rev 28, 685-705.

Josephson, R., Muller, T., Pickel, J., Okabe, S., Reynolds, K., Turner, P.A., Zimmer, A., McKay, R.D., 1998. POU transcription factors control expression of CNS stem cell-specific genes. Development 125, 3087-3100.

Kamachi, Y., Uchikawa, M., Kondoh, H., 2000. Pairing SOX off: with partners in the regulation of embryonic development. Trends Genet 16, 182-187.

Kamachi, Y., Uchikawa, M., Tanouchi, A., Sekido, R., Kondoh, H., 2001. Pax6 and SOX2 form a co-DNA-binding partner complex that regulates initiation of lens development. Genes Dev 15, 1272-1286.

Kapoor, M., Zhou, Q., Otero, F., Myers, C.A., Bates, A., Belani, R., Liu, J., Luo, J.K., Tzima, E., Zhang, D.E., Yang, X.L., Schimmel, P., 2008. Evidence for annexin II-S100A10 complex and plasmin in mobilization of cytokine activity of human TrpRS. J Biol Chem 283, 2070-2077.

Kapsimali, M., Caneparo, L., Houart, C., Wilson, S.W., 2004. Inhibition of Wnt/Axin/beta-catenin pathway activity promotes ventral CNS midline tissue to adopt hypothalamic rather than floorplate identity. Development 131, 5923-5933.

Kaufman, M.H., 1992. The Atlas of Mouse Development. Elsevier Academic Press, London, UK.

Kawahara, A., Stainier, D.Y., 2009. Noncanonical activity of seryl-transfer RNA synthetase and vascular development. Trends Cardiovasc Med 19, 179-182.

Kelberman, D., Dattani, M.T., 2006. The role of transcription factors implicated in anterior pituitary development in the aetiology of congenital hypopituitarism. Ann Med 38, 560-577.

Kelberman, D., Dattani, M.T., 2009. Role of transcription factors in midline central nervous system and pituitary defects. Endocr Dev 14, 67-82.

Kelberman, D., Rizzoti, K., Avilion, A., Bitner-Glindzicz, M., Cianfarani, S., Collins, J., Chong, W.K., Kirk, J.M., Achermann, J.C., Ross, R., Carmignac, D., Lovell-Badge, R., Robinson, I.C., Dattani, M.T., 2006. Mutations within Sox2/SOX2 are associated with abnormalities in the hypothalamo-pituitary-gonadal axis in mice and humans. J Clin Invest 116, 2442-2455.

Kermany, M.H., Parker, L.L., Guo, Y.K., Miller, D., Swanson, D.J., Yoo, T.J., Goldowitz, D., Zuo, J., 2006. Identification of 17 hearing impaired mouse strains in the TMGC ENU-mutagenesis screen. Hear Res 220, 76-86.

Kiefer, J.C., 2007. Back to basics: Sox genes. Dev Dyn 236, 2356-2366.

Kikuchi, M., Yatabe, M., Fujiwara, K., Takigami, S., Sakamoto, A., Soji, T., Yashiro, T., 2006. Distinctive localization of N- and E-cadherins in rat anterior pituitary gland. Anat Rec A Discov Mol Cell Evol Biol 288, 1183-1189.

Kikuchi, M., Yatabe, M., Kouki, T., Fujiwara, K., Takigami, S., Sakamoto, A., Yashiro, T., 2007. Changes in E- and N-cadherin expression in developing rat adenohypophysis. Anat Rec (Hoboken) 290, 486-490.

Kioussi, C., O'Connell, S., St-Onge, L., Treier, M., Gleiberman, A.S., Gruss, P., Rosenfeld, M.G., 1999. Pax6 is essential for establishing ventral-dorsal cell boundaries in pituitary gland development. Proc Natl Acad Sci U S A 96, 14378-14382.

Klagsbrun, M., D'Amore, P.A., 1996. Vascular endothelial growth factor and its receptors. Cytokine Growth Factor Rev 7, 259-270.

Kondoh, H., Uchikawa, M., Kamachi, Y., 2004. Interplay of Pax6 and SOX2 in lens development as a paradigm of genetic switch mechanisms for cell differentiation. Int J Dev Biol 48, 819-827.

Korf, I., Flicek, P., Duan, D., Brent, M.R., 2001. Integrating genomic homology into gene structure prediction. Bioinformatics 17 Suppl 1, S140-148.

Krstic, A., Mojsin, M., Stevanovic, M., 2007. Regulation of SOX3 gene expression is driven by multiple NF-Y binding elements. Arch Biochem Biophys.

Krzanowska, H., 1974. The passage of abnormal spermatozoa through the uterotubal junction of the mouse. J Reprod Fertil 38, 81-90.

Krzanowska, H., Lorenc, E., 1983. Influence of egg investments on in-vitro penetration of mouse eggs by misshapen spermatozoa. J Reprod Fertil 68, 57-62.

Kuroda, T., Tada, M., Kubota, H., Kimura, H., Hatano, S.Y., Suemori, H., Nakatsuji, N., Tada, T., 2005. Octamer and Sox elements are required for transcriptional cis regulation of Nanog gene expression. Mol Cell Biol 25, 2475-2485.

Lampugnani, M.G., Resnati, M., Raiteri, M., Pigott, R., Pisacane, A., Houen, G., Ruco, L.P., Dejana, E., 1992. A novel endothelial-specific membrane protein is a marker of cell-cell contacts. J Cell Biol 118, 1511-1522.

Laron, Z., Pertzelan, A., Mannheimer, S., 1966. Genetic pituitary dwarfism with high serum concentation of growth hormone--a new inborn error of metabolism? Isr J Med Sci 2, 152-155.

Laumonnier, F., Ronce, N., Hamel, B.C., Thomas, P., Lespinasse, J., Raynaud, M., Paringaux, C., Van Bokhoven, H., Kalscheuer, V., Fryns, J.P., Chelly, J., Moraine, C., Briault, S., 2002. Transcription factor SOX3 is involved in X-linked mental retardation with growth hormone deficiency. Am J Hum Genet 71, 1450-1455.

Lawrence, C.E., Altschul, S.F., Boguski, M.S., Liu, J.S., Neuwald, A.F., Wootton, J.C., 1993. Detecting subtle sequence signals: a Gibbs sampling strategy for multiple alignment. Science 262, 208-214.

Le Tissier, P.R., Carmignac, D.F., Lilley, S., Sesay, A.K., Phelps, C.J., Houston, P., Mathers, K., Magoulas, C., Ogden, D., Robinson, I.C., 2005. Hypothalamic growth hormone-releasing hormone (GHRH) deficiency: targeted ablation of GHRH neurons in mice using a viral ion channel transgene. Mol Endocrinol 19, 1251-1262.

Lee, D.K., Nathan Grantham, R., Trachte, A.L., Mannion, J.D., Wilson, C.L., 2006. Activation of the canonical Wnt/beta-catenin pathway enhances monocyte adhesion to endothelial cells. Biochem Biophys Res Commun 347, 109-116.

Lee, J.C., Smith, S.B., Watada, H., Lin, J., Scheel, D., Wang, J., Mirmira, R.G., German, M.S., 2001. Regulation of the pancreatic pro-endocrine gene neurogenin3. Diabetes 50, 928-936.

Lefebvre, V., Dumitriu, B., Penzo-Mendez, A., Han, Y., Pallavi, B., 2007. Control of cell fate and differentiation by Sry-related high-mobility-group box (Sox) transcription factors. Int J Biochem Cell Biol 39, 2195-2214.

Li, B., Nair, M., Mackay, D.R., Bilanchone, V., Hu, M., Fallahi, M., Song, H., Dai, Q., Cohen, P.E., Dai, X., 2005. Ovol1 regulates meiotic pachytene progression during spermatogenesis by repressing Id2 expression. Development 132, 1463-1473.

Li, X., Zhao, X., Fang, Y., Jiang, X., Duong, T., Fan, C., Huang, C.C., Kain, S.R., 1998. Generation of destabilized green fluorescent protein as a transcription reporter. J Biol Chem 273, 34970-34975.

Lin, S.C., Li, S., Drolet, D.W., Rosenfeld, M.G., 1994. Pituitary ontogeny of the Snell dwarf mouse reveals Pit-1-independent and Pit-1-dependent origins of the thyrotrope. Development 120, 515-522.

Lin, S.C., Lin, C.R., Gukovsky, I., Lusis, A.J., Sawchenko, P.E., Rosenfeld, M.G., 1993. Molecular basis of the

little mouse phenotype and implications for cell type-specific growth. Nature 364, 208-213.

Lin-Su, K., Wajnrajch, M.P., 2002. Growth Hormone Releasing Hormone (GHRH) and the GHRH Receptor. Rev Endocr Metab Disord 3, 313-323.

Lindahl, P., Johansson, B.R., Leveen, P., Betsholtz, C., 1997. Pericyte loss and microaneurysm formation in PDGF-B-deficient mice. Science 277, 242-245.

Lindsay, R., Feldkamp, M., Harris, D., Robertson, J., Rallison, M., 1994. Utah Growth Study: growth standards and the prevalence of growth hormone deficiency. J Pediatr 125, 29-35.

Liu, J., Yang, X.L., Ewalt, K.L., Schimmel, P., 2002. Mutational switching of a yeast tRNA synthetase into a mammalian-like synthetase cytokine. Biochemistry 41, 14232-14237.

Liu, J.P., Baker, J., Perkins, A.S., Robertson, E.J., Efstratiadis, A., 1993. Mice carrying null mutations of the genes encoding insulin-like growth factor I (Igf-1) and type 1 IGF receptor (Igf1r). Cell 75, 59-72.

Magoulas, C., McGuinness, L., Balthasar, N., Carmignac, D.F., Sesay, A.K., Mathers, K.E., Christian, H., Candeil, L., Bonnefont, X., Mollard, P., Robinson, I.C., 2000. A secreted fluorescent reporter targeted to pituitary growth hormone cells in transgenic mice. Endocrinology 141, 4681-4689.

Malas, S., Postlethwaite, M., Ekonomou, A., Whalley, B., Nishiguchi, S., Wood, H., Meldrum, B., Constanti, A., Episkopou, V., 2003. Sox1-deficient mice suffer from epilepsy associated with abnormal ventral forebrain development and olfactory cortex hyperexcitability. Neuroscience 119, 421–432.

Manning, L., Ohyama, K., Saeger, B., Hatano, O., Wilson, S.A., Logan, M., Placzek, M., 2006. Regional morphogenesis in the hypothalamus: a BMP-Tbx2 pathway coordinates fate and proliferation through Shh downregulation. Dev Cell 11, 873-885.

Martinis, S.A., Plateau, P., Cavarelli, J., Florentz, C., 1999. Aminoacyl-tRNA synthetases: a family of expanding functions. Mittelwihr, France, October 10-15, 1999. Embo J 18, 4591-4596.

Mathieu, J., Barth, A., Rosa, F.M., Wilson, S.W., Peyrieras, N., 2002. Distinct and cooperative roles for Nodal and Hedgehog signals during hypothalamic development. Development 129, 3055-3065.

Mazilu, J.K., Powers, J.W., Lin, S., McCabe, E.R., 2010. ff1b, the SF1 ortholog, is important for pancreatic islet cell development in zebrafish. Mol Genet Metab 101, 391-394.

McAninch, D.C., 2008. The Identification of Target Genes of the Transcription Factor Sox3 (Honours Thesis), Biochemistry. University of Adelaide, Adelaide, South Australia, Australia.

McGuinness, L., Magoulas, C., Sesay, A.K., Mathers, K., Carmignac, D., Manneville, J.B., Christian, H., Phillips, J.A., 3rd, Robinson, I.C., 2003. Autosomal dominant growth hormone deficiency disrupts secretory vesicles in vitro and in vivo in transgenic mice. Endocrinology 144, 720-731.

Mehta, A., Dattani, M.T., 2008. Developmental disorders of the hypothalamus and pituitary gland associated with congenital hypopituitarism. Best Pract Res Clin Endocrinol Metab 22, 191-206.

Mehta, A., Hindmarsh, P.C., Mehta, H., Turton, J.P., Russell-Eggitt, I., Taylor, D., Chong, W.K., Dattani, M.T., 2009. Congenital hypopituitarism: clinical, molecular and neuroradiological correlates. Clin Endocrinol (Oxf) 71, 376-382.

Mellitzer, G., Bonne, S., Luco, R.F., Van De Casteele, M., Lenne-Samuel, N., Collombat, P., Mansouri, A., Lee, J., Lan, M., Pipeleers, D., Nielsen, F.C., Ferrer, J., Gradwohl, G., Heimberg, H., 2006. IA1 is NGN3-dependent and essential for differentiation of the endocrine pancreas. Embo J 25, 1344-1352.

Melmed, S., 2010. The Pituitary, 3rd edition. Acadmic Press, San Diego, CA, USA.

Metherell, L.A., Savage, M.O., Dattani, M., Walker, J., Clayton, P.E., Farooqi, I.S., Clark, A.J., 2004. TPIT mutations are associated with early-onset, but not late-onset isolated ACTH deficiency. Eur J Endocrinol 151, 463-465.

Miyagi, S., Kato, H., Okuda, A., 2009. Role of SoxB1 transcription factors in development. Cell Mol Life Sci 66, 3675-3684.

Miyagi, S., Masui, S., Niwa, H., Saito, T., Shimazaki, T., Okano, H., Nishimoto, M., Muramatsu, M., Iwama, A., Okuda, A., 2008. Consequence of the loss of Sox2 in the developing brain of the mouse. FEBS Lett.

Miyagi, S., Nishimoto, M., Saito, T., Ninomiya, M., Sawamoto, K., Okano, H., Muramatsu, M., Oguro, H., Iwama, A., Okuda, A., 2006. The Sox2 regulatory region 2 functions as a neural stem cell-specific enhancer in the telencephalon. J Biol Chem 281, 13374-13381.

Miyagi, S., Saito, T., Mizutani, K., Masuyama, N., Gotoh, Y., Iwama, A., Nakauchi, H., Masui, S., Niwa, H., Nishimoto, M., Muramatsu, M., Okuda, A., 2004. The Sox-2 regulatory regions display their activities in two distinct types of multipotent stem cells. Mol Cell Biol 24, 4207-4220.

Mody, S., Brown, M.R., Parks, J.S., 2002. The spectrum of hypopituitarism caused by PROP1 mutations. Best Pract Res Clin Endocrinol Metab 16, 421-431.

Molina, G., Rodriguez, A., Derpich, M., Missarelli, C., Cassorla, F., Mericq, V., Carvallo, P., 2003. Isolated growth hormone deficiency in Chilean patients: clinical and molecular analysis. J Pediatr Endocrinol Metab 16, 1143-1155.

Morey, J.S., Ryan, J.C., Van Dolah, F.M., 2006. Microarray validation: factors influencing correlation between oligonucleotide microarrays and real-time PCR. Biol Proced Online 8, 175-193.

Morrison, T.B., Weis, J.J., Wittwer, C.T., 1998. Quantification of low-copy transcripts by continuous SYBR Green I monitoring during amplification. Biotechniques 24, 954-958, 960, 962.

Mortimer, D., Leslie, E.E., Kelly, R.W., Templeton, A.A., 1982. Morphological selection of human spermatozoa in vivo and in vitro. J Reprod Fertil 64, 391-399.

Mueller, O., Lightfoot, S., Schroeder, A., 2004. RNA Integrity Number (RIN)- Standardization of RNA Quality Control. Application Note. Agilent Technologies, Waldbrown, Germany.

Mullis, P.E., 2005. Genetic control of growth. Eur J Endocrinol 152, 11-31.

Murtaugh, L.C., 2007. Pancreas and beta-cell development: from the actual to the possible. Development 134, 427-438.

Nair, M., Teng, A., Bilanchone, V., Agrawal, A., Li, B., Dai, X., 2006. Ovol1 regulates the growth arrest of embryonic epidermal progenitor cells and represses c-myc transcription. J Cell Biol 173, 253-264.

National Health and Medical Research Council, 2004. Australian code of practice for the care and use of animals for scientific purposes, 7th Edition, 7th edition ed. National Health and Medical Research Council, Canberra, ACT.

Neves, J., Kamaid, A., Alsina, B., Giraldez, F., 2007. Differential expression of Sox2 and Sox3 in neuronal and sensory progenitors of the developing inner ear of the chick. J Comp Neurol 503, 487-500.

Ng, C.T., 2010. Mechanism of a novel dwarfism mutation in WARS (Honours Thesis), Biochemistry. University of Adelaide, Adelaide, South Australia, Australia, p. 123.

Nicosia, R.F., Villaschi, S., 1999. Autoregulation of angiogenesis by cells of the vessel wall. Int Rev Cytol 185, 1-43.

Nikcevic, G., Savic, T., Kovacevic-Grujicic, N., Stevanovic, M., 2008. Up-regulation of the SOX3 gene expression by RA: characterization of the novel promoter- response element and the retinoid receptors involved. J Neurochem.

Nilsson, O., Marino, R., De Luca, F., Phillip, M., Baron, J., 2005. Endocrine regulation of the growth plate. Horm Res 64, 157-165.

Nishiguchi, S., Wood, H., Kondoh, H., Lovell-Badge, R., Episkopou, V., 1998. Sox1 directly regulates the gamma-crystallin genes and is essential for lens development in mice. Genes Dev 12, 776-781.

Nishimoto, M., Fukushima, A., Okuda, A., Muramatsu, M., 1999. The gene for the embryonic stem cell coactivator UTF1 carries a regulatory element which selectively interacts with a complex composed of Oct-3/4 and Sox-2. Mol Cell Biol 19, 5453-5465.

Niwa, H., Toyooka, Y., Shimosato, D., Strumpf, D., Takahashi, K., Yagi, R., Rossant, J., 2005. Interaction between Oct3/4 and Cdx2 determines trophectoderm differentiation. Cell 123, 917-929.

Nussey, S., Whitehead, S., 2001. Endocrinology: An Integrated Approach. Oxford: BIOS Scientific Publishers, London, UK.

Ohyama, K., Das, R., Placzek, M., 2008. Temporal progression of hypothalamic patterning by a dual action of BMP. Development 135, 3325-3331.

Oka, N., Soeda, A., Inagaki, A., Onodera, M., Maruyama, H., Hara, A., Kunisada, T., Mori, H., Iwama, T., 2007. VEGF promotes tumorigenesis and angiogenesis of human glioblastoma stem cells. Biochem Biophys Res Commun 360, 553-559.

Oliver, B., Perrimon, N., Mahowald, A.P., 1987. The ovo locus is required for sex-specific germ line maintenance in Drosophila. Genes Dev 1, 913-923.

Olsson, A.K., Dimberg, A., Kreuger, J., Claesson-Welsh, L., 2006. VEGF receptor signalling - in control of vascular function. Nat Rev Mol Cell Biol 7, 359-371.

Osterstock, G., Escobar, P., Mitutsova, V., Gouty-Colomer, L.A., Fontanaud, P., Molino, F., Fehrentz, J.A., Carmignac, D., Martinez, J., Guerineau, N.C., Robinson, I.C., Mollard, P., Mery, P.F., 2010. Ghrelin stimulation of growth hormone-releasing hormone neurons is direct in the arcuate nucleus. PLoS ONE 5, e9159.

Otani, A., Slike, B.M., Dorrell, M.I., Hood, J., Kinder, K., Ewalt, K.L., Cheresh, D., Schimmel, P., Friedlander, M., 2002. A fragment of human TrpRS as a potent antagonist of ocular angiogenesis. Proc Natl Acad Sci U S A 99, 178-183.

Overton, P.M., Meadows, L.A., Urban, J., Russell, S., 2002. Evidence for differential and redundant function of the Sox genes Dichaete and SoxN during CNS development in Drosophila. Development 129, 4219-4228.

Park, S.G., Schimmel, P., Kim, S., 2008. Aminoacyl tRNA synthetases and their connections to disease. Proc Natl Acad Sci U S A 105, 11043-11049.

Patten, I., Placzek, M., 2002. Opponent activities of Shh and BMP signaling during floor plate induction in vivo. Curr Biol 12, 47-52.

Pawlak, C.R., Sanchis-Segura, C., Soewarto, D., Wagner, S., Hrabe de Angelis, M., Spanagel, R., 2008. A phenotype-driven ENU mutagenesis screen for the identification of dominant mutations involved in alcohol consumption. Mamm Genome 19, 77-84.

Pescovitz, O.H., Eugster, E.A., 2004. Pediatric Endicrinology: Mechanisms, Manifestations, and Management. Lippincott Williams & Wilkins, Philadelphia, PA.

Petri, A., Ahnfelt-Ronne, J., Frederiksen, K.S., Edwards, D.G., Madsen, D., Serup, P., Fleckner, J., Heller, R.S., 2006. The effect of neurogenin3 deficiency on pancreatic gene expression in embryonic mice. J Mol Endocrinol 37, 301-316.

Pevny, L.H., Lovell-Badge, R., 1997. Sox genes find their feet. Curr Opin Genet Dev 7, 338-344.

Pevny, L.H., Sockanathan, S., Placzek, M., Lovell-Badge, R., 1998. A role for SOX1 in neural determination. Development 125, 1967-1978.

Phelps, C.J., Hurley, D.L., 1999. Pituitary hormones as neurotrophic signals: update on hypothalamic differentiation in genetic models of altered feedback. Proc Soc Exp Biol Med 222, 39-58.

Phelps, C.J., Saleh, M.N., Romero, M.I., 1996. Hypophysiotropic somatostatin expression during postnatal development in growth hormone-deficient Ames dwarf mice: peptide immunocytochemistry. Neuroendocrinology 64, 364-378.

Phillips, J.A., 3rd, Hjelle, B.L., Seeburg, P.H., Zachmann, M., 1981. Molecular basis for familial isolated growth hormone deficiency. Proc Natl Acad Sci U S A 78, 6372-6375.

Plate, K.H., Risau, W., 1995. Angiogenesis in malignant gliomas. Glia 15, 339-347.

Pombo, C.M., Zalvide, J., Gaylinn, B.D., Dieguez, C., 2000. Growth hormone-releasing hormone stimulates mitogen-activated protein kinase. Endocrinology 141, 2113-2119.

Potok, M.A., Cha, K.B., Hunt, A., Brinkmeier, M.L., Leitges, M., Kispert, A., Camper, S.A., 2008. WNT signaling affects gene expression in the ventral diencephalon and pituitary gland growth. Dev Dyn 237, 1006-1020.

Procter, A.M., Phillips, J.A., 3rd, Cooper, D.N., 1998. The molecular genetics of growth hormone deficiency. Hum Genet 103, 255-272.

Quek, S.I., Chan, W.K., 2009. Transcriptional activation of zebrafish cyp11a1 promoter is dependent on the nuclear receptor Ff1b. J Mol Endocrinol 43, 121-130.

Rathkolb, B., Decker, T., Fuchs, E., Soewarto, D., Fella, C., Heffner, S., Pargent, W., Wanke, R., Balling, R., Hrabe de Angelis, M., Kolb, H.J., Wolf, E., 2000. The clinical-chemical screen in the Munich ENU Mouse Mutagenesis Project: screening for clinically relevant phenotypes. Mamm Genome 11, 543-546.

Raverot, G., Weiss, J., Park, S.Y., Hurley, L., Jameson, J.L., 2005. Sox3 expression in undifferentiated spermatogonia is required for the progression of spermatogenesis. Dev Biol 283, 215-225.

Ray, P.S., Fox, P.L., 2007. A post-transcriptional pathway represses monocyte VEGF-A expression and angiogenic activity. Embo J 26, 3360-3372.

Reijmers, L.G., Coats, J.K., Pletcher, M.T., Wiltshire, T., Tarantino, L.M., Mayford, M., 2006. A mutant mouse with a highly specific contextual fear-conditioning deficit found in an N-ethyl-N-nitrosourea (ENU) mutagenesis screen. Learn Mem 13, 143-149.

Renner, U., Lohrer, P., Schaaf, L., Feirer, M., Schmitt, K., Onofri, C., Arzt, E., Stalla, G.K., 2002. Transforming growth factor-beta stimulates vascular endothelial growth factor production by folliculostellate pituitary cells. Endocrinology 143, 3759-3765.

Rhodes, S.J., DiMattia, G.E., Rosenfeld, M.G., 1994. Transcriptional mechanisms in anterior pituitary cell differentiation. Curr Opin Genet Dev 4, 709-717.

Ribas de Pouplana, L., Geslain, R., 2008. Not just because it is there: aminoacyl-tRNA synthetases gain control of the cell. Mol Cell 30, 3-4.

Risau, W., 1997. Mechanisms of angiogenesis. Nature 386, 671-674.

Rizzoti, K., Brunelli, S., Carmignac, D., Thomas, P.Q., Robinson, I.C., Lovell-Badge, R., 2004. SOX3 is required during the formation of the hypothalamo-pituitary axis. Nat Genet 36, 247-255.

Rizzoti, K., Lovell-Badge, R., 2005. Early development of the pituitary gland: induction and shaping of Rathke's pouch. Rev Endocr Metab Disord 6, 161-172.

Rizzoti, K., Lovell-Badge, R., 2007. SOX3 activity during pharyngeal segmentation is required for craniofacial morphogenesis. Development 134, 3437-3448.

Rohr, K.B., Barth, K.A., Varga, Z.M., Wilson, S.W., 2001. The nodal pathway acts upstream of hedgehog signaling to specify ventral telencephalic identity. Neuron 29, 341-351.

Rolinski, B., Arnecke, R., Dame, T., Kreischer, J., Olgemoller, B., Wolf, E., Balling, R., Hrabe de Angelis, M., Roscher, A.A., 2000. The biochemical metabolite screen in the Munich ENU Mouse Mutagenesis Project: determination of amino acids and acylcarnitines by tandem mass spectrometry. Mamm Genome 11, 547-551.

Ronchi, A., Bellorini, M., Mongelli, N., Mantovani, R., 1995. CCAAT-box binding protein NF-Y (CBF, CP1) recognizes the minor groove and distorts DNA. Nucleic Acids Res 23, 4565-4572.

Rosenthal, N., Brown, S., 2007. The mouse ascending: perspectives for human-disease models. Nat Cell Biol 9, 993-999.

Rozen, S., Skaletsky, H.J., 2000. Primer3 on the WWW for general users and for biologist programmers. Human Press, Totowa, NJ.

Rubenstein, J.L., Shimamura, K., Martinez, S., Puelles, L., 1998. Regionalization of the prosencephalic neural plate. Annu Rev Neurosci 21, 445-477.

Salvatori, R., Fan, X., Phillips, J.A., 3rd, Espigares-Martin, R., Martin De Lara, I., Freeman, K.L., Plotnick, L., Al-Ashwal, A., Levine, M.A., 2001. Three new mutations in the gene for the growth hormone (gh)-releasing hormone receptor in familial isolated gh deficiency type ib. J Clin Endocrinol Metab 86, 273-279.

Sambrook, J., Russell, D.W., 2001. Molecular cloning : a laboratory manual, 3rd. ed. Cold Spring Harbor Laboratory, Cold Spring Harbor, N.Y.

Schaiber, R., Gowen, J., 1961. A new dwarf mouse. Genetics 46.

Schell-Apacik, C., Rivero, M., Knepper, J.L., Roessler, E., Muenke, M., Ming, J.E., 2003. SONIC HEDGEHOG mutations causing human holoprosencephaly impair neural patterning activity. Hum Genet 113, 170-177.

Schroeder, A., Mueller, O., Stocker, S., Salowsky, R., Leiber, M., Gassmann, M., Lightfoot, S., Menzel, W., Granzow, M., Ragg, T., 2006. The RIN: an RNA integrity number for assigning integrity values to RNA measurements. BMC Mol Biol 7, 3.

Schultze, J.L., Eggle, D., 2007. IlluminaGUI: graphical user interface for analyzing gene expression data generated on the Illumina platform. Bioinformatics 23, 1431-1433.

Schwind, J.L., 1928. The development of the hypophysis cerebri of the albino rat. American Journal of Anatomy 41, 295-315.

Schwitzgebel, V.M., Scheel, D.W., Conners, J.R., Kalamaras, J., Lee, J.E., Anderson, D.J., Sussel, L., Johnson, J.D., German, M.S., 2000. Expression of neurogenin3 reveals an islet cell precursor population in the pancreas. Development 127, 3533-3542.

Scully, K.M., Rosenfeld, M.G., 2002. Pituitary development: regulatory codes in mammalian organogenesis. Science 295, 2231-2235.

Segen, J., 2006. Concise Dictionary of Modern Medicine. McGraw-Hill New York.

Sheng, H.Z., Moriyama, K., Yamashita, T., Li, H., Potter, S.S., Mahon, K.A., Westphal, H., 1997. Multistep control of pituitary organogenesis. Science 278, 1809-1812.

Sheng, H.Z., Westphal, H., 1999. Early steps in pituitary organogenesis. Trends Genet 15, 236-240.

Sinclair, A.H., Berta, P., Palmer, M.S., Hawkins, J.R., Griffiths, B.L., Smith, M.J., Foster, J.W., Frischauf, A.M., Lovell-Badge, R., Goodfellow, P.N., 1990. A gene from the human sex-determining region encodes a protein with homology to a conserved DNA-binding motif. Nature 346, 240-244.

Sinha, Y.N., Salocks, C.B., Vanderlaan, W.P., 1975. Pituitary and serum concentrations of prolactin and GH in Snell dwarf mice. Proc Soc Exp Biol Med 150, 207-210.

Smith, S.B., Gasa, R., Watada, H., Wang, J., Griffen, S.C., German, M.S., 2003. Neurogenin3 and hepatic nuclear factor 1 cooperate in activating pancreatic expression of Pax4. J Biol Chem 278, 38254-38259.

Snell, G.D., 1929. Dwarf, a New Mendelian Recessive Character of the House Mouse. Proc Natl Acad Sci U S A 15, 733-734.

Soewarto, D., Fella, C., Teubner, A., Rathkolb, B., Pargent, W., Heffner, S., Marschall, S., Wolf, E., Balling, R., Hrabe de Angelis, M., 2000. The large-scale Munich ENU-mouse-mutagenesis screen. Mamm Genome 11, 507-510.

Solomon, N.M., Ross, S.A., Morgan, T., Belsky, J.L., Hol, F.A., Karnes, P.S., Hopwood, N.J., Myers, S.E., Tan, A.S., Warne, G.L., Forrest, S.M., Thomas, P.Q., 2004. Array comparative genomic hybridisation analysis of boys with X linked hypopituitarism identifies a 3.9 Mb duplicated critical region at Xq27 containing SOX3. J Med Genet 41, 669-678.

Sommer, L., Ma, Q., Anderson, D.J., 1996. neurogenins, a novel family of atonal-related bHLH transcription factors, are putative mammalian neuronal determination genes that reveal progenitor cell heterogeneity in the developing CNS and PNS. Mol Cell Neurosci 8, 221-241.

Soufla, G., Porichis, F., Sourvinos, G., Vassilaros, S., Spandidos, D.A., 2006. Transcriptional deregulation of VEGF, FGF2, TGF-beta1, 2, 3 and cognate receptors in breast tumorigenesis. Cancer Lett 235, 100-113.

Stenn, K.S., Link, R., Moellmann, G., Madri, J., Kuklinska, E., 1989. Dispase, a neutral protease from Bacillus polymyxa, is a powerful fibronectinase and type IV collagenase. J Invest Dermatol 93, 287-290.

Stevanovic, M., 2003. Modulation of SOX2 and SOX3 gene expression during differentiation of human neuronal precursor cell line NTERA2. Mol Biol Rep 30, 127-132.

Stevanovic, M., Lovell-Badge, R., Collignon, J., Goodfellow, P.N., 1993. SOX3 is an X-linked gene related to SRY. Hum Mol Genet 2, 2013-2018.

Strachan, T., Read, A.P., 1999. Human Molecular Genetics, 2nd edition. Wiley-Liss, New York.

Suh, H., Gage, P.J., Drouin, J., Camper, S.A., 2002. Pitx2 is required at multiple stages of pituitary organogenesis: pituitary primordium formation and cell specification. Development 129, 329-337.

Suhr, S.T., Rahal, J.O., Mayo, K.E., 1989. Mouse growth-hormone-releasing hormone: precursor structure and expression in brain and placenta. Mol Endocrinol 3, 1693-1700.

Sun, J., Wang, D.A., Jain, R.K., Carie, A., Paquette, S., Ennis, E., Blaskovich, M.A., Baldini, L., Coppola, D., Hamilton, A.D., Sebti, S.M., 2005. Inhibiting angiogenesis and tumorigenesis by a synthetic molecule that blocks binding of both VEGF and PDGF to their receptors. Oncogene 24, 4701-4709.

Sun, Y., Wang, P., Zheng, H., Smith, R.G., 2004. Ghrelin stimulation of growth hormone release and appetite is mediated through the growth hormone secretagogue receptor. Proc Natl Acad Sci U S A 101, 4679-4684.

Sutton, E., Hughes, J., White, S., Sekido, R., Tan, J., Arboleda, V., Rogers, N., Knower, K., Rowley, L., Eyre, H., Rizzoti, K., McAninch, D., Goncalves, J., Slee, J., Turbitt, E., Bruno, D., Bengtsson, H., Harley, V., Vilain, E., Sinclair, A., Lovell-Badge, R., Thomas, P., 2011. Identification of SOX3 as an XX male sex reversal gene in mice and humans. J Clin Invest 121, 328-341.

Szabo, N.E., Zhao, T., Cankaya, M., Theil, T., Zhou, X., Alvarez-Bolado, G., 2009. Role of neuroepithelial Sonic hedgehog in hypothalamic patterning. J Neurosci 29, 6989-7002.

Szarek, E., Cheah, P.S., Schwartz, J., Thomas, P., 2010. Molecular genetics of the developing neuroendocrine hypothalamus. Mol Cell Endocrinol 323, 115-123.

Tanaka, S., Kamachi, Y., Tanouchi, A., Hamada, H., Jing, N., Kondoh, H., 2004. Interplay of SOX and POU factors in regulation of the Nestin gene in neural primordial cells. Mol Cell Biol 24, 8834-8846.

Taranova, O.V., Magness, S.T., Fagan, B.M., Wu, Y., Surzenko, N., Hutton, S.R., Pevny, L.H., 2006. SOX2 is a dose-dependent regulator of retinal neural progenitor competence. Genes Dev 20, 1187-1202.

Terman, B.I., Dougher-Vermazen, M., 1996. Biological properties of VEGF/VPF receptors. Cancer Metastasis Rev 15, 159-163.

Thomas, P.Q., Dattani, M.T., Brickman, J.M., McNay, D., Warne, G., Zacharin, M., Cameron, F., Hurst, J., Woods, K., Dunger, D., Stanhope, R., Forrest, S., Robinson, I.C., Beddington, R.S., 2001. Heterozygous HESX1 mutations associated with isolated congenital pituitary hypoplasia and septo-optic dysplasia. Hum Mol Genet 10, 39-45.

Thomas, P.Q., Johnson, B.V., Rathjen, J., Rathjen, P.D., 1995. Sequence, genomic organization, and expression of the novel homeobox gene Hesx1. J Biol Chem 270, 3869-3875.

Tolstrup, A.B., Bejder, A., Fleckner, J., Justesen, J., 1995. Transcriptional regulation of the interferon-gamma-inducible tryptophanyl-tRNA synthetase includes alternative splicing. J Biol Chem 270, 397-403.

Tomioka, M., Nishimoto, M., Miyagi, S., Katayanagi, T., Fukui, N., Niwa, H., Muramatsu, M., Okuda, A., 2002. Identification of Sox-2 regulatory region which is under the control of Oct-3/4-Sox-2 complex. Nucleic Acids Res 30, 3202-3213.

Tzima, E., Schimmel, P., 2006. Inhibition of tumor angiogenesis by a natural fragment of a tRNA synthetase. Trends Biochem Sci 31, 7-10.

Uchikawa, M., Ishida, Y., Takemoto, T., Kamachi, Y., Kondoh, H., 2003. Functional analysis of chicken Sox2 enhancers highlights an array of diverse regulatory elements that are conserved in mammals. Dev Cell 4, 509-519.

Varlet, I., Collignon, J., Robertson, E.J., 1997. nodal expression in the primitive endoderm is required for specification of the anterior axis during mouse gastrulation. Development 124, 1033-1044.

Vetere, A., Li, W.C., Paroni, F., Juhl, K., Guo, L., Nishimura, W., Dai, X., Bonner-Weir, S., Sharma, A., 2010. OVO homologue-like 1 (Ovol1) transcription factor: a

novel target of neurogenin-3 in rodent pancreas. Diabetologia 53, 115-122.

Vikkula, M., Boon, L.M., Carraway, K.L., 3rd, Calvert, J.T., Diamonti, A.J., Goumnerov, B., Pasyk, K.A., Marchuk, D.A., Warman, M.L., Cantley, L.C., Mulliken, J.B., Olsen, B.R., 1996. Vascular dysmorphogenesis caused by an activating mutation in the receptor tyrosine kinase TIE2. Cell 87, 1181-1190.

Villasenor, A., Chong, D.C., Cleaver, O., 2008. Biphasic Ngn3 expression in the developing pancreas. Dev Dyn 237, 3270-3279.

Wakasugi, K., 2010. An exposed cysteine residue of human angiostatic mini tryptophanyl-tRNA synthetase. Biochemistry 49, 3156-3160.

Wakasugi, K., Schimmel, P., 1999. Two distinct cytokines released from a human aminoacyl-tRNA synthetase. Science 284, 147-151.

Wakasugi, K., Slike, B.M., Hood, J., Ewalt, K.L., Cheresh, D.A., Schimmel, P., 2002a. Induction of angiogenesis by a fragment of human tyrosyl-tRNA synthetase. J Biol Chem 277, 20124-20126.

Wakasugi, K., Slike, B.M., Hood, J., Otani, A., Ewalt, K.L., Friedlander, M., Cheresh, D.A., Schimmel, P., 2002b. A human aminoacyl-tRNA synthetase as a regulator of angiogenesis. Proc Natl Acad Sci U S A 99, 173-177.

Waldner, M.J., Wirtz, S., Jefremow, A., Warntjen, M., Neufert, C., Atreya, R., Becker, C., Weigmann, B., Vieth, M., Rose-John, S., Neurath, M.F., 2010. VEGF receptor signaling links inflammation and tumorigenesis in colitis-associated cancer. J Exp Med 207, 2855-2868.

Walls, J.R., Coultas, L., Rossant, J., Henkelman, R.M., 2008. Three-dimensional analysis of vascular development in the mouse embryo. PLoS ONE 3, e2853.

Wang, H., Chan, S.A., Ogier, M., Hellard, D., Wang, Q., Smith, C., Katz, D.M., 2006a. Dysregulation of brain-derived neurotrophic factor expression and neurosecretory function in Mecp2 null mice. J Neurosci 26, 10911-10915.

Wang, T.W., Stromberg, G.P., Whitney, J.T., Brower, N.W., Klymkowsky, M.W., Parent, J.M., 2006b. Sox3 expression identifies neural progenitors in persistent neonatal and adult mouse forebrain germinative zones. J Comp Neurol 497, 88-100.

Wang, X., Chu, L.T., He, J., Emelyanov, A., Korzh, V., Gong, Z., 2001. A novel zebrafish bHLH gene, neurogenin3, is expressed in the hypothalamus. Gene 275, 47-55.

Ward, R.D., Raetzman, L.T., Suh, H., Stone, B.M., Nasonkin, I.O., Camper, S.A., 2005. Role of PROP1 in pituitary gland growth. Mol Endocrinol 19, 698-710.

Wegner, M., 1999. From head to toes: the multiple facets of Sox proteins. Nucleic Acids Res 27, 1409-1420.

Weiss, J., Meeks, J.J., Hurley, L., Raverot, G., Frassetto, A., Jameson, J.L., 2003. Sox3 is required for gonadal function, but not sex determination, in males and females. Mol Cell Biol 23, 8084-8091.

Wilson, M.E., Kalamaras, J.A., German, M.S., 2002. Expression pattern of IAPP and prohormone convertase 1/3 reveals a distinctive set of endocrine cells in the embryonic pancreas. Mech Dev 115, 171-176.

Wong, J., Farlie, P., Holbert, S., Lockhart, P., Thomas, P.Q., 2007. Polyalanine expansion mutations in the X-linked hypopituitarism gene SOX3 result in aggresome formation and impaired transactivation. Front Biosci 12, 2085-2095.

Wood, H.B., Episkopou, V., 1999. Comparative expression of the mouse Sox1, Sox2 and Sox3 genes from pre-gastrulation to early somite stages. Mech Dev 86, 197-201.

Woods, K.S., Cundall, M., Turton, J., Rizotti, K., Mehta, A., Palmer, R., Wong, J., Chong, W.K., Al-Zyoud, M., El-Ali, M., Otonkoski, T., Martinez-Barbera, J.P., Thomas, P.Q., Robinson, I.C., Lovell-Badge, R., Woodward, K.J., Dattani, M.T., 2005. Over- and underdosage of SOX3 is associated with infundibular hypoplasia and hypopituitarism. Am J Hum Genet 76, 833-849.

Workman, C., Jensen, L.J., Jarmer, H., Berka, R., Gautier, L., Nielser, H.B., Saxild, H.H., Nielsen, C., Brunak, S., Knudsen, S., 2002. A new non-linear normalization method for reducing variability in DNA microarray experiments. Genome Biol 3, research0048.

Wright, E.M., Snopek, B., Koopman, P., 1993. Seven new members of the Sox gene family expressed during mouse development. Nucleic Acids Res 21, 744.

Wu, W., Cogan, J.D., Pfaffle, R.W., Dasen, J.S., Frisch, H., O'Connell, S.M., Flynn, S.E., Brown, M.R., Mullis, P.E., Parks, J.S., Phillips, J.A., 3rd, Rosenfeld, M.G., 1998. Mutations in PROP1 cause familial combined pituitary hormone deficiency. Nat Genet 18, 147-149.

Yakar, S., Rosen, C.J., Beamer, W.G., Ackert-Bicknell, C.L., Wu, Y., Liu, J.L., Ooi, G.T., Setser, J., Frystyk, J., Boisclair, Y.R., LeRoith, D., 2002. Circulating levels of IGF-1 directly regulate bone growth and density. J Clin Invest 110, 771-781.

Yang, X.L., Otero, F.J., Skene, R.J., McRee, D.E., Schimmel, P., Ribas de Pouplana, L., 2003. Crystal structures that suggest late development of genetic code components for differentiating aromatic side chains. Proc Natl Acad Sci U S A 100, 15376-15380.

Yoshida, S., Takakura, A., Ohbo, K., Abe, K., Wakabayashi, J., Yamamoto, M., Suda, T., Nabeshima, Y., 2004. Neurogenin3 delineates the earliest stages of spermatogenesis in the mouse testis. Dev Biol 269, 447-458.

Zappone, M.V., Galli, R., Catena, R., Meani, N., De Biasi, S., Mattei, E., Tiveron, C., Vescovi, A.L., Lovell-Badge, R., Ottolenghi, S., Nicolis, S.K., 2000. Sox2 regulatory sequences direct expression of a (beta)-geo transgene to telencephalic neural stem cells and precursors of the mouse embryo, revealing regionalization of gene expression in CNS stem cells. Development 127, 2367-2382.

Zhang, D., Stumpo, D.J., Graves, J.P., DeGraff, L.M., Grissom, S.F., Collins, J.B., Li, L., Zeldin, D.C., Blackshear, P.J., 2006. Identification of potential target genes for RFX4_v3, a transcription factor critical for brain development. J Neurochem 98, 860-875.

Zhao, L., Bakke, M., Krimkevich, Y., Cushman, L.J., Parlow, A.F., Camper, S.A., Parker, K.L., 2001a. Hypomorphic phenotype in mice with pituitary-

specific knockout of steroidogenic factor 1. Genesis 30, 65-69.

Zhao, L., Bakke, M., Krimkevich, Y., Cushman, L.J., Parlow, A.F., Camper, S.A., Parker, K.L., 2001b. Steroidogenic factor 1 (SF1) is essential for pituitary gonadotrope function. Development 128, 147-154.

Zhou, Q., Kapoor, M., Guo, M., Belani, R., Xu, X., Kiosses, W.B., Hanan, M., Park, C., Armour, E., Do, M.H., Nangle, L.A., Schimmel, P., Yang, X.L., 2010. Orthogonal use of a human tRNA synthetase active site to achieve multifunctionality. Nat Struct Mol Biol 17, 57-61.

Zhou, Y., Xu, B.C., Maheshwari, H.G., He, L., Reed, M., Lozykowski, M., Okada, S., Cataldo, L., Coschigamo, K., Wagner, T.E., Baumann, G., Kopchick, J.J., 1997. A mammalian model for Laron syndrome produced by targeted disruption of the mouse growth hormone receptor/binding protein gene (the Laron mouse). Proc Natl Acad Sci U S A 94, 13215-13220.

Zhu, X., Gleiberman, A.S., Rosenfeld, M.G., 2007a. Molecular physiology of pituitary development: signaling and transcriptional networks. Physiol Rev 87, 933-963.

Zhu, X., Wang, J., Ju, B.G., Rosenfeld, M.G., 2007b. Signaling and epigenetic regulation of pituitary development. Curr Opin Cell Biol 19, 605-611.

INDEX

PUBLICATIONS

The following review was written during my PhD candidature. It is reprinted here with permission from Elsevier (license number 2634590295366).

Molecular and Cellular Endocrinology 323 (2010) 115–123

Contents lists available at ScienceDirect

Molecular and Cellular Endocrinology

journal homepage: www.elsevier.com/locate/mce

Review

Molecular genetics of the developing neuroendocrine hypothalamus

Eva Szarek[a,b], Pike-See Cheah[b,c], Jeff Schwartz[a,d], Paul Thomas[b,*]

[a] Discipline of Physiology, School of Molecular and Biomedical Sciences, University of Adelaide, Adelaide, Australia
[b] Discipline of Biochemistry, School of Molecular and Biomedical Sciences, University of Adelaide, Adelaide, Australia
[c] Department of Human Anatomy, Faculty of Medicine and Health Sciences, University Putra Malaysia, Malaysia
[d] School of Medicine, Centre for Medicine and Oral Health, Griffith University, Southport, Queensland, Australia

ARTICLE INFO

Keywords:
Hypothalamus
Development
Neuroendocrine

ABSTRACT

Formation of the mammalian endocrine system and neuroendocrine organs involves complex regulatory networks resulting in a highly specialized cell system able to secrete a diverse array of peptide hormones. The hypothalamus is located in the mediobasal region of the brain and acts as a gateway between the endocrine and nervous systems. From an endocrinology perspective, the parvicellular neurons of the hypothalamus are of particular interest as they function as a control centre for several critical physiological processes including growth, metabolism and reproduction by regulating hormonal signaling from target cognate cell types in the anterior pituitary. Delineating the genetic program that controls hypothalamic development is essential for complete understanding of parvicellular neuronal function and the etiology of congenital disorders that result from hypothalamic–pituitary axis dysfunction. In recent years, studies have shed light on the interactions between signaling molecules and activation of transcription factors that regulate hypothalamic cell fate commitment and terminal differentiation. The aim of this review is to summarize the recent molecular and genetic findings that have advanced our understanding of the emergence of the known important hypophysiotropic signaling molecules in the hypothalamus. We have focused on reviewing the literature that provides evidence of the dependence on expression of specific genes for the normal development and function of the cells that secrete these neuroendocrine factors, as well as studies of the elaboration of the spatial or temporal patterns of changes in gene expression that drive this development.

Contents

* Corresponding author at: School of Molecular and Biomedical Sciences, University of Adelaide, North Terrace, Adelaide 5005, Australia. Tel.: +61 8 8303 7047; fax: +61 8 8303 4362.
E-mail address: paul.thomas@adelaide.edu.au (P. Thomas).

0303-7207/$ – see front matter © 2010 Elsevier Ireland Ltd. All rights reserved.
doi:10.1016/j.mce.2010.04.002

1. Introduction

The hypothalamus influences a broad spectrum of physiological functions, including pituitary hormone synthesis and secretion, autonomic nervous system activity, energy intake and expenditure, body temperature, reproduction and behavior. Despite its physiological importance, we are only beginning to understand the molecular mechanisms underlying neural differentiation and development within the hypothalamus and the ontogeny of its connections with the pituitary. The hypothalamic parvicellular neurosecretory neurons are of particular interest due to their role in controlling anterior pituitary (AP) hormone secretion. For this reason, many studies have focused on the signaling molecules and transcription factors that control hypothalamic morphogenesis and the emergence of the seven known parvicellular neurosecretory neuronal subtypes (described in detail below). While much of the early research into hypothalamic development and function has been conducted in rats, recent advances in murine transgenesis and mutagenesis techniques have established mice as the principal model for the analysis of the central nervous system (CNS) development. Therefore, in this review we have focused primarily on rodent hypothalamic development but have also included key findings from other developmental models, such as chick and zebrafish, which have contributed to our understanding of this field.

2. Functional anatomy of the neuroendocrine hypothalamus

The vertebrate hypothalamus is located ventral to the thalamus and dorsal to the pituitary gland, at the mediobasal region of the CNS. It extends from the optic chiasm (located anteriorly) to the mammillary body (located posteriorly) and is organized into four distinct rostral-to-caudal regions: preoptic, anterior, tuberal, and mammillary. It is also divided into three medial-to-lateral areas: periventricular, medial and lateral. The periventricular hypothalamus contains four distinct cell clusters: the paraventricular nucleus (PVN), arcuate nucleus (ARC), supra-chiasmatic nucleus (SCN), and the periventricular nucleus (PeVN; Fig. 1A). The medial hypothalamic zone is comprised of the medial preoptic nucleus, the anterior hypothalamus (AH), the dorsomedial nucleus, the ventromedial nucleus (VMN) and the mammillary nuclei. The lateral hypothalamus consists of the preoptic area (POA) and hypothalamic area. Located throughout hypothalamus are hypothalamic neurosecretory cells that are divided into two populations: the parvicellular and magnocellular neurosecretory systems. The former consists of neurons controlling the release of specific AP neurohormones: thyrotropin-releasing hormone (TRH; located within the medial part of the medial parvicellular subdivision of the PVN), corticotropin-releasing hormone (CRH; located within the lateral part of the medial parvicellular subdivision of the PVN), growth hormone-releasing hormone (GHRH; located within the lateral part of the ARC), somatostatin (SS; located within the PeVN), gonadotropin-releasing hormone (GnRH; located within the medial POA), dopamine (DA; located within the medial part of the ARC and detected by the enzymatic activity of tyrosine hydroxylase) and, the recently discovered gonadotropin-inhibiting hormone (GnIH; located within the dorsomedial nuclei in rodents; Fig. 1B). The magnocellular neurosecretory system consists of neuronal cells secreting two neurohormones, vasopressin (AVP) and oxytocin (OT), whose axons project directly into the posterior pituitary (neurohypophysis) and release peptides systemically in response to various homeostatic cues (osmotic, cardiovascular and reproductive). The primary focus of this review is the development and function of the parvicellular neurons. For in-depth information and discussion on the magnocellular neurosecre-

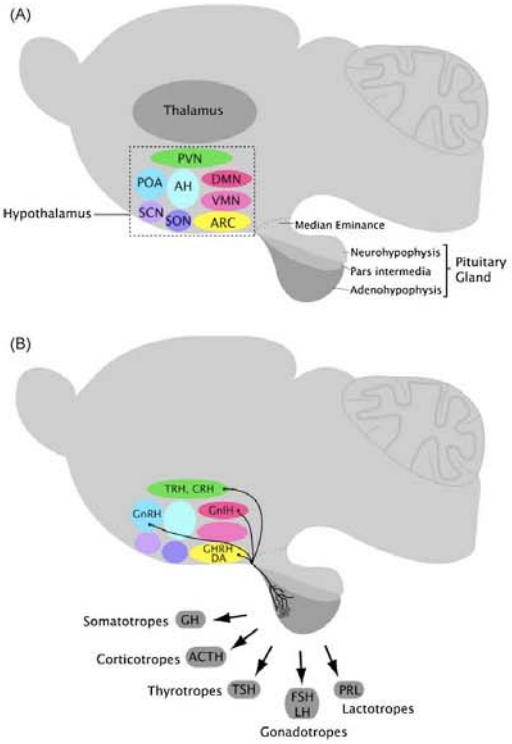

Fig. 1. Illustration of the organization of hypothalamic nuclei, in the murine brain. (A) A lateral view of the organization of the hypothalamic nuclei. The hypothalamus is organized into distinct zones containing tight clusters of cell bodies. (B) Representation of the neuroendocrine hypophysiotropic factors and their neuronal projections through the median eminence (ME) and into the adenohypophysis (anterior pituitary). PVN: paraventricular nucleus; POA: preoptic area; AH: anterior hypothalamus; SCN: supra-chiasmatic nucleus; SON: supra-optic nucleus; DMN: dorsal-medial nucleus; VMN: Ventro-medial nucleus; ARC: arcuate nucleus; GH: growth hormone; ACTH: adrenocorticotropin hormone; TSH: thyroid stimulating hormone; FSH: follicle-stimulating hormone; LH: luteinizing hormone; PRL: prolactin. GnRH: gonadotropin-releasing hormone; GHRH: GH-releasing hormone; GnIH: gonadotropin-inhibiting hormone; DA: dopamine.

tory system we refer the reader to the paper by Caqueret et al. (2006).

3. Hypothalamic induction and the role of signaling pathways

The hypothalamus develops from the ventral region of the diencephalon (Figdor and Stern, 1993) and, in the mouse, its primordium is morphologically evident from approximately 9.5 days post-coitum (dpc; where 0.5 dpc is defined as noon of the day on which a copulation plug is present). Developmental studies performed in mice, chick and zebrafish indicate that sonic hedgehog (SHH) signaling plays an important role in the induction and early patterning of the hypothalamus (Manning et al., 2006; Mathieu et al., 2002; Szabo et al., 2009). Secretion of SHH from the murine axial mesendoderm, from 7.5 dpc, is essential for correct patterning of the anterior midline. In humans as well as in mice, mutations in the *SHH/Shh* gene (and several other components of this pathway) result in holoprosencephaly due to a failure of hypothalamic anlagen induction and optic field separation (Chiang et al., 1996; Schell-Apacik et al., 2003). Increased SHH activity leads to ectopic expression of hypothalamic markers in zebrafish, suggesting that SHH signaling has an instructive rather than a permissive role in shaping the hypothalamus (Barth and Wilson, 1995; Hauptmann and Gerster, 1996; Rohr et al., 2001). Studies in chick have shown that once the hypothalamic primordium is established, down-regulation of *Shh* is critical for the progression of ventral cells into proliferating hypothalamic progenitors, at least within the ventral tubero-mammillary region (Manning et al., 2006). In addition, *Shh* down-regulation is mediated, to some extent, by local production of Bone Morphogenetic Proteins (BMPs), which belong to the transforming growth factor-beta (TGFβ) super-family of signaling proteins (Manning et al., 2006). This antagonism between SHH (ventral gradient morphogen) and BMP (dorsal gradient morphogen) in the hypothalamus is reminiscent of their opposing actions in dorsal-ventral patterning of the neural tube. However, in the developing hypothalamus this incorporates a temporal aspect (SHH early–BMP late) that appears necessary for establishing region-specific transcriptional profiles (Ohyama et al., 2008; Patten and Placzek, 2002). Although axial secretion of another member of the TGFβ super-family, NODAL, is also necessary for hypothalamic induction, the early lethality of *Nodal* mutants has precluded detailed assessment of its role in hypothalamic development in mice (Brennan et al., 2001; Conlon et al., 1994; Varlet et al., 1997). Genetic studies in zebrafish have shown that the Wnt signaling pathway is required for specification of the hypothalamic anlagen, its regionalization and neurogenesis (Kapsimali et al., 2004; Lee et al., 2006). Together, these studies have shown that hypothalamic induction and pattern formation depends on the activities of major protein signaling pathways involved in patterning, regional identity and cell fate determination.

4. Patterning the hypothalamic primordium

Embryonic neurogenesis in vertebrates follows a stereotypical progression that begins with the generation of the neural tube, which is composed of a pseudostratified columnar epithelium of cycling stem cells. As a general rule, these neuronal precursors acquire distinct positional identities, commit to a neuronal fate, exit mitosis, migrate away from the periluminal progenitor zone and terminally differentiate. A large body of evidence, gained principally from mouse and chick embryos, has established that transcription factors belonging to the homeodomain and basic Helix-Loop Helix (bHLH) families play a major role in neurogenesis (reviewed in Guillemot, 2007). Regionally restricted expression of these factors is induced in response to local signaling cues (see above), establishing a transcription factor "code" that directs the generation of distinct neuronal cell types at each neuroaxial level. Mouse mutagenesis has identified several transcription factor pathways critical for the development of the parvicellular neurons in the POA, PVN, PeVN, VMN and ARC, which together provide the foundation for a rudimentary "hypothalamic transcription factor code" and are outlined below.

4.1. *Sim1/Arnt2-Brn2 pathway*

The bHLH-PAS transcription factor SIM1 is expressed in the incipient PVN, supra-optic nucleus (SON), and anterior PeVN (aPeVN) from 10.5 dpc and is maintained in these regions into postnatal development (Caqueret et al., 2006; Michaud et al., 1998). Homozygous *Sim1* mutants die shortly after birth and exhibit significant hypoplasia of the anterior hypothalamus. Histological and molecular marker analysis has revealed that these mutants lack virtually all neurons of the SON and PVN, including those expressing TRH and CRH. SS neurons in the aPeVN and other populations of TRH neurons in the lateral hypothalamus and in the POA region are also missing. Interestingly, mutant mice lacking the *Sim1* dimerisation partner ARNT2 have a strikingly similar phenotype, indicating that these proteins function cooperatively in the AH (Hosoya et al., 2001; Keith et al., 2001). A key downstream target of SIM1/ARNT2 is *Brn2*, which encodes a POU domain transcription factor and is required for the differentiation of CRH (as well as OT and AVP) neurons of the PVN/SON. *Brn2* expression in the prospective PVN/SON region is absent in *Sim1* and *Arnt2* mutants, indicating that *Brn2* is regulated by SIM1/ARNT2, although it is not currently known if this is a direct or indirect interaction.

4.2. *Otp*

The homeobox gene *Orthopedia* (*Otp*) is expressed in neurons giving rise to the PVN, SON, aPeVN and ARC throughout their development. *Otp* mutants die as neonates and fail to generate the parvicellular and magnocellular neurons of the anterior PeVN, PVN, SON, and ARC (Acampora et al., 1999; Wang and Lufkin, 2000). These defects are associated with reduced cell proliferation, abnormal cell migration, and failure of terminal differentiation. Like the *Sim1* and *Arnt2* mutants, *Otp* null embryos fail to maintain *Brn2* expression. However, OTP does not appear to directly interact with SIM1 or ARNT2 (Caqueret et al., 2006) and SIM1 and OTP do not regulate each other's expression (Acampora et al., 1999), suggesting that OTP and SIM1/ARNT2 operate in parallel or convergent pathways.

4.3. *Nkx2.1*

During early CNS development, signals produced from the anterior axial mesendoderm induce expression of the homeodomain transcription factor gene *Nkx2.1* (also known as *T/ebp*) in the overlying presumptive hypothalamus (Ericson et al., 1998; Kimura et al., 1996). *Nkx2.1* mutant mice die at birth and, in addition to lung and thyroid defects, exhibit profound abnormalities in the ventral hypothalamus, including agenesis of the ARC and VMN. Interestingly, null mutants also fail to generate the Rathke's pouch (which does not express *Nkx2.1*), confirming the ventral diencephalon/infundibular recess is essential for induction of the AP (Kimura et al., 1996; Takuma et al., 1998).

4.4. *Sf1*

The *Sf1* gene encodes an orphan nuclear hormone receptor that is required for normal development of the gonads and adrenals and function of pituitary gonadotropes (Ingraham et al., 1994; Shinoda

et al., 1995). Within the CNS, *Sf1* is specifically expressed within the VMN and is required for multiple phases of VMN development. Analysis of *Sf1* null embryos indicates that this transcription factor is initially involved in the survival and migration of VMN precursors from the ventricular zone and at later stages is required for aggregation and condensation of the VMN nucleus and terminal differentiation.

4.5. Hmx2/Hmx3

Two closely related homeobox genes, *Hmx2* and *Hmx3*, are expressed in overlapping domains of the ventral hypothalamus from 10.5 dpc (Wang et al., 2004). While single gene mutants do not have any discernable hypothalamic phenotype (although it bears noting that ear development is affected), *Hmx2;Hmx3* null mice exhibit postnatal dwarfism and a severe deficiency of GHRH neurons in the ARC, but not the VMN (Wang et al., 2004). Expression of the homeobox gene *Gsh1*, which overlaps with *Hmx2* and *Hmx3* and is required for *Ghrh* expression, is also absent in *Hmx2;Hmx3* null embryos. Neuronal cell numbers in the ARC are not significantly different in double mutants indicating that, despite their widespread expression, *Hmx2* and *Hmx3* are not required for early determination of neuroprogenitors in this region of the hypothalamus.

4.6. Mash1

MASH1 is a proneural protein that belongs to the bHLH family of transcription factors and is required for neurogenesis and subtype specification in many regions of the CNS (Parras et al., 2002). *Mash1* is expressed throughout the ventral retrochiasmatic neuroepithelium from 10.5 to 12.5 dpc. *Mash1* null embryos exhibit hypoplasia of the ARC and VMN nuclei due to neurogenic failure and increased apoptosis (McNay et al., 2006). Using a knock-in strategy, McNay et al. (2006) elegantly showed that this phenotype could be rescued by ectopic expression of *Ngn2*, which is also a member of the bHLH proneural gene family. *Mash1* also appears to have a role in subtype specification (that cannot be rescued by *Ngn2*), and is absolutely required for expression of *Gsh1* and the subsequent generation of *Ghrh*-expressing neurons.

4.7. Sox3

Sox3 is a member of the *SOX* (Sry-related HMG box) family of transcription factor genes and is located on the X chromosome (Lefebvre et al., 2007). This gene was initially implicated in hypothalamic development from clinical and genetic studies of families with the male-specific congenital disorder X-linked Hypopituitarism (XH). XH males have GH deficiency and, in some cases, additional pituitary hormone deficiencies as well as intellectual disability (Solomon et al., 2002). Magnetic resonance imaging analysis of affected males has revealed abnormalities of the hypothalamic region including ectopic posterior pituitary and thin pituitary stalk, indicating that XH results primarily from a hypothalamic defect (Woods et al., 2005). Interestingly, XH is associated with duplications and mutations in *SOX3*, suggesting that over-expression and loss-of-function mutations result in a similar developmental defect (Solomon et al., 2002; Woods et al., 2005). Although the mechanism by which altered *SOX3* dosage causes XH is not fully understood, genetic studies in mice have provided some clues. *Sox3* null animals exhibit multiple pituitary hormone deficiency, variable dwarfism and CNS abnormalities, indicating that SOX3 function is broadly conserved in mice and humans (Rizzoti et al., 2004; Weiss et al., 2003). Importantly, *Sox3* is expressed in the developing hypothalamus (see below) but has minimal expression in the AP, suggesting that hypothalamic (and not AP) dysfunction is the primary cause of pituitary hormone deficiency in *Sox3* mutants.

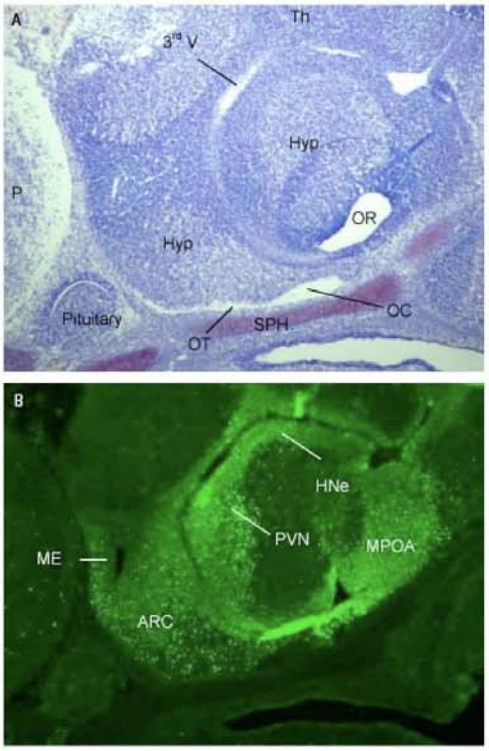

Fig. 2. SOX3 is expressed in the developing murine hypothalamus. (A) Nissl stain of the hypothalamus (Hyp) in the sagittal orientation. (B) Neighboring section showing SOX3 expression (green) throughout the hypothalamic neuroepithelium (HNe), medial preoptic area (MPOA), median eminence (ME), arcuate nucleus (ARC) and paraventricular nucleus (PVN). 3rd V: third ventricle, OC: optic chiasm, OR: optic recess, OT: optic tract, P: pons, SPH: sphenoid cartilage, Th: thalamus.

Studies from our laboratory have shown that *Sox3* is expressed in the hypothalamus from inception to maturity suggesting that it may have multiple roles in hypothalamic development and function (Fig. 2 and data not shown). Analysis of *Sox3* mutants has indicated that early expression in the ventral diencephalon/infundibular recess (at 10.5 dpc) is required for normal induction and morphogenesis of the AP, but, remarkably, not AP function (Rizzoti et al., 2004). From approximately 12.5 dpc, *Sox3* expression is restricted to multiple hypothalamic regions/nuclei including the hypothalamic neuroepithelium, median eminence, ARC, PVN, medial POA and VMN (unpublished data). Interestingly, all of these nuclei contain parvicellular neuronal subtypes. It is therefore possible that the multiple pituitary hormone deficiencies in *Sox3* null mice (and some XH patients) may reflect a specific requirement for *SOX3* in the generation and/or maintenance of some, if not all, parvicellular neuronal subtypes. Alternatively, or in addition, defective development of the median eminence, which also expresses *Sox3* (Rizzoti et al., 2004 and our unpublished data), may compromise the functional connection to the portal vasculature, resulting in altered regulation of AP hormone synthesis and secretion by parvicellular neuronal factors.

5. Birthdate analysis of hypothalamic nuclei

Detailed birth-dating studies of hypothalamic nuclei have been performed in rats, and to a lesser extent, in mice (Markakis, 2002; Markakis and Swanson, 1997). For extensive discussion of these reports we refer the reader to the excellent review by Markakis (2002). The general conclusion arising from birth-dating analyses is that the hypothalamus matures "from outside to inside" such that the lateral nuclei are generated before those located at more medial positions. This developmental sequence is opposite to that occurring in the cerebral cortex, where nascent neurons migrate past older neurons as they move radially towards the pial surface (from "inside to outside") (Misson et al., 1991). The order in which hypothalamic nuclei are generated may reflect, to some extent, a passive process by which the third ventricle is progressively reduced in volume due to accumulation of nascent neurons in a lateral to medial sequence. This is supported by gene expression analysis of the developing anterior hypothalamus, whereby it has been revealed that laminar patterns of gene expression may correspond to distinct waves of neurogenesis (Caqueret et al., 2006). However, birth-dating studies of the six parvicellular neural subtypes suggest that this model is an oversimplification as peak generation of parvicellular neurons occurs before the peak generation of their cognate nuclei (Markakis and Swanson, 1997). These observations imply that nascent parvicellular neurons exhibit a delayed migratory phase. Apart from the exceptional case of GnRH neurons, which undergo extensive migration from their source in the olfactory placode (Verney et al., 1996), this area is poorly understood. Perturbation of this migratory pathway could contribute to the altered distribution of anterior hypothalamic neurons in *Sim1* mutant embryos (see above) (Caqueret et al., 2006) although further studies are required to determine the precise mechanism. A second intriguing finding from parvicellular birth-dating studies is that there is no obvious correlation between the time at which the neurons are born and the neuronal subtype (in rats the peak parvicellular neuron generation occurs at 12.5–13.5 dpc, regardless of cell type). It therefore appears that, apart from GnRH, the parvicellular neurons are generated concurrently from the ventricular neuroepithelium that spans the hypothalamic region. Almost nothing is known about the coordination of progenitor cell selection and lineage commitment in the hypothalamus but it seems possible that similar genetic mechanisms to those employed in other CNS regions (e.g. Notch signaling) may be utilized.

6. Generation and function of parvicellular hypophysiotropic factors

Hypothalamic control of the AP became an accepted principle and the entire field took a major step forward with the discovery that (pyro)Glu-His-Pro(amide), synthesized in the hypothalamus, acted as a releasing factor for TSH (Guillemin et al., 1963). Along with the discovery of additional hypophysiotropic factors, subsequent research has focused on better understanding of the expression of these factors in the hypothalamus and the mechanisms by which they exert physiological activity at the pituitary. The developmental sequence of expression of the known hypothalamic hypophysiotropic factors has been investigated in numerous species including rat, mouse, human and chicken (Table 1).

7. Origin and birthdate of neuroendocrine hypophysiotropic factors

The availability of genetically engineered mouse models has added a new dimension to studies of the ontogeny of parvicellular neuronal subtypes. In recent years, a clearer picture has emerged of the precise steps in development and the factors involved in the

Table 1
Differentiation of hypothalamic parvicellular neurons in rat, mouse, human and chicken. MPON: medial preoptic nucleus; DMN: dorsal-medial nucleus; ARC: arcuate nucleus; PVN: paraventricular nucleus; PeVN: periventricular nucleus; g.w.: gestation week; e: embryonic day; N.D.: not determined.

Hypothalamic factor	Location of neuronal nuclei	Action on pituitary cell(s)	Neuronal appearance date			
			Rat	Mouse	Human	Chicken
GnRH	MPON	Stimulates gonadotropes	e11 (Markakis and Swanson, 1997)	e10.5 (Wray et al., 1989)	5.5 g.w. (Verney et al., 1996) 6 g.w. (Schwanzel-Fukuda et al., 1996)	e4.5 (Sullivan and Silverman, 1993)
GnIH	DMN (in rodent species)	Inhibits gonadotropes	Adult stage[a] (Kriegsfeld et al., 2006)	Adult stage[a] (Kriegsfeld et al., 2006)	N.D.	Adult stage[a] (Dockray et al., 1983)
DA	ARC	Inhibits lactotropes	e11 (Markakis and Swanson, 1997) e12 (Balan et al., 1996) e13.5 (Daikoku et al., 1986)	e10.5 (Son et al., 1996)	4.5 g.w. (Verney et al., 1991; Verney et al., 1996; Zecevic and Verney, 1995)	e5 (Ohyama et al., 2005)
GHRH	ARC	Stimulates somatotropes	e11 (Markakis and Swanson, 1997)	N.D.	29 g.w. (Bloch et al., 1984)	N.D.
SS	PeVN	Inhibits somatotropes	e12.5 (Daikoku et al., 1983) e12 (Markakis and Swanson, 1997)	e17[b] (Gross and Longer, 1979)	10 g.w. (Aubert et al., 1977)	e14[b] (Geris et al., 1998)
CRH	PVN	Stimulates corticotropes	e12 (Markakis and Swanson, 1997)	e13.5 (Keegan et al., 1994)	16 g.w. (Bugnon et al., 1982)	e15 (Józsa et al., 1986)
TRH	PVN	Stimulates thyrotropes	e12 (Markakis and Swanson, 1997)	e13 (Fèvre-Bauman et al., 1978)	8 g.w.[b] (Winters et al., 1974)	e5.5 (Thommes et al., 1985)

[a] Birth-dating studies have not been examined.
[b] Hypothalamic neurons may arise earlier during development; no known earlier stages have been investigated.

differentiation of and acquisition of function by cells that secrete hypothalamic releasing factors. Below we outline some of the key advances in this field.

7.1. GnRH

A total of 14 forms of GnRH have been described (for review see Wray, 2002), with the physiologically most important form being GnRH-1 (referred to here as GnRH). GnRH is a central regulator in the hypothalamic–pituitary–gonadal axis and is produced by neurosecretory cells located throughout the basal hypothalamus including the preoptic nucleus and AH. The release of GnRH triggers the synthesis and release of the gonadotropins, luteinizing hormone (LH) and follicle-stimulating hormone (FSH), which regulate gonadal steroidogenesis and gametogenesis (for review see Lee et al., 2008).

Unlike all other parvicellular neurons that arise from within the hypothalamic anlagen, GnRH neurons originate in the olfactory placode (Wray, 2002) and migrate through the ventral forebrain. In mice, GnRH neuron migration terminates in the medial septum, POA and anterior hypothalamic regions (Wray, 2001). Recent evidence indicates that the initial population of GnRH neurons (9.5–10.5 dpc) is generally located rostral to later-born (11.5–12.5 dpc) GnRH neurons and that the GnRH neurons located at different rostral–caudal positions may be functionally distinct (Jasoni et al., 2009). Several extracellular cues that direct the emergence and migration of nascent GnRH neurons have been identified which include Fibroblast Growth Factor 8 (Chung et al., 2008), hepatocyte growth factor (Giacobini et al., 2007) and secreted-class 3 semaphorins (Cariboni et al., 2007). Of particular interest is semaphorin-4D (Sema4D) which belongs to the semaphorin protein family group of axon/cell guidance proteins and is expressed along GnRH migratory route (Tran et al., 2007). The Sema4D receptor, PlexB1, is expressed in migratory cells that are exiting the olfactory placode (Giacobini et al., 2004). *PlexB1* deficient mice exhibit aberrant migration of the principal GnRH fibers that project to the ME (Giacobini et al., 2008) confirming the importance of Sema4D/PlexB1 interaction during GnRH cell migration.

A number of transcription factors have been implicated in GnRH differentiation such as GATA-4 and Activator Protein-2α (AP-2α). GATA-4, a member of the GATA family of zinc finger-domain transcription factors, binds to the GnRH enhancer and regulates GnRH gene transcription (Lawson et al., 1996). In the 13.5 dpc mouse brain, GnRH neurons express GATA-4 along their migration from the olfactory placode into the brain (Lawson and Mellon, 1998). The Activator Protein transcription factors are critical regulators of gene expression during embryogenesis. AP-2α has been detected in olfactory placode epithelium (Mitchell et al., 1991). It has been reported that GnRH neurons express AP-2α as they migrate into the forebrain (Kramer et al., 2000).

7.2. GnIH

GnIH was recently discovered in the Japanese quail and acts directly on the pituitary to inhibit gonadotropin release (Tsutsui et al., 2007; Tsutsui and Ukena, 2006). The identification of GnIH arose when neurons immuno-positive for the molluscan cardioexcitatory neuropeptide Phe-Met-Arg-Phe-NH_2 (FMRFamide, Price and Greenberg, 1977) were found in the vertebrate nervous system to contain an unknown, but similar, neuropeptide (Raffa, 1988). In the amphibian brain, some of these neurons were seen to project to the hypothalamic region close to the pituitary (Raffa, 1988; Rastogi et al., 2001). In turn, in the Japanese quail brain, clusters of these distinct neurons were seen localized in the PVN in the hypothalamus, with wide distribution in the diencephalic and mesencephalic regions and the most prominent fibers within the ME (Tsutsui et al., 2007). Recent studies have confirmed the effects of GnIH in rodents and sheep (Ducret et al., 2009; Johnson et al., 2007; Kriegsfeld et al., 2006; Murakami et al., 2008). Birth-dating and neuronal migration, however, have yet to be examined.

7.3. DA

DA is a catecholamine neurotransmitter, which in the pituitary is primarily involved in the inhibition of prolactin (PRL) release. In order to detect DA and the cells that produce it, tyrosine hydroxylase (the rate-limiting enzyme in synthesis of dopamine) expression is used as a surrogate marker. Secretion of PRL is regulated by three populations of hypothalamic dopaminergic neurons, originally identified in rats (DeMaria et al., 1999): (1) the tuberoinfundibular (TIDA) dopaminergic neurons, arising from the dorsomedial ARC and project to the external zone of the median eminence (Bjorklund et al., 1973); (2) tuberohypophysial (THDA) dopaminergic neurons, arising from the rostral ARC and project into the hypothalamic-hypophysial tract and into the intermediate and neural lobes of the pituitary gland (Fuxe, 1964); and (3) the periventricular hypophysial (PHDA) dopaminergic neurons, arising from the more rostral PeVN and their axons terminate within the intermediate region of the pituitary gland (Goudreau et al., 1992). The PHDA neuronal populations control basal regulation of PRL secretion. Early immunohistochemical detection shows the first appearance of dopaminergic neurons at 11.5 dpc in the rat (Daikoku et al., 1984).

Insight into the role of specific transcription factors in the development and differentiation of dopamine neurons, specifically the THDA and PHDA subtypes is limited. The LIM-homeodomain transcription factor *Lmx1a* has been shown to play critical roles in the determination of midbrain dopaminergic neurons during brain development (Failli et al., 2002). More recently, it was identified that *Lmx1a* is expressed at high levels within the posterior hypothalamic area, ventral pre-mammillary nucleus, sub-thalamic nucleus, ventral tegmental area, compact part of the substantia nigra and parabrachial nucleus from birth to adulthood (Zou et al., 2009). However, the exact role of *Lmx1a* in the dopaminergic neurons that regulate secretion of prolactin is yet to be determined. *Otp* has also been found to be a key determinant of hypothalamic differentiation, including the DA neurons (Blechman et al., 2007). Recent studies have begun to uncover the factors that regulate OTP expression and function. In zebrafish, Blechman et al. (2007) have shown that *Otp* is transcriptionally regulated by the zinc finger-containing transcription factor Fezl. Furthermore, epistasis and cell culture experiments indicate that signaling via the G-protein-coupled receptor PAC1 increases the level of OTP protein by promoting OTP synthesis. Further research into the role of transcription factors, such as *Lmx1a* and *Otp*, on postnatal maturation, survival and/or function of midbrain dopaminergic neurons will help to provide a better understanding of the complexity of PRL inhibition and its regulation of secretion.

7.4. GHRH

GHRH stimulates the release of growth hormone (GH) from the pituitary. GHRH is expressed during the later stages of development and is essential for the expansion of somatotropes. Hypophysiotropic GHRH neurons are confined to the ventrolateral part of the ARC (Niimi et al., 1990; Sawchenko et al., 1985) and first appear at 11.5 dpc in rat (Markakis and Swanson, 1997).

The development and transcriptional control of GHRH neurons has been studied in mouse models using both gene disruption and transgenic approaches. One example of GHRH reduction has been identified using targeted disruption of *Gsh1*, a homeobox gene identified as a direct transcriptional activator of *Ghrh* (Mutsuga et al.,

2001). Targeted disruption of *Gsh1* leads to the complete absence of *Ghrh* expression resulting in severe attenuation of growth and an associated decrease in overall pituitary size (Li et al., 1996). The haematopoietic transcription factor Ikaros is also expressed in GHRH neurons and is required for *Ghrh* expression (Ezzat et al., 2006). In contrast, GHRH over-expression in a mouse model harboring the human GHRH gene coupled to the murine metallothionein I promoter (Hammer et al., 1985) results in massive pituitary hyperplasia and an overabundance of somatotropes (Kineman et al., 2001; Mayo et al., 1988). These transgenic mice also exhibit pituitary tumors, albeit with incomplete penetrance, indicating that sustained elevated GHRH exposure predisposes somatotropes to neoplastic transformation.

7.5. SS

SS acts as an inhibitor of GH and TSH secretion. The inhibition of GH by SS appears to be independent of GHRH, although the precise mechanism remains unknown. GH secretion stimulates somatostatinergic neurons in the PeVN to secrete SS from the nerve terminals located at the ME into the hypothalamo-hypophysial portal circulation for delivery to the AP (Chihara et al., 1981). SS neurons that project into the ME are located within the rostral PeVN and the PVN. They first appear at 12.5 dpc in the rat (Markakis and Swanson, 1997). To date, transcription factors that specifically regulate the differentiation of hypothalamic SS neurons have not been identified, although it is possible that similar pathways to those that control SS neuron differentiation in other parts of the brain (e.g. the cerebral cortex) may be employed (Du et al., 2008).

7.6. TRH

TRH-synthesizing neurons exert multiple, species-dependent hypophysiotropic activities. However, for the purpose of this review, we will focus on the effects of TRH on TSH. Anatomically, the TRH neuroendocrine cells are situated in the hypothalamic PVN. TRH stimulates the secretion of TSH from the anterior pituitary thereby initiating thyroid hormone synthesis and release from the thyroid gland (Engel and Gershengorn, 2007; Nikrodhanond et al., 2006). TRH, identified by mRNA expression of the biosynthetic precursor pre-pro-TRH, was initially localized within the rat lateral hypothalamus at 13.5 dpc, and in the presumptive PVN at 15.5 dpc (Burgunder and Taylor, 1989). Immunohistochemical analysis of the TRH peptide revealed the first TRH-immunoreactive perikarya at 16.5 dpc as well as 17.5 dpc within the presumptive PVN (Okamura et al., 1991). There are four populations of TRH neurons (appearing at different developmental stages in the rat): (1) lateral hypothalamus (14.5 dpc); (2) VMN (15.5 dpc); (3) PVN (16.5 dpc); and (4) the POA (17.5 dpc). Thus, the differentiation and development of these neuronal populations will differ. Additionally, the identity and origin of the cues that direct TRH neuronal differentiation are poorly understood. However, it has been shown that brain derived neurotropic factor (BDNF) effects TRH neuronal differentiation by tropomyosin-related kinase B receptors during early development (Huang and Reichardt, 2001). BDNF also regulates the expression of pre-pro-TRH throughout development and into postnatal life in the rat (Ubieta et al., 2007).

7.7. CRH

CRH-synthesizing neurons are the principal hypothalamic regulators of the glucocorticoid axis and, like the TRH-synthesizing neurons, are closely situated in the hypothalamic PVN. Immunohistochemical analysis in rat embryos shows CRH expression as early as 15.5 dpc, with immunopositive fibers seen at 16.5 dpc in the ME (Daikoku et al., 1984). *Crh* mRNA expression studies have also identified CRH expressing cells from 16.5 dpc (Grino et al., 1989). Given that most CRH neurons are born at around 13.5 dpc (Markakis and Swanson, 1997), it appears that approximately 3 days is required for CRH neuron differentiation. While this process is poorly understood, one protein that has been shown to be required for generating CRH neurons is the homeodomain transcription factor OTP (Acampora et al., 1999). As discussed above, *Otp* is expressed in the developing PVN, SON, aPeVN and ARC and mutants lack CRH, as well as TRH and SS neurons (Acampora et al., 1999).

7.8. Other hypothalamic releasing hormones

In addition to the well-characterized hypothalamic releasing/inhibiting hormones, described above, there are several other hypothalamic specific factors that play a role during hypothalamic neuron differentiation and development and impact on pituitary function. For simplicity, we will not examine the other hypothalamic releasing/inhibiting hormones in this review because our purpose is to provide an in-depth review that covers hypophysiotropic factors that have a direct impact in AP function. However, of the well-characterized hypothalamic releasing/inhibiting hormones it is worth briefly mentioning kisspeptins. Kisspeptins, a family of peptides that activate G-protein-coupled receptors (GPCR), are strongly implicated in puberty onset as well as in the regulation of the hypothalamo–pituitary gonadal axis in mammals (Mikkelsen and Simonneaux, 2008). By directly stimulating GnRH release and subsequent LH release (Messager et al., 2005), achieved through a GPCR (KISS1R), kisspeptins prepare entry into puberty and the preovulatory LH surge. Kisspeptin neurons located in discrete regions of the hypothalamus make close appositions with GnRH. However, the distribution of neurons varies between species.

8. Summary and future perspectives

The past decade has witnessed significant progress in the identification of genetic determinants that control hypothalamic development. Although the full cast of characters is yet to be identified, it is clear that distinct sets of transcription factors play a role in the differentiation of hypothalamic progenitor cells into neurons and the commitment of subsets of neurons into cells that secrete hypophysiotropic factors. These factors provide an important framework for further functional studies that may lead to the generation of a transcriptional code for hypothalamic development. This process will likely be informed by parallel studies of other brain regions where knowledge of neuronal subtype specification and differentiation is further advanced. While parallel studies will provide useful intellectual synergy, it will also be necessary to focus on the discovery of novel hypophysiotropic cell molecules and pathways. This will be facilitated by recent advances in molecular and cellular biology including the identification of hypothalamic transcription factor gene targets using ChIP sequencing analysis, directed differentiation of ES cells into hypothalamic neuronal fates (Wataya et al., 2008) and characterization of novel mouse models using N-ethyl-N-nitrosourea (ENU) mutagenesis. Together, these approaches will help address critical issues such as the role of morphogens in establishing regional identify in the hypothalamic primordium, the timing and mechanism of parvicellular neuronal subtype specification, and the composition of the genetic program controlling terminal differentiation. As the role of new hypothalamic genes is deciphered it may become possible to detect patterns that will lead to a clearer understanding of brain development and evolution of the neuroendocrine system. This information will also advance our understanding of the molecular pathogenesis of hypothalamic dysfunction in humans and, perhaps, lead to improved therapies for related disorders.

References

Acampora, D., Postiglione, M.P., Avantaggiato, V., Di Bonito, M., Vaccarino, F.M., Michaud, J., Simeone, A., 1999. Progressive impairment of developing neuroendocrine cell lineages in the hypothalamus of mice lacking the Orthopedia gene. Genes Dev. 13, 2787–2800.

Aubert, M.L., Grumbach, M.M., Kaplan, S.L., 1977. The ontogenesis of human fetal hormones. IV. Somatostatin, luteinizing hormone releasing factor, and thyrotropin releasing factor in hypothalamus and cerebral cortex of human fetuses 10-22 weeks of age. J. Clin. Endocrinol. Metab. 44, 1130–1141.

Balan, I.S., Ugrumov, M.V., Borisova, N.A., Calas, A., Pilgrim, C., Reisert, I., Thibault, J., 1996. Birthdates of the tyrosine hydroxylase immunoreactive neurons in the hypothalamus of male and female rats. Neuroendocrinology 64, 405–411.

Barth, K.A., Wilson, S.W., 1995. Expression of zebrafish nk2.2 is influenced by sonic hedgehog/vertebrate hedgehog-1 and demarcates a zone of neuronal differentiation in the embryonic forebrain. Development 121, 1755–1768.

Bjorklund, A., Moore, R.Y., Nobin, A., Stenevi, U., 1973. The organization of tuberohypophyseal and reticulo-infundibular catecholamine neuron systems in the rat brain. Brain Res. 51, 171–191.

Blechman, J., Borodovsky, N., Eisenberg, M., Nabel-Rosen, H., Grimm, J., Levkowitz, G., 2007. Specification of hypothalamic neurons by dual regulation of the homeodomain protein Orthopedia. Development 134, 4417–4426.

Bloch, B., Gaillard, R.C., Brazeau, P., Lin, H.D., Ling, N., 1984. Topographical and ontogenetic study of the neurons producing growth hormone-releasing factor in human hypothalamus. Regul. Pept. 8, 21–31.

Brennan, J., Lu, C.C., Norris, D.P., Rodriguez, T.A., Beddington, R.S., Robertson, E.J., 2001. Nodal signalling in the epiblast patterns the early mouse embryo. Nature 411, 965–969.

Bugnon, C., Fellmann, D., Bresson, J.L., Clavequin, M.C., 1982. Immunocytochemical study of the ontogenesis of the CRF-containing neuroglandular system in the human hypothalamus. C. R. Seances Acad. Sci. III 294, 491–496.

Burgunder, J.M., Taylor, T., 1989. Ontogeny of thyrotropin-releasing hormone gene expression in the rat diencephalon. Neuroendocrinology 49, 631–640.

Caqueret, A., Boucher, F., Michaud, J.L., 2006. Laminar organization of the early developing anterior hypothalamus. Dev. Biol. 298, 95–106.

Cariboni, A., Hickok, J., Rakic, S., Andrews, W., Maggi, R., Tischkau, S., Parnavelas, J.G., 2007. Neuropilins and their ligands are important in the migration of gonadotropin-releasing hormone neurons. J. Neurosci. 27, 2387–2395.

Chiang, C., Litingtung, Y., Lee, E., Young, K.E., Corden, J.L., Westphal, H., Beachy, P.A., 1996. Cyclopia and defective axial patterning in mice lacking Sonic hedgehog gene function. Nature 383, 407–413.

Chihara, K., Minamitani, N., Kaji, H., Arimura, A., Fujita, T., 1981. Intraventricularly injected growth hormone stimulates somatostatin release into rat hypophysial portal blood. Endocrinology 109, 2279–2281.

Chung, W.C., Moyle, S.S., Tsai, P.S., 2008. Fibroblast growth factor 8 signaling through fibroblast growth factor receptor 1 is required for the emergence of gonadotropin-releasing hormone neurons. Endocrinology 149, 4997–5003.

Conlon, F.L., Lyons, K.M., Takaesu, N., Barth, K.S., Kispert, A., Herrmann, B., Robertson, E.J., 1994. A primary requirement for nodal in the formation and maintenance of the primitive streak in the mouse. Development 120, 1919–1928.

Daikoku, S., Hisano, S., Kawano, H., Okamura, Y., Tsuruo, Y., 1983. Ontogenetic studies on the topographical heterogeneity of somatostatin-containing neurons in rat hypothalamus. Cell Tissue Res. 233, 347–354.

Daikoku, S., Kawano, H., Okamura, Y., Tokuzen, M., Nagatsu, I., 1986. Ontogenesis of immunoreactive tyrosine hydroxylase-containing neurons in rat hypothalamus. Brain Res. 393, 85–98.

Daikoku, S., Okamura, Y., Kawano, H., Tsuruo, Y., Maegawa, M., Shibasaki, T., 1984. Immunohistochemical study on the development of CRF-containing neurons in the hypothalamus of the rat. Cell Tissue Res. 238, 539–544.

DeMaria, J.E., Lerant, A.A., Freeman, M.E., 1999. Prolactin activates all three populations of hypothalamic neuroendocrine dopaminergic neurons in ovariectomized rats. Brain Res. 837, 236–241.

Dockray, G.J., Reeve Jr., J.R., Shively, J., Gayton, R.J., Barnard, C.S., 1983. A novel active pentapeptide from chicken brain identified by antibodies to FMRFamide. Nature 305, 328–330.

Du, T., Xu, Q., Ocbina, P.J., Anderson, S.A., 2008. NKX2.1 specifies cortical interneuron fate by activating Lhx6. Development 135, 1559–1567.

Ducret, E., Anderson, G.M., Herbison, A.E., 2009. RFamide-related peptide-3 (RFRP-3), a mammalian gonadotropin-inhibitory hormone ortholog, regulates gonadotropin-releasing hormone (GnRH) neuron firing in the mouse. Endocrinology.

Engel, S., Gershengorn, M.C., 2007. Thyrotropin-releasing hormone and its receptors—a hypothesis for binding and receptor activation. Pharmacol. Ther. 113, 410–419.

Ericson, J., Norlin, S., Jessell, T., Edlund, T., 1998. Integrated FGF and BMP signaling controls the progression of progenitor cell differentiation and the emergence of pattern in the embryonic anterior pituitary. Development 125, 1005–1015.

Ezzat, S., Mader, R., Fischer, S., Yu, S., Ackerley, C., Asa, S.L., 2006. An essential role for the hematopoietic transcription factor Ikaros in hypothalamic–pituitary-mediated somatic growth. Proc. Natl. Acad. Sci. U.S.A. 103, 2214–2219.

Failli, V., Bachy, I., Retaux, S., 2002. Expression of the LIM-homeodomain gene Lmx1a (dreher) during development of the mouse nervous system. Mech. Dev. 118, 225–228.

Faivre-Bauman, A., Grouselle, D., Nemeskeri, A., Tixier-Vidal, A., 1978. Ontogenesis of thyroliberin in the mouse hypothalamus. Brain Res. 154, 382–387.

Figdor, M.C., Stern, C.D., 1993. Segmental organization of embryonic diencephalon. Nature 363, 630–634.

Fuxe, K., 1964. Cellular localization of monoamines in the median eminence and the infundibular stem of some mammals. Z. Zellforsch. Mikrosk. Anat. 61, 710–724.

Geris, K.L., Berghman, L.R., Kühn, E.R., Darras, V.M., 1998. Pre- and posthatch developmental changes in hypothalamic thyrotropin-releasing hormone and somatostatin concentrations and in circulating growth hormone and thyrotropin levels in the chicken. J. Endocrinol. 159, 219–225.

Giacobini, P., Kopin, A.S., Beart, P.M., Mercer, L.D., Fasolo, A., Wray, S., 2004. Cholecystokinin modulates migration of gonadotropin-releasing hormone-1 neurons. J. Neurosci. 24, 4737–4748.

Giacobini, P., Messina, A., Morello, F., Ferraris, N., Corso, S., Penachioni, J., Giordano, S., Tamagnone, L., Fasolo, A., 2008. Semaphorin 4D regulates gonadotropin hormone-releasing hormone-1 neuronal migration through PlexinB1-Met complex. J Cell Biol. 183, 555–566.

Giacobini, P., Messina, A., Wray, S., Giampietro, C., Crepaldi, T., Carmeliet, P., Fasolo, A., 2007. Hepatocyte growth factor acts as a motogen and guidance signal for gonadotropin hormone-releasing hormone-1 neuronal migration. J. Neurosci. 27, 431–445.

Goudreau, J.L., Lindley, S.E., Lookingland, K.J., Moore, K.E., 1992. Evidence that hypothalamic periventricular dopamine neurons innervate the intermediate lobe of the rat pituitary. Neuroendocrinology 56, 100–105.

Grino, M., Young 3rd, W.S., Burgunder, J.M., 1989. Ontogeny of expression of the corticotropin-releasing factor gene in the hypothalamic paraventricular nucleus and of the proopiomelanocortin gene in rat pituitary. Endocrinology 124, 60–68.

Gross, D.S., Longer, J.D., 1979. Developmental correlation between hypothalamic somatostatin and hypophysial growth hormone. Cell Tissue Res. 202, 251–261.

Guillemin, R., Yamazaki, E., Gard, D.A., Jutisz, M., Sakiz, E., 1963. In vitro secretion of thyrotropin (Tsh): stimulation by a hypothalamic peptide (Trf). Endocrinology 73, 564–572.

Guillemot, F., 2007. Spatial and temporal specification of neural fates by transcription factor codes. Development 134, 3771–3780.

Hammer, R.E., Brinster, R.L., Rosenfeld, M.G., Evans, R.M., Mayo, K.E., 1985. Expression of human growth hormone-releasing factor in transgenic mice results in increased somatic growth. Nature 315, 413–416.

Hauptmann, G., Gerster, T., 1996. Complex expression of the zp-50 pou gene in the embryonic zebrafish brain is altered by overexpression of sonic hedgehog. Development 122, 1769–1780.

Hosoya, T., Oda, Y., Takahashi, S., Morita, M., Kawauchi, S., Ema, M., Yamamoto, M., Fujii-Kuriyama, Y., 2001. Defective development of secretory neurones in the hypothalamus of Arnt2-knockout mice. Genes Cells 6, 361–374.

Huang, E.J., Reichardt, L.F., 2001. Neurotrophins: roles in neuronal development and function. Annu. Rev. Neurosci. 24, 677–736.

Ingraham, H.A., Lala, D.S., Ikeda, Y., Luo, X., Shen, W.H., Nachtigal, M.W., Abbud, R., Nilson, J.H., Parker, K.L., 1994. The nuclear receptor steroidogenic factor 1 acts at multiple levels of the reproductive axis. Genes Dev. 8, 2302–2312.

Jasoni, C.L., Porteous, R.W., Herbison, A.E., 2009. Anatomical location of mature GnRH neurons corresponds with their birthdate in the developing mouse. Dev. Dyn. 238, 524–531.

Johnson, M.A., Tsutsui, K., Fraley, G.S., 2007. Rat RFamide-related peptide-3 stimulates GH secretion, inhibits LH secretion, and has variable effects on sex behavior in the adult male rat. Horm. Behav. 51, 171–180.

Józsa, R., Vigh, S., Mess, B., Schally, A.V., 1986. Ontogenetic development of corticotropin-releasing factor (CRF)-containing neural elements in the brain of the chicken during incubation and after hatching. Cell Tissue Res. 244, 681–685.

Kapsimali, M., Caneparo, L., Houart, C., Wilson, S.W., 2004. Inhibition of Wnt/Axin/beta-catenin pathway activity promotes ventral CNS midline tissue to adopt hypothalamic rather than floorplate identity. Development 131, 5923–5933.

Keegan, C.E., Herman, J.P., Karolyi, I.J., O'Shea, K.S., Camper, S.A., Seasholtz, A.F., 1994. Differential expression of corticotropin-releasing hormone in developing mouse embryos and adult brain. Endocrinology 134, 2547–2555.

Keith, B., Adelman, D.M., Simon, M.C., 2001. Targeted mutation of the murine arylhydrocarbon receptor nuclear translocator 2 (Arnt2) gene reveals partial redundancy with Arnt. Proc. Natl. Acad. Sci. U.S.A. 98, 6692–6697.

Kimura, S., Hara, Y., Pineau, T., Fernandez-Salguero, P., Fox, C.H., Ward, J.M., Gonzalez, F.J., 1996. The T/ebp null mouse: thyroid-specific enhancer-binding protein is essential for the organogenesis of the thyroid, lung, ventral forebrain, and pituitary. Genes Dev. 10, 60–69.

Kineman, R.D., Teixeira, L.T., Amargo, G.V., Coschigano, K.T., Kopchick, J.J., Frohman, L.A., 2001. The effect of GHRH on somatotrope hyperplasia and tumor formation in the presence and absence of GH signaling. Endocrinology 142, 3764–3773.

Kramer, P.R., Krishnamurthy, R., Mitchell, P.J., Wray, S., 2000. Transcription factor activator protein-2 is required for continued luteinizing hormone-releasing hormone expression in the forebrain of developing mice. Endocrinology 141, 1823–1838.

Kriegsfeld, L.J., Mei, D.F., Bentley, G.E., Ubuka, T., Mason, A.O., Inoue, K., Ukena, K., Tsutsui, K., Silver, R., 2006. Identification and characterization of a gonadotropin-inhibitory system in the brains of mammals. Proc. Natl. Acad. Sci. U.S.A. 103, 2410–2415.

Lawson, M.A., Mellon, P.L., 1998. Expression of GATA-4 in migrating gonadotropin-releasing neurons of the developing mouse. Mol Cell Endocrinol. 140, 157–161.

Lawson, M.A., Whyte, D.B., Mellon, P.L., 1996. GATA factors are essential for activity of the neuron-specific enhancer of the gonadotropin-releasing hormone gene. Mol. Cell Biol. 16, 3596–3605.

Lee, J.E., Wu, S.F., Goering, L.M., Dorsky, R.I., 2006. Canonical Wnt signaling through Lef1 is required for hypothalamic neurogenesis. Development.

Lee, V.H., Lee, L.T., Chow, B.K., 2008. Gonadotropin-releasing hormone: regulation of the GnRH gene. FEBS J. 275, 5458–5478.

Lefebvre, V., Dumitriu, B., Penzo-Mendez, A., Han, Y., Pallavi, B., 2007. Control of cell fate and differentiation by Sry-related high-mobility-group box (Sox) transcription factors. Int. J. Biochem. Cell Biol..

Li, H., Zeitler, P.S., Valerius, M.T., Small, K., Potter, S.S., 1996. Gsh-1, an orphan Hox gene, is required for normal pituitary development. EMBO J. 15, 714–724.

Manning, L., Ohyama, K., Saeger, B., Hatano, O., Wilson, S.A., Logan, M., Placzek, M., 2006. Regional morphogenesis in the hypothalamus: a BMP-Tbx2 pathway coordinates fate and proliferation through Shh downregulation. Dev. Cell 11, 873–885.

Markakis, E.A., 2002. Development of the neuroendocrine hypothalamus. Front. Neuroendocrinol. 23, 257–291.

Markakis, E.A., Swanson, L.W., 1997. Spatiotemporal patterns of secretomotor neuron generation in the parvicellular neuroendocrine system. Brain Res. Brain Res. Rev. 24, 255–291.

Mathieu, J., Barth, A., Rosa, F.M., Wilson, S.W., Peyrieras, N., 2002. Distinct and cooperative roles for Nodal and Hedgehog signals during hypothalamic development. Development 129, 3055–3065.

Mayo, K.E., Hammer, R.E., Swanson, L.W., Brinster, R.L., Rosenfeld, M.G., Evans, R.M., 1988. Dramatic pituitary hyperplasia in transgenic mice expressing a human growth hormone-releasing factor gene. Mol. Endocrinol. 2, 606–612.

McNay, D.E., Pelling, M., Claxton, S., Guillemot, F., Ang, S.L., 2006. Mash1 is required for generic and subtype differentiation of hypothalamic neuroendocrine cells. Mol. Endocrinol. 20, 1623–1632.

Messager, S., Chatzidaki, E.E., Ma, D., Hendrick, A.G., Zahn, D., Dixon, J., Thresher, R.R., Malinge, I., Lomet, D., Carlton, M.B., et al., 2005. Kisspeptin directly stimulates gonadotropin-releasing hormone release via G protein-coupled receptor 54. Proc. Natl. Acad. Sci. U.S.A. 102, 1761–1766.

Michaud, J.L., Rosenquist, T., May, N.R., Fan, C.M., 1998. Development of neuroendocrine lineages requires the bHLH-PAS transcription factor SIM1. Genes Dev. 12, 3264–3275.

Mikkelsen, J.D., Simonneaux, V., 2008. The neuroanatomy of the kisspeptin system in the mammalian brain. Peptides.

Misson, J.P., Austin, C.P., Takahashi, T., Cepko, C.L., Caviness Jr., V.S., 1991. The alignment of migrating neural cells in relation to the murine neopallial radial glial fiber system. Cereb. Cortex 1, 221–229.

Mitchell, P.J., Timmons, P.M., Hebert, J.M., Rigby, P.W., Tjian, R., 1991. Transcription factor AP-2 is expressed in neural crest cell lineages during mouse embryogenesis. Genes Dev. 5, 105–119.

Murakami, M., Matsuzaki, T., Iwasa, T., Yasui, T., Irahara, M., Osugi, T., Tsutsui, K., 2008. Hypophysiotropic role of RFamide-related peptide-3 in the inhibition of LH secretion in female rats. J. Endocrinol. 199, 105–112.

Mutsuga, N., Iwasaki, Y., Morishita, M., Nomura, A., Yamamori, E., Yoshida, M., Asai, M., Ozaki, N., Kambe, F., Seo, H., et al., 2001. Homeobox protein Gsh-1-dependent regulation of the rat GHRH gene promoter. Mol. Endocrinol. 15, 2149–2156.

Niimi, M., Takahara, J., Sato, M., Kawanishi, K., 1990. Immunohistochemical identification of galanin and growth hormone-releasing factor-containing neurons projecting to the median eminence of the rat. Neuroendocrinology 51, 572–575.

Nikrodhanond, A.A., Ortiga-Carvalho, T.M., Shibusawa, N., Hashimoto, K., Liao, X.H., Refetoff, S., Yamada, M., Mori, M., Wondisford, F.E., 2006. Dominant role of thyrotropin-releasing hormone in the hypothalamic–pituitary–thyroid axis. J. Biol. Chem. 281, 5000–5007.

Ohyama, K., Das, R., Placzek, M., 2008. Temporal progression of hypothalamic patterning by a dual action of BMP. Development 135, 3325–3331.

Ohyama, K., Ellis, P., Kimura, S., Placzek, M., 2005. Directed differentiation of neural cells to hypothalamic dopaminergic neurons. Development 132, 5185–5197.

Okamura, Y., Kawano, H., Daikoku, S., 1991. Spatial-temporal appearance of developing immunoreactive TRH neurons in the neuroepithelial wall of the diencephalon. Brain Res. Dev. Brain Res. 63, 21–31.

Parras, C.M., Schuurmans, C., Scardigli, R., Kim, J., Anderson, D.J., Guillemot, F., 2002. Divergent functions of the proneural genes Mash1 and Ngn2 in the specification of neuronal subtype identity. Genes Dev. 16, 324–338.

Patten, I., Placzek, M., 2002. Opponent activities of Shh and BMP signaling during floor plate induction in vivo. Curr. Biol. 12, 47–52.

Price, D.A., Greenberg, M.J., 1977. Structure of a molluscan cardioexcitatory neuropeptide. Science 197, 670–671.

Raffa, R.B., 1988. The action of FMRFamide (Phe-Met-Arg-Phe-NH2) and related peptides on mammals. Peptides 9, 915–922.

Rastogi, R.K., D'Aniello, B., Pinelli, C., Fiorentino, M., Di Fiore, M.M., Di Meglio, M., Iela, L., 2001. FMRFamide in the amphibian brain: a comprehensive survey. Microsc. Res. Tech. 54, 158–172.

Rizzoti, K., Brunelli, S., Carmignac, D., Thomas, P.Q., Robinson, I.C., Lovell-Badge, R., 2004. SOX3 is required during the formation of the hypothalamo–pituitary axis. Nat. Genet. 36, 247–255.

Rohr, K.B., Barth, K.A., Varga, Z.M., Wilson, S.W., 2001. The nodal pathway acts upstream of hedgehog signaling to specify ventral telencephalic identity. Neuron 29, 341–351.

Sawchenko, P.E., Swanson, L.W., Rivier, J., Vale, W.W., 1985. The distribution of growth-hormone-releasing factor (GRF) immunoreactivity in the central nervous system of the rat: an immunohistochemical study using antisera directed against rat hypothalamic GRF. J. Comp. Neurol. 237, 100–115.

Schell-Apacik, C., Rivero, M., Knepper, J.L., Roessler, E., Muenke, M., Ming, J.E., 2003. SONIC HEDGEHOG mutations causing human holoprosencephaly impair neural patterning activity. Hum. Genet. 113, 170–177.

Schwanzel-Fukuda, M., Crossin, K.L., Pfaff, D.W., Bouloux, P.M., Hardelin, J.P., Petit, C., 1996. Migration of luteinizing hormone-releasing hormone (LHRH) neurons in early human embryos. J. Comp. Neurol. 366, 547–557, javascript:PopUpMenu2_Set('Menu8907364').

Shinoda, K., Lei, H., Yoshii, H., Nomura, M., Nagano, M., Shiba, H., Sasaki, H., Osawa, Y., Ninomiya, Y., Niwa, O., et al., 1995. Developmental defects of the ventromedial hypothalamic nucleus and pituitary gonadotroph in the Ftz-F1 disrupted mice. Dev. Dyn. 204, 22–29.

Solomon, N.M., Nouri, S., Warne, G.L., Lagerstrom-Fermer, M., Forrest, S.M., Thomas, P.Q., 2002. Increased gene dosage at Xq26–q27 is associated with X-linked hypopituitarism. Genomics 79, 553–559.

Son, J.H., Min, N., Joh, T.H., 1996. Early ontogeny of catecholaminergic cell lineage in brain and peripheral neurons monitored by tyrosine hydroxylase-lacZ transgene. Brain Res. Mol. Brain Res. 36, 300–308.

Sullivan, K.A., Silverman, A.J., 1993. The ontogeny of gonadotropin-releasing hormone neurons in the chick. Neuroendocrinology 58, 597–608.

Szabo, N.E., Zhao, T., Cankaya, M., Theil, T., Zhou, X., Alvarez-Bolado, G., 2009. Role of neuroepithelial Sonic hedgehog in hypothalamic patterning. J. Neurosci. 29, 6989–7002.

Takuma, N., Sheng, H.Z., Furuta, Y., Ward, J.M., Sharma, K., Hogan, B.L., Pfaff, S.L., Westphal, H., Kimura, S., Mahon, K.A., 1998. Formation of Rathke's pouch requires dual induction from the diencephalon. Development 125, 4835–4840.

Thommes, R.C., Caliendo, J., Woods, J.E., 1985. Hypothalamo-adenohypophyseal-thyroid interrelationships in the developing chick embryo. VII. Immunocytochemical demonstration of thyrotrophin-releasing hormone. Gen. Comp. Endocrinol 57, 1–9.

Tran, T.S., Kolodkin, A.L., Bharadwaj, R., 2007. Semaphorin regulation of cellular morphology. Annu. Rev. Cell Dev. Biol. 23, 263–292.

Tsutsui, K., Bentley, G.E., Ubuka, T., Saigoh, E., Yin, H., Osugi, T., Inoue, K., Chowdhury, V.S., Ukena, K., Ciccone, N., et al., 2007. The general and comparative biology of gonadotropin-inhibitory hormone (GnIH). Gen. Comp. Endocrinol. 153, 365–370.

Tsutsui, K., Ukena, K., 2006. Hypothalamic LPXRF-amide peptides in vertebrates: identification, localization and hypophysiotropic activity. Peptides 27, 1121–1129.

Ubieta, R., Uribe, R.M., Gonzalez, J.A., Garcia-Vazquez, A., Perez-Monter, C., Perez-Martinez, L., Joseph-Bravo, P., Charli, J.L., 2007. BDNF up-regulates pre-pro-TRH mRNA expression in the fetal/neonatal paraventricular nucleus of the hypothalamus. Properties of the transduction pathway. Brain Res. 1174, 28–38.

Varlet, I., Collignon, J., Robertson, E.J., 1997. nodal expression in the primitive endoderm is required for specification of the anterior axis during mouse gastrulation. Development 124, 1033–1044.

Verney, C., el Amraoui, A., Zecevic, N., 1996. Comigration of tyrosine hydroxylase- and gonadotropin-releasing hormone-immunoreactive neurons in the nasal area of human embryos. Brain Res. Dev. Brain Res. 97, 251–259.

Verney, C., Zecevic, N., Nikolic, B., Alvarez, C., Berger, B., 1991. Early evidence of catecholaminergic cell groups in 5- and 6-week-old human embryos using tyrosine hydroxylase and dopamine-beta-hydroxylase immunocytochemistry. Neurosci. Lett. 131, 121–124.

Wang, W., Grimmer, J.F., Van De Water, T.R., Lufkin, T., 2004. Hmx2 and Hmx3 homeobox genes direct development of the murine inner ear and hypothalamus and can be functionally replaced by Drosophila Hmx. Dev. Cell 7, 439–453.

Wang, W., Lufkin, T., 2000. The murine Otp homeobox gene plays an essential role in the specification of neuronal cell lineages in the developing hypothalamus. Dev. Biol. 227, 432–449.

Wataya, T., Ando, S., Muguruma, K., Ikeda, H., Watanabe, K., Eiraku, M., Kawada, M., Takahashi, J., Hashimoto, N., Sasai, Y., 2008. Minimization of exogenous signals in ES cell culture induces rostral hypothalamic differentiation. Proc. Natl. Acad. Sci. U.S.A. 105, 11796–11801.

Weiss, J., Meeks, J.J., Hurley, L., Raverot, G., Frassetto, A., Jameson, J.L., 2003. Sox3 is required for gonadal function, but not sex determination, in males and females. Mol. Cell Biol. 23, 8084–8091.

Winters, A.J., Eskay, R.L., Porter, J.C., 1974. Concentration and distribution of TRH and LRH in the human fetal brain. J. Clin. Endocrinol. Metab. 39, 960–963.

Woods, K.S., Cundall, M., Turton, J., Rizotti, K., Mehta, A., Palmer, R., Wong, J., Chong, W.K., Al-Zyoud, M., El-Ali, M., et al., 2005. Over- and underdosage of SOX3 is associated with infundibular hypoplasia and hypopituitarism. Am. J. Hum. Genet. 76, 833–849.

Wray, S., 2001. Development of luteinizing hormone releasing hormone neurones. J. Neuroendocrinol. 13, 3–11.

Wray, S., 2002. Development of gonadotropin-releasing hormone-1 neurons. Front. Neuroendocrinol. 23, 292–316.

Wray, S., Grant, P., Gainer, H., 1989. Evidence that cells expressing luteinizing hormone-releasing hormone mRNA in the mouse are derived from progenitor cells in the olfactory placode. Proc. Natl. Acad. Sci. USA 86, 8132–8136.

Zecevic, N., Verney, C., 1995. Development of the catecholamine neurons in human embryos and fetuses, with special emphasis on the innervation of the cerebral cortex. J. Comp. Neurol. 351, 509–535.

Zou, H.L., Su, C.J., Shi, M., Zhao, G.Y., Li, Z.Y., Guo, C., Ding, Y.Q., 2009. Expression of the LIM-homeodomain gene Lmx1a in the postnatal mouse central nervous system. Brain Res. Bull. 78, 306–312.